Development of multi-step biorefinery schemes for the production of nanocellulose and high value-added bioproducts from mango seed

by

Fatimatu Bello

Dissertation presented for the Degree

of

DOCTOR OF PHILOSOPHY

(CHEMICAL ENGINEERING)

in the Faculty of Engineering

at Stellenbosch University

The financial assistance of the National Research Foundation (NRF), South Africa, the Department of Science and Innovation (DSI)/Council for Scientific and Industrial Research (CSIR), South Africa, and the Process Engineering Department, Stellenbosch University, South Africa**,** towards this research is hereby acknowledged. Opinions expressed and conclusions arrived at, are those of the author and are not necessarily to be attributed to the NRF

Supervisor

Prof. Annie Chimphango

Co-supervisor

Prof. Johann Ferdinand Görgens

April 2022

Declaration

By submitting this thesis electronically, I declare that the entirety of the work contained therein is my own, original work, that I am the sole author thereof (save to the extent explicitly otherwise stated), that reproduction and publication thereof by Stellenbosch University will not infringe any third-party rights and that I have not previously in its entirety or in part submitted it for obtaining any qualification.

This dissertation includes 2 original papers published in peer-reviewed journals and 3 unpublished papers. The development and writing of the papers (published and unpublished) were the principal responsibility of myself and, for each of the cases where this is not the case, a declaration is included in the dissertation indicating the nature and extent of the contributions of co-authors.

Date: *April 2022*

Plagiarism Declaration

1. Plagiarism is the use of ideas, material, and other intellectual property of another's work and to present it as my own.
2. I agree that plagiarism is a punishable offense because it constitutes theft.
3. I also understand that direct translations are plagiarism.
4. Accordingly, all quotations and contributions from any source whatsoever (including the internet) have been cited fully. I understand that the reproduction of text without quotation marks (even when the source is cited) is plagiarism.
5. I declare that the work contained in this assignment, except where otherwise stated, is my original work and that I have not previously (in its entirety or in part) submitted it for grading in this module/assignment or another module/assignment.

Initials and surname: F. Bello

Abstract

Due to environmental and health concerns associated with non-renewable and synthetic-based packaging materials, there is an upward demand for bioproducts from renewable sources, particularly for food packaging. Nanocellulose is one such bioproduct and is generally produced from woody biomass due to its fibrous nature, however, woody biomass is in high demand. Mango (*Mangifera Indica L.*) seed is a major lignocellulosic waste from mango fruit processing, whose management is limited to disposal by incineration, burning, or landfilling with no current commercial use, resulting in environmental and economic burdens such as green-house gas emissions and land use concerns. However, mango seed has potentials for various bioproduct exploits including nanocellulose, due to the high cellulose content comparable to woody biomass and valuable co-products (hemicellulose, starch, polyphenols, and lignin). Thus, compared to the woody biomass, biorefinery exploits for the mango seed focused on the comprehensive fractionation and conversion into bioproducts and the nanocellulose offers additional advantages of enhancing the economic exploits through the additional product recoveries. However, the conventional nanocellulose production processes involving controlled sulphuric acid treatment of bleached cellulose-rich Kraft pulp, degrades the valuable components of polyphenols, lignin, and hemicellulose, and the sulphuric acid applied lowers the thermal stability of the nanocellulose thereby limiting its application in thermo-processing. In addition, due to the different biomass components responding differently to process conditions and the specificity of optimal extraction conditions for each product, challenges of low product yields and qualities could be envisaged for non-optimized extraction processes. Thus, establishing appropriate and optimal multi-step fractionation/conversion processes for the multi-product biorefinery schemes is essential for the sustainable recovery of the bioproducts. Therefore, this study aimed at developing multi-step biorefinery schemes for fractionating mango seed into high-value products such as hemicellulose, lignin, starch, cellulose, and polyphenols. Furthermore, produce nanocellulose from the cellulose fibers using organic acids and compare with the classical sulphuric acid-based process. Additionally, evaluate the potential of the hemicellulose extract as a material for biocomposite film development for food packaging without external additives.

A multi-step biorefinery process consisting of sequential organosolv extraction (OE) [ethanol concentration (50–80% v/v), temperatures (20–60°C)], enzymatic hydrolysis (EH) [Termamyl®SC; (300 mL of Termamyl SC per ton starch in MSK) and Saczyme®Plus; (800 ml Saczyme Plus/ ton starch in MSK)] and alkaline pretreatment (AP) [(40–90 °C), NaOH

concentrations (1–2 M), time (2–4 h)] for the recovery of polyphenols, starch, and bioactive hemicellulose from mango seed kernel (MSK) while minimizing the degradation of cellulose and lignin in the residual solids was developed. In addition, a multi-step sequential AP and rotor-stator high shear homogenization-assisted organosolv (HSHO) [ethanol concentration (50–70%), temperature (130–150 °C), homogenizing time (10–20 min)] process to recover hemicellulose (xylan/xyloglucan), lignin and cellulose-rich fibers from mango seed husk (MSH) was developed. The feasibility of the MSH hemicellulose extract to form self-supporting biocomposite film without external additives as applicable with xylan-based films was assessed. In addition, the feasibility of producing nanocellulose from the cellulose-rich fibers obtained from the multi-step process via optimized non-catalyzed formic acid-based treatment was investigated. Effect of an alternative CNC production process involving acetic acid treatment [pulp-to-acid ratio (1:20–1:40), reaction time (6–12 h)] on the preparation and acetylation of CNCs from the cellulose-rich fibers was also evaluated versus the combined acetic acid plus high shear homogenization and the classical sulphuric acid-based process. Results from the optimized multi-step sequential OE, EH, and AP process route for the fractionation of MSK led to the recovery of polyphenols, starch, bioactive hemicellulose, and solid residue enriched in cellulose and lignin. The optimized OE process (64.99%w/w ethanol, 54.18 ºC) resulted in an extract with total polyphenol content (TPC) and antioxidant activity (AA) of 95.21 mg GAE/g and 84.69% respectively with >90% cellulose, lignin, starch, and hemicellulose retention in the residual solids. The EH of the OE process resulted in >90% starch removal (as simple sugars). The optimized conditions for the subsequent AP of the destarched OE solids resulted in >50% hemicellulose recovery with 34.96 mg GAE/g TPC and 55.05% AA, and solids having 88.3% and 91.12% cellulose and lignin retention respectively that could be further valorized to increase the product range from the MSK.

At the optimized AP process conditions (1.92 M NaOH, 86.0 °C, and 3.84 h), the recovered MSH hemicellulose extract possess suitable properties for thermally stable biocomposite film for food packaging. Subsequently, at the optimized HSHO pretreatment conditions (60% ethanol, 148.41 ºC, 15 min homogenization), over 70% lignin dissolution with high purity (>95%), 3247 g/mol molecular weight (M_w), and 298 ºC maximum thermal degradation temperature (T_{max}) were obtained based on the AP MSH. The recovered solids post-HSHO process had >77% cellulose with fibers separated into individual strands of diameters <1 to 10 µm, and >55% crystallinity suitable for CNC production. Thus, the multi-step sequential AP and HSHO biorefinery route is promising for multi-products recovery in addition to the cellulose-rich material for CNC production.

Opsomming

As gevolg van omgewings- en gesondheidskommer geassosieer met nie-herwinbare en sinteties-gebaseerde verpakkingsmateriaal, is daar ’n opwaartse aanvraag vir bioprodukte uit herwinbare bronne, veral vir voedselverpakking. Nanosellulose is só ’n bioproduk en word oor die algemeen geproduseer uit houtagtige biomassa as gevolg van sy veselagtige natuur. Houtagtige biomassa is egter in hoë aanvraag. Mangosaad (*Mangifera Indica L.*) is ’n groot lignosellulose-afval van mangovrugprosessering, wat se bestuur beperk is tot verwydering deur verassing, verbranding, of landopvulling met huidig geen kommersiële gebruik nie, wat omgewings- en ekonomiese laste soos groenhuisgasemissie en landgebruik bekommernisse tot gevolg het. Mangosaad het egter die potensiaal vir verskeie bioprodukontginning insluitend nanosellulose, as gevolg van die hoë sellulose-inhoud in vergelyking met houtagtige biomassa en waardevolle ko-produkte (hemisellulose, stysel, polifenole en lignien). Dus, in vergelyking met die houtagtige biomassa, het die bioraffinadery se ontginning van die mangosaad gefokus op die omvattende fraksionering en omsetting in bioprodukte en die nanosellulose bied addisionele ekonomiese ontginning deur addisionele produkherwinning. Die konvensionele nanoselluloseproduksieproses wat die beheerde swawelsuurbehandeling van gebleikte sellulose-ryke Kraft-pulp insluit, het egter die waardevolle komponente van polifenole, lignien en hemisellulose gedegradeer, en die swawelsuur toegepas het die termiese stabiliteit van die nanosellulose verlaag, daardeur sy toepassing in termoprosessering beperk. Daarby, as gevolg van die verskillende biomassakomponente wat verskillend op die proseskondisies reageer en die spesifisiteit van optimale ekstraksiekondisies vir elke produk, is uitdagings van lae produkopbrengste en kwaliteit voorsien vir nie-geoptimeerde ekstraksieprosesse. Dus, is dit essensieel om die gepaste en optimale multi-stap fraksionering/omsettingprosesse vir die multi-produk bioraffinaderyskema vas te stel, vir die volhoubare herwinning van die bioprodukte. Daarom het hierdie studie beoog om multi-stap bioraffinaderyskemas vir fraksionering van mangosaad in hoë-waarde produkte soos hemisellulose, lignien, stysel, sellulose en polifenole, te ontwikkel. Verder het die studie beoog om nanosellulose uit sellulose vesels te produseer deur organiese sure te gebruik en te vergelyk met die klassieke swawelsuur-gebaseerde proses. Daarby het dit die potensiaal van die hemisellulose ekstraksie as ’n materiaal vir biosaamgestelde film geëvalueer vir voedselverpakking sonder eksterne bymiddels.

’n Multi-stap bioraffinaderyproses is ontwikkel wat bestaan uit sekwensiële organosolv ekstraksie (OE) [etanolkonsentrasie (50–80% v/v), temperatuur (20–60 °C)], ensimatiese hidrolise (EH) [Termamyl®SC; (300 mL Termamyl SC per ton stysel in MSK) en

Saczyme®Plus; (800 ml Saczyme Plus/ton stysel in MSK)] en alkaliese voorbehandeling (AP) [40–90 °C), NaOH-konsentrasies (1–2 M), tyd (2–4 h)] vir die herwinning van polifenole, stysel en bio-aktiewe hemisellulose uit mangosaadpit (MSK) terwyl die degradasie van sellulose en lignien in die residuele vaste stowwe geminimeer is. Daarby is 'n multi-stap sekwensiële AP en rotor-stator hoë skuifkrag homogenisering geassisteerde organosolv (HSHO) [etanolkonsentrasie (50–70%), temperatuur (130–150 °C), homogeniseringstyd (10–20 min)] proses ontwikkel om hemisellulose (xilan/xiloglukaan), lignien en sellulose-ryke vesels van mangosaadpeul (MSH) te herwin. Die uitvoerbaarheid van die MSH hemisellulose ekstrak om self-ondersteunende biosaamgestelde film sonder eksterne bymiddels te vorm, soos toepaslik met xilaan-gebaseerde films, is geassesseer. Daarby is die uitvoerbaarheid van nanoselluloseproduksie uit die sellulose-ryke vesels verkry uit die multi-stap proses via nie-gekataliseerde metanoësuur-gebaseerde behandeling wat geoptimeer is, ondersoek. Die effek van 'n alternatiewe CNC-produksieproses wat asynsuurbehandeling insluit [pulp-tot-suur-ratio (1:20–1:40), reaksietyd (6–12 h)] op die voorbereiding en asetilasie van CNCs van die sellulose-ryke vesels is ook geëvalueer teenoor die gekombineerde asynsuur plus hoë skuifkrag homogenisering en die klassieke swawelsuur-gebaseerde proses. Resultate van die geoptimeerde multi-stap sekwensiële OE-, EH- en AP-prosesroete vir die fraksionering van MSK het tot die herwinning van polifenole, stysel, bio-aktiewe hemisellulose en lignien gelei. Die OE-proses wat geöptimeer is (64.99% w/w etanol, 54.18 °C) het 'n ekstrak tot gevolg gehad met totale polifenole inhoud (TPC) en antioksidant aktiwiteit (AA) van 95.21 mg GAE/g en 84.69% onderskeidelik, met >90% sellulose, lignien, stysel en hemisellulose retensie in die residuele vaste stowwe. Die EH van die OE-proses het >90% styselverwydering tot gevolg gehad (as eenvoudige suikers). Die geöptimeerde kondisies vir die daaropvolgende AP van die ontstyselde OE-vaste stowwe het tot >50% hemisellulose herwinning gelei met 34.96 mg GAE/g TPC en 55.05% AA, en vaste stowwe wat 88.3% en 91.12% sellulose en lignien retensie onderskeidelik het, wat verder gevaloriseer kan word om die produkbestek van die MSK te verhoog.

By die geöptimeerde AP-proseskondisies (1.92 M NaOH, 86.0 °C, en 3.84 h), het die herwinde MSH-hemisellulose-ekstrak gepaste eienskappe vir termies stabiele biosaamgestelde film vir voedselverpakking. Daaropvolgens, by die geöptimeerde HSHO voorbehandelingkondisies (60% etanol, 148.41 °C, 15 min homogenisering), is meer as 70% lignienoplossing met hoë suiwerheid (>95%), 3247 g/mol molekulêre gewig (M_w), en 298 °C maksimum termiese degradasie temperature (T_{max}) verkry gebaseer op die AP MSH. Die herwinde vaste stowwe na-HSHO-proses het >75% sellulose met vesels geskei in individuele

stringe van deursnit <1 tot 10 µm, en >55% kristalliniteit gehad, gepas vir CNC-produksie. Dus, die multi-stap sekwensiële AP- en HSHO-bioraffinaderyroete is belowend vir multi-produkherwinning buiten die sellulose-ryke materiaal vir CNC-produksie.

Acknowledgments

I am very much grateful to the omnipotent God for his protection and grace during my study. My profound gratitude goes to my supervisors, Prof. Annie Chimphango and Prof. Johann F. Görgens for their support and guidance throughout this study. I am forever grateful to my mum, Mrs. Dinah Bello, my sisters, Mariama Bello, Madinatu Bello, Afusatu Bello, Risikatu Bello, Selia Bello, and my brothers, Alex Atuahene Ofosu and Richard Kingley Padi for their unflinching support. I am indebted to my son Uriel Ampiah-Kumi Jnr. for his support and motivation during the period of my study. I extend my appreciation to the National Research Foundation (NRF), DST/CSIR Waste Roadmap program, and the Department of Process Engineering for their financial support. I would like to thank all the analytical staff members of the Process Engineering Department: Mrs. Hanlie Botha, Mr. Jaco van Rooyen, and Mrs. Levine Simmers,) and the technical staff (Mr. Alvin Peterson and Mr. Oliver) for their time and assistance. My gratitude goes to the staff of the Forestry and Wood Science Department (Mr. Wilmour Hendrikse and Mr. Henry Solomon), Department of Chemistry (Dr. Leigh Loots), Department of Polymer Science (Dr. Helen Pfukwa), and The Central Analytical Facility (Mrs. Madalene Frazenburg, Mr. Mokwena Lucky, Dr. D. Brand) for their support in various analyses. Finally, I appreciate the support and motivation from my friends and colleagues.

Dedication

I dedicate this work to the Almighty God, my mum Dinah Bello, and my son Uriel Ampiah-Kumi Jnr.

Table of Contents

DECLARATION ..... **II**

PLAGIARISM DECLARATION ..... **III**

ABSTRACT ..... **IV**

OPSOMMING ..... **VI**

ACKNOWLEDGMENTS ..... **IX**

DEDICATION ..... **X**

TABLE OF CONTENTS ..... **XI**

LIST OF FIGURES ..... **XVII**

LIST OF TABLES ..... **XXI**

LIST OF ABBREVIATIONS ..... **XXIII**

KEY PUBLICATIONS ..... **XXIV**

1. INTRODUCTION **1**

1.1. BACKGROUND AND MOTIVATION 1

1.2. THESIS LAYOUT 7

2. LITERATURE REVIEW **9**

2.1. INTRODUCTION 9

2.2. MANGO FRUIT PRODUCTION, PROCESSING, AND WASTE GENERATION 9

2.3. THE BIOREFIERY CONCEPT 11

2.4. BIOREFINERY POTENTIAL OF MANGO SEED WASTE 11

2.5. THE MANGO SEED COMPOSITION AND POTENTIAL APPLICATIONS 12

2.5.1. Cellulose *14*

2.5.2. Nanocellulose *16*

2.5.3. Hemicellulose *18*

2.5.4. Lignin *21*

2.5.5. Other components of mango seed *24*

2.6. REPORTED STUDIES ON BIOPRODUCT EXPLOIT FROM MANGO SEED WASTE 25

2.7. FRACTIONATION OF LIGNOCELLULOSIC BIOMASS 28

2.8. LIGNOCELLULOSIC BIOMASS FRACTIONATION FOR THE RECOVERY OF CELLULOSE-RICH PULP FOR NANOCELLULOSE: THE CONVENTIONAL APPROACH 28

2.9. PRETREATMENT/FRACTIONATION OF LIGNOCELLULOSIC BIOMASS FOR THE RECOVERY OF MULTI-PRODUCTS 31

2.9.1. Polyphenol extraction *31*

2.9.2. Starch removal *35*

2.9.3. Hemicellulose extraction *36*
2.9.4. Lignin extraction *46*
2.10. COMBINATION OF PRETREATMENT METHODS FOR LIGNIN EXTRACTION 52
2.11. MULTI-STEP BIOREFINERY OF LIGNOCELLULOSIC BIOMASS 54
2.12. FRACTIONATION OF MANGO SEED INTO A CELLULOSE-RICH PULP AND VALUABLE BIOPRODUCTS: THE MULTI-STEP BIOREFINERY APPROACH 57
2.13. TREATMENT METHODS FOR NANOCELLULOSE PRODUCTION FROM CELLULOSE-RICH PULP 58
2.13.1. Chemical treatments *59*
2.13.2. Mechanical treatment processes for nanocellulose production *67*
2.14. HEMICELLULOSE-BASED BIOCOMPOSITE FILM DEVELOPMENT 69
2.15. METHODS FOR DEVELOPING HEMICELLULOSE-BASED BIOCOMPOSITE FILMS 70
2.16. RESEARCH AIMS AND OBJECTIVES 71
2.16.1. Aim *71*
2.16.2. Specific objectives *71*
2.17. SCIENTIFIC CONTRIBUTION 73

3. RESEARCH METHODOLOGY 76
3.1. INTRODUCTION 76
3.2. EXPERIMENTAL PROCEDURE 76
3.2.1. Feedstock selection and handling *76*
3.2.2. Biomass size-reduction *77*
3.3. MANGO SEED FRACTIONATION 77
3.3.1. Multi-step biorefinery route for fractionation of mango seed kernel *77*
3.3.2. Mango seed husk fractionation *82*
3.3.3. Cellulose nanocrystal production from cellulose-rich pulp obtained via a multi-step biorefinery process *84*
3.3.4. Hemicellulose-based biocomposite film development *88*
3.3.5. Characterization of bioproducts *88*

4. DEVELOPMENT OF A MULTI-STEP BIOREFINERY SCHEME FOR THE RECOVERY OF POLYPHENOLS, STARCH, AND BIOACTIVE HEMICELLULOSE FROM MANGO SEED KERNEL 90
4.1. DEVELOPMENT AND OPTIMIZATION OF A MULTI-STEP BIOREFINERY PROCESS FOR THE RECOVERY OF POLYPHENOLS, STARCH, AND BIOACTIVE HEMICELLULOSE FROM MANGO SEED KERNEL 92
4.2. ABSTRACT 92
4.3. INTRODUCTION 93
4.4. MATERIALS AND METHODS 95

4.4.1. Chemicals *95*
4.4.2. First extraction stage: organosolv extraction of polyphenols *95*
4.4.3. Second extraction stage: Enzymatic hydrolysis of starch from the organosolv extracted solid residue *96*
4.4.4. Third extraction stage: Alkaline extraction of bioactive hemicellulose from the destarched solids *96*
4.4.5. Optimization of polyphenol and bioactive hemicellulose extraction *96*
4.4.6. Characterization of kernel and products from the pretreatment processes *97*
4.5. RESULTS AND DISCUSSIONS 97
4.5.1. Optimization of organosolv extraction conditions for free polyphenols *97*
4.5.2. Optimization of alkaline bioactive hemicellulose extraction from the solid residue obtained after organosolv extraction and destarching *105*
4.5.3. Product recoveries from the multi-step biorefinery processes *114*
4.6. INFLUENCE OF THE TREATMENT STEPS IN THE MULTI-STEP BIOREFINERY 115
4.7. CONCLUSIONS 118

5. DEVELOPMENT OF A MULTI-STEP BIOREFINERY SCHEME FOR THE RECOVERY OF HEMICELLULOSE, LIGNIN, AND CELLULOSE-RICH FIBERS FOR NANOCELLULOSE PRODUCTION FROM MANGO SEED HUSK 119

5.1. TAILOR-MADE CONVERSION OF MANGO SEED HUSKS TO OBTAIN HEMICELLULOSE SUITABLE FOR THE PRODUCTION OF THERMALLY STABLE FILM 121
5.2. ABSTRACT 121
5.3. INTRODUCTION 122
5.4. MATERIALS AND METHODS 125
5.4.1. Materials *125*
5.4.2. Feedstock preparation and analysis *125*
5.5. HEMICELLULOSE EXTRACTION 127
5.6. OPTIMIZATION OF EXTRACTION CONDITIONS 127
5.7. HEMICELLULOSE SUGAR COMPOSITION ANALYSIS 128
5.7.1. Determination of neutral sugars *128*
5.7.2. Determination of uronic acids *129*
5.8. PREPARATION OF BIOCOMPOSITE FILMS 129
5.9. STRUCTURAL CHARACTERIZATION OF FEEDSTOCK, HEMICELLULOSE, SOLID RESIDUES, AND BIOCOMPOSITE FILMS 130
5.10. RESULTS AND DISCUSSIONS 132
5.10.1. Composition of untreated and alkali-treated mango seed husks *132*
5.10.2. Yield and composition of mango seed husk hemicellulose *134*

5.10.3. Effects of extraction conditions on yield and composition of mango seed husk hemicelluloses *136*
5.11. OPTIMAL CONDITIONS FOR EXTRACTING HEMICELLULOSE SUITABLE FOR SELF-FORMING FILMS FROM MANGO SEED HUSKS 140
5.12. SUITABILITY OF HEMICELLULOSE FOR SELF-SUPPORTING FILM FORMATION 141
5.13. CONCLUSION 148
5.14. OPTIMIZATION OF LIGNIN EXTRACTION FROM ALKALINE TREATED MANGO SEED HUSK BY HIGH SHEAR HOMOGENIZATION-ASSISTED ORGANOSOLV PROCESS USING RESPONSE SURFACE METHODOLOGY 150
5.15. ABSTRACT 150
5.16. INTRODUCTION 151
5.17. MATERIALS AND METHODS 153
5.17.1. Materials and sample preparation *153*
5.17.2. Mango seed husk delignification *153*
5.17.3. Experimental design and statistical analysis *154*
5.17.4. Regression analysis and optimization *155*
5.17.5. Characterization of starting material, hydrolysate, recovered lignin, and solid residue *155*
5.18. RESULTS AND DISCUSSIONS 156
5.18.1. Yields and compositions of solubilized lignin and solid residue after homogenization-assisted organosolv pretreatment/fractionation process *156*
5.18.2. Optimization of high shear homogenization-assisted organosolv process conditions for isolating pure lignin fraction from alkaline treated mango seed husk *159*
5.18.3. Optimal conditions for lignin extraction of alkaline treated mango seed husk *166*
5.18.4. Structural features of extracted lignin at optimum homogenization-assisted and non-assisted organosolv processes *167*
5.18.5. Elemental composition of lignin samples *170*
5.18.6. Molecular weight and molecular weight distributions of lignin samples *171*
5.18.7. Thermal stabilities of lignin samples *171*
5.18.8. Scanning electron microscopy analysis for the morphology of solid residue *172*
5.19. CONCLUSIONS 173
6. EFFECT OF THE MULTI-STEP BIOREFINERY PROCESS ON THE YIELD AND PROPERTIES OF CELLULOSE NANOCRYSTALS PRODUCED VIA RECOVERABLE ORGANIC ACID TREATMENTS 174
6.1. OPTIMIZING NON-CATALYZED FORMIC ACID HYDROLYSIS OF UNBLEACHED PRETREATED MANGO SEED HUSK PULP TO GENERATE CELLULOSE NANOPARTICLES WITH IMPROVED MORPHOLOGY AND THERMAL STABILITY 176

6.2. ABSTRACT 176
6.3. INTRODUCTION 177
6.4. MATERIALS AND METHODS 180
6.4.1. Materials 180
6.4.2. Preparation of cellulose nanoparticles from unbleached cellulose-rich material from mango seed husk 180
6.4.3. Experimental design and statistical analysis 181
6.4.4. Characterization of starting material and cellulose nanocrystals 181
6.5. RESULTS AND DISCUSSIONS 183
6.5.1. Preparation and functionalization of cellulose nanoparticles from unbleached organosolv-treated mango seed husk using non-catalyzed formic acid hydrolysis 183
6.5.2. Optimization of reaction time and acid-to-pulp ratio for cellulose nanocrystal preparation and building of regression models 185
6.5.3. Verification of optimal formic acid treatment conditions for cellulose nanocrystal preparation 192
6.5.4. Characterization of pulp and cellulose nanoparticles (at optimum conditions) 193
6.6. CONCLUSIONS 200
6.7. SIMULTANEOUS PREPARATION AND ACETYLATION OF CELLULOSE NANOCRYSTALS FROM A CELLULOSE-RICH PULP OBTAINED VIA A MULTI-STEP BIOREFINERY ROUTE USING A NON-CATALYZED ACETIC ACID-BASED TREATMENT 201
6.8. INTRODUCTION 202
6.9. EXPERIMENTAL 205
6.9.1. Materials 205
6.9.2. Acetic acid treatment of unbleached organosolv-treated mango seed husk to produce nanocellulose 205
6.9.3. Homogenization of acetic acid produced nanocellulose 206
6.9.4. Experimental design and statistical analysis 206
6.9.5. Characterization of starting material and cellulose nanoparticles 206
6.9.6. Degree of substitution of nanocellulose 206
6.10. RESULTS AND DISCUSSION 207
6.10.1. Yield and properties of acetic acid produced cellulose nanoparticles from the two-stage alkaline and organosolv treated pulp 207
6.10.2. Effect of solid-to-acid ratio and reaction time on the yield and properties of acetic acid hydrolyzed nanocellulose 209
6.10.3. Morphology and size distribution analysis 211
6.10.4. Structural analysis of starting material and cellulose nanoparticles 214

6.10.5. Crystallinity analysis of starting material and cellulose nanoparticles using X-ray diffraction *215*

6.10.6. Thermal stability of starting material and cellulose nanocrystals *217*

6.11. CONCLUSIONS 220

7. GENERAL DISCUSSIONS, CONCLUSIONS, AND RECOMMENDATIONS 221

7.1. SUMMARY OF STUDY OUTCOMES AND IMPLICATIONS 221

7.1.1. Multi-step biorefinery route for mango seed kernel fractionation *221*

7.1.2. Multi-step biorefinery process for fractionating mango seed husk *225*

7.2. NANOCELLULOSE PRODUCTION 232

7.2.1. The formic acid-based treatment process for cellulose nanoparticles production *232*

7.2.2. Acetic acid-based treatment for nanocellulose production from cellulose-rich fibers obtained via a multi-step biorefinery process *234*

7.3. CONCLUSIONS 236

7.4. RECOMMENDATIONS 238

REFERENCES 239

APPENDIX 289

List of Figures

Figure 2.1: Chemical structure of cellulose (Redrawn from Harmsen et al. [96].....15
Figure 2.2: Physical and chemical structure of hemicellulose (Redrawn from Lee et al. [145]) 20
Figure 2.3: Monolignols of lignin (Redrawn from Lee et al. [145]).....22
Figure 2.4: Biorefining of lignocellulosic biomass based on organosolv fractionating pretreatment (Redrawn from Zhao et al., [310]). *OFP- Organosolv fractionating pretreatment 48
Figure 3.1: Integrated multi-step biorefinery route for multi-product generation from mango seed 78
Figure 4.1: Pareto and response surface plots of the effect of ethanol concentration and temperature on the total polyphenol content, scavenging activity, and recovered solids.....101
Figure 4.2: Pareto and response surface plots of the effect of ethanol concentration and temperature on the cellulose, hemicellulose, lignin, and starch content of solid residue 103
Figure 4.3: Pareto chat for (a) hemicellulose yield (b) lignin content of extract (c) total phenolic content of extract (d) antioxidant activity of extract (e) cellulose content of recovered solids (f) hemicellulose content of recovered solids and (g) lignin content of recovered solids. 108
Figure 4.4: Response surface plots of (a–b) hemicellulose yield (c–d) lignin content of hemicellulose extract (e–f) total phenolic content of extract (g–h) antioxidant activity of extract 110
Figure 4.5: Response surface plots of (a–b) cellulose content of recovered solids (c–d) hemicellulose content of recovered solids (e–f) lignin content of recovered solids.....112
Figure 4.6: Component recovery from mango seed kernel fractionation via multi-step organosolv extraction, enzymatic hydrolysis, and alkaline pretreatment under the optimal organosolv extraction (64.99% ethanol, 54.18 °C) and alkaline pretreatment (1.07 M NaOH, 44 °C, 2.16 h) process conditions 115
Figure 4.7: FTIR spectra of untreated and pretreated solids after the multi-step biorefinery of mango seed kernel.....116
Figure 4.8: Scanning electron microscopy of (a) untreated mango seed kernel, (b) organosolve extracted residue (c) destarched residue and (d) alkaline extracted residue 117
Figure 5.1: Fourier Transform Infra-red spectroscopy (FTIR) spectra showing functional groups in (a) alkaline extracted hemicellulose (b) commercial beechwood xylan (c) commercial

tamarind seed xyloglucan (d) alkaline treated mango seed husk and (e) untreated mango seed husk, and (f) CP/MAS solid-state spectra of mango seed husk hemicellulose.....133
Figure 5.2: Effects of NaOH concentration, temperature, and reaction time on (a) hemicellulose yield, (b) xyloglucan/xylan ratio, (c) lignin, and (d) uronic acid contents of hemicellulose extract with interactions between (i) temperature and NaOH concentration, (ii) extraction time and NaOH concentration and (iii) extraction time and temperature.....139
Figure 5.3: Significance and sizes of effects of NaOH concentration, temperature, and reaction time on the (a) yield, (b) xyloglucan/xylan ratio (c) lignin, and (d) uronic acid contents of hemicellulose extract extracted from mango seed husks.....140
Figure 5.4: Biocomposite films prepared using (a) (i) Mango seed husk hemicellulose (MHH) with xyloglucan (XGN) and xylan (XLN) ratio of 0.13 obtained with mixtures of commercial XGN (CXGN) and XLN (CXLN) and in ratios of 0.29, (iii) 0.47 and (iv) 0.13, (b) Fourier Transform infrared spectra (FTIR) for the films i– iv prepared using CXGN/CXLN ratios of. 0.29, 0.47, 0.13 and MHH with XGN/XLN = 0.13. 143
Figure 5.5: Thermal degradation and derivative thermal degradation thermographs of **a**. Mango seed husk hemicelluloses (MHH) at optimum extraction conditions, **b**. Commercial xylan (CXLN), **c**. Commercial xyloglucan (CXGN), **d.** CXGN/CXLN (0.29), **e.** CXGN/CXLN (0.47), **f.** CXGN/CXLN (0.13), **g.** MHH with XGN/XLN (0.29), **f.** MHH XGN/XLN (0.47), and **i.** MHH XGN/XLN (0.13).....144
Figure 5.6: Thermal degradation and derivative thermal degradation thermographs of **a**. Mango seed husks hemicellulose (MHH) film at optimum extraction conditions, **b**. Commercial xylan (CXLN) film, **c**. Commercial xyloglucan (CXGN) film, **d.** CXGN/CXLN (0.29) film, **e.** CXGN/CXLN (0.47) film, **f.** CXGN/CXLN (0.13) film, **g.** MHH with XGN/XLN (0.29) film, **f.** MHH XGN/XLN (0.47) film, and **i.** MHH XGN/XLN (0.13) film.....145
Figure 5.7: Mechanical properties of mango seed husk hemicellulose films with varying percentages (0 – 40%) of plasticizer.....148
Figure 5.8: Pareto charts showing the significance of the effects of ethanol concentration, temperature, and homogenizing time on (a) solubilized lignin, (b) recovered lignin, and (c) lignin purity, (d) cellulose, (e) lignin, and (f) hemicellulose contents of solid residue. 160
Figure 5.9: Response surface plots showing the effect of ethanol concentration, temperature, and homogenization time on (a) solubilized lignin (b) recovered lignin (c) and lignin purity. 161

Figure 5.10: Response surface plots showing the effect of ethanol concentration, temperature, and homogenization time on (a) cellulose, (b) lignin, and (c) hemicellulose contents of solid residue. 165
Figure 5.11: Fourier transform infrared and nuclear magnetic resonance spectra of organosolv lignin obtained under optimum high shear homogenization-assisted organosolv process (COL) and non-assisted organosolv process (REL). 169
Figure 5.12: Thermogravimetric (TG) and derivative thermogravimetric (DTG) curves of optimum high shear homogenization-assisted organosolv lignin (COL) and non-assisted organosolv lignin (REL). 172
Figure 5.13: Scanning electron microscopy (SEM) images of residues obtained at different magnifications after high-shear homogenization-organosolv process under optimal conditions (a and b) and non-assisted ethanol organosolv (c and d). 173
Figure 6.1: Pareto charts and Response surface showing the effect of acid-to-pulp ratio and reaction time on (a, b) cellulose nanoparticle yield, (c, d) average particle size, and (e, f) ζ-potential 187
Figure 6.2: Pareto charts and Response surface showing the effect of acid-to-pulp ratio and treatment time on the (a, b) polydispersity index, (c, d) crystallinity, and (e, f) formate content of formic acid nanocellulose 189
Figure 6.3: Scanning Electron Microscopy images of (a) unbleached organosolv treated pulp (b) bleached pulp (c) formic acid cellulose nanocrystals, (d**)** sulphuric acid cellulose nanocrystals, and Scanning Transmission Electron microscopy of (**e)** formic acid cellulose nanoparticles and (**f)** sulphuric acid cellulose nanocrystals 195
Figure 6.4: (a) Fourier Transform Infrared spectra and (b) x-ray diffractograms of unbleached organosolv treated mango seed husk, bleached pulp, formic acid cellulose nanoparticles, and sulphuric acid cellulose nanoparticles 197
Figure 6.5: Scanning electron microscopy images of (a) unbleached organosolv treated mango seed husk pulp (b) bleached mango seed husk (c) acetic acid cellulose nanocellulose, (d) homogenized acetic acid nanocellulose (e) sulfuric acid cellulose nanocellulose 212
Figure 6.6: Particle distribution analysis of (a) acetic acid cellulose nanoparticles (b) homogenized acetic acid cellulose nanocellulose analyzed using images from scanning electron microscopy 213
Figure 6.7: FTIR analysis of unbleached pretreated mango seed husk, bleached treated mango seed husk, acetic acid nanocellulose, homogenized acetic acid nanocellulose, and sulfuric acid nanocellulose 215

Figure 6.8: X-ray diffractograms of unbleached organosolv-treated mango seed husk, bleached mango seed husk, acetic acid nanocellulose, homogenized acetic acid nanocellulose, and sulfuric acid nanocellulose.....217
Figure 6.9: Thermogravimetric analysis of organosolv treated mango husk, bleached pulp, acetic acid cellulose nanocellulose, homogenized acetic acid cellulose nanocellulose, and sulfuric acid cellulose nanocellulose. 219

List of Tables

Table 2.1: Worlds ten major mango producing countries for selected years since 2000 (metric tons: [110])....10
Table 2.2: Different components of mango fruit....11
Table 2.3: Composition (dry weight) of mango waste versus other agricultural waste that has been exploited as feedstock in bioproducts production. 13
Table 2.4: Structural and chemical composition of hemicellulose, cellulose, and lignin in lignocelluloses [142]. 15
Table 2.5: Predominant linkages in lignin (Adapted from Santos et. al. [208]) 22
Table 2.6: Summary of reported studies on bioproduct from mango seed waste....27
Table 2.7: The comparison of chemical pre-treatment methods (Adapted from Makheta 2016) 29
Table 2.8: Extraction of polyphenols from mango seed kernel and other agro-waste 34
Table 2.9: Hemicellulose extraction from various hardwood....41
Table 2.10: Hemicellulose extraction from various agro-industrial waste 44
Table 2.11: Lignin extraction from various lignocellulosic biomass 50
Table 2.12: Nanocellulose production from various feedstocks....60
Table 3.1: Selected products, treatment processes, and justification....86
Table 3.2: Characterization of the bioproducts....89
Table 4.1: Total polyphenol content and, scavenging activity of extracts and composition of recovered solids 99
Table 4.2: Verification of predicted optimal conditions....105
Table 4.3: Centarl composite experimental design of independent variables and corresponding responses (independent variables) for hemicellulose extraction. 107
Table 4.4: Predicted and experimental values of the responses at optimum conditions for hemicellulose extraction 114
Table 5.1: Composition of untreated and alkaline treated mango seed husk....132
Table 5.2: Yield and composition of hemicellulose extracted from mango seed husk under varying extraction conditions....134
Table 5.3: *O*-methyl ether derivatives obtained from permethylation of mango seed husk hemicellulose extract 136
Table 5.4: Hemicellulose yield and composition at optimized extraction conditions 141

Table 5.5: Molecular weight, polydispersity and zeta potential of mango seed husk and commercial hemicelluloses 142
Table 5.6: Maximum degradation temperatures (T_{max}) of MHH, different XGN/XLN ratios, and their corresponding biocomposite films 146
Table 5.7: Effect of high shear homogenization-organosolv process conditions on lignin yields, purity, solid recovery and composition, sugar, and ash contents of recovered lignin 157
Table 5.8: Predicted and observed values of responses for optimum high shear homogenization-assisted organosolv process conditions 167
Table 5.9: Elemental composition, weighted average, number average and polydispersity of organosolv lignin samples 171
Table 6.1: Yield and properties of formic acid prepared cellulose nanoparticles from unbleached organosolv-treated mango seed husk 183
Table 6.2: Analysis of variance for formic acid nanocellulose yield, average particle size, ζ-potential, polydispersity index, crystallinity, and formate content regression models 186
Table 6.3: Predicted versus observed values of formic acid nanocellulose at optimum conditions and commercial cellulose nanocrystals 192
Table 6.4: Effect of reaction time and solid-to-acid ratio on the properties of acetic acid nanocellulose from organosolv pulp 208
Table 6.5: Analysis of variance (p-values) for yield, average particle size, degree of substitution, zeta-potential, and polydispersity of acetic acid produced cellulose nanocrystals 209
Table 7.1: Composition of untreated mango seed husk and kernel 221
Table 7.2: Recovered bioproduct yields and properties 227
Table 7.3: Mass balance for fractionation of mango seed kernel 231
Table 7.4: Mass balance for fractionation of mango seed husk 232
Table 7.5: Reaction conditions for nanocellulose production 235

List of Abbreviations

1-G First generation
2-G Second generation
AA Antioxidant activity
ADF Acid detergent fiber
ADL Acid detergent lignin
AP Alkaline pretreatment
ASL Acid soluble lignin
ATR Attenuated Total Reflectance
BHA Butylated hydroxy anisole
BHT Butylated hydroxytoluene
BP Bleached pulp
CCD Central Composite Design
CNF Cellulose nanofibril
CNP Cellulose nanocrystals
CNP Cellulose nanoparticle
CrI Crystallinity Index
CXGN Commercial Xyloglucan
DP Degree of polymerization
DS Degree of substitution
DSROP Destarched organosolv treated solids
FCNP Spherical formic acid cellulose nanoparticles
FTIR Fourier Transform Infra-Red Spectroscopy
GX Glucuronoxylan
HPH High-Pressure Homogenizer
HPLC High-Performance Liquid Chromatography
HSCN Homogenization assisted acetic acid-based nanocellulose
HSH High shear homogenization
HSH High Shear Homogenizer
HSHO High Shear homogenization organosolv pretreatment
LCC Lignin Carbohydrate Complex
LCF Lignocellulosic Feedstock
MHH Mango husk hemicellulose
MKH Mango kernel hemicellulose
MS Mass spectroscopy
MSH Mango seed husk
MSK Mango seed kernel
NAAH Non-catalyzed acetic acid hydrolysis
NDF Neutral detergent fiber
NFAH Non-catalyzed formic acid hydrolysis
NFAH Non-catalyzed formic acid-based hydrolysis
NMR Nuclear Magnetic Resonance Spectroscopy
NREL-TP National Renewable Energy Laboratory
OP Organosolv pretreatment
PDI Polydispersity index
RSM Response Surface Methodology
SAH Sulphuric acid-based hydrolysis
SCNP Sulphuric acid cellulose nanoparticles
SEC Size Exclusion Chromatography
SEC Size Exclusion Chromatography
SEM Scanning Electron Microscope
SROP Solid residue after organosolv pretreatment
TEMPO 2,2,6,6-tetramethyl piperidinyl-1-oxyl
TGA Thermogravimetric Analysis
TPC Total polyphenol content
UMH Unbleached mango seed husk
UMP Unbleached organosolv treated husk
XLN Xylan
XRD X-ray Diffraction

Key publications

Journal Papers

1. **Bello, F.,** Chimphango, A., 2021. Optimization of lignin extraction from alkaline treated mango seed husk by high shear homogenization-assisted organosolv process using response surface methodology. Int. J. Biol. Macromol. 167, 1379–1392 (Published online).
2. **Bello, F.,** Chimphango, A., 2021. Tailor-made conversion of mango seed husks to obtain hemicellulose suitable for the production of thermally stable films. Waste and Biomass Valorization. 1, p. 3 (Published online).

Conference presentation

Bello F. and Chimphango, A., 2019 Mango Waste Biorefinery: Extraction of Hemicellulose from Mango Seed. Presented at the 7th International Conference on Biorefinery (ICB2019), Johannesburg, South Africa. Program available at http://ddl.escience.cn/f/TgAw.

1. Introduction

1.1. Background and motivation

The diminishing fossil fuel reserves coupled with the detrimental effects of fossil-based products on the environment are steering global research trends towards the development of bioproducts from renewable feedstocks. Natural sources that include crops such as corn, sugarcane, etc. termed first-generation feedstock (1G), and lignocellulosic biomass such as agro-processing waste (e.g. sugarcane bagasse, mango seed & peels) termed second-generation feedstock (2G) [1], [2] are targeted due to their rich composition for valuable bioproducts. However, 2G feedstocks are economically and environmentally viable alternatives to both the fossil resources and the 1G feedstock [3], attributable to the associated low acquisition cost, renewability, abundance, and non-competing use with food either directly on a consumption basis as applicable to 1G or indirectly through land use as with fossil resources [4], [5]. In South Africa, approximately 26 million tons of 2G biomass (forest waste, invasive plants, and agricultural waste) are generated annually [6], providing an opportunity to contribute towards fulfilling the demand of the bioproducts for a sustainable bioeconomy. To this end, the mango processing industries present opportunities for bioproduct generation from the waste generated during mango fruit processing [7].

On a global scale, approximately 14.7 to 25.2 million tons of mango seed and peel are generated annually from the industrial processing of ripe mango fruits of which the mango seed forms >1 million tons [8], [9]. The mango seed, which constitutes 35–55% of the mango fruit [10], is partly used in the formulation of animal feed or largely disposed of via landfills with no commercial usage [11], [12]. Hence, it is mostly regarded as waste. However, the valuable components of the mango seed waste could be exploited for more beneficial bioproducts [13], [14]. The mango seed waste is composed of an outermost layer (i.e. husk – comprising mainly cellulose, hemicellulose, and lignin) and an inner stone called kernel [10], [15]. The composition of the kernel is lignin, starch, fatty acids, proteins, polyphenols, hemicellulose, and cellulose [16], [17]. Several bioproduct exploitation studies on the mango seed kernel have focused on free extractable polyphenols, starch, fat, oil, and protein as single products with little attention given to the lignocellulosic components i.e. hemicellulose, cellulose (for nanocellulose), and lignin in a biorefinery [16], [18]. Similar to the kernel, mango seed husk utilization as a biorefinery feedstock has received little attention despite an appreciable composition of lignin (9.0–21.0%), hemicellulose (15.6–52.4%), and cellulose (39.5–55%) [15], [19], [20]. The few research on bioproduct attempts from the husk focused on single

product schemes either for nanocellulose, bioethanol, or activated carbon production [19]–[22]. However, the implementation of biorefineries could be considered a possible approach to recover most/all of the valuable bioproducts from the mango seed waste for both economic and environmental gains [23].

Nanocellulose is one of the most sought after bioproducts for several applications like fillers in biocomposites for food packaging [24]–[26] due to its unique properties such as high specific surface area, low polydispersity, nanoscale dimension, high thermal stability, high modulus of elasticity, crystallinity and biodegradability [27], [28]. Owing to its superior properties compared to macromolecular cellulose, the market demand for nanocellulose has been projected to increase from the estimated global market value of $297 million to $783 million by 2023 [(i.e. compound annual growth rate (CAGR) of 21.3%)] [29]. Consequently, industries such as CelluForce Inc. of Canada, and Paperlogic of the United Sates have embarked on the commercial production of plant-based cellulose nanocrystals (CNC) and cellulose nanofibrils (CNF) [30], [31].

Presently, commercial CNC production is based on the use of woody biomass due to its fibrous nature, however wood is in high demand for other applications such as paper making and construction [32]. Related studies have shown advantages of using the 2G-agro-industrial waste for CNC vs woody biomass, including the lower lignin contents of the former that makes them easier to fibrillate mechanically, and thus, lesser energy requirement [33]–[35]. CNC production requires cellulose-rich material (cellulose purity >65%) with high crystallinity (>55%) such as microcrystalline cellulose (MCC), which is one of the products that can be obtained by fractionation of agro-waste for example mango seed husk, resulting in the removal of the amorphous components (hemicellulose, lignin, and polyphenols) of the biomass [36]–[38]. In relation to the agro-industrial waste (e.g., mango seed), the conventional approach to obtain the cellulose-rich material involves pretreatment schemes targeted at selective recovery of the cellulose material from the biomass [20], [39]–[41], resulting in the usage of the other components (e.g. hemicellulose, lignin, and polyphenols) as low-value products or their degradation and loss during downstream processing [20], [39]–[41] and thus, the inefficient utilization of the bioresource potential. However, the hemicellulose, starch, polyphenols, lignin, and nanocellulose with diverse properties could be recovered from the mango seed for various applications (e.g. in biocomposite films, resins, as antioxidants, etc.) if appropriate pretreatment/fractionation processes are selected and integrated into the right sequence to develop multi-step biorefinery schemes, that could potentially improve revenue generation from mango processing [14], [42], [43].

Generally, hemicellulose polymers (xylan is mostly preferred due to the formation of transparent films) are well known for biocomposite film development for food packaging with good oxygen and gas barrier properties [42]. The composition of hemicellulose (xylan and xyloglucan) in the mango seed [44], [45] presents an opportunity for the extraction of hemicellulose with diversified properties for varied applications such as barrier films, active packaging films, and coatings [43], [46]. Extracted polyphenols could serve as antioxidants in both food and non-food applications [13], [47]. The starch could be used in biofuel production or composite development [45], [48]. The derived lignin, with its numerous phenolic groups, could be used as antioxidants in various applications or the preparation of phenol-formaldehyde resins [43], [49], [50]. Lastly, the recovered cellulose component could be used for CNC production for application as a reinforcement agent, and fillers in biocomposites [40], [43], [51]. Therefore, more efficient exploitation of the mango seed could consider the preservation and extraction of the polyphenols, starch, hemicellulose, lignin, and cellulose (for CNC production) to deliver multi-products rather than a single-product stream. Success in this regard would provide a robust alternative to incorporate waste-based biorefineries into mango fruit processing thereby expanding the product range to include both food and non-food bioproducts. Moreover, the recovery of multi-products from a single feedstock could contribute to the economic robustness of mango processing industries by protecting against unpredictable market demands and single product value [23].

In targeting recoveries of all the referred bioproducts from the mango seed, due to the heterogeneous nature and the specificity of optimal extraction conditions (e.g. temperature, chemicals, and mechanical treatment) for each component, a drawback of low yields and/or cross-contamination (i.e. low-quality) of the various bioproducts could be encountered [52]. For instance, the substantial amount of starch component in the mango seed kernel (≈ 32–65%) [53]–[55] could impede the solid-liquid separation during the fractionation processes by increasing the viscosity of the extraction medium and thereby limiting the bioproducts extraction potential [56]. Likewise, polyphenols (both free and bound) are interconnected with proteins, leading to the formation of insoluble polyphenol-protein complexes that hinder starch extraction [57], [58]. Furthermore, lignin acts as a glue and protects hemicellulose, cellulose, and other biomass components from chemical and enzymatic attack, whereas lignin carbohydrate complexes limit the selective extraction of lignin and hemicellulose, therefore requiring the selection of appropriate pretreatment/fractionation methods to aid in the recovery of the referred bioproducts of interest [59].

Pretreatment of lignocellulosic biomass for the recovery of bioproducts has been well established in the literature [14], [60], [61], with ongoing research aimed to mitigate production costs (e.g. increase product yields and reduce process energy demands) [14], [62]. In general, the majority of the previously considered pretreatment methods applied in CNC production aimed at high crystalline cellulose-rich material generation. The conventional Kraft and bleaching pretreatment processes for the targeted cellulose-rich material result in degradation of the hemicellulose, lignin, and other valuable components, which are subsequently used as low-value fuel to fire boilers [20], [39]–[41]. Other considered pretreatment methods include alkaline, enzymatic, steam explosion, organosolv, dilute acid, and ionic liquid where the choice selection is based on feedstock source, the desired product properties, and end-use of the resultant bioproducts [14], [49], [63], [64]. Additionally, the pretreatment options cause different degrees of structural modifications and come with varying costs [5], [65] hence calls for optimized process conditions that could support economic benefits for target applications [66]. Different pretreatment/fractionation methods and optimal extraction conditions are required for the recovery of the various bioproducts from the mango seed husk and kernel [64], [67]–[69].

Generally, polyphenols, starch, and hemicellulose are thermo-chemically liable to degradation and are thus extracted under less severe conditions (low temperatures, concentrations of chemicals, and shorter reactions times) [47], [70]–[72]. On the other hand, high severities are required to remove lignin and improve the accessibility of enzymes and chemicals to cellulose for conversion into CNC [73]. Therefore, the initial stage of the multi-step biorefinery scheme could consider lower severities to target the more thermo-chemically labile components of polyphenols, starch, and hemicellulose [74], [75]. The latter stage could then employ medium to severe conditions to pretreat the remaining solid residue for lignin and cellulose recovery [73], [76]. It is noteworthy that starch is often extracted from biomass with alkali, water, or enzymes [69], [77], [78]. The water extraction method results in low yields (≈32–59%) [48], [79], [80] while the alkali method could result in hemicellulose and lignin co-extraction thereby lowering their yield recoveries and quality (e.g., purity) in the subsequent stages of the multi-step biorefinery process. Such adverse effects are undesirable for the proposed multi-step biorefinery scheme. Conversely, enzymes are substrate specific [81], thus could mitigate the degradation potential for the other biomass components when applied as the starch extraction agent [82]. In addition, enzymes can remove up to 100% starch from biomass [69] and therefore a more suitable method than acidic, alkaline and water extraction to obtain the starch from the mango seed waste.

Alkaline and organosolv pretreatment/fractionation processes have been effectively employed to fractionate components of agro-industrial biomass waste albeit at different extraction conditions [83]–[85]. Alkaline pretreatment (AP) that employs reagents such as calcium, sodium, and potassium hydroxides are favored due to their effective extraction of hemicellulose polymers at lower severities that could minimize lignin cross-contamination [56]. Considering that the extraction of lignin increases with AP severity [42], [43], [86], application of mild reaction conditions could result in hemicellulose polymers with minimal lignin contamination for potential application in biocomposite film for food packaging while still ensuring high cellulose and lignin contents in the residual solids for further fractionation in the next stage of the multi-step biorefinery process [56]. Conversely, organosolv pretreatment (OP) uses organic solvents or their aqueous mixtures to fragment and separate mostly lignin from the biomass. The OP process operates at temperatures above 185 ºC without catalyst or below 185 ºC with a catalyst (acid or base), to separate lignin and reduce biomass recalcitrance [87], [88]. Some of the organic solvents used for lignin extraction are lower molecular weight (M_w) alcohols (ethanol and methanol), and high M_w polyols (ethylene glycol, glycerol, and xylitol) [5], [89]. The lignin obtained from the OP process has different properties from other technical lignin as they have relatively higher purity, lower M_w, and narrow M_w distributions [90].

However, the referred OP processes for lignin extraction result in lignin condensation reactions [due to severe extraction conditions (>180 ºC) and the use of acid catalysts] that negatively affect the M*w*, polydispersity (PDI), and reactivity (number of aliphatic and phenolic hydroxyl groups) of the lignin. In addition, the yield of the hemicellulose and cellulose is reduced due to their conversion into sugars and subsequent degradation into furfural and 5-hydroxymethylfurfural respectively in the presence of acid catalyst [59], [91]. As a result, treatment techniques such as steam explosion, ultrasonication, and high-pressure homogenization, which increases the feedstock surface area and contact with the OP solvent, could be coupled with less severe OP process conditions (e.g. <150 ºC) for efficient less modified lignin extraction and carbohydrate preservation [14], [68], [92], [93]. In this regard, the integration of a rotor-stator high shear homogenization with ethanol OP process (HSHO) to improve lignin dissolution and quality (purity, PDI, M*w*, etc.) was considered in this study due to its advantages of low pressure and mechanical effect and thus improved surface area for extraction versus the other mechanical/physical techniques [94] [95].

Hence, concerning the mango seed husk (MSH), since lignin recovery requires harsher OP conditions that degrade the hemicellulose into simple sugars instead of the desired polymers

[96], a multi-step biorefinery scheme involving first an AP followed by a second stage of HSHO could be strategic for the selective extraction of the hemicellulose polymers and lignin, and recover cellulose respectively, while aiming for high cellulose retention in the solids for CNC production. On the other hand, for the kernel, due to co-extraction of polyphenols at the starch and hemicellulose extraction conditions, a potential multi-step process involving first an organosolv extraction (OE), followed by enzymatic hydrolysis (EH) and then AP could facilitate the extraction of the polyphenols, starch, and hemicellulose, respectively while maximizing the retention of cellulose and lignin in the solid residue. However, the referred treatment process and sequence in the multi-step biorefinery schemes will impact the biomass structure and performances of the subsequent stages, including the requirements for energy, process severity, and product recovery and quality (i.e. purity, crystallinity, etc.) [76], which calls for optimization of the process stages that will ensure optimal product recoveries while safeguarding the components of the solid residues for subsequent recoveries.

With regard to the CNC production, due to limitations of the conventional sulphuric acid-based process, including concerns of the high toxicity of acid, the requirement of corrosive-resistant equipment, and the low thermal stability of the CNCs vs the thermal stability of starting bleached cellulose-rich pulp [97], [98], alternative production approaches that involve the use of organic acids (e.g. Formic, maleic, acetic acids) treatments have been investigated and found to be promising regarding low toxicity, less corrosiveness, and ease of recovery through simple distillation [42], [91], as well as producing CNCs with high thermal stabilities (355–360 ºC) [89], [91]. However, the relatively weak acidity of such organic acids vs the conventional sulphuric acid limits their CNCs production potentials particularly for highly crystalline cellulose-rich pulp with strong hydrogen bonding [42]. Nonetheless, mineral acids or metal catalysts have shown potentials for improving the hydrolytic effect of the organic acids when incorporated into the organic acid processes as catalysts [42], [89], [403]. However, in the proposed multi-step biorefinery scheme, the synergistic effects of the preceding pretreatments of the biomass (to recover hemicellulose and high purity lignin respectively) could yield cellulose-rich pulp with improved fiber accessibility [182], which could be amenable to organic acid (e.g., formic and acetic acids) treatment for the CNC production without the need for incorporating the referred catalysts. Thus, towards a more sustainable CNC production process scheme, this study tested the impact of the multi-step biorefinery process on the production of CNCs using the recoverable organic acids without external mineral acid or catalysts from the mango seed.

Some advantages of the multi-step biorefinery approach for lignocellulosic biomass include recovery of much purer bioproducts due to limited interference and reduction in the formation of product inhibitors such as furfural and 5-hydroxymethylfurfural from hemicellulose and cellulose respectively [23], [99]. Several authors [100]–[102] have reported on the use of multi-step biorefinery schemes to obtain various products from lignocellulosic biomass. Most of the multi-step processes employed in the literature significantly improved the yields of hemicellulose and cellulose sugars with lower requirements of enzymes for bioethanol production compared to the single-stage processes [59], [73], [76]. However, little has been reported in the literature regarding multi-step biorefinery schemes for mango seed kernel and husk involving the proposed sequential three-stage (organosolv, enzymatic and alkaline) and two-stage (alkaline and homogenization-assisted ethanol organosolv) biorefinery schemes respectively as well as the potential impacts of each pretreatment step on bioproducts in the multi-step process. In addition, the use of cellulose-rich pulp obtained after the multi-step biorefinery process for CNC production using mild recoverable organic acid treatments as alternative nanocellulose treatment methods to sulphuric acid-based process has not been reported.

Overall, cellulose-rich fibers, high purity less modified lignin, hemicellulose polymers (different hemicellulose polysaccharides), starch, bioactive hemicellulose, and high activity polyphenols could be recovered from the mango seed via the combination of carefully designed pretreatment/fractionation processes in an integrated multi-step biorefinery scheme with further conversion of the cellulose-rich solids into CNCs via sustainable non-catalyzed recoverable organic acid treatments. Therefore, this study explored an integrated multi-step biorefinery for the holistic fractionation of the mango seed waste with an overall objective of developing optimal multi-step biorefinery that can effectively fractionate the mango seed biomass complex into the targeted multiple products in good yields and qualities, while preserving the cellulose-rich residue for nanocellulose production.

1.2. Thesis layout

This dissertation consists of seven Chapters. Chapter 1 focuses on the background and motivation. In Chapter 2, which is the literature review, detailed background on production trends of mango and its waste generation, the typical compositions of mango seed as lignocellulosic biomass for multi-product generation in a multi-step biorefinery are provided. Identified pretreatment/fractionation process steps and sequence for the fractionation of potential products and their recovery routes from mango seed before nanocellulose production are reviewed. This Chapter further provides evidence suggesting the insufficient information

in literature with regards to the full valorization of mango seed in a multi-step biorefinery and how this seed is suitable for producing multi-products including nanocellulose due to its composition. Finally, it provides the research aim, objectives, and research contributions. Chapter 3 outlines the research design and methodology. Chapters 4, 5, and 6 consist of articles for journal publications focusing on the objectives, methodology, results, and discussions. In Chapter 4, the effectiveness of the developed multi-step biorefinery scheme that involves organosolv extraction, enzymatic hydrolysis, and alkaline pretreatment processes for the selective extraction of antioxidants (free extractable polyphenols), starch, and bioactive hemicellulose (hemicellulose with bound polyphenols) while preserving the cellulose and lignin in the solid residue for other applications from mango seed kernel was evaluated. Chapter 5 discusses how the developed multi-step biorefinery scheme could separate the various components of MSH into the respective products. In addition, how process parameters (NaOH concentration, temperature, and reaction time) affect the dissolution, composition, and properties of hemicellulose from MSH and the potential suitability of the hemicellulose extract to form self-supporting thermally stable films. This chapter (Chapter 5) further focuses on how a combination of high shear homogenization and organosolv pretreatment (HSHO) affects the yields and properties of lignin and cellulose from the alkaline treated mango seed husk and finally the impact of the preceding treatment process on the performance of the subsequent stages. The feasibility of the unbleached cellulose-rich pulp obtained via the multi-step process consisting of sequential AP and HSHO to produce thermally stable nanocellulose via a non-catalyzed formic or acetic acid or its combination with high shear homogenization treatment processes as alternative CNC production methods to the sulphuric acid-based process was evaluated in Chapter 6. Chapter 7 outlines the main research findings, general discussion, conclusions, and recommendations.

2. Literature review

2.1. Introduction

This chapter discusses the literature on mango production and processing trends, associated biomass waste generation, and compositions as well as potential products that could be obtained from the waste and their recovery pathways (section 2.2). The biorefinery and biorefinery potential of mango seed waste is discussed in sections 2.3 and 2.4. Section 2.5 discuss the mango waste composition and potential applications. Studies on mango seed has been discussed in section 2.6. The conventional pretreatment/fractionation route for nanocellulose production and the proposed multi-step biorefinery route for the multi-product recoveries are presented in sections 2.7 and 2.8.

2.2. Mango fruit production, processing, and waste generation

Mango (*Mangifera Indica L.*) is the fifth tropical fruit in terms of production and consumer acceptance [103], [104]. It is among the most economically important tropical crops and one of the major fruits exploited industrially for mesocarp production. Mango is grown globally on an area of 3.7 million ha [105] with over 100 million metric tons as the estimated production in 2018 with different productions since 2000 (Table 2.1) [106]. Currently, Asia accounts for 75.6% of the mangoes grown worldwide, while 13.3% and 11% come from America and Africa, respectively. India is the leading producer followed by China, Thailand, Mexico, and Indonesia [107]. South Africa produced 112,537 tons in 2019 and this value is envisaged to increase due to improved practices such as cultivar pairing and off-season flowering [7], [108]. Although mango is a seasonal fruit, countries like Brazil have climatic features that allow year-round production enabling the world market to last throughout the year [7], [17].

Mango fruits have found applications both in the beverage and food industries due to their succulent taste and pleasant flavor [109]. The ripe mango fruit is usually processed into dried fruit pulp, concentrates, frozen mango pulp, jams, ready-to-serve beverages, canned mango pulp, and as basic supplements in functional foods [8], [10], [107]. Mango conversion generates large quantities of mango peels and seeds as by-products [103] accounting for 35–60% of the total wet weight of the mango fruit [8], [47]. The peel constitutes 13–18% whereas, the seed constitutes 10–45% of the whole fruit on a wet basis depending on the variety (Table 2.2).

Table 2.1: Worlds ten major mango producing countries for selected years since 2000 (metric tons: [110])

					Percent change	
Country	**2000**	**2005**	**2010**	**2013**	**2000-13**	**2010-13**
India	10.50	11.83	15.03	18.00	71.39	19.80
China	3.00	4.10	4.00	4.45	48.33	11.25
Thailand	1.62	1.80	2.55	3.14	93.57	23.18
Indonesia	0.88	1.41	1.29	2.06	134.99	59.92
Mexico	1.56	1.68	1.63	1.90	21.97	16.49
Pakistan	0.94	1.67	1.85	1.66	76.87	-10.13
Brazil	0.54	1.00	1.19	1.16	116.05	-2.24
Bangladesh	0.19	0.62	1.05	0.95	408.02	-9.34
Nigeria	0.73	0.73	0.85	0.85	16.44	0.00
Egypt	0.30	0.42	0.51	0.83	179.22	65.01
Others	4.46	6.36	7.21	7.66	71.51	6.24
World Total	24.72	31.63	37.14	42.67	72.61	14.87

Currently, the bulk of mango seeds produced during agro-industrial processing has no commercial use hence is discarded as waste in landfills and open dumpsites [9], [111]. This waste degrades and releases unpleasant odors and hazardous leachate that pollute the environment [112]. The minute fraction of the generated mango seeds that is consumed is utilized as low-value animal feed supplements and compost [113], [114]. However, reports indicate that some of the chemicals (e.g. antiseptics) applied during the fruit processing may present health risks in the animal feed applications and the use of the seed for compost is not economical [113], [114]. Fractionation/conversion of the mango seed waste into bioproducts (such as hemicellulose and nanocellulose) in a biorefinery could reduce the dependence on fossil products such as low desity polyethylene (LDPE) for packaging applications, reduce environmental pollution associated with mango processing waste, and lower cost associated with waste disposal [115]. Thus, there is potential for higher-end uses of the mango seed waste when valorized into useful bioproducts such as polyphenols, hemicellulose, and nanocellulose via appropriate pretreatment/fractionation and conversion processes.

Table 2.2: Different components of mango fruit

Mango fruit composition	Pulp	Seeds	Peels	Reference
Percentage composition	45-65	10-25	15-20	[10]
	60-75	14-22	11-18	[116]
	77	11	10	[117]
	76	10	14	
	75	10.6	14.4	
	75.8-76.1	8.5-10.1	13.7-15.5	
	-	9.5-25	13-16	[107]
	-	30-45	-	[118]

2.3. The biorefiery concept

The major idea behind a biorefinery is to produce marketable products such as biofuels, biochemicals, fuel, power, and biomaterials from different biomass sources using a combination of different pretreatment/conversion techniques such as combined chemical and biotechnological techniques that minimize waste, thus improving the biomass value [68], [119]. Biorefinery is analogous to the present petroleum refinery where multiple fuel and products are recovered and it is considered sustainable due to the renewability of the starting material (biomass). The biorefinery takes advantage of the differing biomass composition in addition to their intermediates to maximize the value that can be obtained from the biomass. Generally several high-value but low volume bioproducts (eg. nanocllulose) and low-value high volume fuel such as bioethanol are produced. In addition, the biorefinery can produce electricity for local consumption [113], [120]. There are various biorefinery such as 1G biorefinery (use of food crops such as corn, etc.), 2G biorefinery (use of lignocellulosic biomass such as wheat straw etc.), 3G biorefinery (microalgae) and 4G biorefinery (use of genetically modified microorganisms) [89], [121], [122]. The lignocellulosic biorefinery is attractive because the feedstocks do not compete with food directly on consumption basis.

2.4. Biorefinery potential of mango seed waste

Developing and applying biorefinery processes is one way of meeting the goal of a sustainable bioeconomy [123], [124]. The use of biorefinery schemes for multi-products has the advantage of tailoring the properties of the components generated to specific applications [119], [125]. However, the suitability of the biomass feedstock for targeted biorefinery products lies in the composition of the feedstock. The mango seed serves as a suitable biorefinery feedstock due to its composition of polyphenols, hemicellulose, starch, cellulose, proteins, lignin, among other components [9], [15], [126].

The polyphenols when selectively extracted can be used as antioxidants in many applications [16], [127]; the starch and hemicellulose when extracted in the polymeric form can be applied in biocomposite film development for the food industries or biofuel production when extracted in the monomeric form [42], [43], [48]; lignin can be used in resin applications or as plasticizers, UV-absorbents and many more [14], [68]; and the cellulose when treated under controlled conditions can yield nanocellulose for a wide array of applications such as reinforcement purposes or biofuel production when hydrolyzed into monomers with further fermentation processes [20], [128]. Hence, the mango seed could serve as suitable lignocellulosic biomass for application in a biorefinery.

2.5. The mango seed composition and potential applications

The mango seed is made up of an outer layer known as husk (teguments), and an inner stone, called kernel [107], [118] with about 1–2 mm of a thin lining surrounding the kernel [8], [10]. Of the total seed weight, the kernel (MSK) constitutes 45–85% [105] and is composed of 34–84.9% carbohydrates, 6–13% crude protein, 2% crude fiber, 2–3.88% ash, and some bioactive compounds such as polyphenols [107], [129]–[131]. The MSK also contains 32.0–65.0% starch as part of the carbohydrates [15], [55]. The husk (MSH) represents 15–25% of the total seed weight [19], [109] and is largely composed of cellulose, hemicellulose, and lignin [131] as shown in Table 2.3. A larger proportion of the MSH is cellulose, accounting for 35–55% of the cell wall components (Table 2.3). Hemicellulose and lignin components of the MSH ranges between 15.6–28.6% and 5.6–25.5%, respectively, [10], [118], [131].

The referred compositions of the MSH and MSK are comparable to other agricultural residues that have been exploited in bioproducts (e.g., nanocellulose, hemicellulose, lignin) generation (Table 2.3). Therefore, the generation capacities and diverse biomass composition of the mango seed makes it a good bioresource for the generation of multi-products such as cellulose for nanocellulose, plus recoveries of the hemicellulose, lignin, starch and polyphenols [14], [42], [43]. To effectively recover multi-products from the mango seed, it is crucial to understand the chemical interactions of these components for the development of a robust biorefinery scheme that will deconstruct the biomass into the desired fractions [96] since the desired products' qualities depend on the biomass structure, which further dictates the type and combination of pretreatment/fractionation processes, sequence and reaction conditions required, as detailed in the following subsections.

Table 2.3: Composition (dry weight) of mango waste versus other agricultural waste that has been exploited as feedstock in bioproducts production.

Biomass source	**Cellulose (%)**	**Hemicellulose (%)**	**Lignin (%)**	**Starch (%)**	**Reference**
Barley straw	34.8	27.9	14.6	-	[132]
Coastal Bermuda grass	25.0	35.7	6.4	-	[133]
Corn Cobs	43.2 – 45.0	31.8 – 35.0	14.6 – 15.0	-	[133] [132]
Corn stover	29.7	25.0	12.3	-	[56]
Cotton seed hair	80.0 – 95.0	5.0 – 20.0	0	-	[133]
Esparto	35.8	28.7	17.8	-	[132]
Grasses	25.0 – 40.0	35.0 – 50.0	10.0 – 30.0	-	[133]
Maize stems	38.5	28.0	15.0	-	[132]
Mango husk	34.7 – 55.0	15 – 28.63	5.6 – 25.5	-	[15], [19]–[21][131]
Mango kernel	2.8 – 25.2	14.3 – 52.4	2.03-15.0	32 – 65	[130], [134], [135][136],[131][15], [55]
Mango peel	38.3	13.9	27.9	-	[103], [137], [138]
Nutshell	25.0 – 30.0	25.0 – 30.0	30.0 – 40.0	-	[133]
Oil palm fiber	40.2	32.1	18.7	-	[132] [132]
Pear Pomace	32.4	20.2	25.9	-	[139]
Rape straw	37.6	31.4	21.3	-	[132]
Sugar beet pulp	18.4	14.8	5.9	-	[132]
Sugar cane bagasse	39.2 – 43.6	27.7 – 28.7	19.4 – 27.7	-	[98], [140]
Switch grass	45.0	31.4	12.0	-	[133]
Wheat straw	30.0 – 38.6	21.0 – 50.0	11.0 – 22.9	-	[132], [133], [141]

2.5.1. Cellulose

Cellulose is a renewable organic polymer consisting of D-glucose units connected by β-1,4-glycosidic linkages (Table 2.4) which is present in lignocellulosic biomass [142]. The dimensions of the cellulose fibrils are in the nanometer range (approximately 3 nm), some of which have well-organized intramolecular/intermolecular hydrogen bonding forming a crystalline domain and usually present in large proportions in various lignocelluloses (50–90% of the total cellulose) [20], [98], [133]. The high crystalline portion decreases cellulose reactivity and solubilization and increases its thermal stability due to the stable intermolecular/intramolecular hydrogen and glycosidic bonds [115]. The other portion is disordered, forming the amorphous region, thus, cellulose can be classified as a semi-crystalline biopolymer [143]. This amorphous portion constitutes a smaller percentage of the cellulose with less organized hydrogen bonding and more accessible hydroxyl groups making it vulnerable to chemical and enzyme attacks for producing material such as nanocellulose and biofuel [144], [145].

The glucose units in cellulose bear three hydroxyl groups each and crosslink each other through intermolecular and intramolecular hydrogen bonding as illustrated in Figure 2.1. The sheet of cellulose chains formed overlay each other through weak Van der Waals forces [35], [146]. These forces together with the strong hydrogen bonding between the cellulose fibrils result in cellulose recalcitrance and high tensile strength making cellulose hydrophobic with no solubility in many solvents including water and dilute acids at room temperature and atmospheric pressure [89]. However, the few exposed hydroxyl (-OH) groups on the cellulose surface that do not partake in any bonding can interact with water molecules, thus, cellulose can absorb 8–14% water [96], [147]. In alkaline solutions, cellulose fibers swell and fractions with lower molecular weights [degree of polymerization (DP) < 200] dissolve, reducing the cellulose DP [96]. The cellulose DP or the number of glucose units per molecule influences its accessibility by enzymes and chemicals for nanocellulose production. Harmsen et al. [96] indicated that the DP of cellulose could range between 800 to 17000 units for various lignocelluloses. The reduction in cellulose DP influences cellulose crystallinity which further affects yield and the properties of nanocellulose, particularly cellulose nanocrystals (CNC). Lee et al. [145] asserted that a portion of the crystalline cellulose should be converted to less-ordered amorphous portions to aid in cellulose accessibility for conversion into products such as nanocellulose.

Table 2.4: Structural and chemical composition of hemicellulose, cellulose, and lignin in lignocelluloses [142].

Hemicellulose	Cellulose	Lignin	
D-Xylose, mannose, L-arabinose, galactose, glucuronic acid	D-Pyran glucose units	Guaiacylpropane (G), syringylpropane (S), phydroxyphenylpropane (H)	Subunit
Three-dimensional inhomogeneous molecular with a small crystalline region	Three-dimensional linear molecular composed of the crystalline region and the amorphous region	Amorphous, inhomogeneous, nonlinear three-dimensional polymer	Composition
Polyxylose, galactoglucomannan, (Gal-Glu-Man), glucomannan (Glu-Man)	β-Glucan	G lignin, GS lignin, GSH lignin	Polymer
β-1,4-Glycosidic bonds in main chains; β-1.2-, β-1.3-, β-1.6-glycosidic bonds inside chains	β-1,4-Glycosidic bonds	Various ether bonds and carbon-carbon bonds, mainly β-O-4 ether bond	Bonds between subunits
Contains chemical bonds with lignin	Without chemical bonds	Contain chemical bonds with hemicellulose	Bonds between three components
Less than 200	Several hundred to tens of thousands	4000	Polymerization

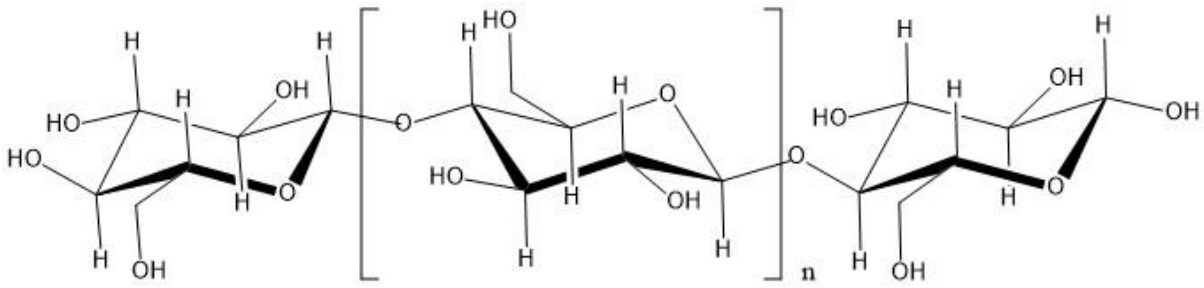

Figure 2.1: Chemical structure of cellulose (Redrawn from Harmsen et al. [96]

As shown in Table 2.3, a higher proportion of the MSH is cellulose accounting for up to 55% of the cell wall components. This cellulose content is higher compared to other agro-industrial waste, except for cotton that contains almost pure cellulose (see Table 2.3). The cellulose content of biomass affects its crystallinity index which is an important parameter in cellulose conversion to nanocellulose. Henrique et al. [20] reported a high crystallinity of 74.3% for cellulose obtained from MSH after purification. This suggests that MSH can be a reliable source of cellulose, which may be utilized in nanocellulose production with an

expected crystallinity of up to 90% [20], [48]. On the other hand, the MSK contains 5.0–25.2% cellulose indicating low crystallinity that has been confirmed with a reported low crystallinity index of 29.4% [80]. This makes the MSK a less attractive feedstock for nanocellulose considering it would require extensive purification before nanocellulose production. However, it could be explored for other valuable bioproducts such as polyphenols and starch.

Obtaining cellulose from lignocellulosic biomass poses some difficulty arising from the complex interaction of cellulose with lignin and hemicellulose and the strong hydrogen bonding within the crystalline region of cellulose [96]. To overcome this difficulty, it is best to first isolate the non-cellulosic components such as starch, lignin, and hemicellulose from the biomass through pretreatment/fractionation processes [147] such as chemical (alkaline, organosolv, ionic liquids, etc.), mechanical (milling, and homogenization), or enzymatic methods with different levels of effectiveness [144], [148]. The chemical methods are the most effective techniques due to their high reactivity with the components [56]. After separation, cellulose has been widely converted to biofuel (butanol, ethanol, etc.), food additives (e.g. cellulose gum), with a recent focus on its nanostructures for application in food packaging, pharmaceutical, medical applications, and cosmetics due to the unique properties [65], [149], [150].

2.5.2. Nanocellulose

Nanocellulose is the smallest unit of cellulose in terms of fiber size [52]. The plant-based nanocelluloses are categorized, based on preparation methods, dimensions, and feedstock used, into cellulose nanofibrils (CNF) and cellulose nanocrystals (CNC) [144] with a subcategory of the CNC being spherical nanocellulose (SCN) [151], [152]. The preparation of CNC, CNF, or SCN requires a cellulose-rich material with cellulose purity in the range of 65–95% [38], [97]. Recently, lignin-containing cellulose nanocrystals (LCNCs) and nanofibrils (LCNF) are being touted as low-cost alternative materials to the CNC, CNF, and SCN because their production involves the application of milder treatment processes compared to the harsher treatments applied in the conventional nanocellulose production processes [153]. However, due to their brown color resulting from a large amount of lignin (up to 12.42%) [154]–[158], they are mostly applied in fluting papers and test liners or liner boards where brightness and color are not a requirement [153], [155]. For application as reinforcement agents or fillers in biocomposites for food packaging, brown and opaque films are less desirable and less attractive to consumers [153], [159].

2.5.2.1. Cellulose nanofibrils (CNF)

Cellulose nanofibrils (CNF) are produced by the destruction of the cellulose fibers along its longitudinal axis [144] and are comprised of alternating crystalline and amorphous cellulose regions. Mechanical techniques such as grinding, high-pressure/shear homogenization, ultrasonication, and micro-fluidization (mostly preferred because it leads to uniform fiber dimensions) are used to break the hydrogen bonds and defibrillate cellulose into CNF and in some cases in combination with chemicals or enzymes [51], [160]. This leads to the destruction of the fibers into fibrils of width 10 to a few 100 nm and length in the micron-scale [144], [161]. CNF exhibits a high aspect ratio, specific surface area, and tensile strength and is used as reinforcement agents and nanofillers due to their high tensile strength in nano/biocomposites [144]. However, their high hydrophilicity limits dispersion in hydrophobic counterparts and the use of mechanical means is regarded as energy-intensive [33].

2.5.2.2. Cellulose nanocrystals

Cellulose nanocrystals (CNC), also known as nanocrystalline cellulose (NCC), OR cellulose whiskers (CW) [162] comprise pure cellulose with crystallinity (Crl) ranging from 54–90.3% [20], [163]. It exists as an elongated particle-like crystalline structure having a rod-like or whisker-like shape with length and width ranging between 100–500 nm and 2–20 nm, respectively [161]. The main process involved in CNC preparation is acid hydrolysis. As previously mentioned in section 2.5.1, the cellulose macromolecule consists of both crystalline and amorphous portions, with the amorphous region susceptible to degradation by enzymes and chemicals. Therefore, addition of acid cleaves the amorphous cellulose fibers. Consequently, the amorphous portion that exists around and between the cellulose microfibril is hydrolyzed leaving the crystalline portion unaltered [144], [164]. This is followed by hydrolysis of glycosidic bonds that can be accessed easily in the cellulose crystalline structure [165].

Depending on the raw material, and the operating conditions (cellulose purification process and CNC treatment process conditions of temperature, time, acid type and concentration, and solid loading), different CNC morphologies, dimensions, and Crl have been reported [20], [166]. The most common acids used in CNC preparation are sulphuric (H_2SO_4) and hydrochloric (HCl) acids [69], [167]. The H_2SO_4 results in stable aqueous suspensions due to sulfate ester groups introduced onto the CNC during hydrolysis. However, CNC from HCl treatment does not form stable aqueous suspensions because of the acids inability to introduce

surface charges [33]. Other acids that have also been used in CNC preparation are formic acid, acetic acid, maleic acids, and oxalic acid [51], [97], [166]. These acids are considered environmentally benign due to their recoverability and reusability compared to inorganic acids, although their weaker acidity limits their sole application in nanocellulose production, thus requiring the addition of catalysts [51], [168].

2.5.2.3. Spherical nanocellulose (SCN)

Through mixed acids, microbial, enzymatic hydrolysis and other alkaline processes, a sub-category of cellulose nanocrystal called spherical nanocellulose (SNC) has been obtained [166], [169], [170]. The diameters of SNC produced from a bleached waste paper by sodium hydroxide/thiourea/urea under ultrasonication were 50 nm [169], while that produced from enzymatic hydrolysis of microcrystalline cellulose for several days had diameters in the range of 43–119 nm [170]. Due to its spherical shape, SCN could have one dimension but with similar qualities defined for CNC and is mostly used in personal hygiene products, biocomposite film for packaging, cosmetics, and drug delivery. This is attributed to their shape since the rod-like CNC could injure human tissues and cells and therefore are less suitable for medical applications [170], [171]. The usage of enzymatic treatment and ultrasonication is expensive and limits the industrial scale nanocellulose preparation and applications [172]. However, due to the diverse applications of SCN and its advantages over the rod-shaped CNCs in terms of medical applications, several studies are developing alternative low-cost processes for its production [173], [174].

2.5.3. Hemicellulose

Unlike cellulose, hemicellulose represents a range of alternative biopolymer structures, made up of mixtures of monosaccharides of β-D-mannose, β-D-glucose, α-D-galactose, β-D-xylose, α-L-arabinose, β-D-galacturonic acid, β-D-glucuronic acid, and α-D-4-*O*-methyl glucuronic acid. The types of hemicellulose differ from plant to plant and this variation is mainly due to the different compositions of the main and branched sugar chains [142], [175]. Hemicelluloses have both lower molecular weight and DP (80–200) compared to cellulose due to their highly branched structure and shorter chain lengths [132], [176] and can be homogeneous or heterogeneous with their monosaccharide sugars exhibiting varied sites for binding interactions [175]. Depending on the plant species and structural features, hemicelluloses are categorized into various forms including xylan, xyloglucan, glucomannan, glucuronoxylans, and galactomannans [177], [178].

The hemicellulose contents of mango seed kernel and husk are comparable to most of the listed feedstock sources in Table 2.3. Literature reports a gradual reduction of both pectic and hemicellulose sugar chains during mango fruit ripening due to enzymatic and ethylene-induced partial depolymerization resulting in significant loss of the side chains including arabinose and galactose [179]. The depolymerization of side chains from the mango seed hemicellulose can be an added advantage as high yields of hemicellulose with diversified functionalities could be obtained due to reduced degree of substitution (reduced steric hindrance) [180] and ripening induced structural changes that may not be found in other agro-industrial waste like wheat straw and sugarcane bagasse. Xylan and xyloglucan being the major hemicellulose types identified in most agro-industrial waste and dicotyledons such as mango seed are discussed in the following sections [45], [106], [179], [181].

2.5.3.1. Xylan

Xylan is the most abundant hemicellulose type in agro-industrial waste and hardwood. It is found in different variations based on the type of feedstock, but with a common backbone of 1,4 xylopyranosyl units. Arabinoxylan, homoxylan, heteroxylan, and glucuronoxylan are the various xylan sub-classes, arising from the type of side chain and degree of substitution on the xylan backbone [182]. Arabinoxylans are typically found in cereal grains and endosperm of starchy feedstock. It is composed of a β-1,4-xylopyranosyl backbone with α-1, 2, and/or α-1,3 arabinofuranosyl substitution. It may be partly esterified with some phenolic acids [183]. Homoxylans are rare in higher plants but exist abundantly in green and red algae. They are made of mixed linkages of β-1,3- and 1,4-xylopyranosyl units [184], [185]. Heteroxylans are also complex groups of xylans mostly obtained from seeds, exudates, and cereals. They consist of a backbone of xylopyranosyl units that are branched heavily by one, two, or three sugar units of arabinose, galactose, and xylose [184], [186].

Glucuronoxylan (GX) is the main type of hemicellulose found in hardwood and most agro-industrial solid waste with a high degree of acetylation mostly at C-2 and C-3 positions [187]. The backbone of GX is β-D-1,4 linked xylofuranose residue, usually esterified with 7 acetyl groups on every 10 xylose units. Other substitutions through α-1,2 linkages by 4-*O*-methylglucuronosyl and glucuronosyl residues can also be found on the GX [182]. The degree of substitution and the type of substituents (particularly 4-O-methyl-D-glucuronic acid) influence the hydroxide ion concentration on the xylan surface, which in effect influences the rate of the hemicellulose reaction [188]. Xylan can be soluble in water, organic solvents, or

alkaline solutions depending on the type because the different substituents on the xylan chains can result in changes in the conformation of the xylan and consequently the solubility [183], [189].

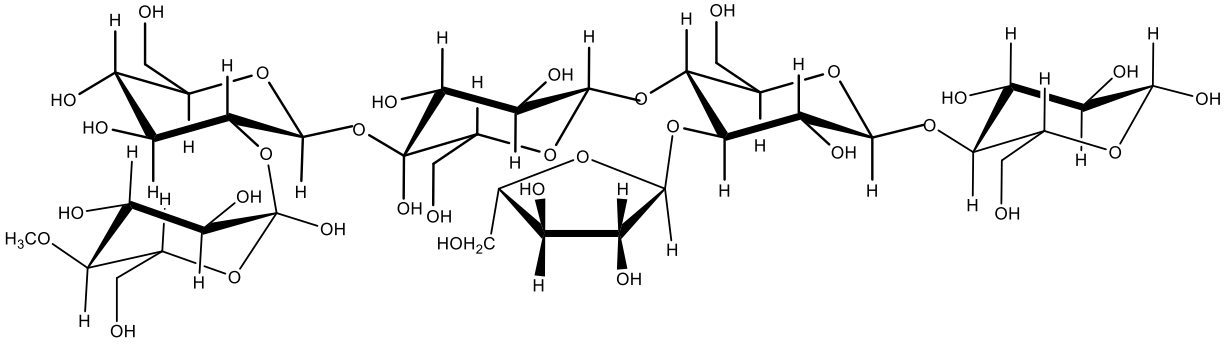

Figure 2.2: Physical and chemical structure of hemicellulose (Redrawn from Lee et al. [145])

2.5.3.2. Xyloglucan

Xyloglucan (XGN) exists as storage polysaccharides in the secondary cell walls of dicotyledonous seeds and as a component of the primary cell wall (about 20–25%) of many higher plants and some non-graminaceous monocotyledons [190], [191]. This type of hemicellulose has a β-1-4 glucopyranosyl backbone like that of cellulose with *O*-6 linked α-D-xylopyranosyl substitution. The xylopyranose may further be substituted at *O*-2 by galactopyranosyl and/or fucosyl moiety. The substitution of the sugars on the XGN varies considerably depending on the plant species [192], [193]. In the cell wall, XGN extensively coats the cellulose microfibrils surfaces through hydrogen bonding and tethers them together leading to the formation of an extensive network of cellulose-xyloglucan structures [193], [194]. These properties of xyloglucan could aid in cellulose protection from hydrolyzing agents during biomass fractionation and reduce cellulose degradation for nanocellulose production. Generally, the storage XGN lacks the presence of a fucose residue, which could be a reason why it undergoes extensive self-association in solution [190], [195]. The M_w of XGN from the primary cell wall is estimated to range between 9 kDa and >900 kDa while that of storage XGN are relatively large with various reports estimating over 2000 kDa [189], [190], [193]. This suggests that storage XGN could be easily isolated than cell wall XGN. Thus, the relatively higher M_w of storage XGN renders their extraction much easier than the cell wall XGN based on literature studies. Nevertheless, high viscosities may be encountered during dissolution, which should also be taken into consideration during storage XGN isolation.

Hemicellulose has a strong association through ester and α-benzyl ether covalent bonds with lignin, hydrogen bonds with cellulose, and ester bonds with hydroxycinnamic acids and acetyl units as previously stated [132], [177]. This kind of association in addition to the amorphous nature of hemicellulose makes it a challenge to isolate hemicellulose from their sources in the intact form [175]. In nanocellulose production, there is a limit to the amount of hemicellulose that could be present in the cellulose (approximately 0.5–26% is allowed), to allow chemicals and enzyme access to produce nanocellulose because of the protective nature of hemicellulose through cellulose shielding [69], [158], [196]. Thus, the various isolation methods developed for hemicellulose include mild alkaline, organosolv, alkaline peroxide, and steam explosion [177], [197], [198]. In mild alkaline and organosolv (without acidic catalysts), polymeric hemicellulose is usually obtained [89], [96]. However, alkaline peroxide and steam explosion (without acidic catalysts) lead to partial degradation of hemicellulose resulting in the production of oligomeric and monomeric sugars [199], [200]. After isolation, hemicellulose polymers can be used in the modified or native form in non-food (adhesives, biocomposite films, and pharmaceutical) and food (gelling agents, viscosity enhancing additives in food, and stabilizers) industries [42], [201].

2.5.4. Lignin

Lignin is second to cellulose in terms of most abundant biopolymer in nature. It usually occurs in the cellular wall of the organic material and accounts for 15–40 wt% of plant biomass depending on the variety [202]. Lignin is amorphous and provides structure and resistance to biological and chemical degradations for the cell wall. Unlike cellulose and hemicellulose, lignin is not a polysaccharide but a polyphenolic macromolecule [85], [203] formed from three different aromatic monomers of phenylpropane alcohols; coniferyl, *p*-coumaryl, and synapyl alcohols [204], [205]. Guaiacyl (G), *p*-hydroxyphenyl (H), and syringyl (S) are the three structural moieties formed from the dehydrogenative cross-linking of the phenylpropane monomers by enzymes [91] as indicated in Figure 2.3 and Table 2.4.

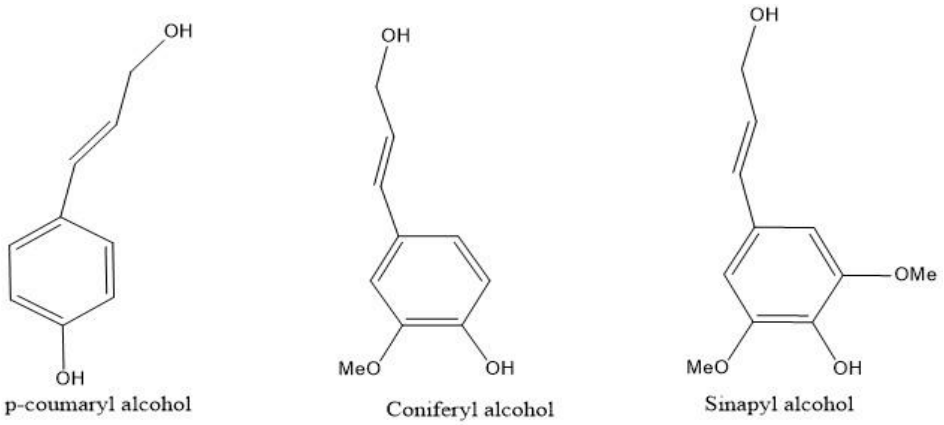

Figure 2.3: Monolignols of lignin (Redrawn from Lee et al. [145])

Several inter-unit linkages are formed during the radical coupling of the phenylpropane monomers which include carbon-carbon biphenyl (5-50), resinol (5-5), 1,2-diaryl propane (b-1), phenyl coumaran (b-5/a-O-4), biphenyl ether (4-O-5), and β-O-4 [206]. The type and proportion of the lignin monomers and bonds vary based on factors such as biomass origin, and species [50], [203]. Hardwoods and dicotyledons comprise diverse proportions of sinapyl and coniferyl alcohols [207]. The different functional groups and the major linkages that connect the different phenylpropane units in the lignin are shown in Table 2.5. The majority of the phenolic hydroxyl groups are used in bond formation between other lignin units, making them less available [208]. Apart from the linkages present in lignin units, lignin forms cross-link with hemicellulose and other polymers in the plant cell wall. This association leads to the formation of lignin carbohydrate complexes (LCCs) [96].

Table 2.5: Predominant linkages in lignin (Adapted from Santos et. al. [208])

Linkage type	Dimer structure	% Linkage in SWD	% Linkages in HWD
β-O-4	Arylglycerol β-aryl ether	45-50	60
5-5	Biphenyl and Dibenzodioxocin	18-25	20-25
β-5	Phenyl coumaran	9-12	6
β-1	1,2-Diaryl propane	7-10	7
α-O-4	Phenylpropane α-aryl ether	6-8	7
4-O-5	Diaryl ether	4-8	7
β- β	β- β-linked structures	3	3

*SWD-softwood dimers and HWD-hardwood dimers

Depending on the biomass material, different covalent bonds can be seen in the LCCs. For example, the main LCC bonds present in woody biomass are ester bonds, phenyl-glycoside bonds, and benzyl ether bonds, while that in herbaceous plants and grasses are mainly ester bonds between hemicellulose and ferulic acid [204], [209]. The LCCs contribute to the difficulty in isolating lignin from lignocellulosic biomass [96]. Cordeiro et al. [15] reported a lignin content of 21.07% for mango seed husk. Another report by Henrique et al. [20] showed mango husk to contain 24% lignin. These reported values of lignin in mango seed husk are comparable to the lignin contents of most of the agro-industrial waste presented in Table 2.3. This quantity of lignin present in mango seed makes it an attractive bioresource for extraction and valorization.

Although there is the emergence of lignin-containing nanocellulose [153], most of its production process involves the so-called mild pretreatment to remove part of the lignin leaving approximately 0.54–12.42% in the biomass [154]–[158]. Thus, the difference between the CNCs, CNF, and lignin-containing cellulose nanomaterials (LCNM) is the extent of delignification [153], [156]. Moreover, for application as reinforcement agents in biocomposite for food packaging, purity of the starting cellulose material and the CNC are important as this property affects the appearance of the final composite product. Cellulose-rich solids with purities of 65.6 to 95.2% have been applied in CNC production with final CNC purity of 77 to 99% [38], [97], [210]. Although the presence of lignin in the packaging material could protect the food from exposure to light (i.e. oxidation caused by UV radiation), lignin could impact negatively on the appearance (opaque films) of the films [210], [211].

Therefore, the content of lignin in the cellulose fiber during nanocellulose production needs to be limited due to its recalcitrant nature, and impact on color in the final composite product [210]. Thus, part of the lignin can be isolated and recovered for other applications such as resins. Selective removal of lignin will improve the cellulose purity, allow easy defibrillation, and improve the nanocellulose yield. Besides, the lignin, when recovered as a co-product of the nanocellulose process will diversify the product range from the feedstock. The isolation of lignin is mainly done by the pulping industries to obtain cellulose-rich material for various applications including processing into paper and nanocellulose. Practically, it is not feasible to isolate appreciable amounts of lignin in its intact structure from the cell wall of biomass i.e., lignin is always modified during the extraction. The isolated lignin can be obtained with different functional groups depending on the source and the separation process [207], [212].

Organosolv, acid treatment, alkaline treatment, Kraft, and sulfite treatments are among the developed treatment methods used for lignin extraction with different levels of effectiveness [96], [213]. Details on the extraction processes are provided in section 2.9.4. The versatility of lignin has been proven and therefore used as emulsifiers, dispersants, pesticides, UV-absorption, activated carbon fiber, and as a stabilizer for food and feed. When added to synthetic polymers, purified lignin stabilizes materials against thermal and photo-oxidation [214]. Lignin can as well be applied in devices such as supercapacitors, batteries, fuel cells, and solar cells [207], [215]. To enhance the economic benefits from the isolation and continuous supply of purified lignin with desired properties (lower molecular weight and molecular weight distributions, high purity, etc.) for application in areas such as resin production [216] from different sources while improving the cellulose purity for nanocellulose production, appropriate pretreatment/fractionation methods are required which is one of the objectives of this study.

2.5.5. Other components of mango seed

2.5.5.1. Starch

Starch exists as granules used for energy storage in the plant material. It composes of two high molecular weight carbohydrates, amylose, and amylopectin. The amylose is made up of α-(1–4)-linked chains of glucose units leading to the formation of a linear structure. However, small portions of α-(1–6) linkages may be seen in its structure. Unlike amylose, amylopectin is made up of both α-(1–4) linear glucose unit linkages (94–96%) and α-(1–6) branched units (4–6%) [217]. Different sources of starch differ in their particle size distribution, appearance, and functional properties [218].

Starch has been extensively studied for application as matrices for producing biodegradable composites [15]. For example, Oliveira et al. [219] produced biocomposite films using mango seed kernel starch and starch nanocrystals. They reported an increased modulus and tensile strength and reduced water vapor permeability after the addition of 5% starch nanocrystals to the starch biocomposite [219]. Several studies on starch-based staple foods like maize, wheat, legumes, rice, mango seed kernel, and wheat have been made available in the literature [15], [220], [221]. The use of these sources in biocomposite film applications competes with the consumption of food causing a rise in food prices. Starch from MSK (32–65%) has an advantage over the referred sources since the MSK is regarded as waste and does not compete with food consumption. Starch removal from the kernel before nanocellulose

production is necessary to limit the production of monomeric sugars that results in low nanocellulose yields. In addition, the removal of starch will reduce the number of interfering components and improve the cellulose purity for nanocellulose production.

2.5.5.2. Antioxidants

Antioxidants are substances capable of inhibiting the damage of nucleic acids and proteins due to oxidation, and inhibiting the damage of lipids resulting from increased reactive oxygen species during stress [71], [222]. Antioxidants work by scavenging free radicals, quenching singlet oxygen species, and reducing free radical activity [10], [103], [223]. They are classified as primary and secondary antioxidants based on their ability to protect during oxidation. The primary antioxidants work by delaying or stopping oxidation by hydrogen atoms or electron donation to free radicals. In so doing they become more stable. The secondary antioxidants work by scavenging oxygen, binding metal ions, deactivating singlet oxygen or absorbing UV radiation, and converting hydroperoxides to non-radical species [10]. Butylated hydroxyanisole (BHA) and butylated hydroxytoluene (BHT) are two major synthetic antioxidants used in the food industry, which are reported to be toxic and carcinogenic. For this reason, natural antioxidants have attracted significant interest as they are considered safe [10], [103]. Accordingly, many researchers have focused on evaluating the antioxidant potential of extracts from vegetables, fruits, cereals, and herbs. However, most attention has been on fruits, perceived to contain appreciable amounts of phenolic compounds [103]. The MSK, as mentioned in section 2.3, contains appreciable amounts of bioactive compounds that have antioxidant properties, thus could be extracted as additional valuable products from the mango seed [224].

2.6. Reported studies on bioproduct exploit from mango seed waste

Various studies have been focused on the recovery of a variety of bioproducts from mango seed, which includes bioactive compounds, starch, and polysaccharides (pectin/hemicellulose complex) from MSK (Table 2.6), and xylooligosaccharides, nanocellulose, activated carbon, and biofuel from the MSH. Most of these studies considered only one valuable bioproduct for extraction, rather than multiple products obtained from a multi-step process (Table 2.6). There is limited information on the hemicellulose and lignin extraction from both MSH and MSK although these biomasses contain an appreciable amount of these bioproducts (Table 2.3). Additionally, there is limited data on the production of nanocellulose from MSK which could be due to its low cellulose and high starch content. The

recovery of only a single product however limits the full economic potentials of the biomass. Thus, a multi-step biorefinery scheme could enhance the complete utilization of the biomass feedstock for multi-products including nanocellulose, which requires compatible and efficient biomass pretreatment/fractionation technologies [201]. For instance, the biomass components that are liable to degradation can be extracted first followed by those that are more stable.

The suitability of the lignocellulosic biomass for nanocellulose depends on its composition of cellulose, lignin, and hemicellulose [145], [225]. Generally, the hemicellulose and lignin contents in the cellulose pulp should be limited to 0.5–26% and <0.1–16% respectively, indicating that majority of lignin and hemicellulose should be removed from the biomass [98], [157], [169], [226]. The hemicellulose and lignin inhibit the accessibility of the cellulose to the hydrolyzing agents (e.g. enzymes and chemicals) for conversion to nanocellulose [145], [163], [227]. High lignin content in cellulose provides rigidity that results in difficult mechanical defibrillation and controlled hydrolysis of amorphous cellulose, thus, obstructing the formation of the nanocellulose [159]. In addition, high lignin-containing nanocellulose result in brown and opaque films as indicated in section 2.5.2 compared to the low-lignin and lignin-free nanocellulose that produces less opaque and transparent films [153], [159]. Hemicellulose is also labile to heat and chemicals and degrade into simple sugars with further conversion into undesired products of furfural and 5-hydroxymethyl furfural (HMF) under the chemical treatment for nanocellulose [228], [229]. Thus, the hemicellulose and lignin could be recovered for other beneficial uses such as in biocomposite films for packaging application and phenol formaldehyde resins respectively. For such applications, hemicellulose polymers and purity are essential whereas less condensed, lower molecular weight and high purity lignin are required respectively [230], [231]. The single products that have been recovered from mango seed contributed to the selection of the variety of bioproducts and the sequence of the treatment steps to be applied in the multi-step biorefinery in the present study, as detailed in section 2.11.

Table 2.6: Summary of reported studies on bioproduct from mango seed waste

Substrate (%)	Treatment conditions (%)	Product (s)	Reference
Husk	Hydrothermal treatment (sonicated distilled water, 180 ºC, 30 min, 2.5–10 MPa)	Xylooligosaccharides	[106]
Husk	Acid hydrolysis (11.21 M H_2SO_4, 10 min, 40 ºC)	Nanocellulose	[20]
Kernel	Water extraction (89ºC, 1:9 solid to solvent ratio, 2.9 h)	Polysaccharides (pectin and hemicellulose)	[232]
Husk	Soaking tine; (4h), impregnation ratio; (0.25), and temperature; (500 °C)	Activated Carbon	[21]
Kernel	Microwave-assisted extraction (600 W, 90% ethanol, 75ºC, 2 cycles and 1:60.4 g/mL, 22 min)	Antioxidants	[16]
Husk	Dilute acid treatment (1–5% v/v H2SO4, 95 °C, solid-to-solvent ratio of 1:10 (w/v), 60 min), enzymatic hydrolysis (Cellic CTec3 HS cellulase, 50 °C, 150 rpm, 24 to 72 h),	Biofuel	[45]
Husk	NaOH treatment, bleaching, Acid hydrolysis using 52% (w/w) sulfuric acid, 1:20 solid: solvent) 45ºC, under vigorous stirring for 2 h	Nanocellulose	[15]
Kernel	80 ml 0.16% sodium hydrogen sulfite, 10% solid loading, 50˚C, 24hrs + grinding in 50 ml of distilled water+filtering +drying	Starch	[55]
Husk	Acetosolv pulping, bleaching, Sulfuric acid: hydrochloric acid (11.3M:8M) at a ratio of 3:1 hydrolysis, 1:20 solid: solvent, 45ºC, 1 h	Nanocellulose	[48]
Kernel	Solvent extraction: Methanol, solvent reflux for 24 h, 10% solid loading, 0.30 atm	Phenolic compounds	[233]
Kernel	Solvent extraction (80% methanol, 120rpm in a shaker overnight, room temperature, 1:7.5 solid: solvent)	Polyphenols	[234]
Kernel	Solvent extraction (Ethanol/water mixtures, room temperature, 200 rpm, 1 h, 10% solid loading),	Bioactive compounds	[235]

2.7. Fractionation of lignocellulosic biomass

Biomass fractionation involves the extraction and separation of components from biomass in good yield and with quality for the specified application [23]. Fractionation is the fundermental process in biorefinery and employs different pretreatment methods [83], [213]. There are different pretreatment fro lignocellulosic biomass fractionation including mechanical, enzymatic and chemical processes with different levels of effectiveness. The chemical pretreatment methods are regards more promising in biorefinery applications owing to their high selectivity towards the components. Table 2.7 shows some comparison of chemical pretreatments. Generally, pretreatments such as acidic, and ionic acids results in hemicellulose in the form of oligomers and monomers, whereas alkaline pretreatment results in hemicellulose polymers. Therefore, depending of the desired product properties each of these pretreatments could be considered.

2.8. Lignocellulosic biomass fractionation for the recovery of cellulose-rich pulp for nanocellulose: The conventional approach

The conventional lignocellulosic biomass-based nanocellulose process involves mechanical size reduction, followed by pretreatment steps to remove the non-cellulosic components of hemicellulose, lignin, polyphenols, and pectin to obtain the cellulose-rich pulp. This is followed by a bleaching stage where remnant lignin is removed to increase cellulose content and purity before subjecting the cellulose-rich pulp to mechanical fibrillation or controlled chemical/enzyme treatment [24], [89], [236]. The referred pretreatment steps usually involve the use of chemicals (Kraft pulping and bleaching processes) and/or mechanical processes. The Kraft process is the most widely established chemical pretreatment method for obtaining more than 80% of the total cellulose produced worldwide [237]. In the Kraft pulping stage, biomass is subjected to hydrolytic treatment using white liquor (a combination of sodium hydroxide and sodium sulfide) at temperatures of about 170 °C and high pH (>10) to fragment and dissolve the lignin and most of the hemicelluloses from the biomass thereby releasing the cellulosic fibers [24], [238]. Kraft pulping retains fiber strength, however, there is considerable loss in yield of pulp due to the enhanced cleavage of covalent bonds in the biopolymers at such severe conditions. This leads to degradation of hemicellulose to lower molecular weight and to some extent cellulose into the spent liquor [208], [237]. The cellulose fibers are processed further to obtain the pulp after the removal of the spent liquor.

Table 2.7: The comparison of chemical pre-treatment methods (Adapted from Makheta 2016)

Pretreatment	Mode of action	Recovered sugar	Inhibitor production	Byproduct's formation	Need for chemical resuse	Applicable to diverse biomass	Operational cost	Pilot scale attempts	Advantages	Disadvantages	Hemicellulose quality
Dilute acid	Hemicellulose removal, lignin transformation and removal	High	High	High	Yes	Yes	Moderate	Yes	Lignin removal is achieved	High equipment cost	Oligomers Monomers
Liquid hot water	Hemicellulose removal	High	Low	No	No	Yes	Low	Yes	Minimum degradation products Low coat of solvents Low residence time	Use of high temperature products and pressures Low cost of solvent Low lignin removal Low residence time pH monitoring required	Mostly oligomers
Steam explosion	Hemicellulose removal Lignin transformation	High	High	Low	No	Yes	Low	Yes	Low residence time Limited use of chemical Low environmental impact	Use of high temperature and pressures Low lignin removal	Mostly oligomers
AFEX	Lignin removal Minimum hemicellulose dissolution Cellulose decrystallisation	High	Low	-	Yes	Yes(with limitations on softwood)	High	-	Considerable lignin removal Minimum degradation products Moderate temperature Short residence time	Costly solvent (ammonia) High environmental impact (issues)	Oligomers
Alkaline	Lignin removal Hemicellulose removal	High	Low	High	Yes	Yes	Low	Yes	Low reagents cost Low and moderate temperatures	Long residence times Irreversible salt formation Large volumes of water used for washing pulp Need for neutralizing liquid fractions	Polymers
Organosolv	Considerable lignin removal Hemicellulose remova	High	Low(for auto alkaline and neutral catalyst)	Low	Yes	Yes	High	Yes	Sulphur-free high purity and quality lignin Does not require significant size reduction of feedstock	Solvent recovery required Costly solvents Inherent fire and explosion hazards Environmental, health and safety concerns	Oligomers Monomers
Ionic liquids	Dissolution of biomass Use of antisolvents Selective dissolution (either lignin or carbohydrate	High	Low	-	Yes	Yes	-	-	Solvents are thermally stable, highly polar and have negligible vapour pressure	Requirement of antisolvents Need for solvent recovery and reuse Low solid loading capacity	Polymers Oligomers Monomers (for acidic ionic liquids)

Approximately 80% of the dissolved solid components in the spent liquor are lignin and hemicellulose products that are commonly combusted as fuel for boilers due to product separation difficulties. In addition, the Kraft process uses excessive sodium sulfide which generates and releases sulfur gases into the environment [2]. Kraft lignin is also modified with aliphatic thiols (1–2%), reducing its quality for many applications like in resins and carbon fiber production [239]. The Kraft process thus focuses mostly on the recovery of a single cellulose product, which limits the economic value of the biomass.

Other biomass pretreatment processes presented in the literature for obtaining high purity cellulose fibers (purity ≥65%) for nanocellulose production include combined acid chlorite and alkaline pretreatment [20], [240]. The acid chlorite process, also known as the bleaching process, is used to delignify biomass to obtain holocellulose (a material with mainly cellulose and hemicellulose). The acid chlorite process is performed at about 80 °C using sodium chlorite, acetic acid, and distilled water with constant stirring for a period of up to 12 h or more [161]. The sodium chlorite and acetic acid are added in batches to control the pH of the mixture. Although chlorite bleaching is the most preferred in the nanocellulose production process, other bleaching agents such as hydrogen peroxide have been used as a greener treatment approach [48]. Following the bleaching stage is the removal of hemicelluloses and the remnant lignin using alkaline pretreatment, mostly performed using 4–20%wt NaOH for a period of 1–5 h. After the process, the solids are removed, washed with distilled water, and dried [161]. Many researchers [20], [39], [40] have used these treatment methods to obtain cellulose from agro-industrial waste for nanocellulose production. In the referred treatments, lignin, pectin, polyphenols, and hemicellulose are usually not recovered for further valorization and their value is lost. Hence, it could be economically beneficial if efficient pretreatment/fractionation processes are applied to recover the polyphenols, lignin, and hemicellulose in good yields and with properties (molecular weight, polydispersity, purity, antioxidant activity, etc.) suitable for diverse industrial applications (e.g., biocomposite film development, antioxidants, resin production) while obtaining cellulose-rich material for nanocellulose in a biorefinery context.

2.9. Pretreatment/fractionation of lignocellulosic biomass for the recovery of multi-products

Pretreatment/fractionation of lignocellulosic biomass can also be achieved by two or more steps to recover multi-products i.e. cellulose, hemicellulose, and lignin [241]. For the two-step fractionation process, the hemicellulose and lignin can first be extracted using a suitable method, thereby generating the cellulose-rich pulp. This is then followed by a second step that separates the dissolved hemicellulose and lignin. On the other hand, selective extraction of one component (mostly components that are easily degraded i.e. hemicellulose) is carried out, leaving the lignin and cellulose in the biomass, followed by a second step that separates the lignin from the biomass residue thereby yielding the cellulose-rich material [241]. One could also use a single-step process to hydrolyze the three components, however, a major drawback is the difficulty in the separation of the product streams resulting in co-contamination and extensive downstream purification processes [241].

Some important factors to consider during pretreatment/fractionation of the biomass are: (1) the pretreatment method or combination of methods required, (2) the sequence in which the fractionation steps are applied such that there is the preservation of properties and minimal degradation of the products and, (3) components in the solid residue to be used in the subsequent stage(s) of the process. In addition, the selected processes and sequence should reduce waste/pollution and the cost of processing, while maximizing the product recoveries [242]–[244]. The components fractionated should also be in good yields and of good quality (e.g. purity, molecular weight, polydispersity, crystallinity, etc.) for their intended applications [89], [213]. The following section describes single product extraction methods for the bioproducts of interest to the present study.

2.9.1. Polyphenol extraction

The presence of antioxidants (polyphenols), starch, and other non-structural components interferes with the fractionation of components from lignocellulosic biomass [56]. Polyphenols interact with proteins and hemicellulose and could obstruct the hemicellulose fractionation step. In addition, the hemicellulose extraction step could degrade the polyphenols particularly the free extractable polyphenols [81], [245]. The pre-extraction of polyphenols using appropriate conditions will allow the recovery of polyphenols with high bioactivity (DPPH scavenging activity

of up to 85.85%) for application as antioxidants [8], [71], [234], [235], [246]. In the recovery of multi-products using the multi-step biorefinery approach, the selection of the extraction method and conditions needs to consider potential impacts on the stability of the polyphenols in addition to other biomass components. A suite of methods including solvent extraction, subcritical water extraction, Soxhlet extraction, and maceration has been used to obtain polyphenols from MSK and other agro-industrial residues [47], [247], [248]. Solvent extraction is the most commonly used method for mango waste as it is effective, has broad application potential, and is easy to operate to obtain the desired product at a lower cost [12], [249]. Although solvent extraction is considered simple, the chemicals used and required conditions such as temperature and reaction time affects the polyphenol extraction yields and bioactivity [235].

Generally, the solubility of polyphenols from plant materials depends on both the polarity of the solvents used and the nature of the compounds to be extracted [71]. The solvent selected should ideally be able to selectively extract the compounds of interest [12], [47]. For example, different polyphenolic compounds such as tannins, phenolic acids among others in different proportions may exist in the biomass with some associated with proteins, polysaccharides, and other inorganic acids [12], [16], [67]. Thus, based on the selected extraction solvent, different polyphenolic compounds could be recovered. Solvents with low viscosity such as ethanol, methanol, their aqueous mixtures, and water are the most preferred for obtaining bioactive extracts from MSK due to their ability to easily penetrate the biomass and dissolve the compounds of interest into the extraction medium [47], [250]. Generally, binary solvent mixtures (ethanol/water, methanol/water, acetone/water mixtures) are preferred over the pure solvents due to their synergistic effect, however, ethanol/water mixtures are the most preferred for food and pharmaceutical applications due to compliance with good-grade standards [67], [235], [251]. It is worth noting that, the polyphenols in seeds such as MSK exist in both free and bound forms [71]. The free polyphenols are located on the surface of the bulk material while the bound polyphenols associate with carbohydrates and proteins [71], [235], [252].

Several studies, as shown in Table 2.8, have reported on the extraction of free polyphenols from MSK and other agro-industrial waste with some studies optimizing the extraction conditions to obtain the desired product qualities (antioxidant activity, anticancer activity, etc.). Dorta et al. [47] extracted antioxidants from MSK using solvent extraction method varying temperature (25, 50 and 75 °C) and solvent type (methanol, ethanol, acetone, methanol-water [1:1], acetone-water

[1:1], and ethanol-water [1:1]). They reported the solvent type to be the most significant factor for polyphenol extraction. In addition, extracts obtained using methanol: water, ethanol: water, methanol, and acetone: water exhibited high antioxidant activities (AA). However, ethanol/water mixture was concluded to be a safer solvent for food security due to its compliance with good manufacturing practices [235], [253]. Ethanol-water mixture, at 50:50% ratio, has been found optimal in most polyphenol extraction processes [235], [254]. Work done by Lim et al [235] showed that 50%v/v ethanol gave the highest TPC (101.68 mg GAE/g) of the extract with AA of 85.85% followed by 75%v/v ethanol (93.41 mg GAE/g) with AA of 72.78%. Below the 50% ethanol and above 75%v/v ethanol the TPC was less than 52%.

Siacor et al. [251] optimized the organosolv process conditions [ethanol concentration (25.0–75.0% v/v) and temperature (30–60 ºC)] to extract polyphenols from MSK and reported that a temperature of 63.21 ºC and percentage ethanol of 53.21% was optimal for obtaining maximum polyphenol yield (14.18%). Furthermore, Rawdkuen et al. [256] varied the ethanol concentration (40–80% v/v), time (1–3 h), and temperature (40–80 ºC) for the extraction of polyphenols from MSK. They reported a 62% v/v ethanol concentration, 63 ºC temperature, and 1.5 h reaction time as optimal conditions for obtaining maximum polyphenol yield, AA, and TPC. Generally, from Table 2.8, the most widely employed ethanol concentrations for polyphenol extraction from MSK is 50% v/v [67], [129], [135], [253].

Apart from the solvent type and polarity, temperature also significantly influences the extractability of polyphenols from plant material although different temperatures may be required for different feedstock [47], [251]. Numerous studies revealed that the efficiency of polyphenol extraction is enhanced when the temperature is above 25 ºC due to improved mass transfer, reduced solvent viscosity, and improved solvent-solute interaction [16], [71], [135], [257]. However, extreme temperatures (>70–110 ºC) degrade and cause volatilization of polyphenols, which affect the antioxidant activity and yield [127], [235], [258]–[260]. Therefore, in free polyphenol extraction, the temperature should be limited to ≤70 ºC to preserve the bioactivity of the extracts.

Table 2.8: Extraction of polyphenols from mango seed kernel and other agro-waste

Substrate (%)	Organic solvent: water ratio	Temperature [ºC]	Time [min]	Total polyphenol content (mg GAE/g)	Antioxidant activity (% DPPH)	Type of polyphenol	Reference
Mango seed kernel	Ethanol/water 0:100	25	60	27.21	54.51	Free extractable	[235]
	10:90	25	60	51.34	66.53	Free extractable	
	25: 75	25	60	76.52	73.10	Free extractable	
	50:50	25	60	101.68	85.85	Free extractable	
	75:25	25	60	93.41	72.78	Free extractable	
	90: 10	25	60	38.05	32.99	Free extractable	
	100:0	25	60	18.19	8.19		
Mango seed kernel	Methanol: water 80:20	25	60	42.83	-	Free extractable	[255]
Mango seed kernel	Methanol: water 80: 20	25	overnight	174	-	Free extractable	[234]
Tamarind seed flesh	Ethanol: water 50:50	70	60	94.5	-	Free extractable	[135]
Mango kernel flesh	Ethanol: water 50:50	70	60	117.0	-	Free extractable	
Avocado seed flesh	Ethanol: water 50:50	70	60	88.2	-	Free extractable	
Defatted mango kernel	Ethanol: water 50:50	70	60	78.0	-	Free extractable	
Longman seed flesh	Ethanol: water 50:50	70	60	62.6	-	Free extractable	
Jackfruit seed flesh	Ethanol: water 50:50	70	60	27.7	-	Free extractable	

Previous works on the polyphenol extraction from MSK were mostly focused on the free polyphenols using organic solvents (Table 2.8), while studies on the bound polyphenol extraction are limited [81]. The bound polyphenols have been reported to be much higher in the plant biomass and exhibit stronger bioactivity than the free counterpart [81]. According to Galili and Hovav [71], the bound polyphenols that associate with biomolecules are extractable in alkaline solvents. Other studies have reported on the co-extraction of bound polyphenols and hemicellulose under alkaline conditions to obtain bioactive hemicelluloses [261]. Due to the stability of bioactive hemicelluloses than the free polyphenols, less severe treatment conditions could be applied to recover the free polyphenols, followed by more/less severe process conditions for the bioactive hemicellulose. Thus, in the present study, an organosolv extraction and mild alkaline treatment processes have been considered for the recovery of the free polyphenol and bioactive hemicellulose (bound polyphenols plus hemicellulose) from the MSK respectively (Chapter 4).

2.9.2. Starch removal

Removing starch from the biomass feedstock is important to improve the yields, purity, and properties of the recovered components due to limited interference [69]. There are different methods of extracting starch from the biomass of which enzymatic hydrolysis and water extraction are predominant [69], [262], [263] due to their respective less severity (temperatures <50 ºC, no chemical application) and substrate specificity (in the case of enzymatic hydrolysis), and therefore could have minimal degradation effect on hemicellulose, lignin, and cellulose for subsequent extraction [263]. Using these processes, many research works have shown feasibility for obtaining starch from feedstocks including MSK, wheat bran, and potato peels [10], [220], [264]–[266]. The use of water extraction results in obtaining starch in its native form. Matavire [263] removed over 90% of starch from wheat bran with an accompanied protein dissolution of approximately 18% after treating the material in 400 mL distilled water at 40 °C for 15 min with constant shaking.

Sonthalia & Sikdar [55] in their study extracted starch from the kernel of three different Indian mango varieties by water extraction after sodium hydrogen sulfite treatment. The yields of the starches were 59.06%, 47.45%, and 48.42% respectively for *sindhoori, Totapuni* and *Bagenepalli* varieties. Cordeiro et al. [15] obtained a lower yield (32%) of starch from the Tommy Atkins mango variety. Their extraction process involved the treatment of seed kernel with sodium metabisulphite, followed by water extraction and NaOH treatment. Generally,

water extraction processes could result in substantial (<50%) removal of starch, however, some hemicelluloses (e.g., water-soluble xylan, storage xyloglucan, and mannan) are water-soluble, resulting in their loss when water is used to extract starch at the referred conditions. Hence, water extraction is not a suitable option for MSK starch removal before the fractionation of lignocellulosic components such as hemicellulose proposed in this study.

With the use of enzymes, literature studies have demonstrated that most or all of the starch content of biomass can be removed due to the substrate-specificity of the enzymes. In addition, enzymes hydrolyze the starch into oligomeric and monomeric glucose units with minimal effect on the hydrolysis of hemicellulose, lignin, and cellulose [69]. Some of the commonly employed enzymes for starch hydrolysis from agro-industrial waste are amyloglucosidase and α-amylase [69]. Amyloglucosidase and Termamyl SC from Novozymes have been used to achieve significant removal (≈100%) of starch [69], [267]. For example, Ceaser [69] removed almost all the starch in wheat bran by using Termamyl SC and Saczyme Plus enzymes. Thus, starch hydrolysis in the present study would be based on enzymatic hydrolysis using Termamyl SC and Saczyme plus enzymes.

2.9.3. Hemicellulose extraction

Using appropriate pretreatment methods and conditions could result in hemicellulose recovery in polymeric form (which has high economic value) for diverse applications [196]. The hemicellulose extraction is dependent on its source and level of interaction (through hydrogen and covalent bonding) with other biomass components of lignin, cellulose, proteins, among others [231]. Generally, due to their amorphous nature and low DP, hemicellulose requires less severe extraction conditions (lower temperatures such as room temperature and in some cases the use of water or low alkali concentrations <2M) to recover it in the polymeric form for applications such as biocomposite film development [74], [192]. For ethanol production, hemicellulose is required in the monomeric form and thus, high severities (high temperature, alkaline concentrations, longer reaction times) are applied during its extraction [268]. This means the end-use of the hemicellulose influences the selection of the extraction method and the severity of the extraction conditions.

For potential application in food packaging films, the purity of the hemicellulose should be considered due to its impact on the appearance of the films [42], [178]. In most cases, lignin is the main impurity since it leads to the production of brown and opaque films [42], [178]. However, other studies revealed that at least 1% lignin should be present in the hemicellulose (particularly xylan) to improve its film formation due to the plasticizing effect of lignin [42],

[178], [269]. In addition, Hansen et al. [270] asserted that although transparent films are desirable for food packaging, the present demand does not exclude brown films as they can be used as UV-barrier films [271]. Hemicellulose purities of ≤80% with lignin as the major impurity have been used in hemicellulose-based film formation [42], [178], [216]. However, due to the formation of less appealing brown films, lower severity conditions could be applied, and the process optimized to minimize lignin co-extraction. In addition, optimizing the hemicellulose extraction process conditions can result in significant improvement in the cellulose purity before nanocellulose production. Therefore, the selection of a pretreatment method should be based on the composition of the feedstock, type of hemicellulose to be extracted, target field of application of the hemicellulose, and the desired properties of the solid residue, one of which is to retain the lignin and cellulose in their intact forms in the solid residue (i.e. selective extraction of the hemicellulose) [236]. Several research works have focused on hemicellulose extraction from lignocellulosic biomass using various pretreatment/fractionation methods. The most common being dilute acid treatment, steam explosion, water extraction, and alkaline pretreatments [61], [83], [191], [272]. Table 2.6 shows a summary of hemicellulose extraction from various lignocellulosic biomass.

2.9.3.1. Dilute acid pretreatment

The use of dilute acid (1–4 wt% at 120–210 ºC for several minutes) pretreatments results in oligomeric or monomeric sugars of hemicellulose (mainly suitable for ethanol production or other microbial bioprocesses), partial disruption in the structure of lignin, and in some cases the degradation of amorphous cellulose depending on the severity of the operation [24], [236], [273]. The most common acid employed is sulphuric acid, although nitric, hydrochloric, and phosphoric acids have been used [145], [167]. Hemicellulose hydrolysis by acids involves the hydrolytic cleavage of the glycosidic linkages to give oligosaccharides and monosaccharides. The application of acids however is limited to the requirement of special reactors, cumbersome downstream processing, and cost implications [89]. Moreover, dilute acid pretreatment is associated with furfural, 5-hydroxymethylfurfural, and other degradation products generation, which affect the overall processing yields and cost [274], [275]. Therefore, acidic pretreatment was avoided in this study.

2.9.3.2. Steam explosion

Steam explosion (SE) works by breaking the glycosidic bonds in hemicellulose structure when biomass is heated in steam at temperatures between 160 °C to 240 °C under high pressures (7–50 bar) for a specified period (up to a few minutes) after which the pressure

is released to that of the atmosphere [89], [242]. Under high pressures, the steam condenses and acts as a solvent for the material, and the sudden release of pressure causes an explosion and rupturing in the cellulose fibers [276]. The combined effect of acetic acid production from hemicelluloses and the acidic nature of water at high temperatures reduces the pH of the reaction medium and (auto)catalyzes hemicellulose hydrolysis into oligomeric and monomeric sugars [275]. SE is not an appropriate method for this study since the hemicelluloses are recovered in the oligomeric and monomeric forms that are not suitable for application in biocomposite film development.

2.9.3.3. Ammonia Fibre Expansion

During Ammonia Fiber Explosion (AFEX), lignocellulosic biomass is treated with liquid anhydrous ammonia with pressure of about 17–20 bar and temperatures of 60–100°C for 5–30 minutes and pressure immediately released as in steam explosion. It is a low cost process since lower temperatures are used which helps lower the energy and capital involved. Moreover, upon expansion of ammonia, hemicellulose degrade to oligomers, lignin-polysaccharide crosslinks breakdown and cellulose decrystallizes partially, however little amount of lignin is degraded [277], [278]. Only a solid fraction is obtained during AFEX which is different from all the other pretreatment methods that results in the production of slurry containing both solid and liquid fraction [244]. Though there is the removal of only a small amount of lignin as compared to other processes, there is a possibility of obtaining about 90 % conversion of cellulose and hemicellulose [277]. Some advantages associated with AFEX are lower degradation of sugars, no inhibitory compound production and high reducing sugar yield of about 80-90 %. However, the use of high volumes of ammonia during AFEX increases the cost of production [278]. Due to the fact that hemicellulose is mostly recovered in monomeric forms which is not suitable for the envisaged application (in this case biocomposite films), this study did not consider it. Difficulty in scaling of process is also problematic due to high capital requirement for recovering/recycling the ammonia.

2.9.3.4. Alkaline pretreatment

Hemicellulose extraction using alkaline pretreatment (AP) before nanocellulose production presents advantages in the context of multi-product biorefinery due to the resulting high yields with less destruction in the molecular structure (i.e. high DP and *Mw*) [175]. In addition, the volume of chemicals that may be required in the subsequent multi-step fractionation stages could be reduced due to lesser interference resulting from the

hemicellulose removal [64], [102]. Compared to other pretreatments such as acid pretreatments, the AP uses less corrosive reagents like potassium hydroxide, sodium hydroxide, ammonia, sodium carbonate, and calcium hydroxide at milder reaction conditions (low concentrations, shorter reaction time, and low temperature) or severe conditions (high concentration, longer reaction time, and high temperatures) to separate hemicellulose and lignin respectively from cellulose [86], [279]. For the alkali reagents, sodium hydroxide (NaOH) has been recognized as one of the strongest alkalis that effectively solubilizes hemicellulose and lignin, thereby increasing the chemical and enzyme accessibility to cellulose [86], and is considered as an effective catalyst for the fractionation of both agro-industrial waste and hardwood [280]–[282]. Moreover, a report by Xu et al. [283] indicated that the use of NaOH in AP offers an advantage of working effectively at lower temperatures (below 30 ºC).

The AP affects the individual components of the biomass differently due to their structural variations and extent of reactivity with the alkali reagent [89]. Generally, the alkali in the reaction medium promotes deacetylation of hemicellulose, swelling of cellulose, removal of uronic acids, and cleavage of ester bonds between lignin and hemicellulose, resulting in partial hydrolysis of hemicellulose and lignin in the reaction medium [272], [284], [285]. Due to the presence of uronic acids, arabinose, and other substituents on the hemicellulose structure, minimal degradation occurs within its structure, and the hemicellulose in most cases are recovered in the polymeric form suitable for the development of hemicellulose-based biocomposite films, hydrogels, barrier films, among other bioproducts [42], [83], [285], [286]. In addition, the effect of alkali reagents on cellulose is generally less severe compared to other methods such as acids and hydrothermal [287]. Nevertheless, since AP is selective towards both lignin and hemicellulose [284], [288], various studies have proposed a delignification of the starting material (biomass) through bleaching processes to obtain a holocellulose to limit the interference of lignin for effective hemicellulose extraction [64], [289].

As an example, Höije et al. [290] used chlorite delignification to obtain holocellulose prior to AP (1 M NaOH, 16 h, 25 ºC) for hemicellulose extraction from barley husk and reported more than 50% recovery of the original hemicellulose in the biomass. Rabetafika et al. [64] on the other hand recorded a higher yield of 94.5% hemicellulose from pear pomace after alkaline treatment (2 M NaOH, 60 ºC, 18 h) of the holocellulose, which could be due to the higher NaOH concentration and temperature (high severity) employed compared to the 1 M and 25 ºC (low severity) used by Höije et al. [290]. Even though these studies reported high yields of hemicelluloses, bleaching processes cause oxidative degradation of the lignin and to

a certain level, degradation of hemicellulose (≈20% loss) [64], [284], [285], [291], thus inefficient use of the biomass resources. Thus, delignification prior to hemicellulose extraction is not an attractive process in the present study.

Due to the partial loss of hemicellulose and lignin during bleaching treatment prior to AP for hemicellulose extraction, various studies have extracted the hemicellulose from the untreated biomass to limit the loss of hemicellulose and lignin [43], [178], [292]. Svard et al. [43] obtained a hemicellulose yield of 47.0% with 13.0% lignin content from rapeseed straw using AP conditions of 1.5 M NaOH, 110 °C, and 1 h. Another report by Rabetafika et al. [64] revealed that the use of 4 M NaOH at 60 °C for 18 h to extract hemicellulose from pear pomace resulted in a yield of 61.7% with a lignin content of 14.9%. Both reports showed more than 10% lignin content in the hemicellulose extract which could be due to high severity operation (longer reaction time of 18 h, high NaOH concentration of 4 M, and high temperature of 110 ºC), which favor both hemicellulose and lignin extraction [209], [288], [293]. However, although lignin contents could be up to 15% during AP of untreated biomass, this method results in insignificant physical or chemical modification in the structure of the lignin, which makes it useful as a valuable bioproduct for further valorization unlike the bleaching process [64], [294].

The lignin contents in the direct AP extracted hemicellulose could introduce antioxidant, UV-light absorbent, resistance to water vapor permeability, and plasticizing effects into biocomposite films for food packaging application [214], [271]. Although purity is an important property to consider during biocomposite film development, hemicellulose composition (with residual lignin), molecular weight (M_w), and structure also contribute to the formation of the films [178], [295]. In the literature, approximately 1–20% of lignin could be applied in the development of hemicellulose-based biocomposite films for food packaging, although the films were reported to be brownish and unattractive to consumers, thus the lignin content could be minimized during extraction for such an application [42], [43], [216]. Due to the differing AP severity requirements for lignin and hemicellulose, selective extraction of hemicellulose from untreated biomass could be achieved by applying lower severities that limit lignin co-extraction..

Table 2.9: Hemicellulose extraction from various hardwood

Substrate (%)	Reaction conditions (%)	Solid yield (%)	Cellulose recovery (%)	Hemicellulose removal (%)	Lignin removal (%)	Major carbohydrate(s) in extract	Reference
E. *grandis*	2 M NaOH, 90 ºC, 240 min, 1:10 solid: liquid	63.40	73.54	16.00	13.17	Xylan	[238]
E. *grandis*	1 M NaOH, 90 ºC, 240 min, 1:10 solid: liquid	70.08	76.25	8.50	8.98	Xylan	
E. *grandis*	2 M NaOH, 40 ºC, 240 min, 1:10 solid: liquid	68.59	75.00	12.40	8.38	Xylan	
Giant bamboo	1 M NaOH, 90 ºC, 240 min, 1:10 solid: liquid	50.4	96.70	13.6	21.2	Xylan	
Giant bamboo	2 M NaOH, 90 ºC, 240 min, 1:10 solid: liquid	-	87.91	20.4	28.6	Xylan	
Sweet gum	2.63 M NaOH, 50 ºC, 180 min, 1:20 solid: liquid	73.4	88.31	56.68	10.71	Xylan	[284]
E. *nitens*	2.63 M NaOH, 50 ºC, 180 min, 1:20 solid: liquid	70.4	81.98	61.9	17.14	Xylan	
Maple	2.63 M NaOH, 50 ºC, 180 min, 1:20 solid: liquid	72.0	83.80	49.12	16.67	Xylan	
E. globulus	2.5 M NaOH, 100 ºC, 60 min, 1:10 solid: liquid	92.8	97.61	13.75	5.41	Xylan	[297]
Sweet gum	2.5 M NaOH, 60 min, 100 ºC, 1:10 solid: liquid	89.2	95.88	7.94	5.28	Xylan	
E. *grandis*	1.5 M NaOH, 90 ºC, 240 min, 1:10 solid: liquid	78.06	95.63	55.39	26.16	Xylan	[83]
E. *grandis*×*urophylla*	1 M NaOH, 120 ºC, 60 min, 105 kPa, 1:10 solid: liquid	63.4	100.85	12.35	40.72	Xylan	[298]
E. *grandis*	1.5 M NaOH, 90 ºC, 240 min, 1:10 solid: liquid	74.48	89.44	53.25	32.92	Xylan	[241]
E. *grandis*	2 M, 120 ºC, 90 min, 1:4 solid: liquid			15.15			[296]

AP has been documented to effectively isolate hemicellulose from both hardwoods species such as eucalyptus and poplar, and non-woody agro-industrial waste such as sugarcane bagasse, pear pomace, and wheat straw under milder reaction conditions [64], [84], [272], [294]. The MSH has similar physical characteristics as hardwoods whereas the MSK is less rigid with similar characteristics as other agro-industrial waste such as wheat bran, corn fiber, etc. [69], [235], [281]. Tables 2.9 and 2.10 show the AP of hardwood and agro-industrial waste and compare the qualities of the products as influenced by the severity of pretreatment. Generally, for the hardwoods, higher alkali concentrations (>1 M) and temperatures (>40 ºC) favored the hemicellulose dissolution due to hemicellulose susceptibility to such severe AP conditions. Table 2.9 further indicates that application of lower alkaline concentrations (<1.5 M) required either longer reaction times or higher temperatures to extract the hemicellulose. Vena et al. [286] reported a hemicellulose removal of 12.4% from *E. Grandis* at conditions of 40 °C, 240 min, and 2 M NaOH concentration. As compared to the result obtained by Vena et al. [286], Joubert et al. [296] were able to recover 15.15% of hemicellulose from the same type of feedstock, although at a higher temperature and reaction time (2 M, 90 min, 120 °C).

The use of higher temperatures and contact time (i.e. high severities) could be attributed to the higher lignin content (27.7%) of the feedstock due to the formation of lignin carbohydrate complexes (LCCs). It can be observed from Table 2.9 that, to achieve >50% hemicellulose removal from hardwoods using AP, ≥1.5 M alkali concentration and temperatures of ≥90 ºC or reaction times up to 4 h will be required, thus, affecting the severity of the AP process. For example, Pius [241] and Makhetha [83] removed up to 53% and 55% hemicellulose from *E. Grandis* only after the application of 1.5 M NaOH, 90 ºC and 240 min whereas, Geng et al. [284] had to increase the alkali concentration to 2.63 M, when the slightly lower temperature of 50 ºC and reaction time of 180 min were applied to achieve >50% hemicellulose (Table 2.9). Nevertheless, extending the reaction time to 240 min and temperature above 90 ºC resulted in up to 40% lignin removal (Table 2.9). Thus, for selective extraction of hemicellulose, temperatures of ≤90 ºC, NaOH concentrations less than 2.63 M, and reaction time of ≤4 h may be required. Further observations from Table 2.10 revealed that during the AP of agro-industrial waste, significant amounts (up to 85%) of lignin simultaneously solubilized with a significant amount of hemicellulose (up to79%), even under similar AP conditions to those applied for the treatment of hardwoods (Table 2.9). This could be due to less rigidity and less recalcitrant nature of the agro-industrial waste compared to hardwoods. It could therefore be

said that at lower severities, AP is more effective on non-woody agro-industrial waste versus the hardwoods.

AP results in alteration of the molecular weight (M_w), polydispersity (PDI), and DP of hemicellulose, and depending on the severity, different ranges of hemicellulose DP/*Mw* may be obtained. For potential use in the development of biocomposite films for food packaging applications, higher *Mw* (36684–91796 g/mol) hemicellulose has been reported to form self-supporting thermally stable films, whiles the lower *Mw* (30997–31105 g/mol) hemicelluloses results in brittle and thermally unstable films due to the extensive intermolecular and intramolecular H-bonding that occurs between the numerous hydroxyl groups [42], [46], [178], [299]. A study by Wei et al. [300] reported a molecular weight range of 79420–99960 Da of hemicellulose extracted from *Eucalyptus* species when 1M NaOH, 180 min, and 70°C conditions were applied. Júnior et al. [297] also reported recovery of hemicellulose with an *Mw* of 16000 Da from *Eucalyptus globulus* when AP conditions of 12.5 M, 100 °C, and 60 min were applied. Comparing the two reports, it could be deduced that a higher severity used by Júnior et al. [297] led to significant disruption of the hemicellulose macrostructure resulting in a much lower *Mw*, whereas a higher *Mw* resulted from the less severe conditions employed by Wei et al. [300]. This also implies a fewer number of bonds are broken in the presence of less severe conditions and justifies the use of less severity in this study for hemicellulose isolation since higher M_w and DP are expected. Work done by Egüés et al. [42] showed that low *Mw* hemicellulose extracts (30997 and 31105 g/mol) formed cracked films whereas high *Mw* hemicelluloses (91796–36684 g/mol) formed self-supporting and continuous films. Other literature studies have reported 2.64 M NaOH as the optimum concentration for the recovery of high *Mw* hemicelluloses [297], [301].

Tables 2.9 and 2.10 show that most of the hemicellulose polysaccharides extracted using AP were xylan with very few xyloglucan extracts, although this is feedstock dependent. In feedstock sources that contained mixtures of different hemicellulose types, the conditions were optimized to obtain differing optimum points that maximize the yield of each of the major hemicellulose types [61], [192], [261]. In other reports, separate extraction conditions are employed to obtain hemicellulose polymer comprising of the different hemicellulose types. However, optimizing the alkaline process conditions can result in a hemicellulose product with varied ratios of the hemicellulose types (due to structural differences and dissolution capacity in alkaline solution) and obtain a product with diversified functional properties for various applications.

Table 2.10: Hemicellulose extraction from various agro-industrial waste

Substrate (%)	Reaction conditions (%)	Solid yield (%)	Cellulose recovery (%)	Hemicellulose removal (%)	Lignin removal (%)	Major carbohydrate(s) in extract	Reference
Sugarcane bagasse	1.5 M NaOH, 1.53h, 1:10 solid loading, 65 °C	65.10	94.60	69.10	18.70	Xylan	[238]
Sugarcane bagasse	1.5 M NaOH, 1.53 h, 1:10 solid loading, 65 °C	59.31	95.50	71.17	65.72	Xylan	[83]
Corn Stover	2.5 M NaOH, 0.5 h, 1:10 solid loading, 160 °C, 200 rpm	50.7	89.67	36.56	67.05	Xylan	[305]
	1.75 M NaOH, 0.5 h, 1:10 solid loading, 140 °C, 200 rpm	63.1	92.49	23.90	62.70	Xylan	
	1.75 M NaOH, 0.5 h, 1:10 solid loading, 160 °C, 200 rpm	56.6	87.49	36.29	67.05	Xylan	
	2.5 M NaOH, 0.5 h, 1:10 solid loading, 140 °C, 200 rpm	53.5	91.56	31.18	84.78	Xylan	
Sugarcane bagasse	0.2 M NaOH, 121 °C, 1 h, 105 kPa	83	98.30	49.40	63.80	Xylan	[306]
	0.25 M NaOH, 121 °C, 1 h, 105 kPa	63.00	81.90	65.00	79.50	Xylan	
Rice husk	2.08 M $(NH_4)_2CO_3$, 1:10 solid: liquid, 80°C, 12 h	65.9	92.3	17.4	23.9	Xylan	[307]
Rapeseed straw	0.5 M NaOH, 1:10 solid: liquid, 105 °C, 1 h	-	-	21	6.8	Xyloglucan	[178]
	Distilled water, 1:10 solid: liquid, 105 °C, 1 h	-	-	5	11.7	Mannan, xyloglucan	
Hymernaea courbaril var. courbaril seeds	0.5M NaCl, 1:15 solid ratio, 25 °C, 20 min	–	–	72.5	–	Xyloglucan	[308]
Tamarind seed	Distilled water, 100 °C, 6h	–	–	20.0	-	Xyloglucan	[192]
Grape pomace	2.25 M KOH, 1:57 solid: liquid, 2.9 h	-	-	7.9	-	Xyloglucan	[61]
	2.2 M KOH, 1:58 solid: liquid, 2.7 h	-	-	3.6	-	Mannan	
	2.3 M KOH, 1:60 solid: liquid, 3 h	-	-	1.2	-	Xylan	

The mango seed contains hemicellulose polymers including xyloglucan and xylan [45], [106], [302]. Since each of these hemicellulose types solubilize under different extraction conditions [(storage xyloglucan; in water or >1M NaOH, xylan; up to 2.5M NaOH) (Table 2.9), the extraction medium can be designed such that different ratios of these components can be obtained with properties (molecular weight, thermal stability) that can diversify the functional properties of the resultant biocomposite film.

For most of the results presented in Tables 2.9 and 2.10, the cellulose retained in the solids after the AP process for both hardwood and agro-industrial waste was high (>80% of the cellulose in the initial biomass). The high retention of cellulose in the biomass after AP is attractive considering minimal cellulose losses imply high cellulose yield for nanocellulose production. Further observations showed that increases in AP severity (NaOH concentration and temperature) caused an increment in cellulose degradation (Tables 2.9 and 2.10). High AP severities (NaOH concentration >1.5 M, temperature >100 ºC) affect the structure of cellulose by causing swelling in the amorphous cellulose fibers and disruptions in the intermolecular/intramolecular H-bonding in the crystalline portion [303], [304]. Thus, the AP leads to a decrease in the DP of cellulose, whiles the removal of the amorphous hemicellulose increases the Crl, surface area, and porosity depending on the treatment conditions applied [86].

The DP of cellulose reduced by ≈8% when p*opulus* was treated with NaOH for 2 min at 120 ºC, and the reduction in DP further increased to 61 and 76% when the time was extended to 10 and 60 min respectively, thus the increased severities enhanced cellulose accessibility to chemicals and enzymes by reducing the DP [304]. A study by Bali et al. [236] disagreed with the reported increase in Crl of cellulose after AP. They reported that after AP (0.53 M NaOH, 120 ºC, 2–60 min) of different feedstock, less-crystalline cellulose II allomorph fibers were obtained. The Crl of the AP pulp was reduced to 52–54% from Crl of 55% for the untreated biomass. High severities disrupt the crystalline cellulose structure with subsequent conversion into an amorphous portion (from cellulose I to cellulose II) [303]. Nevertheless, a decrease or increase in cellulose Crl depends on the source of biomass and the severity of the AP conditions. In the literature, the AP of different biomass for nanocellulose production were performed at temperatures of ≤100ºC, NaOH concentrations of up to 5M, and reaction time of 4 h [20], [97], [152], [240]. The above conditions are overlaps of treatment conditions that favor both lignin and hemicellulose

solubilization, and the partial degradation of cellulose (Tables 2.9–2.10). Therefore, in the multi-step biorefinery approach, milder treatment conditions would be preferable.

2.9.4. Lignin extraction

Other than hemicellulose, the difficulty in obtaining cellulose from biomass is attributed to lignin since lignin acts as a protective barrier, preventing cell wall destructions by microbes and chemicals [89], [304]. Hence, isolating lignin is mandatory to improve the accessibility of cellulose for further valorization into nanocellulose during downstream processing. Whereas lignin is less essential in nanocellulose production for application in biocomposite for food application, its extraction in a more purified form could open avenues for valorization into high value-added materials such as phenol-formaldehyde resins and carbon fibers [145] while reducing the resistance in biomass for nanocellulose production. Lignin in a more purified form (purity >90%) could open avenues for valorization into high-value products such as phenol-formaldehyde resins, plasticizers, and antioxidants [145], [309]. The most common methods used in the industry for lignin extraction are the Kraft, lignosulfonate, and soda methods [85]. The Kraft lignin is however modified with aliphatic thiol groups, reducing its quality for many applications [239]. The soda and lignosulfonate lignin also contain high ash and sulfur contents, respectively.

Consequently, one of the limitations of the industrial application of lignin is due to these high impurities [201]. It is worth noting that the method for lignin extraction should not only be effective in isolating high quantities of lignin from the biomass but should also produce lignin with valuable qualities (high purity, lower molecular weight, and less condensation) for further valorization. Considering the recent growing interest in commercial utilization of cellulose and lignin derivative products, there is a need to develop pretreatment techniques that can generate less condensed and high purity lignin while obtaining the cellulose for nanocellulose production [124]. Lignin extraction methods have been presented in the literature, including the alkaline and organosolv pretreatment methods [88], [213], [228]. The alkaline methods, discussed in section 2.9.3.4, favor both lignin and hemicellulose dissolution. The use of alkali for delignification purposes requires high pH values (pH 12–13) such that the acetic acid released due to cleavage of acetyl groups of hemicelluloses do not continually neutralize the solution [85], [213]. Most alkaline extracted lignin has low purity due to the co-extraction of carbohydrates and ash unless most of the hemicellulose is selectively pre-extracted prior to lignin extraction using lower severities [69]. The organosolv pretreatment is a promising pretreatment/fractionation method that

has been discovered to produce purified lignin and a cellulose-rich pulp with easy accessibility to enzymes and chemicals for further valorization [310].

2.9.4.1. Organosolv pretreatment

Due to its efficiency in obtaining a range of products, the organosolv pretreatment (OP) process has received attention recently. Various reviews on the OP using different reaction conditions have been presented in the literature [14], [68], [85], [242], [311]. Organosolv is a pretreatment/fractionation method that uses organic solvents or their aqueous mixtures to dissolve and separate largely lignin or co-extract hemicellulose and lignin (when acidic or basic catalysts are added) from biomass, and in so doing increasing the accessibility of cellulose to enzymes and chemicals for further valorization [88]. The resulting pulp after the OP presents increased surface area, increased cellulose content, reduced cellulose DP, and high pore volume with less recalcitrance to subsequent processing [312]. The lignin obtained has a lower molecular weight, high purity, high phenolic aromatic rings with more reactive sites (based on the conditions of operation), thus could be used for producing bio-based chemicals, plasticizers, and phenol-formaldehyde resins [14], [88], [212], [313]. Figure 2.4 shows a typical OP of lignocellulosic biomass to obtain cellulose solids, hemicellulose sugars (based on reaction conditions), and high purity lignin.

Different organic solvents have been applied in the OP, which includes high boiling point alcohols (glycerol, propylene glycol, and ethylene glycol), low boiling point alcohols (ethanol and methanol), and organic acids (performic acid, formic acid, peracetic acid, and acetic acid) [89]. Ethanol and methanol are mostly preferred because they are less costly, have higher water solubility, and are easy to recover by distillation at lower temperatures [87], [242]. The boiling points of methanol and ethanol are 64.7°C and 78.37 °C respectively while that of water is 100 °C. The difference between the boiling point of water and these alcohols makes them easy to be recovered and reused [311]. From Table 2.11, the solvent concentration of 50–80% v/v (60% mostly preferred) at temperatures of 180–250 °C (due to the highly volatile nature of the lower molecular weight alcohols) under pressures of 5–30 bar for 15–120 min are usually employed in OP [87], [89], [242]. In cases where the temperature is below 180 °C, catalysts are added to facilitate the process of lignin removal from the biomass [213], [214], [314], [315]. The different catalysts used in OP include sodium hydroxide, calcium hydroxide, hydrochloric acid, sulphuric acid, magnesium chloride, calcium chloride, magnesium nitrate, formic acid, oxalic acid, and

acetic acid [85], [88], [89], [96], [212], [278], [310]. The concentration and type of catalyst significantly influence the product's yields, product degradation, the formation of inhibitory products, and whether hemicellulose is extracted as polymers, oligomers of monomers.

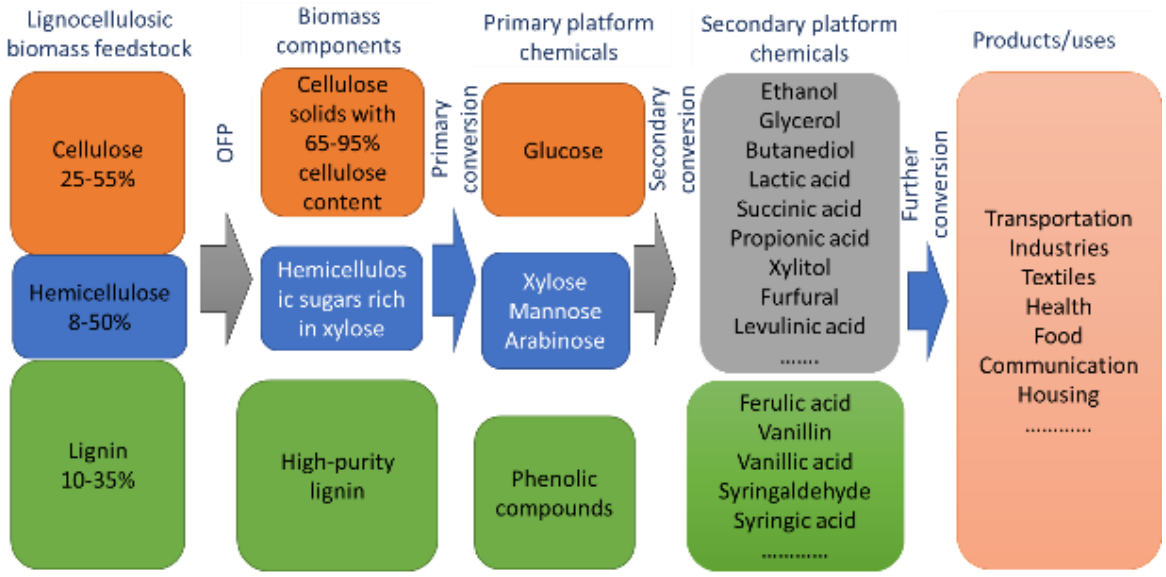

Figure 2.4: Biorefining of lignocellulosic biomass based on organosolv fractionating pretreatment (Redrawn from Zhao et al., [310]). *OFP- Organosolv fractionating pretreatment

For example, Wildschut et al. [213] compared the optimization of acid-catalyzed and non-catalyzed organosolv processes for wheat straw delignification. At the optimized condition for the non-catalyzed organosolv process (210 °C, 50% EtOH, 1:10 solid: liquid ratio), the lignin yield was 84% accompanied by 86% sugar recovery. The acid-catalyzed OP at optimum process conditions of 30 mM H_2SO_4, 190 °C, and 60% EtOH, gave similar yields of lignin and sugar recovery. Thus, the addition of a catalyst allowed the use of lower temperatures. Raita et. al. [316] investigated the impacts of different alkaline catalysts (NaOH, NH_4OH, and tri-ethylene) on the delignification rate of rice straw and the effect on glucose yield from the resultant pulp in the organosolv process. Adding NaOH catalyst resulted in the highest sugar yields of 86.5% with glucose accounting for more than 95%. An increase of about 5.9-fold in sugar yield was achieved when compared to the control (no catalyst). Furthermore, the NH_4OH and ethylene catalysts were less effective, leading to only a 2-fold increase in sugar yields when compared to the control [316].

During OP using mild organic solvents such as methanol or ethanol, the reaction of lignin and hemicellulose involves a chemical reaction that leads to different levels of solubilization of these two components. The hemicellulose dissolution occurs through the partial hydrolysis of acetyl groups and uronic acids from hemicellulose, which is followed by hydrolysis of the glycosidic linkages within the hemicellulose structure [89], [241], [310]. The lignin fragmentation and dissolution through OP are largely dependent on the cleavage of the ether linkages in the lignin structure. The fragmentation will expose more hydroxyl groups and make the lignin more reactive for its intended application. The α-ether linkages are more easily cleaved than the β-linkages. Nevertheless, the β-O-4 ether linkages which form a majority (40–65%) of the lignin linkages need to be cleaved for lignin to fragment and solubilize for recovery. Breaking of the β-O-4 ether linkages follows the mechanism described by McDonough which involves: (1) the solvolytic cleavage with formaldehyde removal, (2) solvolytic, and homolytic cleavage to form Hilbbert's ketone or, 3) through benzyl carbocation formation [2], [215], [312].

The α-ether linkages are broken through the formation of benzyl carbocation, solvolytic cleavage through SN2 nucleophilic substitution, and quinone methide substitution [2]. After breaking the ether linkages, new phenolic groups are generated. In an acidic medium, pseudo lignin is formed by the reaction of the degraded sugar products with the depolymerized lignin [310]. Moreover, condensation reactions (an undesirable side reaction) involving the reaction of depolymerized lignin fragments through intermolecular bonding with lignin on the surface of the solid substrates also occur in the presence of acid catalysts. This results in less dissolution of lignin and subsequently low recovery yields [2]. To prevent condensation reactions, acid catalysts are excluded from this study.

Unlike lignin and hemicellulose, the reaction between cellulose and organic solvents such as ethanol follows a physical process that is limited to cellulose swelling [123], [241], [322]. Thus, after the OP, cellulose-rich solids (Table 2.11) are obtained by removal of the spent liquor and successively washing of the solids with hot ethanol (heated to 40 °C) and then with warm water to remove the remaining ethanol. The spent liquor, comprising of the organic solvent, lignin, hemicelluloses, and degraded products (e.g., furfural, hydroxymethyl furfural (HMF), acetic acid), is distilled to recover the organic solvent. The lignin is then precipitated from the solvent-free liquor by acidification followed by vacuum filtration and drying. The hemicelluloses, acetic acid, furfural, and HMF remain in the water-soluble fraction [89], [213].

Table 2.11: Lignin extraction from various lignocellulosic biomass

Substrate (%)	Treatment conditions (%)	Solid yield (%)	Lignin removal (%)	Hemicellulose removal (%)	Cellulose recovery (%)	Reference
Wheat straw	60% EtOH, 1h, 200 °C, 1:10 solid ratio	67.70	46.30	3.70	97.00	[213]
Pretreated Rice husk	70% EtOH, 1.5h, 200°C, 1:15 solid/liquid ratio,	-	58.58	2.67	-	[212]
Organosolv waste	0.2% NaOH, pH 11, 6 bar O_2 atmosphere, 98 °C, 60 min	-	22.47	8.97	-	
Bleached waste	0.2% NaOH, pH 11, 6 bar O_2 atmosphere, 98 °C, 60 min	56.00	12.04	12.32	-	
Wheat straw	50% acetone, 205°C, 1:7.04 solid ratio,	48.70	78.83	1.94	92.05	[317]
Wheat straw	50% acetone, 190°C, 1:7.04 solid ratio,		71.76	-	92.09	
Wheat straw	60% EtOH, 60 min, 200 ºC, 1:10 solid ratio	63.20	58.60	7.80	96.8	[91]
Wheat straw	50% EtOH, 90 min, 210 ºC,	48.6	83.10	2.00	94.8	
Prehydrolyzed *E. globulus*	60% EtOH, 200 ºC, 11%solid loading	68.6	70.72	43.76	95.01	[318]
Sugarcane bagasse	50% EtOH, 175 ºC, 90 min, 1.5% NaOH, 17% solid loading	73.33	20.76	1.02	88.25	[319]
Sugarcane bagasse	50% EtOH, 175 ºC, 60 min, 1.5% NaOH, 17% solid loading	60.37	44.31	1.09	70.90	
Rice straw	75% EtOH, 150 ºC, 1.0% H_2SO_4, 60 min, 11% solid loading	76.80	39.46	45.03*	85.54	[320]
Buddleja davidii	50% EtOH, 180 ºC, 1.25% H_2SO_4, 60 min, 1:10 solid: liquid	61.95	23.50	45.50	84.95	[321]
	65% EtOH, 195 ºC, 1.75% H_2SO_4, 40.2 min, 1:10 solid: liquid	47.05	74.58	32.83	86.06	
Hybrid poplar	50% EtOH, 180 ºC, 1.25% H_2SO_4, 60 min, 1:10 solid: liquid	52.72	74.13	52.49	88.17	[214]

Organosolv is versatile and has been applied to pretreat different feedstock such as softwood, grasses, agricultural waste, and hardwoods [62], [83], [214], [278]. For instance, Manara and co-workers [323] extracted lignin from the olive kernel, grape pomace, and peach kernels using similar organosolv process conditions. The delignification of the peach kernel was reported to be the highest (15.7%), followed by olive (9.1%) and grape pomace (0.6%). Peach kernel and olive kernel lignin had purities above 95%. The cellulose pulp yields were 67.1%, 75.0%, and 67.1% for peach, olive, and grape pomace, respectively. Grape pomace presented the lowest lignin yield; however, its pulp recovery was the lowest. The pulp recovery for peach was higher than that of grape although peach gave the highest delignification rate, which could have resulted from the severe degradation of components of the grape kernel that could not be accounted for under the conditions investigated. Therefore, different biomasses respond differently to OP conditions due to the differences in compositions, types of side chains, and degree of side-chain substitution [323].

In a multi-step biorefinery for multi-product recovery from mango seed, although OP could be applied for the lignin removal, applying acid catalysts could lead to the hydrolysis of the hemicellulose into monomeric sugars and degradation products (e.g. furfural and 5-hydroxymethylfurfural) [87], [89], [96], [324]. The exception is alkaline catalysts such as NaOH which allows the recovery of polymeric or oligomeric hemicellulose sugars, although very few research works used alkaline catalysts due to their less effectiveness in hydrolyzing the β-O-4 ether linkages in lignin compared to the acid catalyst, resulting in lower lignin yields [311]. Presently, there are limited applications of OP on a commercial scale (the organocell at Kelheim, Germany), yet the potential of organosolv in pretreating biomass motivates various companies to perform the process on a pilot scale. Examples are the pilot-scale formic and acetic acid-based organosolv processes in CIMV in Pomacle, France, and Dedini in Brazil respectively, and the ethanol-based process of Lignol in Burnaby, British Columbia, Canada (former Alcell® process) [91], [312].

2.10. Combination of pretreatment methods for lignin extraction

As shown in Table 2.11, OP is usually performed at high temperatures (>170 °C) for base or acid-catalyzed hydrolysis, and up to 210 °C for auto-catalyzed reactions, to achieve maximum delignification. Although high cellulose-rich material can be recovered in severe conditions, the energy consumption by these processes is very high for commercial-scale implementation [310]. In addition, the recovered lignin is highly modified while the hemicellulose is degraded into undesired products (e.g. HMF). Thus, to alleviate these issues, some studies combined the OP with physical/mechanical processes or physicochemical pretreatments such as ultrasonication and steam explosion, among others [62], [68], [325]. In the work of Matsakas et al. [68], combined organosolv and steam explosion (15–60 min, 200 ºC, 52–65% ethanol, and H_2SO_4 ;0–1%w/w biomass) was used for delignification of Norway spruce. It was established that combining the two methods led to a high yield of cellulose-rich material (72%). The delignification rate was found to be high (79.4%). In all the treatments, no significant cellulose solubilization was observed, but hemicelluloses in the solids decreased by 18.8% (after 15 min), 15.4% (30 min), and 9.6% (60 min). Li et al. [325] combined ultrasound pretreatment with ethanol/methylbenzene organosolv process to increase the delignification efficiency of *Neosinocalamus affinis*. In the first stage, a ball-milled feedstock was subjected to ethanol OP (95% EtOH, 5 min, 20 °C) followed by ultrasonication [325]. The results showed an increase in ethanol-soluble components after ultrasonication when compared with the organosolv without ultrasonication. The lignin yields were found to increase with an increase in ultrasonic time from 38.66 (0 min) to 62.13% (50 min). They concluded that the increase in lignin yield was a result of the action of the ultrasonication, which improved the surface area and pore volume of the biomass enhancing the accessibility of components by the solvent.

A two-stage OP was employed by Sun et al. [326] to pretreat tea oil fruit hulls in a biorefinery. The first process was a combination of OP (mild aqueous conditions: 70% EtOH, 70 °C, 1.5 h) and ultrasonication. The second stage involved only OP. The application of ultrasound led to a recovery of approximately 70% solids after the first stage. After the second stage, (severe organosolv process: 70% glycerol, 1:20 solid/liquid ratio, 1atm) solid recovery of 45% accompanied by 35% lignin and 40% hemicellulose were recorded [326]. The recovered solids had >95% cellulose digestibility. Therefore, combining OP with mechanical/physico-chemical or physical treatment processes improves the rate of lignin dissolution and accessibility

of chemicals and enzymes to cellulose, however, the application of ultrasonication is expensive and not industrially sustainable.

High shear homogenization (HSH) is a technique that employs mechanical shear and cavitation similar to sonochemical treatment to treat biomass. The HSH is an economical and efficient processing method employed purposely for the emulsion and dispersion generation of biological tissues [327]. Figure 2.5 shows a schematic presentation of the operation of the rotor-stator HSH. It consists of a stator with a slant or vertical slots around the homogenizer cell and a rotor with either two or more blades. The rotor is positioned concentrically inside the stator (Figure 2.5). The HSH uses mechanical shear and cavitation to disrupt the cell wall of biomass [94]. It works by pulling up materials into the equipment with the help of a rotating blade, followed by scissor-like mechanical shearing (which takes place within the gap between the stator and rotor), and cavitation leading to breaking and reduction in the particle size of materials [95], [328]. As the rotor rotates, a vacuum is created which draws the mixture in and out of the homogenizer, resulting in circulation [328]. With its open configuration, the HSH allows repeated circulation of the sample. Additionally, due to the variable diameters of the probe, even high viscosity samples with volumes ranging from 0.01 mL to over 60000 L can be processed without clogging [327]. This technique, despite its distinctive effectiveness, is yet to be widely applied for biomass pretreatment probably due to the generation of minor heat, which may pose safety issues, especially with flammable organic solvents. Nevertheless, this issue can be eliminated by operating in well-ventilated areas and with the use of ice baths [327]. Considering the effectiveness of OP and HSH, it is anticipated that integrating these two processes would provide a cost-effective industrial method for producing purified lignin from mango seed at lower operating temperatures versus other methods. Thus, a combination of these processes will be employed in this study to delignify the mango seed. There is limited information on the application of OP in mango seed valorization in the literature. In addition, no reported literature exists on the fractionation of mango seed using the hybrid OP and rotor-stator HSH to recover lignin and cellulose-rich solids.

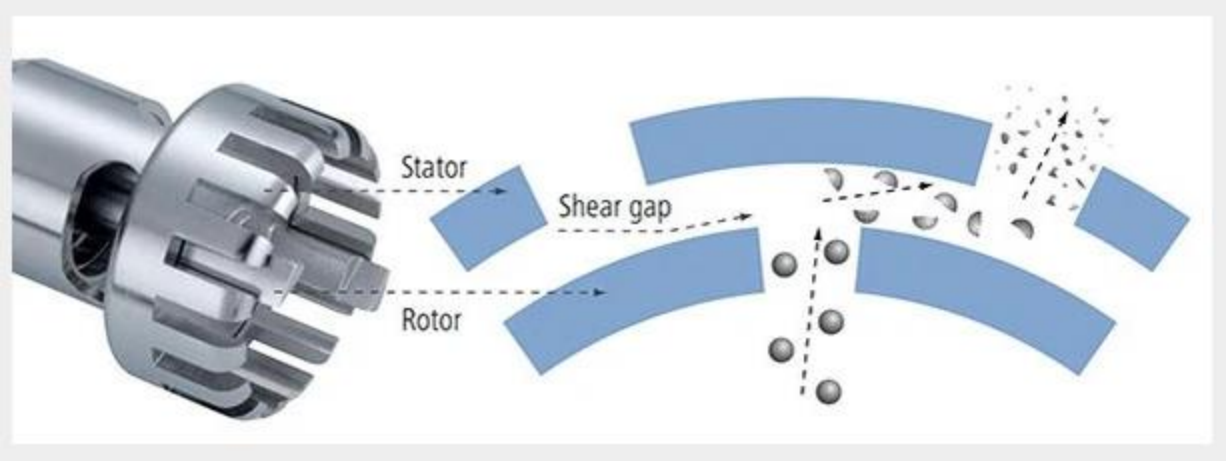

Figure 2.5: Schematic representation of the configuration of a rotor/stator homogenizer. Adapted from O'Driscoll [329].

2.11. Multi-step biorefinery of lignocellulosic biomass

Different pretreatment methods have been used to improve the cellulose content and its accessibility to chemicals and enzymes for conversion into nanocellulose. Each of these pretreatment methods impacts differently on the structure of the biomass and to a large extent on all the subsequent stages of the biomass conversion process, i.e., energy requirement, severity of process conditions, product recoveries, and quality, in addition to the formation of degradation products from hemicellulose and cellulose sugars [76], [89]. Based on work done by Siro´and Plackett [330], the energy consumption during mechanical fibrillation of cellulose could be reduced by 20–30 folds if an efficient pretreatment/fractionation process is used. Choosing an appropriate pretreatment method could increase the cellulose inner surface area, breaks hydrogen bonds, alter the crystallinity, and improve cellulose reactivity, thus, lowering the energy requirement of the nanocellulose production process [331]. However, these pretreatment methods are unable to effectively remove lignin and hemicellulose when applied individually and their sole application is expensive and time-consuming [231], thus, combining such methods in a multi-step biorefinery process to efficiently extract each of the biomass components in its intact form while obtaining the cellulose-rich material with improved accessibility is essential. It is worth noting that the choice of the pretreatment process, combination, and sequence is dependent on the source of the cellulose, its crystallinity, and desired morphology for further treatment into the nanocellulose [331]. In the present study, the main aim is to obtain a cellulose-rich pulp with cellulose content

and crystallinity of ≥60% and ≥55% respectively while minimizing cellulose degradation to <20% and recovering other products of hemicellulose, polyphenols etc. [37], [98], [196], [332].

The main feature of the multi-step biorefinery process is that it limits cross-contamination of products while minimizing the conversion of the hemicellulose and cellulose into simple sugars and degradation products albeit depending on the chosen severities and sequence of steps for the individual pretreatment methods. It could also limit the quantity of chemicals required in subsequent stages of the process [73], [76]. Furthermore, lignin, cellulose, and hemicellulose fractions could be obtained in solid form for the intended applications. Finally, both the structural and non-structural biomass components can be recovered and in a much purer form since there would be fewer interfering compounds and therefore the potential to increase the value of the bioproducts [76], [102], [333]. Several authors [76], [101], [102], [334], [335] have used multi-step biorefinery approach to obtain various bioproducts from biomass. Papatheofanous et al [101] used a multi-step process that involved a mechanical/chemical fractionation process to separate wheat straw into lignin oligomers, hemicellulose sugars, and cellulose fibers and compared with a single step process. They reported that the use of a single-stage alkaline treatment after a mechanical treatment resulted in lower yields (12.2%) of hemicellulose. However, when there was a subsequent introduction of alkaline aqueous ethanol step, hemicellulose yield increased to 88.7%. In addition, an increased hemicellulose yield was observed when acidic treatment was performed in a two-stage process instead of one before aqueous ethanol treatment. Following this, lignin fractionation was improved yielding 70.0% which further resulted in high cellulose content in the residue. In all, three different products, including hemicellulose sugars, lignin, and cellulose were obtained in high yield, though hemicelluloses were obtained in oligomer/monomeric form.

Michelin et al. [102] also showed that the use of multi-step hot water fractionation, enzymatic saccharification, and fungal fermentation on corncobs resulted in the production of multi-products including xylooligosaccharides, enzymes, fermentable sugars, and lignin. Varavadekar et al. [336] developed a multi-step process to fractionate groundnut husk, cotton stalk, and coconut shell into three streams of cellulose, lignin, and hemicellulose. They first pretreated the biomass (under alkaline conditions) and optimized the process conditions for the selective hemicellulose extraction without cellulose degradation (leaching). The recovered alkaline treated solids were subjected to an acidic treatment under conditions of varying reaction time, biomass loading, temperature, and concentration of acid, and the process optimized for the recovery of

cellulose (in soluble form) and lignin. The cellulose and hemicellulose streams were further subjected to enzymatic saccharification using commercial soluble cellulase and hemicellulase, respectively. The results indicated that almost all the hemicellulose (100%) in the biomass was recovered in the first stage of the process using the alkaline treatment. The subsequent acidic treatment of the alkaline treated pulp resulted in 100% and 95% cellulose and lignin recoveries, respectively. Finally, enzymatic hydrolysis of cellulose and hemicellulose streams led to 70% and 99% conversion into glucose and xylose, respectively. It was concluded that the multi-step alkaline, acidic, and enzymatic process could separate lignocellulosic biomass into the main components of cellulose, lignin, and hemicellulose, accompanied by high cellulose conversion into simple sugars.

Another study by Castro and colleagues [76] combined a mild alkaline pretreatment with dilute acid pretreatment in a multi-step process to valorize rice straw in a biorefinery. The alkaline pretreatment process conditions of NaOH concentration (20–80 mg NaOH/g biomass), and temperature (50–70 ºC) were optimized in a central composite design to remove acetyl groups and determine how this treatment step affects the composition of the biomass. The alkali-treated solids were then subjected to acid pretreatment varying sulfuric acid concentration (0.5–1.5% w/v) and reaction time (30–90 min). The results showed that the multi-step alkaline and acid pretreatments led to significant improvement in the xylose ethanol yield (about 4-folds) when treated with *Scheffersomyces stipitis* NRRL Y-7124 enzyme. The enzymatic hydrolysis of cellulose to simple sugars was enhanced from 73 to 89% when the deacetylated cellulignin solids were used. This also increased the cellulosic ethanol production from 12.7 to 20.4 g/L during the simultaneous saccharification and fermentation with *Kluyveromyces marxianus* NRRL Y-6860.

Guo et al. [73] in addition employed a multi-step acidic (temperature;130–190 ºC, H_2SO_4 dosage; 0.25–1.25wt% and time; 5–45 min) and alkaline [(temperature; 175–245 ºC and $Ca(OH)_2$ concentration; 0-0.08 g biomass at 30 min)] pretreatment process with further optimizations to recover pentose and hexose sugars. In the first stage, a low severity acid pretreatment was employed followed by a harsh alkaline pretreatment. The results indicated that the multi-step acid pretreatment conditions of 0.73 wt% H_2SO_4, 6.1 min and 150 °C and alkaline pretreatment conditions of 202 °C, 0.024 g lime/g biomass and 30 min resulted in >70% hemicellulose and 80% cellulose recoveries, which further improved the ethanol yield up to 0.145 g/g biomass (*Miscanthus*). They attributed the improvement in the ethanol fermentation yield to the reduced

formation of inhibitory products like phenols and furans and concluded that instead of using the single-stage pretreatment to obtain one sugar product, the multi-step process could achieve the recovery of both xylose and glucose sugars in high yields while reducing inhibitory product formation during ethanol production.

Based on the results, a multi-step biorefinery process can lead to the recovery of multi-products from the same feedstock while improving subsequent treatment processes and product yields. However, the use of such processes on mango seed is limited. In most of the reported multi-step biorefinery approaches, the hemicellulose and cellulose were recovered in the monomeric sugar forms for ethanol production due to the severity of the treatment conditions applied. In addition, the multi-step processes have been applied on feedstock such as rice straw, coconut shell, groundnut husk, and wheat straw with limited information on MSH and MSK. The following sections thus discuss how the mango MSK and MSH can be fractionated into polyphenol, hemicellulose, lignin, and cellulose-rich fibers in a multi-step biorefinery scheme in addition to the conversion of the cellulose into nanocellulose. The objective of the multi-step biorefinery scheme is to obtain high activity polyphenols, polymeric hemicellulose, high purity lignin, and a pulp rich in cellulose (≥70%) while minimizing cellulose degradation for nanocellulose production (section 2.10).

2.12. Fractionation of mango seed into a cellulose-rich pulp and valuable bioproducts: The multi-step biorefinery approach

The mango seed (husk and kernel) presents both advantages and limitations as a bioresource for multi-product generation in a multi-step biorefinery scheme. This is due to component heterogeneity, low accessibility of cellulose by chemicals, sheathing of cellulose by hemicellulose, and protection of cellulose by lignin [10], [145]. Additionally, for an objective of fractionating the mango seed waste into the multi-products, including the polyphenols, starch, hemicellulose, lignin, and cellulose (for nanocellulose), due to the overlapping extraction conditions for some of the products (e.g., the polyphenols vs starch, hemicellulose vs lignin) (Section 2.9), obtaining the cellulose-rich pulp under conditions that will also ensure minimal losses of the other products could be a challenge. For sustainable value addition to the mango seed and to selectively recover cellulose and other valuable bioproducts, adjustments could be made to a selected number of the existing individual pretreatment/fractionation processes highlighted in section 2.9 which can then be integrated into a multi-step biorefinery process. The non-cellulosic

components that are easily degraded (polyphenols, starch, and hemicelluloses) can be extracted first, followed by the components that are more stable while ensuring minimal cellulose degradation. This multi-step process could ensure the recovery of the majority, if not all, of the mango seed valuable components [101], [102], [337].

To achieve this, the economic and industrial feasibility of the pretreatment/fractionation processes should be considered. Organosolv extraction process has been applied extensively for the recovery of polyphenols (free extractable polyphenols), whereas enzymatic hydrolysis has proven effective for the removal of starch with minimal degradation of the hemicellulose, cellulose, and lignin (section 2.9.1–2.9.2). Mild alkaline pretreatment has been demonstrated to be effective for the extraction of hemicellulose polymers and bound polyphenols while ensuring the recovery of the lignin and cellulose as non-degraded polymers in the solid residue (section 2.9.3). The lignin of high purity in addition to cellulose-rich pulp has also been recovered using organosolv pretreatment and in some instances its combination with physical/mechanical or physicochemical treatment processes (section 2.9.4). Based on these, the mango seed could first be separated into seed kernel and husk, followed by mechanical size reduction to increase the biomass surface area. For the MSK, a multi-step biorefinery process that involves three major stages is proposed:(1) Organosolv extraction (OE) for the recovery of free polyphenols and solid residue; (2) enzymatic hydrolysis (EH) of the recovered OE solid residue to remove starch and recover destarched solids; and then (3) mild alkaline pretreatment (AP) of the destarched solid residue to recover hemicellulose/bound polyphenol (bioactive hemicellulose) while ensuring minimal cellulose and lignin degradation. For the MSH, a multi-step biorefinery process that consists of two major stages could be applied: (1) Mild AP for hemicellulose polymers and solid residue, followed by (2) a high shear homogenization organosolv (HSHO) process of the residual solids for lignin and cellulose-rich fiber recovery.

2.13. Treatment methods for nanocellulose production from cellulose-rich pulp

After obtaining a cellulose-rich pulp through pretreatment/fractionation processes, further treatment is required to obtain nanocellulose as previously indicated in section 2.9. Different cellulose treatment methods have been applied to produce nanocellulose. These methods include mechanical (micro fluidization, grinding, and homogenization), biological (enzymatic treatment), and chemical (acid hydrolysis and oxidation), which can be used individually or in combination with each other [28], [338]. Some of the basic qualities of nanocellulose for most applications

include colloidal stability (attributed to the surface charged groups on the nanocellulose), morphology, polydispersity, crystallinity, thermal stability, and dimensions [97], [167], all of which are dependent on the properties of the starting material (e.g. cellulose content and crystallinity), pretreatment process (cellulose purification), nanocellulose treatment and post-treatment processes [97]. Table 2.12 shows some of the properties of the starting cellulose-rich pulp, some treatment processes used in the nanocellulose preparation, and the properties of the produced nanocellulose. Generally, cellulose-rich pulps with cellulose contents in the range of 65.6–95.2% and Crl of 57.0–74.3% have been used to produce nanocellulose using the different treatment methods (Table 2.12).

2.13.1. Chemical treatments

Acid-based treatment is the most commonly employed chemical treatment method for producing CNC due to its efficacy in removing amorphous cellulose [339]. Sulphuric acid is the most preferred acid for CNC production because of the applicable conditions of lower temperatures (30–60 °C) and shorter reaction times (30–60 min) and up to 65 wt% sulphuric acids [20], [40], [115]. In the acid treatment, the crystalline cellulose regions are insoluble in the acid under the conditions applied, thus, the hydronium ions released by the acid cleave the glycosidic linkages within the amorphous regions to release the CNCs [144], [145], [339]. The use of sulphuric acid results in the formation of CNCs with charged sulfate ester groups on the surface that aids in the formation of stable colloidal suspensions [20], [165], [340]. Many research works have been reported on the use of sulphuric acid hydrolysis on bleached cellulose-rich pulp with cellulose contents of 60.70–97.70%, hemicellulose content of 0.5–26%, the lignin content of <0.1–16%, and cellulose crystallinity of 57.0–77.0% to produce CNCs [37], [38], [97], [226], [341]. These studies have reported different CNC yields (22.8–77%), Crl (50.0–90.6%), particle diameters (2.1–43.1 nm), and particle lengths (140–2000 nm) as indicated in Table 2.12. Apart from sulphuric acid, other mineral acids such as phosphoric [342], nitric [343], hydrobromic, or a mixture of such acids and strong oxidizing agents have been used [167], [339], [340], [344].

Table 2.12: Nanocellulose production from various feedstocks

Feedstock	Cellulose content of starting material [%]	Crystallinity of cellulose pulp [%]	Method of cellulose treatment for nanocellulose	Nanocellulose yield [%]	Crystallinity of nanocellulose [%]	Particle size [nm]	Thermal stability of nanocellulose [°C]		Reference
							T_{onst}	T_{max}	
Bleached usher seeds cellulose pulp	-	57.0	H_2SO_4 acid hydrolysis (64% H_2SO_4, 1:20 fiber: solvent ratio, 50 ºC, 75 min	79.0	70.0	D- 14-24 L- 140-260	240	-	[37]
Bleached usher seeds cellulose pulp	-	57.0	TEMPO-mediated oxidation (0.016g TEMPO, 0.1g sodium bromide, 5.0mM NaClO, 1:100 fiber: solvent ratio	98.0	59.0	D- 10-20 L- NR	200	-	
Bleached mango seed husk cellulose pulp	86.1	74.3	H_2SO_4 acid hydrolysis (11.24 M H_2SO_4, 1:20 fiber: solvent ratio, 40 ºC, 10 min)	22.8	90.6	D- 4.59 L- 123.4	248	271	[20]
Bleached sugarcane bagasse cellulose pulp	-	65.0	H_2SO_4 acid hydrolysis (64% H_2SO_4, 1:10 fiber: solvent ratio, 45 ºC, 60 min)	-	73.0	D- 20-30 L- 160-400	204	-	[345]
Bleached sugarcane bagasse cellulose pulp		65.0	Ball milling (0.25:50 fiber: solvent, 20g cerium doped balls, 1h)	-	68.0	D- 50 L- 2000	299	364	
Bleached corncob cellulose enriched pulp	65.6	73.3	H_2SO_4 acid hydrolysis, (9.17 M H_2SO_4, 1:15 fiber: solvent ratio, 45 ºC, 30 min)	57.0	79.8	D- 4.90 L- 287.3	200	300	[38]
Bleached corncob cellulose pulp	65.6	73.3	H_2SO_4 acid hydrolysis, (9.17 M H_2SO_4, 1:15 fiber: solvent ratio, 45 ºC, 60 min)	50.0	83.7	D- 4.15 L- 210.8	185	276	
Bleached corncob cellulose pulp	65.6	73.3	H_2SO_4 acid hydrolysis, (9.17 M H_2SO_4, 1:15 fiber: solvent ratio, 45 ºC, 90 min)	46.0	78.0	D- 4.03 L- 195.9	180	322	

Table 2.12 continued

Bleached pineapple leaves cellulose pulp	74.5	64.0	H_2SO_4 acid hydrolysis (64% H_2SO_4, 1:20 fiber: solvent ratio, 45 ºC, 5 min)	77.0	69.0	-	245	-	[226]
Bleached pineapple leaves cellulose pulp	74.5	64.0	H_2SO_4 acid hydrolysis (64% H_2SO_4, 1:20 fiber: solvent ratio, 45 ºC, 30 min)	65.0	73.0	D- 4.45 L- 249.7	225	-	
Bleached pineapple leaves cellulose pulp	74.5	64.0	H_2SO_4 acid hydrolysis (64% H_2SO_4, 1:20 fiber: solvent ratio, 45 ºC, 60 min)	55.0	68.0	D- 4.18 L- 190.2	220	-	
Bleached corncob cellulose pulp	95.2	61.5	Formic acid hydrolysis (88% FA, 0.5% HCl, 1:30 fiber: solvent ratio, 95 ºC, 30 min)	66.3	63.8	D- 6.5 L- 421	334	360	[97]
Bleached corncob cellulose pulp	95.2	61.5	H_2SO_4 acid hydrolysis (64% H_2SO_4, 45 ºC, 1:20 fiber: solvent ratio, 60 min)	34.5	55.9	D- 5.5 L- 198	278	313	
Bleached corncob cellulose pulp	95.2	61.5	TEMPO-mediated oxidation (1 mmol/L TEMPO, 10 mmol/L sodium bromide, 10 mmol NaClO/g cellulose, 0.5 M NaOH, 1:100 fiber: solvent ratio, room temperature	78.4	49.9	D- 2.1 L- 438	237	305	
Bleached corncob cellulose pulp	95.2	61.5	PFI refining (4% NaOH, 80 ºC, 2 h, 1:30 fiber: solvent ratio, PFI refiner (10wt%, 1460 rpm, 0.24 mm refining gap, 100k revolution number	100	52.1	D- 43.1 L- several microns	287	336	
Bleached softwood kraft cellulose pulp	85.5	65.76	Formic acid hydrolysis (88% FA, 1g $FeCl_3$, 95 ºC, 12 h, 1:30 fiber: solvent ratio, 300 rpm)	12.5	75.21	D- 5-20 L-50-200	325	356	[51]

*D=diameter of nanocellulose, L: length of nanocellulose

Several studies have attempted optimizing the H_2SO_4 treatment process for CNC production and have reported that the reaction temperature, time, acid concentration, and acid-to-pulp ratio are the most significant factors that influence the properties (surface charge, crystallinity, and PDI) of the CNCs and its application [161], [163], [167], [346]. Generally, when the severity of the treatment conditions is increased (increasing temperature, acid concentration, and reaction time) high yields of CNCs with higher surface charge, (measured as ζ-potential), and lower polydispersity (PDI) is achieved. However, when the hydrolysis severity exceeds a certain limit, the CNC yield, and properties like crystallinity, and thermal stability are compromised as more cellulose is converted to glucose which further degrades into 5-hydroxymethylfurfural (HMF) [163], [167], [347]. On the contrary, when less severe conditions (lower temperatures, shorter reaction time) are used, large fragments of cellulose fibers with higher PDI and lower surface charge resulting in the formation of less stable aqueous suspensions are observed [167], [347]. Therefore, the optimal treatment conditions for the CNC production are highly dependent on the desired output parameter and field of application of the CNCs [167].

Depending on the treatment conditions employed, the yield, Crl, and thermal stability of CNC can vary. For instance, under different extraction conditions of time and temperature, yields of 25–79%, crystallinities of 60–90%, and onset thermal degradation temperatures of 204–278 °C have been reported for sulphuric acid-based CNCs using a concentration of 64 wt% on cellulose-rich pulp (Table 2.12). Silvério et al. [38] evaluated the effect of varying hydrolysis time (30 min, 60 min, and 90 min) at a fixed temperature of 45 °C and 64 wt% H_2SO_4 on the yield and Crl of CNC produced from bleached corncob cellulose pulp (cellulose content of 65.6% and Crl of 73.3%). The yields of CNC obtained were 57%, 50%, and 46% with crystallinities of 79.8%, 83.7%, and 78.05% respectively for 30 min, 60 min, and 90 min. Santos and colleagues [226] on the other hand varied the sulphuric acid hydrolysis time from 5 to 60 min to investigate the impact on the yield and Crl of CNCs from pineapple leaves cellulose pulp (cellulose purity of 74.5% and Crl of 64%) at constant concentration and temperature (64 wt%, 45 °C). They reported yields of 55%, 65%, and 77% and Crl of 69%, 73%, and 68% respectively for 60 min, 30 min, and 5 min, respectively. From these reports, it can be established that increasing the treatment time at a fixed temperature (45 ºC) could lead to a reduction (≈19–28% reduction) in CNC yield, however with improved Crl up to a certain threshold. Beyond this threshold, there is the hydrolysis of crystalline cellulose leading to a reduction in CNC Crl.

Oun & Rhim [37] produced nanocellulose from bleached usher seed pulp fiber using acid hydrolysis (64% H_2SO_4, 1:20 g/mL, 50 °C for 75 min). The resultant needle-like CNC showed a yield of 79% with a Crl of 70%. In another study, mango seed husk CNC was produced using sulphuric acid hydrolysis by Henrique et al. [20]. The mango seed husk was treated 4 times with 2%w/w NaOH at 100 °C for 4 h. The resultant material was bleached twice with 1.7 wt% $NaClO_2$ at 80 °C for 6 h and the bleached cellulose pulp (with cellulose purity of 86.1% and Crl of 74.3%) hydrolyzed using the same acid concentration (64% H_2SO_4) as Oun & Rhim [37] but employing a lower reaction time of 10 min. A stable and homogeneous aqueous suspension of CNC was obtained but with a much lower yield of 22.8% and a Crl of 90.6%, greater than the 70% presented by Oun & Rhim [37]. The lower yield could be due to the insufficient contact time of the solvent with the cellulose for hydrolysis [163]. The difference in Crl could be due to the purification processes, the initial Crl of the different starting materials, and the different compositions of biomass species used by the authors. For all these nanocellulose production processes, the non-cellulosic components such hemicellulose and lignin were not reported as either they were lost through downstream processes or unaccounted for resulting in the loss of such valuable products.

For stability of aqueous suspensions of CNC, it has been established that the zeta potential, is a major influencing factor [167]. In general, CNC colloidal suspensions with an absolute zeta-potential value of 0–10 mV are highly unstable, 10–20 mV are relatively stable, 20–30 mV are moderately stable whereas >30 mV are highly stable [167], [348]. CNC prepared by sulphuric acid has been proven to form stable colloidal suspensions due to the introduced sulfate ester groups that result in high absolute zeta potential values (35.73–48.76 mV) [163], [341], [349]. Since sulphuric acid is a strong acid, during treatment, extensive hydrolysis in the amorphous cellulose region occurs resulting in reduced particle sizes. The lower particle sizes present numerous hydroxyl groups which increase the sulfation through esterification reactions and consequently the surface charge of the CNCs [339], [341]. However, these sulfate groups lower the thermal stability of CNC by lowering the activation energy of cellulose [163], [350], and limits the CNC usage in high-temperature applications [167]. In addition, H_2SO_4 and other mineral acids are corrosive, hence requiring very expensive corrosive-resistant equipment or anti-corrosive reagents, which further delay large-scale production and consequently affect production cost [351]. Over-degradation of cellulose, the use of large volumes of water, and environmental pollution problems are also encountered with the use of mineral acids [352]. Moreover, H_2SO_4 acid-based nanocelluloses are hydrophilic and promote dispersion in

aqueous suspensions but aggregates in non-polar solvents, compromising their dispersion in non-polar solvents. As a result, they are mostly stored as aqueous suspensions (solid contents mostly below 2%wt), increasing transportation costs and limiting large-scale applications [159].

In addressing the issues associated with mineral acids for CNC production, alternative methods involving oxidizing agents like ammonium persulphate (APS) [351], solid acids like phosphotungstic acid [342], 2,2,6,6-Tetramethylpiperidine-1-oxyl (TEMPO) mediated oxidation, and sonochemical assisted hydrolysis [168] have been described in the literature. For example, carboxylated nanocelluloses from different biomasses were produced by Leung et al. [351] using ammonium persulfate (APS) oxidation (1M APS, 60 °C, for 16 h with strong agitation) which were compared with the classical H_2SO_4 hydrolysis method. They reported that the diameters for sulphuric acid-produced nanocellulose from flax and hemp were 16–28 nm and 20–40 nm respectively whereas that of APS were 3–6 nm. Therefore, the APS produced a more fundamental unit fiber of cellulose than the acidic counterpart. Furthermore, H_2SO_4 produced CNCs presented lower thermal stability (150–200 °C) than APS CNCs (220–270 °C). The APS nanocellulose from flax and hemp presented a Crl of 73–75% and a yield of 28–36% while acid hydrolysis gave a yield of only 5%.

Sonochemical-assisted hydrolysis was used by Filson et al. [168] to prepare CNC from Avicel. The process involved the treatment of Avicel with 50 mM maleic acid solution at 15 °C for 9 h. The resultant suspension was centrifuged and washed several times with distilled water to remove maleic acid and further sonicated until turbidity of the suspension was attained. The length of the CNC was 65 nm with a width of 15 nm and a yield of approximately 10%. Torlopov et al. [353] used a novel system consisting of acetic acid/phosphotungstic acid/octanol-1 to produce CNC from cotton. The process involved the catalytic solvolysis of cotton in an acetic acid/octanol-1/phosphotungstic acid mixture. Other experiments were performed as benchmarks for comparison. The cotton powder was placed together with 45 mL of acetic acid in a round bottom flask equipped with a condenser, a thermometer, and a stirrer. The mixture was heated for 60 min at 117 °C. Thereafter, 0.25 mol% of phosphotungstic acid in octanol-1 was added and the temperature lowered to 114 °C and stirred further for 40 min. Hydrogen peroxide (50 µL) was added after every five minutes to decolorize the solution until the reaction was completed. The precipitate was then obtained after centrifugation and dialyzed against deionized water and stored at 4 °C for further analysis. The results showed that when cellulose was treated in only acetic acid without octanol-1, no nanocellulose was produced,

only micrometer size fibers were obtained. Upon addition of octanol-1 to acetic acid in the ratio of 9:1, the yield of CNC was 38% with accompanied particle size of 200 nm. SEM analysis showed a rod-like morphology while XRD showed CrI of 82% for the CNC compared to that of the starting material (89%). The decrease in CrI of the CNC could be attributed to hydrolysis of a portion of the crystalline cellulose region after amorphous cellulose hydrolysis.

The referred methods offer various advantages compared to the classical sulphuric acid, however, using these methods in most cases is unattractive for commercial implementation due to lower yields, longer extraction times, and the use of equipment like sonicators which are expensive and impractical for industrial application [168]. More recently, organic acids such as oxalic and formic acids have been used to produce CNCs because they are less corrosive compared to inorganic acids and can be easily recovered and reused due to the low boiling point [51], [352]. As an example, a sustainable method of producing CNC using formic acid hydrolysis in the presence of $FeCl_3$ catalyst was explored by Du et al. [352] and compared with H_2SO_4 hydrolysis (64%wt H_2SO_4, 45 °C, 30 min). The $FeCl_3$ was varied to investigate its effect on the formation of CNC from the bleached cellulose pulp at 95 °C for 6 h with constant stirring. They reported a yield of 75.7% with CrI of 75.45% at a catalyst concentration of 0.015M with an average size of 594 nm and absolute ζ-potential of 6.34 mV. The yield for the H_2SO_4 was 29.56% but with a higher absolute ζ-potential of 49.35 mV and CrI of 78.82%. The onset thermal degradation temperature for formic acid CNC was higher (≈260 °C) than that of H_2SO_4 (≈190 ºC). With formic acid conditions where a catalyst was not included, 82.26% yield was achieved but only microfibers were obtained with no nanofiber detected. They further recovered the formic acid and the catalyst for reuse and concluded that formic acid in the presence of $FeCl_3$ can result in nanocellulose with improved thermal stability.

Liu et al. [97] further used four different methods (sulphuric, formic, oxidative, and mechanical means) to investigate their effect on the properties of the isolated nanocellulose from bleached corncob cellulose pulp. The corncob was first pretreated with 3 wt% NaOH for 3 h at 100 °C and bleached for 2 h using sodium hypochlorite at 80 °C. The bleached corncob cellulose pulp was used for nanocellulose production using the different methods: sulphuric acid (64 wt%, 45 °C, 60 min), formic acid (88% formic acid, 0.5% HCl, 95 °C, 30 min), TEMPO (1mmol/L TEMPO plus 10 mmol/L sodium bromide, 1:100 solid: liquid, 0.5 M NaOH) and PFI refining (4% NaOH, 80 °C, 2 h, 10 wt%, 1460 rpm). They reported that the formic acid CNC had longer lengths (421 nm) than the sulphuric acid CNC (198 nm) due to the weak acidity of formic acid compared to sulphuric acid. However, the CrI (63.8%) and

thermal stability (360 °C) of the formic acid CNC were higher than the Crl (55.9%) and thermal stability (313 °C) of sulphuric acid CNC. This is due to the selective nature of formic acid to hydrolyze the amorphous cellulose regions leaving the crystalline cellulose intact, in addition to the introduction of formate groups unto the CNC that improved the thermal stability [51], [97]. The Crl of the CNCs were in the order of formic acid (FCNC) > sulphuric acid (SCNC) > refining (PCNF) > TEMPO (TCNF). In terms of yield, the PFI refiner presented 100%, followed by TCNC (78.4%), FCNC (66.3%), and then SCNC (34.5%). It was concluded that FCNC presented several preferable properties including Crl and thermal stability making it a good candidate for reinforcement and gas barrier applications. Considering the weaker acidity of organic acids compared to sulphuric acid, it can be noticed that, in all the nanocellulose treatment processes involving organic acids, inorganic acid catalysts (eg. HCl, H_2SO_4) or salts ($FeCl_3$) were added to improve the hydrolytic effect of the acid to produce CNCs.

A review by García et. al. [115] indicated that the pretreatment approach utilized to obtain the cellulose-rich pulp before further treatment to CNC also affects the final CNC yield and properties such as the crystallinity, particle size, and morphology. The pretreatment path combined with the CNC treatment method could give rise to CNCs with different morphologies such as spherical, whisker-like, or rod-like and crystallinities [166], [173]. As an example, spherical CNC was obtained using acid hydrolysis (47% H_2SO_4, 3 h, 60 °C) under vigorous agitation after pretreating mulberry fiber with a laboratory-scale valley beaker for 60 min [354]. The resultant suspension was sonicated for 5 min using a high-intensity ultrasonic processor. The CNC obtained had a diameter of 40–50 nm with a length of 200–350 nm and a Crl of 69.9%. Hastuti and colleagues [355] produced needle-like CNCs with diameters of 10–13 nm and length of 190–301 nm after bleached kraft oil pulp empty fruit bunches (treated with 4% NaOH, at 60 ºC for 4h) was treated with 3 M HCl at 80 ºC for 120 min followed by mechanical treatment (blending in deionized water) at 10,000 rpm for 30 min. The crystallinity of the as-prepared CNCs ranged from 53–65%. Although organic acids have found applications in the production of thermally stable nanocellulose, their weaker acidity limits their sole application as treatment agents on the bleached cellulose-rich pulp, thus, requiring mineral acids and salts as catalysts.

Other than adding inorganic acid catalysts which are not environmentally sustainable, application of an unbleached cellulose-rich pulp obtained from the multi-step process could allow the use of only the recoverable organic acids (such as formic and acetic) to produce a similar yield and quality (thermal stability, crystallinity, etc.) of nanocellulose from the mango

seed. Thus, the effect of the multi-step process on the qualities of the nanocellulose produced using sole organic acid treatment should be investigated. Among the organic acids, formic acid (plus inorganic acid catalysts) resulted in high yields (>50%) of thermally stable (thermal stability >300 ºC) nanocellulose. Acetic acid is also used in combination with acetic anhydride in nanocellulose modification processes and could be considered for nanocellulose production.

2.13.2. Mechanical treatment processes for nanocellulose production

In general, the mechanical treatment processes use mechanical forces to break the cellulose pulp into smaller particles resulting in the production of mostly cellulose nanofibers (CNFs). The mechanical treatments of cellulose-rich fibers lead to a diagonal cleavage of the cellulose fibers along the longitudinal axis leading to the destruction of the structure of the microfibril and reduction in the degree of cellulose crystallinity [163], [356]. The application of mechanical treatments on cellulose results in CNFs that exhibit improved mechanical properties (tensile strength); 1.6–3.0 GPa for wood CNFs and 3.0–6.0 GPa for tunicins [357]. Mechanical treatment processes such as homogenization (high pressure and high shear homogenization), refining, cryo crushing with liquid nitrogen, and grinding have been used to produce CNF from various lignocellulosic biomass [158], [356], [358], [359]. Due to the high energy requirements resulting in high production costs, chemical treatments are combined to reduce energy consumption [96], [231]. Generally, the mechanical treatment process causes a reduction in cellulose DP from 1200–1400 to 850–500 [359]. One of the major disadvantages of this treatment process stems from the high energy consumption (20,000–70,000 kW/ton) [357], [360], limiting the industrial production of CNFs.

2.13.2.1. Refining and high-pressure homogenization

In this treatment process, the biomass undergoes a refining process followed by high-pressure homogenization [356]. This involves passing the dilute cellulose suspension through the gap between the refiner's rotor and stator disk that are corrugated and fitted with bars. These bars, through repeated cyclic frictional stresses, cause fibrillation resulting in peeling of the external wall layers of the material and exposing the inner wall layers [356], [358]. Refining also causes internal fibrillation that unloosens the fiber wall, which is suitable in the following homogenization process [361], [362]. After refining, the cellulose fibers suspension (2–7%w/v) is subjected to high-pressure homogenization, in which the fibers are pumped through a spring-loaded valve assembly at high pressure (≈551 bar) [359]. With the continual opening and closing of the valves in a cyclic motion, the fibers are exposed to a large pressure drop with

impacting and shearing forces that leads to cellulose fibrillation. In most cases, the procedure is repeated several times to improve the fibrillation rate, reduce the particle size and obtain a more uniform particle size [356], [359], [361]. The diameters of the CNFs produced by this method range between 20 and 100 nm with several hundreds of micrometer lengths [356], [359]. Lee et al. [363] produced CNFs using microcrystalline cellulose as raw material with the help of the high-pressure homogenizer. The results indicated a diameter range of 28–100 nm for CNF after 10 passes. Li et al. [338] also used the high-pressure homogenizer (30 cycles) to isolate CNF from sugarcane bagasse. They, however, reported a much lower diameter range of 10–20 nm which is due to the number of passes through the homogenizer.

One important factor to consider with the application of a homogenizer is the particle size of the starting cellulose material such that clogging of the homogenizer could be minimized. Mahardika et al. [158] produced nanocellulose from pineapple leave fibers after chemical pulping (25% NaOH, 60min, 150 °C, and 9 bar), bleaching (4:1 $NaClO_2$:Acetic acid, 60 °C, 2 h, 600 rpm), and acid hydrolysis (3.5 M HCl, 50 °C, 12 h followed 7.5 M HCl, 50 °C overnight) to remove the amorphous components. The fibers were then subjected to high shear homogenization (diameter of rotor and stator: 130 mm and 180 mm respectively, 12000 rpm, 5% suspension, 25 °C, 10 min) and ultrasonication (400 W, 60 min, at 60 °C). Analysis of particle size after acid hydrolysis indicated an average diameter of 1–5 µm, which reduced to 68 nm upon homogenization and ultrasonication. A Crl index of 82.7% was achieved after acid hydrolysis, however, this value decreased to 69.4% and 61.7% after homogenization and ultrasonication, respectively. Therefore, mechanical treatments destroy the intermolecular hydrogen bonding between crystalline fibers, as shown by the Crl indexes. The thermal degradation temperatures were found to be 300 °C, 310 °C and 320 °C for acid hydrolyzed, homogenized and ultrasonicated nanocelluloses, respectively [158]. The major drawbacks of this treatment process are high energy consumption, clogging of the homogenizer, and damage to cellulose crystalline portion leading to low crystallinity.

2.13.2.2. Grinding

Grinding involves passing a dilute cellulose suspension (1–2 wt%) through a commercial grinder that consists of a static upper stone and rotating grinding lower stones set at a speed of approximately 1500 rpm [356], [359]. Grinding causes the breakdown of the cell structure by the repeated cyclic stresses and shear forces, which in turn, causes evaporation of water from the material due to frictional heat, thereby producing a gel [359], bringing about a change in the morphology and size of the fibers as well as mechanical damage of the cellulose fibers

[356], [362], [364]–[366]. The grinding process has been utilized in the extraction of CNFs from various agro-industrial waste such as soy hulls [359]. Due to the high costs of the single nanocellulose treatment processes, various chemical and enzymatic pretreatments have been combined with mechanical treatment processes to improve CNF liberation from cellulose [357], [367]. Pretreatment before mechanical treatment has been reported to be economical since fewer passes in the homogenizer are required which reduces the energy requirement (1000–2000 kWh/ton) [357].

2.14. Hemicellulose-based biocomposite film development

Due to recent lifestyle changes, the demand for convenience foods has increased tremendously causing an upsurge in the market demand for food packaging materials [368], [369]. Among the existing packaging materials, low-density polyethylene (LDPE) and polyethylene terephthalate (PET) made from petroleum-based materials are the most predominant for food packaging due to their flexibility, high strength, low cost, and barrier properties [46], [368]. Nevertheless, petroleum-based plastics cause serious environmental pollution because they are not biodegradable [368]–[370], and their disposal through incineration causes the release of toxic substances such as furans and dioxins that are detrimental to human health and the environment [368]. Thus, the focus on global sustainability now relies on renewable, non-toxic biodegradable materials such as natural polymers (proteins, hemicellulose, starch, chitosan, nanocellulose, pectin, etc.) for packaging applications [42], [43], [299].

Among these natural polymers, hemicellulose (particularly xylan and glucomannan) has gained increased interest as starting materials for biocomposite films for packaging applications due to their good gas barrier properties arising from their ability to form a dense macromolecular network with less mobility [42]. Xylan films are preferred over glucomannan for food packaging because they form transparent films, nevertheless, the low *Mw* and high glass transition temperature of xylan results in the development of brittle and thermally labile films thus requiring some form of modifications [178], [301], [368], [371]. The physical characteristics of hemicellulose-based films are dependent on the *Mw*, composition, purity, chemical structure, and processing conditions [42], [295]. Some of the properties of films to consider for food packaging application are a good gas barrier, flexibility, and mechanical properties (tensile strength, modulus, and elongation at break). The unmodified hemicellulose-based films exhibit poor mechanical properties due to their amorphous nature and the different

side chains. Therefore, for hemicellulose to be applicable in food packaging, it needs to be modified [369].

Currently, the most common hemicellulose modification processes are chemical and physical processes. The chemical modification process involves a chemical reaction whereby the numerous exposed carboxyl, hydroxyl, and carbonyl groups in the side or main chain of the hemicellulose is replaced by other bulky groups through esterification, etherification, grafting, or crosslinking, among others [369], [372], [373]. The physical modification process involves the blending of high *Mw* materials or lower *Mw* materials such as plasticizers (10-40%w/w sorbitol, xylitol, glycerol) with the hemicellulose [369], [374], [375]. Although the addition of lower *Mw* plasticizers improves the film formation from xylan, their drawbacks of migration into the packaged goods over time pose a health risk to consumers [178], [295], [376]. Other studies have shown that lignin could be used as a replacement for the lower *Mw* plasticizers and due to its numerous phenolic groups, it could provide additional functional properties (antioxidant and UV-barrier property) [42], [176], [295].

The lignin polymer can act as a plasticizer by entangling with the hemicellulose polymer and hindering its migration contrary to the low *Mw* plasticizers, thus, replacing low *Mw* plasticizers with lignin is a green and environmentally feasible way of producing packaging films [178]. Even though hemicellulose purity is a factor to consider during film development for packaging application, literature reports indicate that there is no strict limit to the content of lignin that can be used [295]. Although selective hemicellulose extraction is important and improves hemicellulose purity, the presence of lignin has been advantageous in self-supporting hemicellulose (xylan) film development [270]. Lignin content in the range of 1–15% has been used in hemicellulose-based composite film development although brown and opaque films were reported [178], [295]. Therefore, during AP for hemicellulose extraction, the process conditions could be optimized to limit the lignin content in the hemicellulose extract for self-supporting biocomposite film development. Another important parameter to consider for biocomposite films for food packaging is thermal stability, particularly if the product is to be microwaved or thermo processed [295], [377]. Modification by the addition of substances such as nanocellulose or by acetylation has shown improvements in the thermal stability of xylan-based films [295], [369].

2.15. Methods for developing hemicellulose-based biocomposite films

In developing hemicellulose-based films, the solvent used and its interaction with components being used for the development of the films need to be considered since they affect

the final properties (mechanical, physical, barrier, and thermal properties) of the film. Numerous methods have been reported for such purpose, including the commonly used hot-melt extrusion (HME) and solvent casting particularly for flat films [378], [379]. The HME method is mainly designed for producing pipes, plastics, and fabricating bags and rubber for various applications (domestic and industrial) [380] and involves the pumping of raw materials (polymers) through a heated barrel at high pressures and temperatures. Although HME results in producing film without solubilization [381], its operation under high pressure and temperatures may limit the usage of certain biopolymers such as hemicelluloses since they are thermally liable. Thus, the solvent casting method has been adopted for the development of biopolymer films involving hemicelluloses [381], [382]. The solvent casting method works by dissolving the polymers in an appropriate solvent (such as dimethyl sulphoxide, water, and tetrahydrofuran), casting in a mold (thereby taking the shape of the mold), and drying (in an oven or air drying at room temperature depending on the solvent and composition of the polymers). Solvent casting is a preferred method for the present study since it works under lower temperatures suitable for hemicellulose-based films. Moreover, it leads to the formation of uniform films [383].

2.16. Research aims and objectives

2.16.1. Aim

The main aim of this study was to develop multi-step biorefinery processes for high-value multi-products recoveries from mango seed waste, including (i) free polyphenols, starch, bioactive hemicellulose (i.e. hemicellulose with bound polyphenol), and solids enriched in cellulose and lignin for further valorization from MSK and, (ii) nanocellulose, hemicellulose polymers and high purity lignin from the MSH. To achieve this aim, three specific studies having the following objectives were carried out:

2.16.2. Specific objectives

1. To develop and optimize a multi-step biorefinery process (involving sequential organosolv extraction, enzymatic hydrolysis, and alkaline pretreatment) for recovering multi-products [polyphenols, starch, and bioactive hemicellulose] from MSK while ensuring minimal residual solids substrate (cellulose, and lignin) degradation and determine the effect of each treatment step in the multi-step biorefinery process on the product properties in the subsequent stages. The series of experimental studies include:

(a) Assessing the impacts of organosolv extraction (OE) on the total polyphenol content (TPC) and antioxidant activity (AA) of the derived polyphenol product and the residual solid composition (cellulose, hemicellulose, lignin, and starch) from MSK. Optimal process conditions (ethanol concentration and temperature) that enhances the total polyphenol content and antioxidant activity of the polyphenol extract while maximizing the retention of hemicellulose (≥ 80%), cellulose (≥ 80%), lignin (≥ 80%), and starch (≥ 80%) in the solid residue were investigated.

(b) Assessing the impact of subsequent enzymatic treatment (EH) step on starch removal and the residual solid components (cellulose, hemicellulose, and lignin) from the OE solid residue.

(c) Evaluating the impact of third step alkaline (NaOH) pretreatment (AP) of the destarched solid residue (obtained after enzymatic hydrolysis of the polyphenol extracted solid residue) on the yield, TPC, and AA of hemicellulose product. In addition, optimal process conditions (NaOH concentration, temperature, time) for obtaining ≥50% yield of hemicellulose polymers with high AA while maximizing the recovery of cellulose (≥80%), and lignin (≥80%) in the solid residue was investigated (Paper I).

2. To develop and optimize a multi-step biorefinery process (involving sequential alkaline pretreatment and high shear homogenization-assisted organosolv process) for fractionating MSH of multi-products [hemicellulose polymers, high purity lignin, and cellulose-rich solids] and assess the effect of the individual stages of the multi-process on the qualities of the products. This involves:

(a) Investigating the effect of a first stage alkaline pretreatment process conditions (i.e., NaOH concentration, temperature, and reaction time) on the yield and quality (molecular weight, purity, composition, etc.) of hemicellulose extract from MSH, while ensuring maximum ≥80% cellulose and ≥80% lignin retention in the resultant solid residue (Paper-II). This was followed by the identification of optimal process conditions that maximizes hemicellulose yield, xyloglucan/xylan ratio and improve the hemicellulose purity by minimizing lignin and uronic acid contents in the hemicellulose extract. Further, test the feasibility of the hemicellulose extract to produce

self-supporting thermally stable hemicellulose film for potential application in food packaging.

(b) Investigate the efficacy of a subsequent stage high shear homogenization-assisted organosolv pretreatment/fractionation process for delignification of the alkaline treated mango seed husk solid residue. Specifically, to assess the effect of the HSHO process conditions and determine optimal process conditions (conditions of ethanol concentration, homogenization time, and temperature) that maximizes both lignin dissolution (i.e., solubilize ≥70%), and lignin purity (≥90%) and cellulose recovery (≥ 80% cellulose) in the resultant solid residue (Paper-III).

3. To assess the feasibility of producing nanocellulose from the cellulose-rich pulp obtained from the multi-step biorefinery (sequential AP and HSHO) process in objective 2 using two alternative conversion methods:

(a) a non-catalyzed formic acid treatment process. Precisely study the effect of the process conditions (acid-to-pulp ratio and reaction time) in producing the cellulose nanocrystals from the cellulose-rich pulp with further identification of optimal process conditions that enhance the cellulose nanocrystal yield and properties [(average particle size, polydispersity, (PDI), degree of substitution and crystallinity)] (Paper-IV).

(b) an alternative non-catalyzed acetic acid treatment process. Specifically, the effectiveness of this process for producing a cellulose nanocrystal with hydrophobic properties (high degree of acetylation) for potential application in a hydrophobic biocomposite matrix (without further modification requirement) was analyzed. The influence of acetic acid treatment conditions (acid-to-pulp ratio and reaction time), and potentials for enhancing the nanocellulose product yield and quality through incorporating a high shear homogenization step after the acetic acid treatment were also analyzed (Paper-V).

2.17. Scientific contribution

The present study contributes to the revealing of high value potential for the mango seed waste (kernel and husk) by developing multi-step biorefinery processes and identifying optimal process conditions that could valorize the mango seed waste into multi-products, which

includes nanocellulose, hemicellulose polymers, and high purity less modified lignin from the husk; and polyphenols, starch, bioactive hemicellulose, and solids rich in cellulose and lignin from the kernel. Specifically, the study developed multi-step biorefineries that consist of a unique combination and sequence of pretreatment methods i.e. a sequential organosolv extraction (OE), enzymatic hydrolysis (EH), and alkaline pretreatment (AP) process for recovering multi-products of free polyphenols, bioactive hemicellulose (hemicellulose with bound polyphenols), starch (in simple sugars) and solids enriched in cellulose and lignin for further fractionation and valorization (Chapter 4). Optimal conditions for obtaining the multi-products that respond differently to process conditions from MSK have been provided while preserving their properties for the intended application. Thus, more value could be added to the mango seed, thereby, providing knowledge on alternate ways of increasing product ranges, and revenue while reducing environmental pollution problems associated with waste disposal in the mango processing industries. Even though several authors have developed different multi-step processes for other agro-industrial waste valorization, the combination and sequence of the developed multi-step process involving sequential OE, EH, and AP are the first for MSK.

Concerning the husk (MSH), an innovative optimized alkaline pretreatment process that facilitates the extraction of hemicellulose with different compositions of polysaccharides (xylan-xyloglucan complexes), lignin, and uronic acids for potential uses as a raw material to develop self-supporting, and thermally stable biocomposite film has been established (Chapter 5). Gaps in knowledge with regards to alternative feedstock sources that could yield a hemicellulose extract with compositions that suit self-supporting hemicellulose-based film development have been addressed. In addition, the thermal properties of the xylan-xyloglucan hemicellulose-based biocomposites films for potential high-temperature applications have been addressed (Chapter 5). Furthermore, the feasibility of a subsequent extraction of high-purity/less-condensed lignin (for potential application in phenol formaldehyde resin production) and a cellulose-rich solid residue (with fibrillated, less recalcitrant, improved surface area) from the alkaline treated solids using a novel high-shear homogenization-assisted ethanol organosolv (HSHO) process has been demonstrated (Chapter 5). Particularly, the findings contribute to knowledge on the proficiency of a novel HSHO process for biomass fractionation that maximizes lignin dissolution, recovery, and purity, in addition to fibrillated cellulose-rich solids with high cellulose content (purity), improved surface area and crystallinity, thus suitable lignin and cellulose feedstock supply pathway for varied industrial applications.

In addition, the study demonstrated the feasibility and effectiveness of a hypothesized milder alternative process for producing nanocellulose, involving the use of an unbleached cellulose-rich pulp obtained from a multi-step sequential AP and HSHO pretreatments of MSH followed by direct organic acid (non-catalyzed formic acid (FA)/acetic acid) treatment, versus the conventional method of sulphuric acid-based treatment of bleached Kraft pulp (Chapter 6). Improved nanocellulose (CNCs) product yields and qualities were obtained for the developed non-catalyzed organic acid-based nanocellulose production process versus the conventional sulphuric acid-based process. For instance, the demonstrated processes produced a more thermally stable formylated/acetylated CNCs (T_{max} of 361 ºC /352 ºC vs. 309 ºC respectively), with spherical morphology versus the rod-like shaped CNCs from the conventional process, thus unraveling potentials for CNCs suitable for the preparation of thermally stable nanocomposites for highly sensitive applications such as biomedicine, cosmetics, and food packaging. Additionally, the recoverability and reuse of the organic acids could provide both environmental and economic benefits in terms of their less toxicity and reduced cost associated with re-usage and effluent processing.

Moreover, the novel sequential alkaline and homogenization assisted organosolv treatments of the biomass (MSH) in the developed multi-step biorefinery process results in beneficial recovery of high-value bioproducts (hemicellulose for biocomposite development), (lignin for resin production), alongside the nanocellulose, juxtaposed to the degradation of the hemicellulose/lignin substrates for fuel in the conventional Kraft/bleaching/sulphuric acid-based process for the CNCs. In addition, the functionality of the MSH hemicellulose extract was tested via the development of self-supporting thermally stable biocomposite film without the addition of external additives such as plasticizers contrary to the xylan/plasticizer biocomposite film development in the literature. The application of the MSH hemicellulose extract provides opportunities for developing biocomposite films with no/limited need for lower M_w plasticizers that could migrate from the packaging material into the product over time if not bound to the biopolymer.

3. Research methodology

3.1. Introduction

This chapter presents the approach and methodology followed to achieve the study's objectives of developing the multi-step biorefinery route for the mango seed husk and kernel fractionation/conversion (Chapter 2). The mango seed waste multi-step biorefinery process was aimed at producing cellulose-rich pulp for nanocellulose and co-products of hemicelluloses (bioactive hemicellulose and mixed xylan/xyloglucan), lignin, starch (as simple sugars), and polyphenols (both free and bound) due to their high economic values (nanocellulose= US$25–127/Kg, hemicellulose= US$20–121/Kg, lignin= US$8–25/Kg, polyphenols= US$12.5–98.32/Kg) [384] and diverse fields of application, summarized in Table 3.1 (see Table 3.1). The experimental procedures involving feedstock selection and handling, mango seed fractionation, nanocellulose production, biocomposite film development, and product characterizations are summarized in sections 3.2.1–3.4.2. Details of the experimental procedures are outlined in the respective research papers (Chapter 4–6).

3.2. Experimental procedure

3.2.1. Feedstock selection and handling

Mango seed waste was selected as feedstock in the present study because of the high generation capacities and minimal uses, thus largely discarded as waste, posing serious environmental issues. Furthermore, studies have shown that high-value products, including polyphenols, hemicellulose, nanocellulose, bioethanol can be obtained from the mango seed [9], [45], [235], [255]. The Kent mango variety was chosen because it is one of the most preferred for industrial processing in South Africa for juice due to the large-to-medium size, less fibrous nature, good taste, and ease of transportation due to its toughness. It is also more tolerant to harsher conditions. The ripe mango fruits were first washed with distilled water followed by peeling to remove the peels and pulp to recover the seed, which was further washed to remove the residual pulp and then manually separated into the husk and kernel using a knife. The kernel and husk were then dried in the greenhouse for 48 h at 43 ºC. High-temperature drying of mango seed affects the total polyphenol content and their antioxidant activity [385], thus, the drying temperature was kept at 43 ºC. Both kernel and husk were used because of their different compositions and diverse products that could be recovered. In the prospective industrial setting, the mango seed could be separated into the kernel and husk as described in a patent by Siacor and Taboada [386]. The seed is initially dried in a tray dryer at 50–70 ºC [386].

A decorticator is then used to crack the dried seed, which separates the husk from the kernel. The size reduction and sieving could be similar to the experimental protocols described in section 3.2.2.

3.2.2. Biomass size-reduction

After the drying (to a moisture content of ≈10%), the kernels were milled using a retch mill (Retsch ZM100 mill with a 2 mm circular blade) to obtain particle sizes <2 mm, which was sieved using a vibratory sieve (universal test sieve, ISO 3310) equipped with a series of mesh to achieve particle sizes of 425–800 µm that was stored in black polyethylene bags for the analysis. The husks, due to their hard nature, were first milled in a Hammer mill into ≈2 mm sizes and then in a Retsch ZM100 cutting mill into sizes < 2 mm. The milled samples were sieved using Retsch AS200 shaker to obtain sizes of 250–800 µm that were stored in zip-lock bags for the analysis. The coning-and-quartering method was used to obtain a representative samples of the milled dried mango seed kernel (MSK) and mango seed husk (MSH) before the characterization to determine the cellulose, hemicellulose, lignin, starch, and other (extractives, proteins, ash, etc.) components (Detailed in Chapters 4 to 6).

3.3. Mango seed fractionation

The characterization of the MSK and MSH revealed distinct compositions regarding the structural and non-structural components (Chapters 4 and 5), thus multi-step biorefinery processes were developed for the recovery of the bioproducts [polyphenols (both free and bound), starch, hemicellulose, lignin, and cellulose] of interest. The process route is shown in Figure 3.1a–g and highlights the modifications made to enhance the recovery of the bioproducts while minimizing the degradation of the cellulose to be used for nanocellulose production. Figure 3.1h further shows how nanocellulose was produced from the cellulose-rich pulp obtained after the multi-step biorefinery process. The individual steps in the multi-step fractionation process for the MSK and MSH are presented hereafter.

3.3.1. Multi-step biorefinery route for fractionation of mango seed kernel

The milled MSK was fractionated into polyphenols (free and bound), starch, hemicellulose, and residual solids enriched in cellulose and lignin using a multi-step biorefinery process highlighted in Figure 3.1. Polyphenols extraction from MSK have been widely explored, but mainly focused on the free extractables whereas data on the extraction of the bound polyphenols is limited [11], [16], [67], [81], [387]. Consequently, the bound polyphenols reported to exhibit stronger antioxidative properties than the free polyphenols, are lost, and the total polyphenols in the mango seed are not utilized [81], [245]. In the present

study, a multi-step process consisting of three different treatment steps in a sequential manner, aimed at recovering free polyphenols (Figure 3.1b), starch (Figure 3.1c), bound polyphenols plus hemicellulose (as bioactive hemicellulose) (Figure 3.1d), and solids enriched in cellulose and lignin were explored (detailed in sections 3.3.1.1–3.3.1.3).

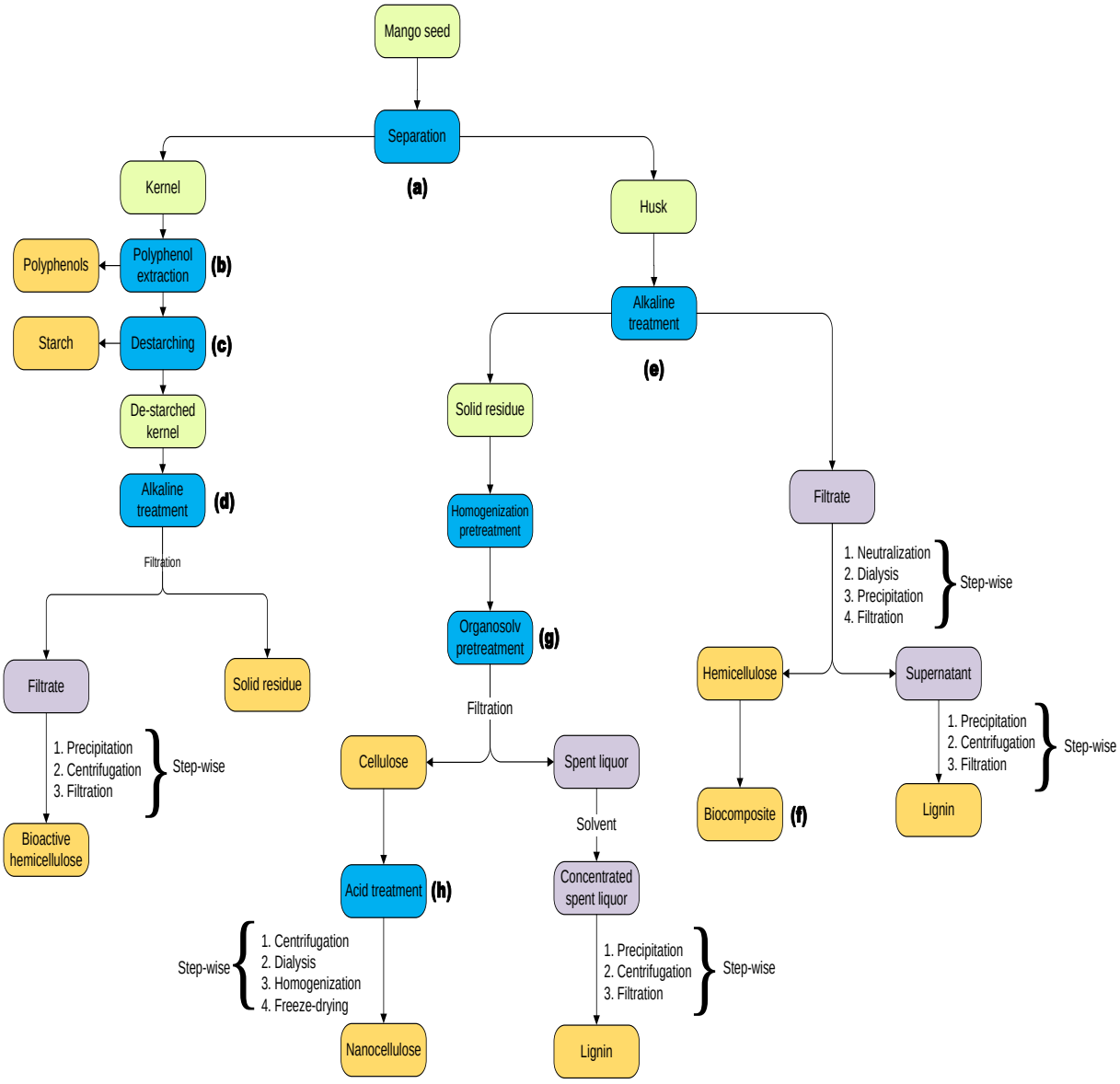

Figure 3.1: Integrated multi-step biorefinery route for multi-product generation from mango seed

3.3.1.1. First step: Free polyphenol extraction

The first step in the multi-step biorefinery process for the MSK fractionation after seed separation and mechanical size reduction (Figure 3.1a) involved free polyphenol extraction using the solvent extraction method (Figure 3.1b). Various extraction methods such as Soxhlet, maceration, and direct solvent extraction have been reported to extract polyphenols (particularly the free extractable ones) from lignocellulosic biomass. From the referred methods, solvent extraction was chosen because it is easy to operate, efficient, and has been widely employed for various feedstock [47], [235]. Generally, due to the nature and diverse polarities of the free polyphenolic compounds, different aqueous organic solvent mixtures such as ethanol/water, acetone/water, methanol/water are preferred to the pure organic solvents for mango seed due to their synergistic behavior. In the present study, ethanol/water mixtures were chosen to comply with good food manufacturing practices [47], [235], [388]. The widely used ethanol concentration for MSK free polyphenol extraction in the literature is 50% v/v [16], [67], [235], combined with temperatures ranging between 25 to 100 ºC and reaction periods of 1 to 12 h [47], [70]–[72], [234], [235]. However, temperatures above 70 ºC result in degradation of the polyphenols and loss of bioactivity [235]. Since one of the objectives is to selectively extract free polyphenols while ensuring maximum retention of other components of biomass for extraction in the subsequent stages of the multi-step process, a compromise was made to the free polyphenol extraction conditions (Figure 3.1b). For example, starch in the mango seed kernel [53]–[55] is insoluble in cold water or organic solvents such as ethanol but gelatinizes at ≈78.2–82.4 ºC (temperatures where polyphenols and hemicellulose may co-extract/degrade) during extraction with water [53], [386]. Additionally, some hemicellulose types such as xyloglucan, and mannan are water extractable and the glycosidic linkages can easily be cleaved at temperatures as low as 80 ºC (particularly, under alkaline or dilute acid treatments) reducing the hemicellulose polymer to monomers or oligomers, and therefore compromising the hemicellulose molecular structure for biocomposite film development [241], [389]. Furthermore, all the three main lignocellulosic biomass components (cellulose, lignin, and hemicellulose) have been reported to partially degrade at extraction times longer than 240 min [241], [390], [391].

Considering the criteria described above, the extreme temperature of the OE process was limited to 60 ºC, thus ensuring temperature lower than the gelatinization temperature of mango seed starch (78.13–82.29 ºC) [53] and the degradative temperatures (75–100 ºC) for free polyphenols under the solvent extraction method [70], [72], [235], [251]. This temperature

is also below the boiling point of ethanol (78 ºC), to avoid evaporation that could lead to changes in the concentrations of the extraction medium, which can affect the extraction yields and bioactivity [71]. The reaction time was set to 1 h similar to reports in the literature [235], [255] to save cost. These selected ranges of conditions could limit the co-extraction of lignin and cellulose due to the less severity to overcome the strong inter/intramolecular bonding, and ester and ether linkages in these components [14], [96]. The MSK was therefore treated with different ethanol concentrations at different temperatures for a period of 1 h. This was followed by the characterization of the extracts [where consideration was given to the polyphenol extract properties such as total polyphenol content (TPC) and antioxidant activity (AA) and solid residue components of starch, hemicellulose, lignin, and cellulose] and optimization of the process conditions to determine the best compromise that could result in maximum TPC and AA of the extract and maximum hemicellulose, starch, lignin, and cellulose contents in the solid residue. The residual solids were then used in the next stage of the multi-step fractionation process (Chapter 4, section 4.1).

3.3.1.2. Second step: Starch removal from polyphenol extracted solid residue

The second step involved the extraction of the starch (as simple sugars) from the solid residue obtained from the organosolv process (Chapter 4, section 4.4.3). The starch, if not removed, will obstruct the fractionation of hemicellulose, lignin, and cellulose by forming highly viscous solutions that impede component separation. As indicated in Chapter 2, section 2.9.2, the starch can be removed from biomass through various methods such as alkali, water, and enzymatic treatment [69], [77], [78]. Water extractions result in ≈32–59% starch removal [48], [79], [80], whereas alkali methods result in ≈84–98% starch removal [77]. Water and alkali treatment methods were not considered because former results in <60% starch removal whereas the use of alkali under the conditions used will lead to hemicellulose and lignin co-extractions thereby reducing the hemicellulose and lignin recoveries in the next stage of the multi-step fractionation process. Enzymatic treatment was the preferred method of choice to hydrolyze the starch into simple sugars because enzymes are substrate specific, and effective in removing up to 100% starch from biomass [69]. The organosolv treated solid residue, therefore, underwent a two-stage enzymatic treatment (Figure 3.1c) using thermostable α-amylase (Termamyl®SC) and amyloglucosidase (Saczyme®Plus) enzymes from Novozymes (Chapter 4, section 4.4.3). The hydrolysis process was performed twice due to the high starch content (≈40 wt%), hence enhancing the removal of starch from the solid residue. After the destarching process, the dried solids obtained, termed destarched MSK, was characterized to

determine the cellulose, hemicellulose, and lignin contents using the Van Soest method for fiber analysis [136], [392], the starch content of the residue was determined using the Megazyme starch assay kit whereas the sugars in the hydrolyste was determined using HPLC. The destarched MSK was then used in the next stage of the process.

3.3.1.3. Third step: Bioactive hemicellulose extraction from the destarched mango seed kernel

This step of the MSK multi-step biorefinery process focused on extracting bioactive hemicellulose (hemicellulose with bound polyphenols) from the residue recovered after EH (termed destarched solids) for use as bioactive hemicellulose while ensuring minimal degradation of cellulose and lignin in the solid residue [81], [245]. Bioactive substances such as polyphenols exist in biomass matrix particularly in seeds in the bound or free form [71]. Bound polyphenols are soluble in alkali solvents that favor hemicellulose extraction [245]. Particularly, alkaline (NaOH) concentrations in the range of 1–8 M, at different reaction times (up to 4 h) and temperatures (up to 60 ºC) have been used to extract bound polyphenols [81], [387], [393]. Whereas, alkaline concentrations of 0.44–2 M, temperatures of 25–80 ºC, and reaction time of 2–6 h [263], [394] have been used to extract hemicelluloses. Thus, in this step, since both hemicellulose and bound polyphenols are soluble in alkali solvents [71], the feasibility of recovering the bioactive hemicellulose using a mild alkaline pretreatment (AP) was investigated (Figure 3.1d) while maintaining its antioxidant activity and retaining maximum cellulose and lignin compositions in the residual solids were investigated. The proposed AP involved protocols of White et al. [387] and Kim et al. [395] (2M NaOH, 0.25–4 h, and 25–60ºC) that favored bound polyphenol extraction, and the condition of Chen et al. [232], Renard et al. [396] and Yashoda et al. [397](1–4 M NaOH, 25–90 ºC and 0.5–16 h) that favored hemicellulose extraction. Based on these protocols and yield compromises for both products and the residual solid components, preliminary experiments were carried out and the applicable ranges of the AP conditions for the bioactive hemicellulose extraction from the destarched MSK were selected (Chapter 4, section 4.4.4). Thus, the destarched MSK was treated in alkaline solutions (1–2 M NaOH) containing 20mM sodium borohydride ($NaBH_4$), at various temperatures (40–90°C) for different reactions times (2–4 h) using a solid loading of 10%wt. Characterization and optimization of the process conditions were carried out to determine the best conditions that favor maximum hemicellulose yield, TPC and AA in the extract, and maximum lignin and cellulose contents in the solid residue (detailed in Chapter 4, section 4.4.5).

3.3.2. Mango seed husk fractionation

For the MSH, due to the insignificant starch and polyphenol contents but significant cellulose, hemicellulose, and lignin contents (Table 2.3), a mild AP followed by homogenization-assisted organosolv pretreatment/fractionation process were selected and combined in a sequence that favors the recovery of the hemicellulose, lignin, and cellulose in their polymeric forms while aiming for minimal losses of each product.

3.3.2.1. First step: Hemicellulose recovery from untreated mango seed husk

The first step for the MSH after mechanical size reduction was AP aimed at recovering hemicellulose polymers while aiming for minimal cellulose and lignin degradation in the residual solids for fractionation in the next stage of the multi-step biorefinery process (Chapter 5, section 5.1). The factors considered in this step of the multi-step biorefinery process were NaOH concentration, temperature, and reaction time (which affects the extractability and qualities of the hemicellulose (i.e. purity, molecular weight, and thermal stability) [83], [272]. Part of the objectives of this study was to recover polymeric hemicellulose and test its suitability for the development of self-supporting biocomposite film for potential application in food packaging (Figure 3.1e-f) while ensuring minimal cellulose and lignin degradation in the solid residue (Objective 2, section 5.1). Acid treatments were avoided due to the hemicellulose monomeric sugars being bound by weak ester bonds that could easily be hydrolyzed by the acids [241]. The water extraction route also has setbacks of low yields (4–7%) and was therefore not considered [43]. The AP has been documented to result in high hemicellulose yields (up to 90%) with high *Mw* (that allows for better mechanical and thermal properties of hemicellulose-based films) [63], [398], [399] due to the ability of the reagent to selectively cleave acetyl groups without cleaving the glycosidic linkages between the hemicellulose sugars at the applied low pressures and temperature conditions [175], [178], [241], [400].

Hemicellulose (particularly xylan) extractions have been achieved with alkaline solvents (0.5–2 M) as indicated in Table 2.10 under temperatures above 40 ºC, facilitated by the reduction in the density of solvents at such high temperatures [401]. Xyloglucan on the other hand is extractable either in the presence of water using reaction times up to 3h [61], [192], [402] or in 1–4 M alkali solutions using reaction times up to 16 h, depending on the composition of the biomass and type of xyloglucan [191], [396], [403]. AP also results in the dissolution of lignin and other phenolic compounds at higher reaction severities [34], [176]. Although purity is one of the attributes of hemicellulose that affects hemicellulose-based film

development, it has been established that lignin and uronic acids serve as natural plasticizers that aids in film development [42], [178]. For hemicellulose-based films, purities of ≤80% with lignin as the major impurity [42], [178], [216] have been reported, nevertheless, lignin results in opaque films, thus, the AP process conditions can be selected and optimized for hemicellulose with high purity [(i.e. minimal lignin contents (<20%)].

Although the AP can be used for the effective recovery of hemicellulose, it is also selective towards lignin and could cause the peeling of cellulose sugars [404]. Generally, temperatures below 100 ºC have been reported to minimally affect peeling reactions in cellulose because of the less energy required to break the inter/intramolecular H-bonding [84]. The glycosidic linkages in hemicellulose are also cleaved at temperatures >150 ºC at high pH [405]. Thus, for the extraction of hemicellulose polymers with high purity (minimum lignin content) and molecular weight using the AP method, milder treatment conditions were employed, as the solubility of lignin and peeling of cellulose, sugars increase with pretreatment severity [42], [86], [404]. Based on data from literature and preliminary studies (Appendix B), the dried MSH samples were subjected to different alkali concentrations [1–2 M NaOH containing 20 mM sodium borohydride ($NaBH_4$) to prevent cellulose peeling reactions [84], temperatures (40–90 °C) and reaction times (2–4 h) (Chapter 5, section 5.2) [83], [272]. After the hemicellulose precipitation with ethanol, the filtrate obtained was distilled to recover the ethanol (using a rotary evaporator) and the residual filtrate was air-dried in a vacuum oven to recover dried lignin. Characterization and optimization of the AP conditions were done to determine the best combination of treatment conditions that results in high yields of an extract with a lower xyloglucan/xylan ratio, lower lignin, and uronic acids (high purity). The recovered MSH hemicellulose was tested to investigate its suitability to produce self-supporting and thermally stable biocomposite film (assessing the thermal and mechanical properties) whereas the residual solids obtained were used in the next stage of the multi-step process for lignin and cellulose recovery (Details are highlighted in Chapter 5).

3.3.2.2. Second step: Lignin recovery from alkaline pretreated mango seed husk

In the next stage of the multi-step biorefinery process for MSH fractionation, the solid residue recovered after the AP optimization of MSH (for hemicellulose extraction) was subjected to HSHO treatment to extract lignin and obtain cellulose-rich fibers. Part of objective 2 was to recover high purity, less condensed lignin (for potential application in resin production) compared to the kraft and lignosulfonate lignin, and cellulose-rich fibers with properties (purity, Crl, etc.) that could suit CNC production (Section 2.13). Organosolv

pretreatment/fractionation (OP) process was considered in the present study due to the recoverability of the organic solvents or their aqueous mixtures and their effectiveness [68], [85] in generating lignin that presents different properties in terms of purity, molecular weight and molecular weight distributions compared to other technical lignin such as Kraft lignin [90]. The application of high temperatures (>160ºC) and acid catalysts in OP however results in undesired lignin condensation reactions, thus, significant lignin modifications for the intended application [89], [213], [316], [406]. To achieve desired product yields and qualities (molecular weight, purity, etc.) other physicochemical/mechanical techniques such as steam explosion have been included in the OP process [68], [407]. In the present study, a rotor-stator high shear homogenization (HSH) technique was combined with the OP to increase biomass surface area and facilitate the fragmentation and dissolution of lignin at reduced temperatures (<150 ºC) to limit lignin condensation and recover cellulose-rich pulp with properties (purity, Crl, etc.) that could suit CNC production (Figure 3.1g). Thus, this stage of the multi-step biorefinery process for the MSH was aimed at recovering high purity and less condensed lignin and cellulose-rich pulp from the AP treated MSH using OP plus high shear homogenization, hereafter called high-shear homogenization assisted organosolv pretreatment (HSHO). The HSHO pretreatment of the AP residual solids was based on optimized RSM for lignin dissolution and purity, high cellulose with low lignin, and hemicellulose contents in residual solids (Chapter 5, section 5.18). The process parameters considered were ethanol concentration, reaction temperature, and homogenization time. The lignin was characterized to determine its properties and suitability for phenol-formaldehyde resin production based on less modification and high purity, whereas the cellulose-rich material was characterized and tested for its suitability to be used in CNC production employing less severe treatment conditions (Figure 3.1h). The present study thus developed a novel HSHO process to pretreat/fractionate the AP MSH in a biorefinery. Detailed information can be found in Chapter 5.

3.3.3. Cellulose nanocrystal production from cellulose-rich pulp obtained via a multi-step biorefinery process

The conventional sulphuric acid-based treatment for CNC production is most preferred because of the production of CNCs that disperse easily in water [25]. However, the CNCs exhibit poor thermal stability making it problematic when applied in biocomposites produced via simple melt blending [408], [409]. The use of organic acids as alternative treatment methods has been suggested owing to their ability to produce thermally stable CNCs but the major drawback is their weaker acidity and thus require inorganic acid catalysts such as HCl,

sulphuric acid among others, and longer reaction times to produce the CNC, which makes the process less sustainable [51], [97], [409]. A non-catalyzed organic acid-based treatment could be a more sustainable alternative process to the sulphuric acid-based treatment, which was tested in the present study because it was observed that the multi-step biorefinery process consisting of AP and HSHO could increase the purity and surface area, reduce the crystallinity (Crl) [although the Crl was within the range (50–90%) required for CNC production] and produce individualized cellulose-rich pulp with particle diameter in the range of <1 µm to 10 µm (Chapter 5, detailed in section 5.2.10). It was hypothesized that due to these qualities of the cellulose-rich pulp, CNCs could be produced using only organic acids (formic and acetic acids) (Chapter 6). Thus, following the multi-step biorefinery process involving sequential AP and HSHO processes, the recovered cellulose-rich pulp was used to produce CNCs via organic acid-based (formic and acetic acids) treatments without prior bleaching contrary to the observed trend in the conventional nanocellulose production processes (bleaching before sulphuric acid hydrolysis). The selected organic acids were formic and acetic acids due to their ease of recovery at lower temperatures (<100 ºC under pressure) and reuse thus could save cost. An RSM was used to optimize the formic acid treatment conditions (acid-to-pulp ratio and reaction time) based on the nanocellulose yield, particle size, polydispersity index (PDI), ζ-potential, formate content, and crystallinity index (Crl). The product from the optimized process was characterized based on thermal stability, morphology, among others, and compared with that produced from the classical sulphuric acid-based hydrolysis of bleached pulp (Chapter 6). The production of CNC using acetic acid was based on a factorial design with considerations given to the yield, average particle size, ζ-potential, PDI, and degree of acetyl substitution. Further, an additional high shear homogenization treatment was included to determine its influence on the yield and quality of the acetic acid nanocellulose. A detailed process for nanocellulose production and characterization is provided in Chapter 6.

Table 3.1: Selected products, treatment processes, and justification

Product	**The rationale for product selection**	**Treatment/fractionation method**	**Novelty**	**The rationale for the selected products and treatment processes**
Polyphenols	Composition of feedstock, field of application, and commercial value	Organosolv extraction (Figure 3.1 b)	(a) For mango seek kernel valorization- Novel multi-step biorefinery scheme consisting of sequential organosolv extraction, enzymatic hydrolysis, and alkaline pretreatment processes was developed (b) Established optimal conditions for step-wise recovery of multi-products while ensuring all products are recovered in good yields and properties for intended applications, thus mitigating biomass component losses for subsequent extraction operations. (c) Recovery of additional bioproducts that would have been discarded as waste in the single product extraction schemes	(a) Serves as antioxidants in food and non-food industries, recoverable solvent, compliance with good food manufacturing practices
Starch	Based on the composition of the feedstock, field of application of bioproduct	Enzymatic treatment (Figure 3.1c		(a) Bioactive hemicellulose for active food packaging or antioxidant (b) AP results in recovery of hemicellulose polymers compared to the conventional Kraft process that results in hemicellulose monomers or oligomers used mainly as fuel. (c) AP increases the surface area and improves the accessibility of biomass for further processing
Bioactive hemicellulose (xyloglucan)	Based on the composition of the feedstock, field of application of bioproduct and commercial value; (Hemicellulose)	Alkaline pretreatment (Figure 3.1 d)		
Solids enriched in cellulose and lignin	Composition of feedstock	Alkaline pretreatment (Figure 3.1c)		(a) Serves as a substrate for further valorization

Table 3.1 continued

Hemicellulose (Xylan/xyloglucan mixtures) High purity lignin Cellulose-rich fibers	Based on the composition of the feedstock, field of application of bioproduct, and commercial value Based on the composition of the feedstock, field of application of bioproduct, and commercial value Lignin Based on the composition of the feedstock, field of application of bioproduct, and commercial value Cellulose	Alkaline pretreatment (Figure 3.1 e) High shear homogenization-assisted organosolv pretreatment (Figure 3.1 f) High shear homogenization-assisted organosolv pretreatment (Figure 3.1 f)	(d) A hemicellulose extract that depends on the inherent properties of the optimized composition to enhance suitability for self-supporting and thermally stable biocomposite film development (e) Developed a novel high shear homogenization assisted organosolv pretreatment process that performs under lower temperatures compared to the conventional organosolv pretreatment process (f) Recovery of cellulose-rich solids from a multi-step AP plus HSHO with properties suitable for cellulose nanocrystal production via mild organic acid treatments	a) Recovery of hemicellulose for potential self-supporting biocomposite film development (a) High purity, less condensed lignin for resin/plasticizer application (b) Numerous phenolic structures of lignin could provide antioxidant activity in biopolymers, act as UV-light absorbents. (d) OP is widely accepted for fractionating high-purity lignin and highly accessible cellulose-rich pulp. (e) Organic solvents can easily be recovered and reused. (c) cellulose-rich solids for controlled hydrolysis into nanocellulose (f) High shear homogenization works under low pressures and improves biomass accessibility to solvent without issues of clogging contrary to high-pressure homogenization
Nanocellulose	Unique inherent properties and diverse applicability, commercial value; Cellulose nanoparticles	Non-catalyzed organic acid (formic and acetic acid) hydrolysis (Figure 3.1 h)	(g) Developed an optimized non-catalyzed formic acid-based treatment for producing thermally stable nanocellulose (h) Identified the impact of a multi-step AP plus HSHO process on the production of hydrophobic cellulose nanocrystals via mild acetic acid-based treatment	(a) Organic acid is less corrosive and can be recovered and reused, unlike the classical sulphuric acid process that requires expensive corrosive-resistant equipment and cumbersome downstream effluent processing. (b) Production of thermally stable formylated/acetylated nanocellulose compared to the sulfated sulphuric acid nanocellulose. (c) Nanocellulose can be obtained with hydrophobic properties, requiring no further modifications for application in hydrophobic matrix.

3.3.4. Hemicellulose-based biocomposite film development

A hemicellulose-based film was developed from the MSH hemicellulose extract using the solvent casting method and compared with commercial beechwood xylan-based and combined xylan/xyloglucan-based films. Previous studies focused on hemicellulose-based film production based on xylan (particularly the water-extractable) due to the formation of transparent films for food packaging. However, its lower molecular weight favors the formation of brittle films with low thermal stability and mechanical properties, thus, requiring modifications (addition of plasticizers and other high *Mw* biopolymers) to aid in film formation. The feasibility of a hemicellulose extract obtained via an optimized AP process (Chapter 5, section 5.12) in biocomposite film development was tested and compared with films made with commercial xylan and xyloglucan. The solvent casting method was chosen over other methods due to its advantage of producing smooth thin films in addition to the requirement of lower operational temperatures such as room temperature [383]. Other methods such as extrusion are performed at high temperatures (90 ºC) which could result in hemicellulose degradation. The effect of varying the xyloglucan/xylan ratio on the formation of self-supporting films, the thermal stabilities, and the mechanical properties of films were studied. Details of the processes involved are provided in Chapter 5.

3.3.5. Characterization of bioproducts

Characterization (i.e., qualitative, and quantitative analysis) of the bioproducts and solid residues is an important part of the fractionation process because it helps in establishing the effectiveness or success of the applied processes. Various characterizations were performed on the recovered products using the selected analytical techniques presented in Table 3.2 and detailed in the respective Chapters (Chapter 4–6). The effectiveness of the multi-step biorefinery process on the product streams and the product qualities (for specific applications or further processing into valuable products) were assessed using various analytical instruments (Chapters 4–6, detailed in the respective chapters). The data obtained from these characterizations will provide essential information with regard to the effect of the multi-step biorefinery processes.

Table 3.2: Characterization of the bioproducts

Product	**Characterization**	**Mode of analysis (Instrument)**
Multi-functional hemicellulose Bioactive hemicellulose	Sugar composition + linkage analysis, Molecular weight, Structural changes, Thermal stability, Antioxidant activity, Total polyphenol content, Zeta-potential	Respectively- High-performance liquid chromatography (HPLC)+Nuclear Magnetic Resonance Spectroscopy (NMR), Gas Chromatography-Mass Spectroscopy (GC-MS), Size-exclusion Chromatography (SEC), Fourier Transform Infrared spectroscopy (FTIR), Thermogravimetric analyzer (TGA), DPPH-radical scavenging, Follin-ciocaltaeu method, Dynamic light scattering (DLS)
High purity lignin	Structural changes + Chemical composition+ Purity, Molecular weight, Elemental composition,	Respectively- HPLC+ FTIR, SEC, X-ray Photoelectron Spectroscopy (XPS)
Cellulose-rich fibers	Crystallinity, Morphology, Particle size, Structural changes,	Respectively- X-ray Diffraction (XRD), SEM, Zetasizer, FTIR
Nanocellulose	Crystallinity, Morphology, Particle size, Structural changes, Zeta-potential +polydispersity	Respectively- XRD, SEM+STEM, DLS, FTIR, Zetasizer
Polyphenols	Antioxidant activity, Total polyphenol content	Respectively- DPPH-radical scavenging, Follin-ciocaltaeu method
Hemicellulose-based films	Thermal stability Mechanical properties	TGA Instron machine

4. Development of a multi-step biorefinery scheme for the recovery of polyphenols, starch, and bioactive hemicellulose from mango seed kernel

Manuscript contributing to this chapter

1. **Title: A multi-step biorefinery process for the sequential recovery of mango seed kernel polyphenols, starch, and bioactive hemicellulose**

Chapter Summary

In this Chapter, a multi-step biorefinery process was developed and optimized for fractionating mango seed kernel (MSK) (Objective 1, section 2.14.2). The multi-step process involved sequential organosolv extraction (OE), enzymatic hydrolysis (EH), and alkaline pretreatment (AP) for recovering polyphenol, starch-based simple sugars, and bioactive hemicellulose polymers with antioxidant properties respectively, while ensuring minimal degradation of cellulose and lignin in the solid residues for further valorization. The OE was performed varying ethanol concentration and temperature and the process was optimized for the recovery of free polyphenols for potential application as antioxidants. The optimized condition (64.99% ethanol concentration, 54.18 ºC) resulted in an extract with 95.21 mg GAE/g total polyphenol content (TPC) having 84.69% antioxidant activity (AA), plus high (>90%) cellulose, hemicellulose, lignin, and starch recoveries in the solid residues. Subsequently, the EH treatment was performed on the OE solids to recover the starch-based simple sugars (for potential application in ethanol production). The applied EH resulted in approximately 96% starch removal from the biomass while retaining >80% cellulose, hemicellulose, and lignin in the solid residue (destarched solids). Finally, the destarched solids were subjected to the AP to recover bioactive hemicellulose for potential application in active biocomposite film development or as natural antioxidants in food. The bioactive hemicellulose yield of 54% with a TPC of 34.96 mg GAE/g and 55% AA was achieved. Thus, resulting in total polyphenol (i.e., both free and bound) recovery of 130.17 mg GAE/g vs 101.68 mg GAE/g achieved for single extraction schemes for only free polyphenol. The established optimal conditions for the bioactive hemicellulose (1.07 M, 44ºC, and 2.16 h) showed better performance in terms of yield than that reported for destarched wheat bran (20.8%; 0.44M NaOH, 80 ºC and 15 h). Hence, the multi-step biorefinery process demonstrated potentials for recovering the multi-products (polyphenols, starch, and bioactive hemicellulose) for the targeted applications, plus

added advantage of collective non-degrading impacts of the multi-step pretreatment on the final solid residue components (cellulose and lignin) for further valorization. Thus, the multi-step biorefinery process is promising for the enhancement of the MSK biomass utilization potential vs the single product extraction schemes.

Declaration by the candidate:

With regard to Chapter 4, pg. 90–118 the nature and scope of my contribution were as follows:

Nature of contribution	**Extent of contribution**
Planning and execution of experiments, data analysis and interpretation, and writing of the chapter	80

The following co-author(s) have contributed to Chapter 4, pg. 90–118:

Name	**E-mail address**	**Nature of contribution**	**Extent of contribution**
Chimphango, A.	achimpha@sun.ac.za	General discussion and chapter review	15
Görgens J. F.	jgorgens@sun.ac.za	General discussion and chapter review	5

4.1. Development and optimization of a multi-step biorefinery process for the recovery of polyphenols, starch, and bioactive hemicellulose from mango seed kernel

Manuscript

4.2. Abstract

The study assessed the potential of a developed multi-step biorefinery for fractionating mango seed kernel (MSK) into multi-products. The multi-step biorefinery scheme that consists of sequential organosolv extraction (OE), enzymatic hydrolysis (EH), and alkaline pretreatment (AP) process was developed to recover free polyphenols, starch (as simple sugars), bioactive hemicellulose (hemicellulose with bound polyphenols) while minimizing the degradation of cellulose and lignin in the residual solids. The first step of the multi-step biorefinery process involved the optimization of an organosolv extraction (OE) process to recover free polyphenols while minimizing the degradation of cellulose, hemicellulose, lignin, and starch in the solid residue. This was followed by a second step enzymatic hydrolysis (EH) of the remaining solid residue to remove starch. Finally, optimization of alkaline pretreatment (AP) was performed on the destarched solids for the recovery of bioactive hemicellulose while ensuring minimal cellulose and lignin degradation in the remaining residual solids. The optimal OE conditions (64.99%v/v ethanol concentration, 54.18 °C) resulted in an extract of 95.21 mg GAE/g total polyphenol content (TPC) with 84.69% antioxidant activity (AA). Enzymatic treatment of the OE residue resulted in recovery of >96% starch. Subsequent AP of destarched OE solids at the optimal conditions (1.07 M NaOH, 43.98 ºC, and 2.16 h) resulted in a xyloglucan-based hemicellulose extract (53.68%) with molecular weight, TPC, and AA of ≈108,163 g/mol, 34.96 mg GAE/g and 55.05%, respectively. The free polyphenols together with polyphenols bound to the hemicellulose, accounted for a total polyphenol recovery of 130.17 mg GAE/g that exceeded recoveries from a single extraction process (101.68 mg GAE/g) while increasing hemicellulose recoveries (53.68% vs 20.8%). The percentage lignin and cellulose retention in the recovered solids after the multi-step OE, EH, and AP biorefinery process were 88.3% and 91.12% respectively, indicating minimal degradation effect of the developed process on these components. Thus, these components can be further fractionated and valorized for diverse applications. FTIR and SEM revealed significant structural and morphological changes in the MSK after each step of the multi-step biorefinery process. Therefore, the sequential OE, EH, and AP processes presented opportunities for increasing the product spectrum while preserving their properties.

4.3. Introduction

Increasing demands for mango and mango products in recent years, due to derived therapeutic and nutritional benefits, results in increases in global mango productions (> 52 million metric tons in 2018) [104]. The associated mango processing waste has correspondingly increased with global generation capacities of above 1 million tons [8]. Management of the seed waste is often limited to disposal by incineration, open discard in dumpsites, or landfilling, leading to environmental and economic detriments such as greenhouse gas (GHG) emissions and land use concerns [410].

The mango seed makes up 10–25% of the mango fruit based on a variety [8]. The seed consists of a husk [cellulose (34.68–55%), hemicellulose (20.6 – 28.63%), and lignin (9.0–25.5%) [20], [21]] and kernel [lignin (2.03–15%), starch (18–50%), fat (11%), protein (6%), polyphenols (21.6–447 mg/g), hemicellulose (14.13–52.4%), and cellulose (2.88–25.2%)] [8], [131]. Thus, the mango seed contains high-value products such as polyphenols, which have established antioxidant, anticancer, and antimicrobial properties [411]. For instance, several studies have shown potential for mango seed kernel (MSK) polyphenols as antioxidants in food and pharmaceutical applications [104]. The lignocellulosic components in the MSK could also be exploited in various bioproduct applications. For instance, hemicellulose is a highly sought-after biopolymer for packaging applications due to its film-forming ability [43]; lignin is used in the preparation of resins and carbon fibers [85]; cellulose is treated further to obtain nanocellulose for reinforcement purposes [20].

Demand for bioproducts increased in recent years, attributable to the rising health and environmental concerns associated with their synthetic or fossil-based counterparts [8]. Accordingly, using the MSK as a biorefinery feedstock for producing multiple valuable products could add value to the waste and increase revenue for the mango processing industry, and also mitigate the economic and environmental detriments of current waste management schemes [410]. However, in targeting multiple products from a single feedstock, there is the drawback of low yields and quality (purity) due to the differing optimal extraction conditions of each product. Thus, the biorefinery set-up will require amenable extraction methods and process conditions including time, solvent type and concentration, and temperature [135]. Previous studies on the bioproduct exploits for the MSK focused on improving the yields for single product extractions such as polyphenols, oils, and protein with little attention paid to solid residue substrates that contain mainly hemicellulose, cellulose, and lignin [11], [111]. For instance, optimized organosolv processes for kernel-based polyphenol extraction in high yields

and with high antioxidant activity, have been investigated, but little has been reported on the fate of the remaining solid residue components [11], [127]. In the organosolv process, the free polyphenols are extracted through the dissolution of the biomass cell membrane while the bound polyphenols are mostly retained in the solid residue due to their strong attachment with other cell wall components such as carbohydrates and proteins [71], [245].

Free polyphenols are extracted using organic solvents concentrations of 50–80% v/v and temperatures of 25–60 ºC; conditions that are not sufficient to extract bound polyphenols [9], [67], [103]. Bound polyphenols are extractable under alkaline conditions of 2–8 M NaOH over a time up to 4 h [81], [245], Likewise, hemicelluloses are extracted using 1–4 M NaOH at temperatures of 25 ºC to 90 ºC [83], [191], [232]; conditions where the free polyphenols are reported unstable [387]. The MSK is also composed of high starch content, which could impede product extraction due to the formation of highly viscous solution and need to be removed. Although starch can be removed from biomass through different processes such as alkaline and acidic treatments, enzymatic treatment will be favorable due to its substrates specificity such that the integrity of the other biomass components could be maintained for extraction in the subsequent fractionation stages.

Thus, the different requirement of process conditions of the individual components could suggest that the integration of the individual extraction processes in the right sequence to develop a multi-step biorefinery to recover the free polyphenols, starch, and bioactive hemicellulose while minimizing the degradation of the cellulose and lignin in the solid residue will be effective for MSK valorization. Although several studies have focused on the development of multi-step biorefineries for the recovery of multi-products from biomass, there is limited data on the application of the proposed multi-step process for the recovery of the envisaged products from MSK. In addition, the effect of each treatment step in the multi-step process is not extensively addressed. Thus, after the free polyphenol extraction, the solid residue could be further processed with enzymes to remove starch and the destarched residue treated with alkaline solutions (e.g. NaOH solution) to extract hemicellulose with bound polyphenols to yield bioactive hemicellulose with antioxidant potential [261], thereby recovering both free and bound polyphenols, hemicellulose, starch, and cellulose/lignin rich solids via the multi-step sequential organosolv extraction (OE), enzymatic treatment (EH) and alkaline pretreatment (AP) processes.

Hemicellulose with bound polyphenols could be used for active food packaging due to the combined functional and physicochemical property of the hemicellulose and antioxidant

activity of the phenolic compounds or as natural antioxidants in food [178], [282]. Thus, understanding the degradation impacts of the OE process on the residual solid substrates is imperative for sustainably recovering multi-products including free extractable polyphenols, starch, bioactive hemicellulose, and solid residue enriched in cellulose and lignin through subsequent EH, and AP in an integrated biorefinery context. The present study developed a multi-step biorefinery process that consists of sequential OE, EH, and AP for the recovery of free polyphenols, starch (as simple sugars), and bioactive hemicellulose from MSK while aiming for minimal degradation of the recovered solid residue substrates (cellulose and lignin), to increase the product spectrum from the MSK. The effect of each treatment stage in the multi-step process was assessed through scanning electron microscopy and Fourier Transform infrared spectroscopy.

4.4. Materials and methods

4.4.1. Chemicals

The mango seed kernel was obtained as detailed in section 3.2.1. Ethanol (95% v/v), and sodium carbonate, were obtained from Science World (Cape Town, South Africa) while gallic acid, Folin Ciocalteu reagent, 1-diphenyl-2-picrylhydrazyl (DPPH), acetic acid, sulphuric acid, carbazole, galacturonic acid, standard glucose, xylose, and arabinose were purchased from Sigma Aldrich (Johannesburg, South Africa). Commercial xyloglucan, D-galacturonic, and D-glucuronic acids were purchased from Megazyme International, Ireland. All chemicals were of analytical grade.

4.4.2. First extraction stage: organosolv extraction of polyphenols

Approximately 10 g of MSK powder was weighed into scotch bottles (250 mL) and 100 mL ethanol (50–80% v/v) was added to give a solid-to-liquid ratio of 1:10. The reaction was carried out in a shaking water bath (150 rpm) at varying temperatures (20–60 °C) for 1 h. All ranges of conditions employed in the study were obtained from preliminary experiments taking into account ranges that include the optimum prior to the optimization. The extracts were centrifuged at 8000 rpm for 10 min and filtrate decanted into plastic tubes, wrapped with aluminium foil, and stored at -4 ºC for analysis. The solid residue was washed with 300 mL distilled water, oven-dried at 30 ºC for 48 h, and stored in zip-lock bags for analysis.

4.4.3. Second extraction stage: Enzymatic hydrolysis of starch from the organosolv extracted solid residue

The solid residue obtained after organosolv extraction was destarched using thermostable α-amylase (Termamyl®SC) and amyloglucosidase (Saczyme®Plus) enzymes (from Novozymes) as detailed in Appendix A2. The glucose concentration from the starch hydrolysis was determined by HPLC as detailed in Appendix A.

4.4.4. Third extraction stage: Alkaline extraction of bioactive hemicellulose from the destarched solids

The destarched kernel was used for hemicellulose extraction using AP, where 10 g of the destarched MSK was weighed into 250 mL scotch bottles before adding 100 mL NaOH solutions (1–2 M) containing 20 mM sodium borohydride ($NaBH_4$). The mixtures were treated at varying temperatures (40–90 °C) and reaction times (2–4 h), centrifuged (Hermie Labortechnik GmbH, Z 366, Germany) at 3000 rpm for 15 min, and the filtrate neutralized to pH 5.5 with 6 M HCl. Experimental conditions were based on preliminary experiments and data from literature [232], [261]. The solids were washed with distilled water, dried at 40 °C and stored for further analysis. The extracts were dialyzed (cellulose membrane dialysis tubing with molecular weight cut-off of 14000 Da) against distilled water for 3 days, followed by precipitation with 95% ethanol, oven-dried at 25 °C for 48 h, and stored for characterization. Hemicellulose yield was calculated based on actual hemicellulose in the feedstock.

4.4.5. Optimization of polyphenol and bioactive hemicellulose extraction

Response Surface Methodology (RSM) was used to optimize the organosolv and alkaline processes for polyphenol and bioactive hemicellulose extraction from MSK. The extraction conditions optimized for higher total polyphenol content (TPC) and antioxidant activity (AA) of the polyphenol extract were ethanol concentration (50–80%) and temperature (20–60 °C), whereas NaOH concentration (1–2 M), temperature (40–90 °C), and reaction time (2–4 h) were optimized for higher hemicellulose yield, TPC and AA to obtain 10 and 16 runs respectively (Table 4.1 and 4.3). Data analysis was performed using Statistica 13.2 software. The coefficient of determination (R^2) and the lack of fit (LOF) were used to determine the adequacy of the models. Analysis of variance (ANOVA) was used to verify the statistical significance of the second-order model Equation 1.

$$Y = A_o + \sum A_i X_i + \sum A_{ii} X_{ii}^2 + \sum \sum A_{ij} X_i X_j + \varepsilon \qquad [1]$$

Where Y is the dependent variable; A_o is the constant for the model; A_i, $A_{ii,}$ and A_{ij} are the coefficients of the model (linear, quadratic, and interaction terms respectively); ε is the model error. The desirability function in Statistica 13.2 software was used to obtain the optimal desirability point. The desirability function in the statistica software works by assigning a desirability value to the responses with 0 being the undesirable and 1 being the desirable. Statistica combine these desirability values and generates desired conditions for the selected responses. Since each response exhibit different optimal condition, the disadvantage is that the best of all the responses will not be obtained in the overall optimal condition.

4.4.6. Characterization of kernel and products from the pretreatment processes

The untreated, organosolv extracted, and alkaline pretreated solids were analyzed for cellulose, hemicellulose, and lignin contents following the method described by Torres-León et al. [136] with modification as detailed in Appendix A. The starch content of residue was determined using the Megazyme starch assay kit (KSTA 09/14) as described in Appendix A. The total polyphenol content (TPC) of organosolv extract and bound polyphenols was estimated by the Folin-Ciocalteau method [135], [261] (see details in Appendix A). The sugar composition, thermal stability, molecular weight, and structural changes of the hemicellulose extracts were analyzed following the protocols elaborated in Appendix A.

4.5. Results and discussions

4.5.1. Optimization of organosolv extraction conditions for free polyphenols

The total polyphenol content (TPC) of the extracts [63.31–101.57 mg (GAE/g)] for the investigated process conditions (Table 4.1) compared favourably with literature values (18.19–292 mg GAE/g MSK) [11], [235], [412]. The maximum TPC and antioxidant activity (AA) were observed at 60 ºC and 50% v/v ethanol, which also corresponds to the highest cellulose, hemicellulose, and lignin contents of the recovered solids (Table 4.1).

The results from the analysis of variance (ANOVA) (Appendix A, Table A1) showed that the process conditions selected had significant influence on the responses. The R^2 values for TPC, AA, and recovered solids were 0.88, 0.83, and 0.99 respectively (Appendix A, Table A1) whereas that for the cellulose, hemicellulose, lignin, and starch contents of recovered solids were 0.96, 0.97, 0.99, and 0.92 respectively (Appendix A, Table A1). The R^2 values show that the developed models can predict accurately the selected responses [385]. The lack of fit (LOF) *p*-value was further used to confirm the model's sufficiency to describe the data. From Appendix A, Table A1, LOF *p*-values of 0.21, 0.06, and 0.20 respectively for TPC,

AA, and recovered solids, and 0.33, 0.05, 0.33, and 0.58 respectively for cellulose, hemicellulose, lignin, and starch contents of recovered solids respectively, indicate that the models were sufficient to describe the data [16]. The actual models developed for each response variable are shown in Appendix A, Equations A5–A10.

Table 4.1: Total polyphenol content and, scavenging activity of extracts and composition of recovered solids

Sample	Temperature (°C)	Ethanol concentration (%v/v)	Total polyphenol content mg (GAE)/g	Scavenging activity (%)	Solid recovery (%)	Hemicellulose content of residue (%)	Cellulose content of residue (%)	Lignin content of residue (%)	Starch content of residue (%)	[a]Others (%)
1	20.00	50.00	77.98	74.95	76.17	22.88	4.04	5.40	42.40	25.28
2	60.00	50.00	101.57	89.69	73.52	23.57	4.19	5.61	38.77	27.86
3	20.00	80.00	74.75	77.79	83.95	20.59	3.64	4.92	38.19	32.66
4	60.00	80.00	76.33	84.34	79.9	21.74	3.86	5.23	39.89	29.28
5	40.00	43.79	66.46	75.48	74.98	22.98	4.06	5.53	38.58	28.85
6	40.00	86.20	63.31	68.47	84.00	20.71	3.66	4.98	39.12	31.53
7	11.64	65.00	74.64	74.54	81.52	21.24	3.78	5.09	39.78	30.11
8	68.36	65.00	98.68	87.13	76.47	22.62	3.99	5.44	38.69	29.26
9	40.00	65.00	86.73	79.46	75.96	22.96	4.03	5.50	40.36	27.15
10	40.00	65.00	88.57	80.04	75.67	22.99	4.07	5.52	41.44	25.98

[a] 'Others' comprise components other than cellulose, hemicellulose, lignin, and starch in the kernel

4.5.1.1. The effect of organosolv process conditions on total polyphenol content and antioxidant activity of extract and recovered solids

The extraction temperature and ethanol concentration significantly affected (p<0.05) the TPC (Figure 4.1a) and AA (Figure 4.1b) of the extracts. The temperature had the largest effect on the TPC and AA as displayed by the linear effects in Figures 4.1a–b, respectively, which were followed by the quadratic effects of ethanol concentration. Both the linear and quadratic temperature and ethanol concentration effects were significant (p<0.05) on the recovered solids unlike their interaction effects (Figure 4.1c). The 3D response surface (RSM) plots relating the effects of temperature and ethanol concentration on the TPC, and AA of extracts are depicted in Figures 4.1d–e. The TPC and AA increased with ethanol concentration (43–65 %v/v) at a fixed temperature of 40 ºC, and and the TPC reduced for further increase in the ethanol concentration (> 65% v/v) (Figures 4.1d–e), which suggests the 65% v/v ethanol as optimum. This trend agrees with work done on MSK [67], [235]. Similarly, at 65% v/v ethanol, the TPC and AA increased with temperature up to the highest of 68 ºC (Figures 4.1d–e), thereby exhibiting a linear increase, consistent with work done by Ghafoor et al. [413] on grape seed. High temperatures (>40 ºC) favored the release of polyphenols in the solid matrix by causing the cell wall to become weak and soft for the solubility of the polyphenols to increase [414]. Additionally, reduced extraction solvent viscosity at increased temperature increases the solvent penetration into the biomass matrix thus, dissolving the polyphenols into the extraction medium with ease [11]. Nevertheless, the temperature cannot be increased after a certain (>70 ºC) threshold because it can cause degradation, evaporation, or oxidation of phenolic compounds through chemical, thermal, or enzymatic reactions [385]. Consequently, the temperature was limited to below 70 ºC in the present study to limit the degradation of polyphenols and other biomass components such as hemicellulose [78], [192]. Overall, to recover free polyphenols with high AA from mango seed kernel, ethanol concentration should be limited to ≤65% to save cost and maintain the bioactivity.

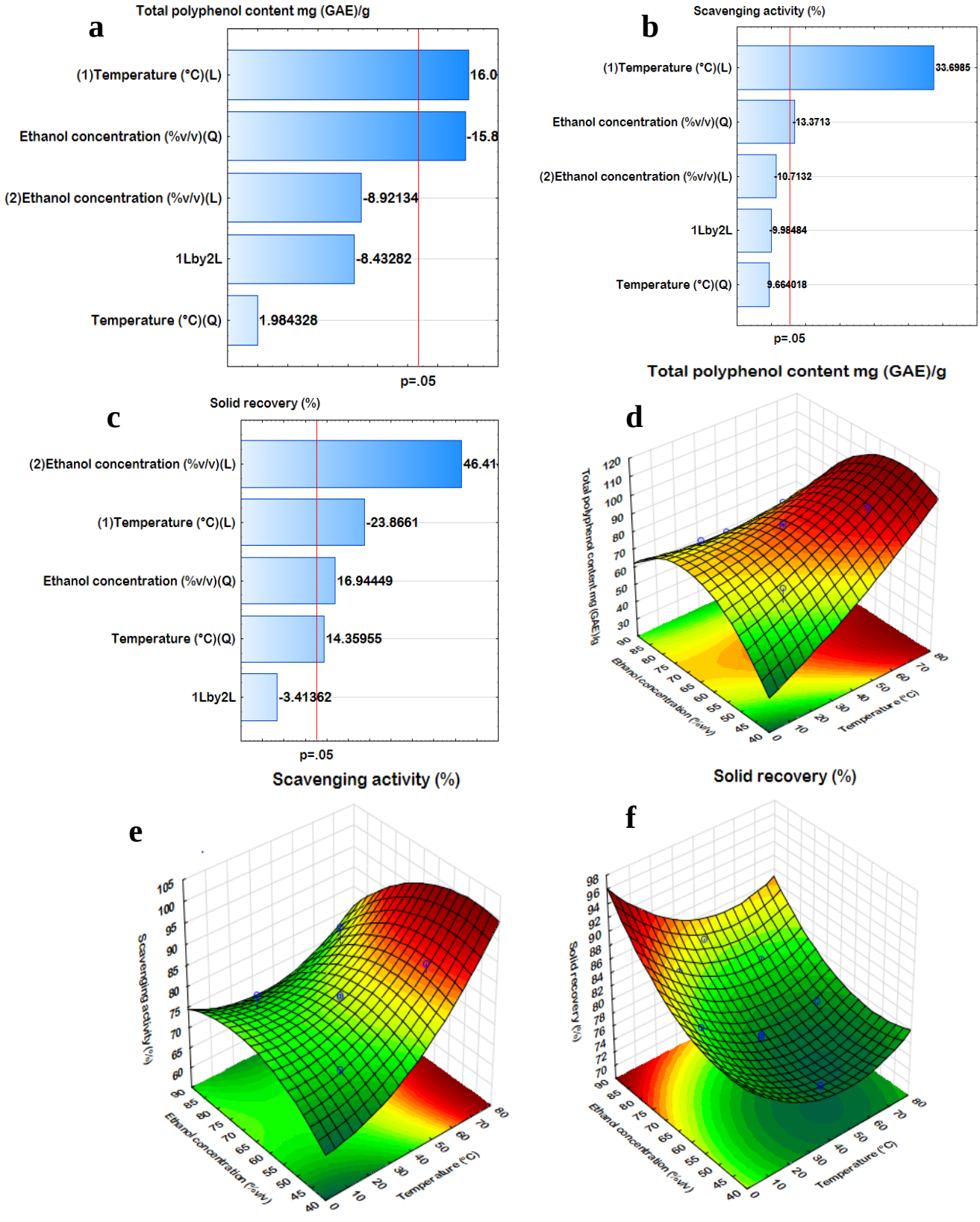

Figure 4.1: Pareto and response surface plots of the effect of ethanol concentration and temperature on the total polyphenol content, scavenging activity, and recovered solids.

The decrease in TPC and AA at elevated ethanol concentrations (>65% v/v) could be related to the polarity of the both the solvent and polyphenols [71]. Binary solvents show a greater contribution to the extraction of bioactive compounds than pure solvents since the solvating power of the mixture increases due to the dipolar moment, thereby leading to the higher dissolution of bioactive compounds [235]. The trend for the TPC and AA is consistent with work by Lim et al. [235], where the TPC and AA of MSK polyphenols increased with ethanol content up to 50% v/v and 65% v/v respectively, and then reduced when the ethanol was increased further.

4.5.1.2. Effect of ethanol concentration and temperature on the yield and composition of recovered solids after polyphenol extraction

The extraction of free polyphenols from the MSK resulted in 73.52–84.00% solid recovery (Table 4.1). ANOVA showed that the cellulose content of the recovered solids (3.66–4.19% (Table 4.1) was significantly (p<0.05) affected by the linear effect of ethanol concentration (Figure 4.2a). The linear and quadratic effects of temperature, the quadratic effect of ethanol concentration, and the interaction effect of temperature and ethanol concentration were not significant (p>0.05) (Figure 4.2a). On the contrary, all the parameters (linear and quadratic) investigated significantly affected both the hemicellulose (20.59–23.57%) and lignin (4.98–5.61%) (Table 4.1) contents except for the interaction of ethanol concentration and temperature (Figures 4.2b and c). For starch, even though the temperature (linear) showed a negative effect, (i.e., starch dissolution during free polyphenol extraction), the linear term of ethanol concentration showed a positive effect due to less solubility of starch in ethanol. However, none of these parameters was significant (p>0.05) at a 95% confidence level (Figure 4.2d).

The cellulose content was marginally affected at ethanol concentrations <50% v/v and temperatures below 50 °C due to the insolubility of cellulose at such conditions, arising from the strong inter/intramolecular hydrogen bonding of the cellulose fibrils (Figure 4.2e). However, as ethanol content and temperature reached and exceeded 60% v/v and 40 °C respectively, a slight reduction in the cellulose content was realized although it was not significant (Figure 4.2e), attributed to carbohydrate-lignin bond disruption or amorphous cellulose dissolution [14]. In a multi-step biorefinery for multi-product recovery, the temperature and ethanol concentration should be limited to 60% v/v and <60 ºC such that product loss will be minimized.

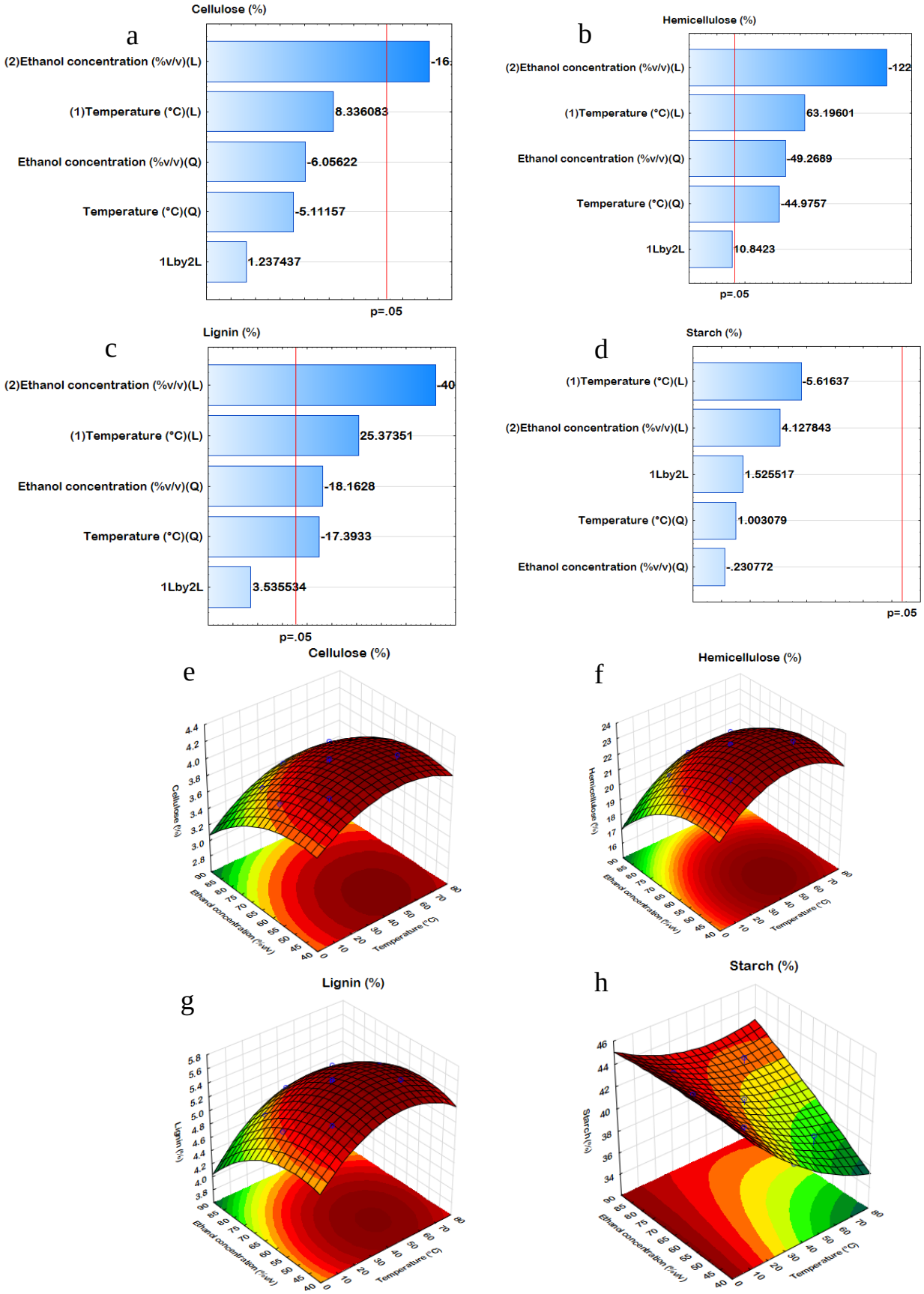

Figure 4.2: Pareto and response surface plots of the effect of ethanol concentration and temperature on the cellulose, hemicellulose, lignin, and starch content of solid residue

Similar to cellulose, the hemicellulose content of the recovered solids reduced at temperatures and ethanol concentrations above 65 °C and 65% v/v respectively (Figure 4.2f), indicating the partial dissolution of hemicellulose into the extraction medium at such conditions. The ester and ether bonds between hemicellulose and lignin and the glycosidic linkages in hemicellulose have been found to cleave at high temperatures and in the presence of organic solvents such as ethanol [14], [83]. The results show that to extract free polyphenols without significant carbohydrate dissolution from the solids in a biorefinery, the extraction should be performed at temperatures of about 50 °C and ethanol concentrations above 60% v/v (Figures 4.2 e and f). Concerning the lignin content of the solid, increasing the temperature and ethanol concentration to 50 °C and 55% v/v (respectively) enhanced polyphenol release from the MSK, resulting in increasing lignin contents in residue (Table 4.1 and Figure 4.2 g). However, as the conditions exceeded 60 °C and 60% v/v ethanol, a reduction in the lignin content was observed (Figure 4.2g), attributable to higher temperatures causing ions to migrate speedily into the biomass matrix, thereby disrupting linkages to disintegrate and solubilize lignin [14]. The starch content of the recovered solids increased until about 45 °C and 50% v/v ethanol (Figure 4.2h). Further increase in both parameters resulted in reduction in the starch content which could be due to gelatinization of starch and subsequent removal during the washing processes [415]. A similar temperature (40 ºC) could dissolve starch from wheat bran [78].

4.5.1.3. Verification of predicted optimal conditions for polyphenol extraction

Free polyphenols with high AA could be extracted from MSK under optimized conditions while still obtaining a solid residue with minimal component degradation for further valorization. The optimal conditions predicted by the model for maximum TPC (93.51 mg GAE/g) and AA (84.15%) of extracts, and maximum cellulose (4.08%), hemicellulose (23.09%), lignin (5.54%), and starch contents (40.01%) of residual solids were 64.99% v/v ethanol and 54.18 °C (Table 4.2). Triplicate experiments performed at the referred optimal conditions showed similar results to the model's prediction, thus confirming the predicted optimal conditions (Table 4.2). The TPC at the optimized condition falls within the 44.7–101.68 mg GAE/g reported for polyphenol from MSK [235], [388]. In conclusion, to maximize product recoveries, the identified optimum conditions could help save costs towards improving the economics of the biorefineries for investments. For instance, excessive temperature (i.e. energy input) and ethanol concentration, beyond the identified optimum, would imply higher operating costs due to the corresponding decrease in product yield and quality.

Table 4.2: Verification of predicted optimal conditions

Variable	Predicted	Observed	% deviation
Total polyphenol content mg (GAE)/g	93.51	95.21	1.79
Antioxidant activity (%)	84.15	84.69	0.64
Cellulose content of recovered solids (%)	4.08	4.19	2.63
Hemicellulose content of recovered solids (%)	23.09	21.11	8.58
Lignin content of recovered solids (%)	5.54	5.68	2.46
Starch content of recovered solids (%)	40.01	42.67	6.23

4.5.2. Optimization of alkaline bioactive hemicellulose extraction from the solid residue obtained after organosolv extraction and destarching

Optimization of AP conditions (NaOH concentration, reaction time, and temperature) for bioactive hemicellulose extraction from destarched OE MSK (3.59 g solids; with compositions of cellulose=8.22%, hemicellulose=38.55%, lignin=11.34%, starch=2.84%, and others=39.05%) was performed and responses are presented in Table 4.3. The hemicellulose yield ranged from 42.05–59.64%. However, the hemicellulose extract contained lignin and TPC of 4.02–11.67% and 30.03–46.43 mg GAE/g respectively and could scavenge 42.04–58.43% of DPPH radicals (Table 4.3). The relationships between the independent and dependent variables as presented in Appendix A, Equation A10–16.

The R^2 values for bioactive hemicellulose yield, the lignin content of hemicellulose extract, TPC, and AA of extract were 0.80, 0.72, 0.87, and 0.76, respectively which showed that the models could adequately describe the respective experimental data [416]. In addition, the lack of fit *p*-values was non-significant ($p > 0.05$) for the models at a 95% confidence level (Appendix A, Table A2). From Figure 4.3a, the temperature and NaOH concentration showed significant ($p<0.05$) individual effects on the hemicellulose yield but not the reaction time (linear and quadratic) and interaction effects of all the variables at a 95% confidence level (Figure 4.3a). For the lignin content of hemicellulose extract, only the linear term of temperature was significant ($p < 0.05$), whereas the rest of the variables and their interactions were insignificant ($p > 0.05$) (Figure 4.3b). In addition, the linear term of temperature and quadratic term of NaOH concentration was the only significant ($p < 0.05$) terms contributing to the TPC (Figure 4.3c), while only the linear term of temperature was significant towards AA (Figures 4.3c–d). With respect to the cellulose content of recovered solids, the quadratic term

of temperature exhibited the greatest effect (p<0.05), which was followed by the interaction of temperature and NaOH concentration, the linear effect of temperature, and then the linear effect of NaOH concentration (Figure 4.3e). For hemicellulose and lignin contents or recovered solids, temperature and NaOH concentration (linear and quadratic) were significant (p<0.05) model terms, while time and all the interaction terms were insignificant (p>0.05) (Figures 4.3 f-g).

Table 4.3: Centarl composite experimental design of independent variables and corresponding responses (independent variables) for hemicellulose extraction.

Conc [M]	Temp [°C]	Time [h]	Yield [%]	Lignin content [%]	Total phenolic content [mg GAE/g]	Antioxidant activity [%]	Cellulose content of recovered solids [%]	Hemicellulose content of recovered solids [%]	Lignin content of recovered solids [%]
1.00	40.00	2.00	55.23	7.13	34.15	54.95	13.06	29.83	18.25
1.00	40.00	4.00	52.18	7.91	33.52	51.79	11.56	33.21	18.29
1.00	90.00	2.00	50.29	8.96	34.68	45.13	11.34	27.45	15.90
1.00	90.00	4.00	47.97	9.73	33.59	46.34	10.44	28.96	13.96
2.00	40.00	2.00	55.17	7.43	41.01	55.48	10.49	31.38	17.29
2.00	40.00	4.00	52.44	9.98	42.98	52.69	12.16	32.17	14.91
2.00	90.00	2.00	50.02	9.22	44.37	45.47	10.23	27.11	15.57
2.00	90.00	4.00	47.54	11.00	40.03	44.54	10.53	27.55	13.24
0.66	65.00	3.00	52.24	4.02	33.32	52.98	12.10	32.94	20.51
2.34	65.00	3.00	48.01	9.35	46.43	55.97	11.38	26.88	13.19
1.50	22.96	3.00	51.54	4.08	38.54	58.43	10.02	36.22	18.29
1.50	107.04	3.00	42.05	11.67	30.03	42.04	9.63	24.12	12.30
1.50	65.00	1.32	50.33	7.02	42.45	59.46	10.96	31.31	13.78
1.50	65.00	4.68	58.52	7.64	35.47	50.23	12.79	28.03	12.56
1.50	65.00	3.00	59.64	6.87	41.04	56.18	11.29	30.87	14.26
1.50	65.00	3.00	57.31	6.68	39.98	52.69	11.06	31.81	16.27
1.50	65.00	3.00	58.26	4.27	37.01	47.89	11.75	32.70	13.90
1.50	65.00	3.00	54.59	6.32	40.11	57.24	11.55	30.74	15.47

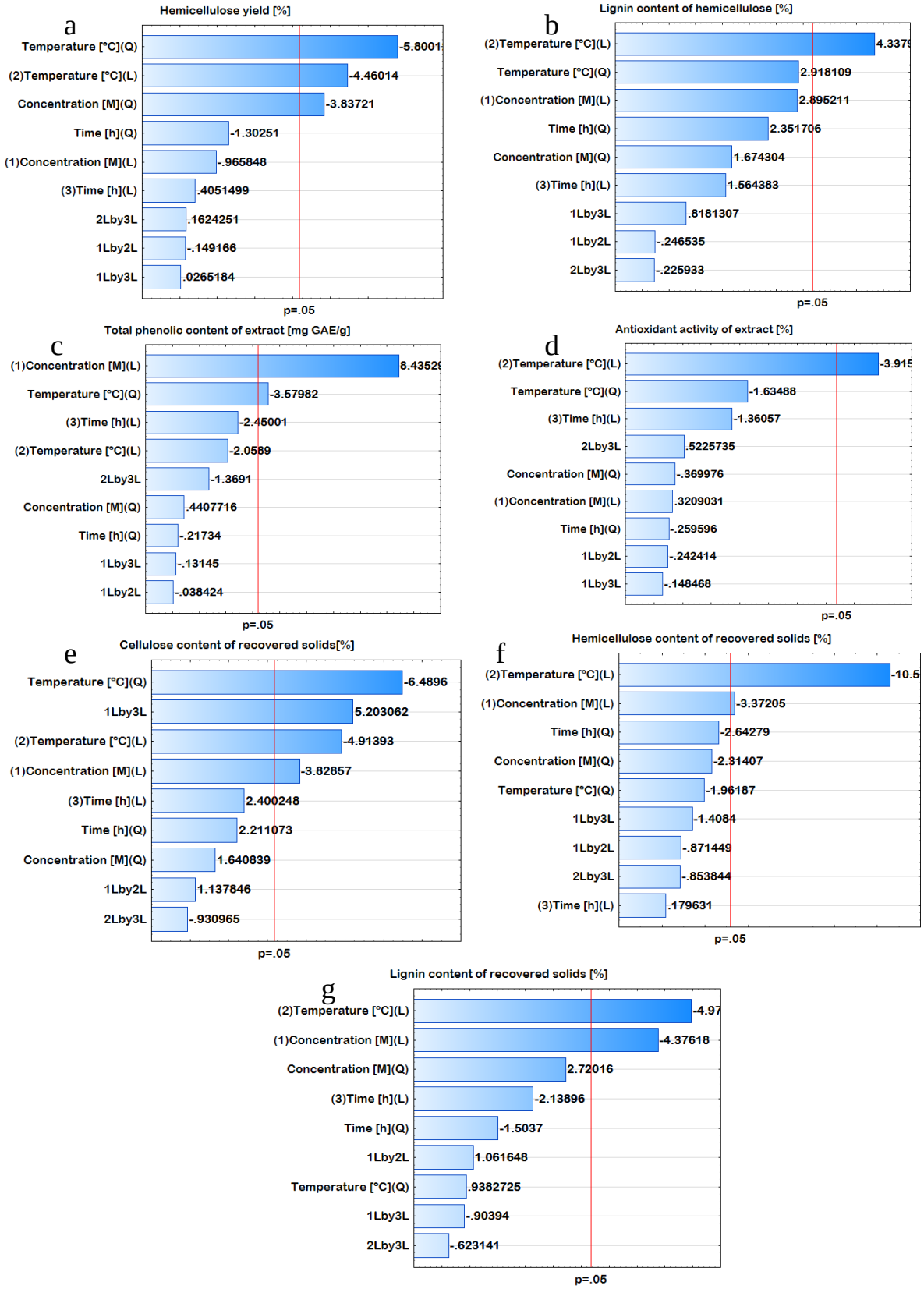

Figure 4.3: Pareto chat for (a) hemicellulose yield (b) lignin content of extract (c) total phenolic content of extract (d) antioxidant activity of extract (e) cellulose content of recovered solids (f) hemicellulose content of recovered solids and (g) lignin content of recovered solids.

4.5.2.1. Effect of alkaline pretreatment conditions on the bioactive hemicellulose extraction and properties

Figures 4.4a–d illustrates the RSM plots of the effect of NaOH concentration, temperature, and time on the yield, lignin content, TPC, and AA of the bioactive hemicellulose extract. At a constant time (3 h), increasing concentration of NaOH and temperature created a dome-shaped surface plot, indicating increasing yield to an optimum at approximately 1.5 M NaOH and 65ºC, and reduced with further increment in NaOH concentration or temperature (Figure 4.4a). Thus, with an increment in NaOH concentration and temperature, more hydrolyzing ions are introduced into the reaction medium that gains enough energy with the application of heat to effectively diffuse into the biomass, causing it to swell and weaken the glycosidic linkages and hydrolyze the alkali-soluble components, particularly the hemicellulose [272], [417]. Nevertheless, excessive increase in ion concentration (due to increment in NaOH) could increase the viscosity of the reaction medium and inhibit the dissolution of hydrolyzed hemicellulose, whereas extreme heat could cause excessive hydrolysis of bonds within the dissolved hemicellulose into simple sugars [43], [418]. A similar trend has been reported in the literature [418].

The relationships between temperature, NaOH concentration, and the lignin content of extract at a constant time (3 h) are shown in Figures 4.3c–d. At low levels of NaOH concentration and temperature, the lignin content was low due to less energy and hydrolyzing ions to overcome the strong C-C, ester, and ether linkages in the structure of lignin and between lignin and carbohydrates [14], [85]. When the temperature and NaOH concentration were increased, enough heat energy was gained by the high concentration of hydroxide ions which accelerated their penetration and aided lignin hydrolysis (Figure 4.4 c-d). Generally, at high temperatures, the kinetic energy of the hydrolyzing ions is high, making it effective to penetrate the biomass at a higher rate to hydrolyze the linkages especially in the amorphous regions [14], [419]. A similar trend was observed as both NaOH concentration and time were increased from 1 to 2 M and 1 to 4 h respectively at constant temperature (Figure 4.4d). This trend has been observed in many studies, whereby solubilized lignin is precipitated with the hemicellulose or dissolution of lignin-carbohydrate complexes that cannot be overcome by the reaction conditions employed [420].

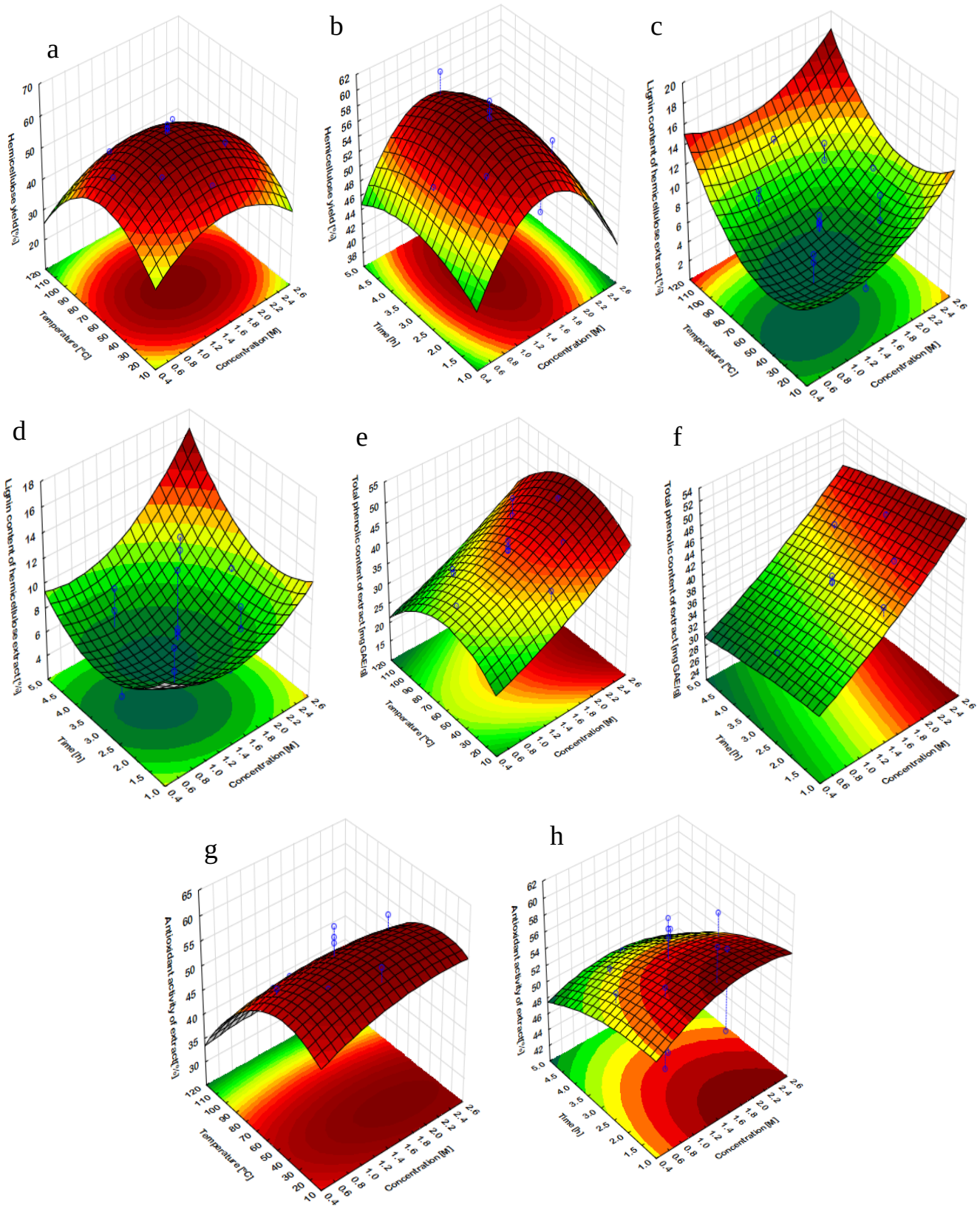

Figure 4.4: Response surface plots of (a–b) hemicellulose yield (c–d) lignin content of hemicellulose extract (e–f) total phenolic content of extract (g–h) antioxidant activity of extract

The RSM plots (Figures 4.4 c–d) show that to obtain hemicellulose extract with low lignin content, the temperature, which is the major factor should be kept below 60°C with NaOH concentration and time of ≈1 M and 3 h respectively. The dependence of the TPC on NaOH concentration, temperature, and time are depicted in Figures 4.4 e–f. The TPC increased with an increase in temperature from approximately 20 to 65 °C, whereas a reduction in TPC was observed with a further temperature rise (Figures 4.4 e-f). A similar trend has been observed in the literature [421]. As previously stated, temperature improves the diffusion of ions into the biomass for linkage hydrolysis; however, beyond a certain limit (in this case 65 °C), the stability of the phenolic compounds is affected by either thermal decomposition, the reaction of phenolic compounds with other components, or vaporization [422]. Another reason could be related to obstructions by other components such as hemicellulose and lignin due to their simultaneous dissolution during alkaline treatment, impeding the extraction of the polyphenolic compounds [421].

In relation to the AA, Figures 4.4 g–h show that extracts with high AA from mango seed kernel can be obtained when the extraction is carried out at reaction temperatures below 65 ºC, reaction times less than 3 h and NaOH concentrations between 1-3 M (Figures 4.4 g–h). This result corroborates that of the TPC (Figures 4.4 e–f). The AA increased with temperature due to improved extraction of phenolic compounds. However, extreme temperatures degrade or volatilize the phenolic compounds, which affect the AA [75]. The maximum AA (59.46%) was predicted at extraction temperature, NaOH concentration, and time of 65 °C, 1.5 M, and 1.32 h, respectively.

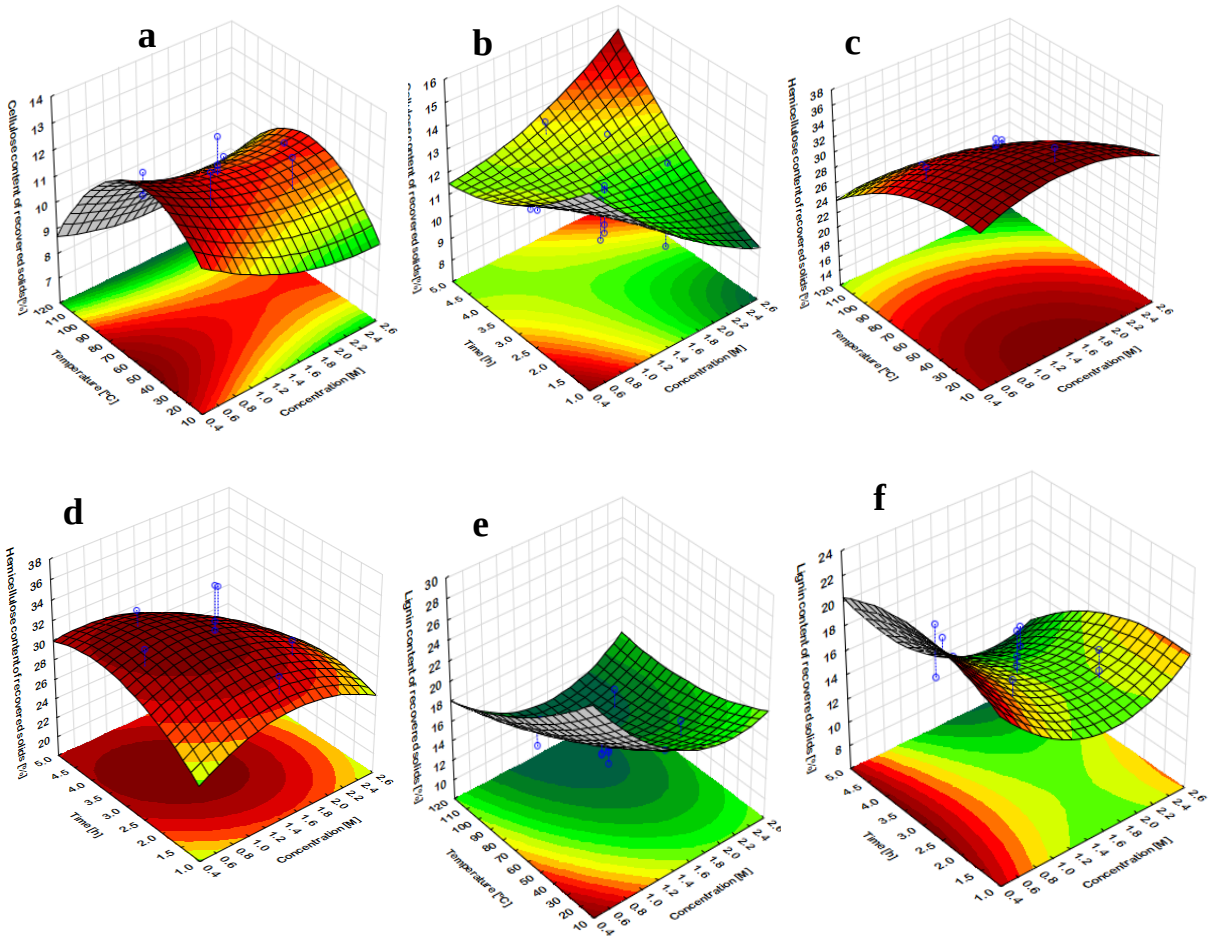

Figure 4.5: Response surface plots of (a–b) cellulose content of recovered solids (c–d) hemicellulose content of recovered solids (e–f) lignin content of recovered solids.

4.5.2.2. Sugar composition and structural features of the hemicellulose extract

Glucose was the main neutral sugar unit present in the extract (72.23%) followed by xylose (17.16%), an indication of the presence of xyloglucan as reported in the literature for mango [179]. The FTIR spectra showed the stretching and bending vibrations of C-O, C-C, and C-OH in hemicellulose at 1148–1150 cm^{-1} (Appendix A, Figure A1). The characteristic peak for xyloglucan was evident at 1078 cm^{-1} [261] and that of absorbed water at 1641 cm^{-1} (Appendix A, Figure A1). The small peak at 1365 cm^{-1} attributed to the phenolic hydroxyl groups of lignin confirms the small lignin content observed in hemicellulose extract [14]. A small peak at 854 cm^{-1} is attributed to the presence of xylose residues [261].

The molecular weight, M_w, and polydispersity (M_w/M_n) of mango kernel hemicellulose (MKH) and commercial tamarind xyloglucan (XGN) are presented in Table A3. The weighted average (M_w, 108,163 g mol^{-1}) and number-average M_w (M_n, 22,685 g mol^{-1}) of the MKH were lower compared to M_w, 2,372,886 g mol^{-1} and M_n, 707,569 g mol^{-1}, for XGN (Table A3). A

wide range of M_w was observed for MKH (PDI=4.77) compared to XGN (PDI=3.35) which could be due to slight degradation of hemicellulose by alkaline conditions [423]. The thermal stability of MKH and XGN is shown in Figure A2. Moisture loss from evaporation was the first phase of reduction of weight observed between 50–120 ºC in both samples (Appendix A, Figure A2). MKH decomposition occurred between 215–350 ºC and that of XGN, 300–420 ºC. For XGN, only a single peak was observed at 380 ºC, whereas two peaks (at 246 ºC, and 293 ºC) were observed for MKH which could be due to present of two different molecular weight polysaccharides (Appendix A, Figure A2). A similar result was obtained by Peng *et al.*, (2012), where two degradation peaks were observed for alkali extracted hemicellulose from a bamboo stem, which could be due to the decomposition of a range of M_w hemicelluloses. At 600 ºC, the char yields were 21.2% and 8.3% for the MKH and XGN, respectively. The lower char yield in XGN could be attributed to its larger M_w and purity [425].

4.5.2.3. Effect of alkaline pretreatment conditions on the composition of the recovered solid

The solubilization of hemicellulose and phenolic compounds from destarched kernel resulted in residual solids enriched in cellulose and lignin (Table 4.3). Figures 4.5 a–b shows higher cellulose content in the recovered solids at lower NaOH concentrations and temperatures due to less degradation at such conditions. The opposite was, however, observed for the hemicellulose content of the recovered solids due to hemicellulose dissolution in alkaline conditions (Figures 4.5 c–d). This trend agrees well with the data for hemicellulose yields (Table 4.3), whereby, hemicellulose dissolution reduces the residual hemicellulose contents and increases the residual cellulose and lignin contents, although their increase is dependent on the employed conditions. At a constant time (3 h), an increased cellulose content from approximately 10% to 12% was observed when the temperature was increased from 22 to 65 °C. Contrarily, both the lignin and hemicellulose contents at these conditions were reduced due to the susceptibility of these components to alkaline hydrolysis conditions [83], [177]. At ≈107 °C, all the components in the residual solids were reduced simultaneously due to improved hydrolysis at a higher temperature. The lignin content of residual solids decreased (Figures 4.5 e–f) with both NaOH concentration and temperature at a fixed time (3h) due to lignin hydrolysis in alkaline conditions as reported in other studies [83]. Overall, extracting hemicellulose from the destarched mango kernel gave residual solids enriched in cellulose and lignin.

4.5.2.4. Validation of optimum extraction conditions for hemicellulose extraction

The predicted optimum conditions were 1.07 M NaOH, 44 °C and 2.16 h (Table 4.4), which resulted in hemicellulose yield of 53.68% with TPC and AA of 34.96 mg GAE/ and 55.08%, respectively, and a solid residue (2.082 g) with 13.06% cellulose and 18.25% lignin corresponding to (Table 4.4). The percentage error values were 2.75%, 3.18%, 2.86%, 7.50%, and 0.60% for yield, TPC, and AA of the extract, and cellulose and lignin contents of residual solids respectively suggesting predictability of the desired responses by the regression models. The bioactive hemicellulose yield is higher than the 13.2% reported for bioactive hemicellulose [282] from a single process for single product recovery.

Table 4.4: Predicted and experimental values of the responses at optimum conditions for hemicellulose extraction

	X_1, (M)	X_2, (°C)	X_3, (h)	Hemicellulose yield, (%)	Total phenolic content, (mg GAE/g)	Antioxidant activity, (%)	Cellulose content of recovered solids (%)	Lignin content of recovered solids (%)
Predicted optimal condition	1.07	43.98	2.16	55.20	36.11	56.67	12.08	18.14
Verified optimal condition	1.07	44.00	2.16	53.68	34.96	55.05	13.06	18.25
% deviation				2.75	3.18	2.86	7.50	0.60

X_1: NaOH concentration (M); X_2: Temperature (◦C); X_3: Extraction time (h)

4.5.3. Product recoveries from the multi-step biorefinery processes

Overall mass balance for the recovery of polyphenols, starch, bioactive hemicellulose, and solid residual components from MSK was performed. The composition of the recovered solids after each treatment process is presented in Figure 4.6. The percent recovered solids after the ethanol organosolv process (SROP) was 7.269 g per 10 g starting material and consisted of 22.71% hemicellulose, 42.81% starch, 4.15% cellulose, 5.61% lignin, 22.59% protein, 1.83% extractives, and 0.29% ash (Figure 4.6). The solid residue was destarched (with a solid recovery of 3.590 g) and further pretreated with the alkaline solution to recover the bioactive hemicellulose (53.68%) (Table 4.4), which yielded 2.082 g solids. The solids residue (2.082 g) after the multi-step OE, EH, and AP were composed of 29.83% hemicellulose, 0.10% starch, 13.06% cellulose, 18.25% lignin, and 38.76% protein (Figure 4.6). Therefore, the multi-step biorefinery process resulted in total recoveries of 130.17 mg GAE/g polyphenols (free plus

bound), 53.68% bioactive hemicellulose, 97% starch, and solids (2.082g) with ≈13% cellulose and 18.3% lignin. The total polyphenol and bioactive hemicellulose recoveries were higher than reported values for their single extraction processes [101 mg GAE/g [235] and 13.2% bioactive hemicellulose [282], respectively], which suggest minimal impacts of the multi-step biorefinery process on the multi-product yields versus the single product extraction schemes.

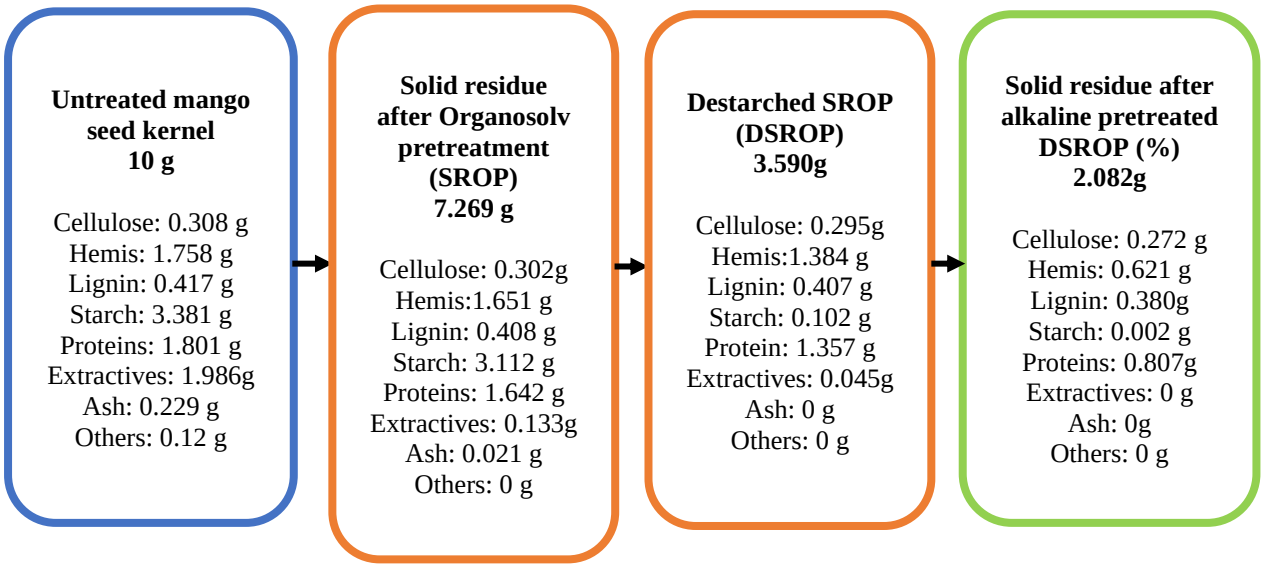

Figure 4.6: Component recovery from mango seed kernel fractionation via multi-step organosolv extraction, enzymatic hydrolysis, and alkaline pretreatment under the optimal organosolv extraction (64.99% ethanol, 54.18 °C) and alkaline pretreatment (1.07 M NaOH, 44 °C, 2.16 h) process conditions

4.6. Influence of the treatment steps in the multi-step biorefinery

The effects of the individual treatment steps in the multi-step biorefinery process were also accessed using FTIR (Figure 4.7). After the polyphenol extraction, the peaks associated with cellulose, hemicellulose, and lignin became more prominent correlating with the results from the compositional analysis. The peak at 2852, 1735, and 1362-1320 cm^{-1} representing the CH stretching vibration of the methyl groups related to lignin, C=O stretching vibration of the carbonyl and acetyl groups in lignin and hemicellulose and the CH deformation of cellulose, hemicellulose, and lignin became more prominent after the polyphenol extraction (Figure 4.7), respectively whereas they were almost absent in the untreated MSK [14], [20], [426].

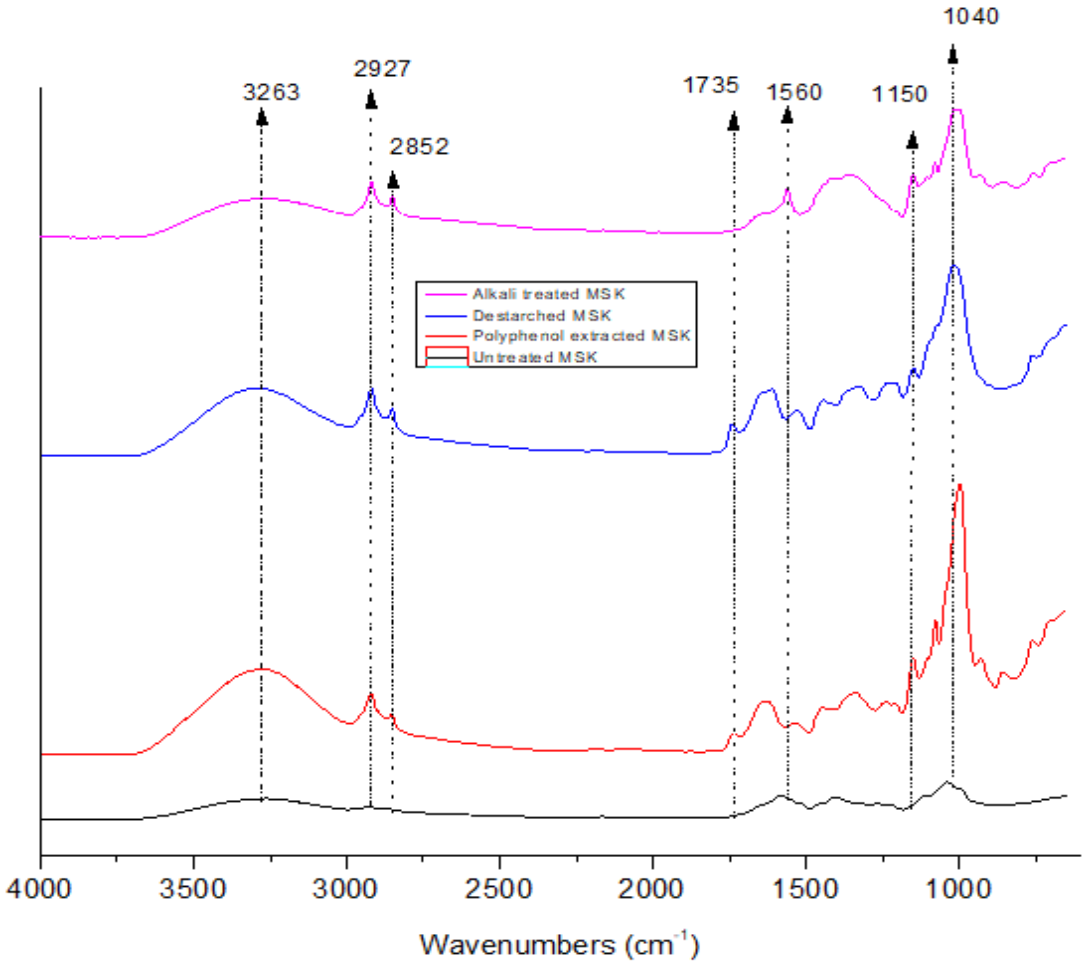

Figure 4.7: FTIR spectra of untreated and pretreated solids after the multi-step biorefinery of mango seed kernel

Furthermore, the presence of the peak at 1735 cm^{-1} shows that the polyphenolic extraction step was only effective for the extraction of the free polyphenols within the MSK whereas the bound phenolics such as ferulic and p-coumaric acid were minimally affected [427], [428]. The destarching step led to an increase in the intensity of all peaks especially peaks associated with lignin and hemicellulose (Figure 4.7). For instance, peaks at 1242-1211 cm^{-1} associated with C—C, C—O, C=O stretching of hemicelluloses and guaicyl ring condensation of lignin were observed to increase after the destarching step whereas the peak at 2919 cm^{-1} representing both the CH_2 stretching of cellulose and lignin also increased slightly in intensity in comparison to that of the polyphenol extracted MSK [302], [428]. However, due to the destarching step, there is a reduction in the peaks related to the OH groups and CO stretching vibrations of the glycosidic compounds at 3263 and 1040 cm^{-1} [429].

Alkaline treatment resulted in the reduction of the intensity of all peaks, indicating that the treatment conditions affected all components of the destarched MSK (Figure 4.7). Although

the cellulose content should be least affected by the alkaline treatment conditions, the reduction of the peaks at 3263 and 1040 cm^{-1} could be attributed to the almost complete removal of the starch content with a significant reduction in hemicellulose content (Figure 4.7). Furthermore, the alkaline treatment was very effective in completely removing the bound polyphenols (ferulic and p-coumaric acid) from the feedstock as represented by the absence of a peak at 1740 cm^{-1} as has been observed by earlier studies [428]. Additionally, the strong presence of the peak at 1560 cm^{-1} representing the C=C aromatic vibration of lignin was prominent indicating that the alkaline treatment conditions were not very severe to reduce the lignin content as was observed in the compositional analysis [302], [430]. The results from the FTIR are consistent with the results from the SEM analysis (Figure 4.8) showing the gradual loosening of the compact structure of the MSK after successive treatments. The cellulose fibere were seen to appear after the multi-step process indication the removal of amorphous components during the multi-step biorefinery process. Therefore, both FTIR and SEM corroborate the results from the compositional analysis.

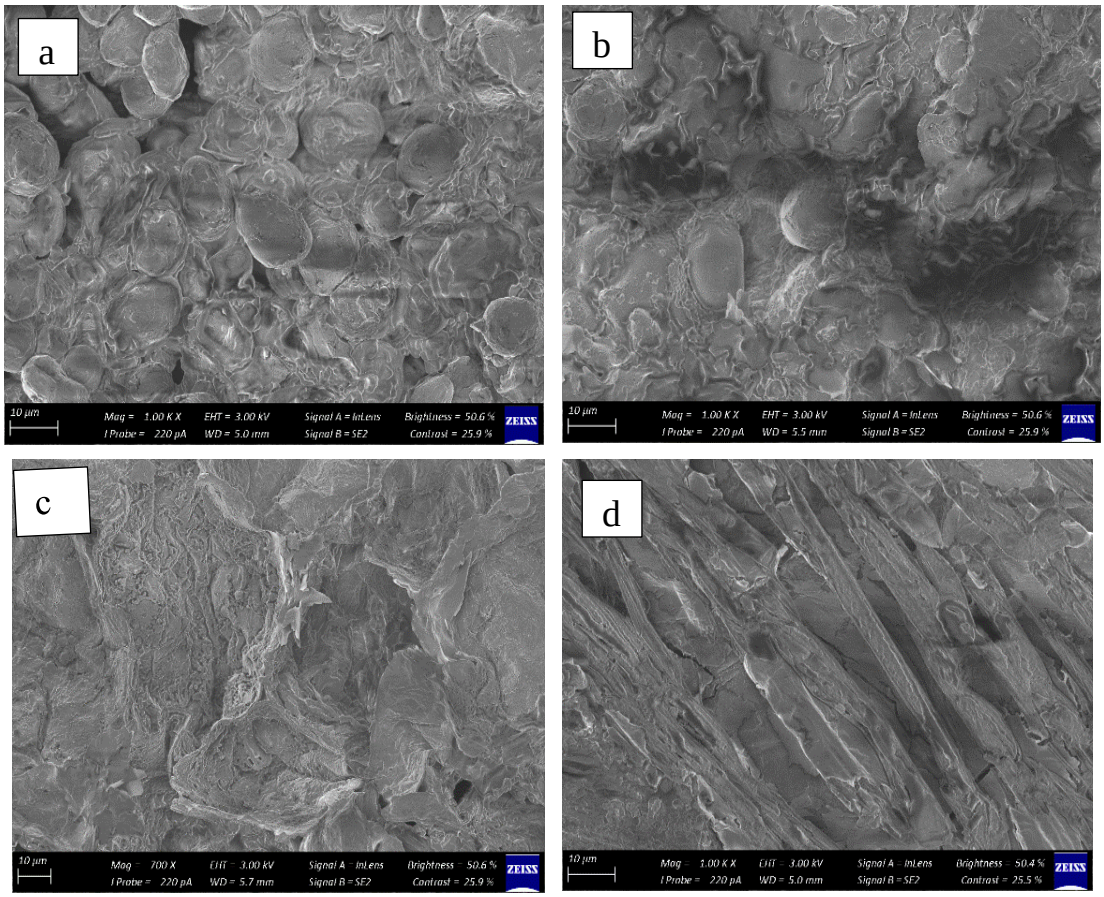

Figure 4.8: Scanning electron microscopy of (a) untreated mango seed kernel, (b) organosolve extracted residue (c) destarched residue and (d) alkaline extracted residue

4.7. Conclusions

A multi-step biorefinery process that consists of sequential organosolv extraction, enzymatic hydrolysis, and alkaline pretreatment for the fractionation of mango seed kernel into multi-products of polyphenols, starch, bioactive hemicellulose, while minimizing the degradation of cellulose and lignin in the solids from MSK was developed. At the optimal conditions for the organosolv extraction process (64.99% ethanol concentration and 54.18 °C), a 95.21 mg GAE/g TPC extract with AA of 84.69% was obtained, with over 90% preservation of cellulose, hemicellulose, and lignin in the solid residue. The subsequent enzymatic treatment of the organosolv treated solid residue resulted in the removal of >95% starch in the monomeric form to recover a destarched solid residue. The successive optimal condition for the alkaline treatment of the destarched kernel (1.07 M NaOH, 43.98 ºC, and 2.16 h) resulted in a 53.68% bioactive hemicellulose yield with TPC and AA of 34.96 mg GAE/g and 55.05% respectively. The total recovery of polyphenols in OE and AP was higher than literature values for their single extraction processes whereas the bioactive hemicellulose yield was higher than literature values (54% vs 13.2%). The solids (2.082 g) recovered after the multi-step OE, EH, and AP process were composed of cellulose - 13.06%, and lignin - 18.25%, corresponding to ≈88.3% and 91.12% retention in the solids. This study has provided optimized multi-step process conditions for recovering multi-products from MSK in an integrated biorefinery scheme. Subsequently, increasing potential revenues to be realized from the bioproducts (polyphenols, starch, bioactive hemicellulose, and solids residue enriched in cellulose and lignin). Compared to the single product recovery, the multi-step biorefinery process results in an increased number of products from a single feedstock toward full valorization of MSK.

5. DEVELOPMENT OF A MULTI-STEP BIOREFINERY SCHEME FOR THE RECOVERY OF HEMICELLULOSE, LIGNIN, AND CELLULOSE-RICH FIBERS FOR NANOCELLULOSE PRODUCTION FROM MANGO SEED HUSK

Papers contributing to this chapter

1. Tailor-made conversion of mango seed husks to obtain hemicellulose suitable for the production of the thermally stable film (Published research paper).
2. Optimization of lignin extraction from alkaline treated mango seed husk by high shear homogenization-assisted organosolv process using response surface methodology (Published research paper).

Authors: Fatimatu Bello, Annie Chimphango,

Chapter summary

This Chapter discusses the novel optimized multi-step biorefinery route for recovering hemicellulose (for biocomposite film), lignin (for phenol formaldehyde resins), and cellulose-rich fibers (for nanocellulose production) from the mango seed husk (MSH) (Objective 2, section 2.14.2). The selection and sequence of the multi-step fractionation steps were based on the physicochemical properties and response of the biomass feedstock components to process conditions; thus, the chemo-thermally liable hemicellulose component was first extracted using an alkaline pretreatment (AP), followed by lignin extraction and cellulose recovery using a combined organosolv and homogenization pretreatment (HSHO). In each referred operation, the process was optimized to ensure low degradation of the solid residue components for the subsequent fractionation stage, thus resulting in the recovery of the cellulose-rich solid residues for the nanocellulose production. The AP was performed varying NaOH concentration, temperature, and time and the process optimized for the recovery of hemicellulose with lower xyloglucan/xylan ratio, lower lignin, and uronic acid contents (high purity) suitable for developing biocomposite films, while retaining the cellulose and lignin in the solid residue for a further fractionation in the next stage of the multi-step process. The optimized condition (1.92 M NaOH, 86 ºC, and 3.84 h) resulted in 46% hemicellulose extract with XGN/XLN ratio, lignin, uronic acid, and molecular weight of 0.13, 16%, 12%, and 70189 g/mol respectively that formed thermally stable films (maximum thermal degradation temperature 290 ºC), plus

high (>90%) cellulose and lignin recoveries in the solid residues. The next step involved subjecting the solid residue from the AP to the HSHO process. In the HSHO, the ethanol concentration, temperature, and homogenization time were optimized to solubilize lignin with high purity and recover cellulose-rich solids with high cellulose and low hemicellulose contents for nanocellulose production. Optimized HSHO conditions of 60% ethanol concentration, 148.41 ºC, and 15 min homogenization resulted in 70.23% lignin solubilization with 96% purity and having the molecular weight and thermal degradation temperature of 3247 mg/mol and 298 ºC respectively. Compared to the HSHO process, the non-assisted organosolv process resulted in 68.58% solubilized lignin with 94.74% purity at a higher temperature (200 ºC). The recovered solid residue was enriched in cellulose (77%) with less than 12% hemicellulose content. After the multi-step sequential AP and HSHO, approximately 80% cellulose was recovered in the solids, indicating that the developed process could preserve a substantial amount of cellulose for nanocellulose production. Thus, the multi-step biorefinery was efficient for the fractionation of the MSH into hemicellulose polymers, high purity lignin, and cellulose-rich pulp while preserving their properties for the intended application. In addition, the temperature required for the lignin extraction was reduced vs the conventional process (148.14 vs 200 ºC). The recovered cellulose had improved surface area, purity, and crystallinity suitable for CNC production. The hemicellulose product was suitable for self-supporting thermally stable film production although with low elongation at break value. Therefore, the integration of the different pretreatment methods into the multi-step process could help enhance the economic value of the mango seed waste while eliminating the cost associated with waste disposal in the mango processing industry.

Declaration by the candidate:

With regard to Chapter 5, pg. 119–173 the nature and scope of my contribution were as follows:

Nature of contribution	**Extent of contribution**
Planning and execution of experiments, data analysis and interpretation, and writing of the chapter	80

The following co-authors have contributed to Chapter 5, pg. 119-173:

Name	**E-mail address**	**Nature of contribution**	**Extent of contribution**
Chimphango, A.	achimpha@sun.ac.za	General discussions, interpretation of results, and revision of chapter	20

5.1. Tailor-made conversion of mango seed husks to obtain hemicellulose suitable for the production of thermally stable film

Published research paper: *Journal of Waste and Biomass Valorization*, 2022, 13: 719-737

Authors: Fatimatu Bello, Annie Chimphango

5.2. Abstract

Mango seed husks were fractionated to obtain hemicellulose extracts with varied xyloglucan (XGN) and xylan (XLN) compositions that suit the development of thermally stable and self-supporting films. A strategy for obtaining the suitable XGN/XLN composition involved optimizing extraction temperatures (40–90 °C), NaOH concentrations (1–2 M), and time (2–4 h) in central composite design experiments, based on the yield, XGN/XLN ratio, uronic acid, and lignin contents. The optimal process conditions of 1.92 M NaOH, 86.0 °C, and 3.84 h gave hemicellulose yield, XGN/XLN ratio, uronic acids, lignin, and Z-potential of 46.24%, 0.13, 12.02%, 16.73%, and -16.1 mV, respectively. Permethylation analysis and Gas chromatography/Mass spectroscopy confirmed the presence of 1,4 linked glucan backbone for xyloglucan in the hemicellulose, with xylose residues branching at the non-reducing end. The molecular weight and maximum degradation temperature of the hemicellulose extract were higher (70189 $gmol^{-1}$ & ≈330 °C, respectively) than of beechwood XLN (27235 $gmol^{-1}$ & 290 °C, respectively). The hemicellulose extract formed self-supporting thermally stable (290 °C) biocomposite films, with potential application in food packaging. Customizing extraction of the hemicellulose with tunable properties, from the mango seed husk, is a novel approach for value addition to food waste that can be integrated into a biorefinery set-up.

5.3. Introduction

It is estimated that more than 42 million tons of mangoes are produced annually, out of which 14.7 to 25.2 million tons are generated as waste after the industrial processing of mango fruits [8]. The mango (*Mangifera indica L.*) seed representing 35–55% of the whole mango fruit constitutes a portion of the waste and consists of approximately 48% kernel, 50% husk, and 2% integuments [15]. The kernel is rich in carbohydrates (58–80%), crude protein (6–13%), crude fiber (2%) with high phenolic content [8], [129] thus, various high-value products are obtained from it. In contrast, utilization of the mango seed husk as a biorefinery feedstock is limited despite containing appreciable amounts of lignin (23.8–26.6%), hemicellulose (15.6–20.6%), and cellulose (39.4–55.1%) [15], [20], [118]. The research on the mango seed husk has focused mainly on the production of nanocellulose and activated carbon [20], [21] as single products with limited information on hemicellulose recovery and application. The extraction of hemicellulose from mango seed husk can increase the number of products obtained from the waste and increase the value of mango waste from food processing.

Hemicelluloses have diverse properties and applicability [431] emanating from the diversity in the sugar composition and structures, thus, can improve the economics of biomass utilization. Hemicelluloses are often extracted using alkaline-based solvents such as calcium, sodium, ammonium, and potassium hydroxides [84], [432], [433]. In the case of biomass containing different types of hemicelluloses such as xylan, xyloglucan, mannan, among others, the alkaline conditions might be optimal for one type and not the other type(s) of hemicelluloses [61]. In addition, the alkaline conditions co-extract hemicelluloses with other compounds such as lignin and uronic acids [42]. Therefore, the combination of the different types of hemicelluloses and the presence of the lignin and uronic acids can influence the functional properties of the extracted hemicelluloses and thus, the end application. For example, a literature study has shown that the nature and source of the hemicellulose significantly influence the formation of composite films [42] and mixtures of two polymers (synthetic or biopolymers) have been reported to help achieve the desired properties of films for varied applications when compared to a single polymer [372].

Xyloglucan (XGN) and xylan (XLN) hemicelluloses exist in many agricultural waste. The XGN is present in *Hymenaea courbaril var. courbaril* seeds, depectinised apple pomace, mango seeds, and tamarind seed (major commercial source) [192], [232], [396], [434]. This XGN exists as storage polysaccharides in some seeds of higher plants, and as structural components in the primary cell wall [434]. Structurally, XGN has a β-1, 4 glucopyranosyl backbone similar to cellulose with α-1, 6 xylose substitution, which may further contain

galactose and fucose residues depending on the plant species [434], [435]. On the other hand, XLN is predominant in woody and non-woody sources [84] and have a β-1,4 xylopyranosyl backbone, side chains of α-D-glucuronic acids or its 4-*O*-methyl derivative (MeGA), some with acetyl groups at C-2 and C-3 positions, and arabinose groups that are in some cases, ferulylated [63], [84], [184].

XGN binds to the surface of cellulose microfibrils in the cell wall of plants through hydrogen bonding and forms tightly bound networks with cellulose microfibrils, resulting in a web-like network of cellulose-xyloglucan chains [436]. The XLN, on the other hand, binds mainly to the cellulose microfibrils surface and is covalently linked to lignin [191], [436]. Notably, the individual biopolymers have varied chemical reactivity under different extraction conditions due to the different covalent and intramolecular, and intermolecular hydrogen bonding to other cell wall components [437], [438], which influence their functional properties, thus, how they behave in a biocomposite. The associations of the XGN and the XLN with cellulose, lignin, and uronic acids provide frameworks for producing biocomposites with diversified properties. For instance, hemicellulose with XGN tends to have a higher maximum thermal degradation temperature than those with XLN [74]. However, XGN could lead to the formation of aggregates in solution due to partial hydration of the individual polymers [439], [440].

On the other hand, increased content of XLN contributes to increased hydrophilicity due to excessive branching, and the hemicellulose thermal degradation occurs at relatively low temperatures (200 ^{o}C vs 332 ^{o}C) [74]. Therefore, there is a need to consider extraction conditions for maintaining the individual polymer functionalities that would enhance the functionality of the biocomposite while minimizing those that could introduce negative attributes to the biocomposites. For example, manipulating and optimizing the alkaline conditions can vary the XGN/XLN ratios, lignin, and uronic acid contents in the hemicellulose extract to make it suitable for specific applications and for diversifying functional properties of biocomposites.

Various studies on biocomposite film formulation are based on xylan hemicelluloses (mostly water-soluble) due to the benefits of transparent film formation, while its disadvantages of inability to form coherent and thermally stable films have been addressed through additives such as external plasticizers, nanocellulose, or biopolymers of higher molecular weights than the xylan [46], [178], [299]. For instance, some studies [46], [371], [441] assessed possibilities of enhancing xylan-based biocomposite film development and properties through additives like cellulose nanocrystals, chitosan, and plasticizers (sorbitol, glycerol, lignin, etc). However, it is

envisaged that this approach involving external additives could increase the costs of industrial production and applications of such biocomposites. Moreover, lower molecular weight plasticizers such as glycerol, sorbitol, etc. that do not bind to the film tend to migrate from the film during usage causing issues in food packaging [178], [442]. In this regard, various reports have projected potentials for feedstocks that have mixed hemicelluloses (e.g. xylan-galactomannan, xylan-xyloglucan), to yield hemicellulose extracts that can produce the desired film properties [43], [299] but their explorations have been minimal in the literature [261], [443].

Although biomass feedstock sources and compositions are major contributors to obtaining hemicellulose extract for self-supporting film development, optimization of the alkaline process conditions is also crucial to tune the hemicellulose properties for the intended end usage. In the literature, optimized processes for the required ratios of xyloglucan/xylan to ensure desirable film properties are unexplored. Kostalova et al. [261] investigated extraction of the xylan-xyloglucan complexes from *Fallopia sachalinensis*, but under unoptimized conditions without testing for its suitability in producing composite films. Kostalova et al. [261] used an alkaline method to extract XGN-XLN complexes from knotweeds without further optimizing for the polysaccharide ratios and purity that could suit biocomposite film development. In addition, the optimization processes presented in the literature on feedstock sources with diverse hemicellulose polysaccharides focused on obtaining an optimum alkaline extraction condition for each of the individual hemicellulose polysaccharides without considerations given to a compromised condition that could result in an extract with compositions that suits diverse applications such as the development of self-supporting thermally stable films.

In this study, mango seed husks were characterized for customized extraction of hemicelluloses with varying compositions to suit the development of thermal stable films. The hemicellulose extraction conditions were optimized based on the yield, XGN/ XLN ratio (to determine if the content of the xyloglucan in the hemicellulose extract influences the formation and thermal stability of xylan films differently), uronic acid, and lignin contents, to produce a hemicellulose fraction with desirable attributes that can be used for the development of thermal stable hemicellulose self-supporting films. It is therefore anticipated that obtaining a hemicellulose extract with a lower XGN/XLN ratio could improve the processability and thermal stability of the films for application in food packaging. This study focused on thermal properties because it is one of the properties that influence the processability and field of application of the composite films [295]. Thus, hemicellulose extract with (1) molecular weight

(M_w) greater than standard XLN (beechwood xylan), (2) lowest XGN/XLN ratio, and absolute Z-potential > 15 mV, and (3) with thermal stability greater than standard XLN. The optimization of hemicellulose extraction was achieved through a central composite design (CCD) experiment based on response surface methodology (RSM). The optimization approach could be applied to other biomass feedstocks with compositions similar to the mango seed husk. The optimization approach means one will be able to tune the properties of the extract before extraction to suit the desired application. Furthermore, the films mechanical properties (tensile strength, elongation at break, and Young's modulus) films were evaluated.

5.4. Materials and methods

5.4.1. Materials

Fresh ripened mango fruits (*Mangifera indica L.*) of the Kent variety were obtained from the Cape Town market, South Africa. Commercial tamarind seed xyloglucan (CXGN), beechwood xylan (CXLN), and analytical grade sugars of D-glucuronic and D-galacturonic acids were purchased from Megazyme International, Ireland. Carbazole, D-glucose, D-xylose, L-arabinose, and D-galactose were purchased from Sigma-Aldrich. Ethanol (95%) and sulphuric acid (72% wt) were purchased from KIMIX, South Africa, NaOH and acetic acid (98%) were purchased from Science world, South Africa. All chemicals were of analytical grade.

5.4.2. Feedstock preparation and analysis

The pulp was manually removed from the mango fruits to obtain the seeds, which were subsequently de-husked using a sharp knife and air-dried at 40 °C in a greenhouse for 48 h followed by milling using a Hammer mill, and a Retch ZM 100 pilot plant scale mill. The ground material was sieved (universal test sieve, ISO 3310) to particle sizes of 250 to 850 µm. The samples with particle sizes of 425 µm were used for the chemical compositional analysis and the remaining samples were used for extraction of the hemicelluloses.

The milled mango seed husks (MSHs) and the alkaline treated residue were analyzed for acid detergent fiber (ADF), neutral detergent fiber (NDF), and acid detergent lignin (ADL) to account for the content of cellulose, hemicellulose, lignin, and other components according to the Van Soest method using Fibertech® system (Velp Scientifica 419278, FIWE, raw fiber extractor). This method allows measurement from a 0.1–100% range allowing repeatability of ± 1% [392]. Approximately, 1 g of sample was weighed into glass crucibles and placed in a Fibertech® extraction unit, followed by the addition of 0.5 g sodium sulfite and 100 mL NDF solution (sodium dodecyl sulfate, EDTA, pH 7.0). The mixture was heated to 100 °C before

adding 0.1 mL thermostable α-amylase (Sigma #A3306). The reaction temperature was, thereafter, reduced to 50 °C. Subsequently, the mixture was refluxed in a reflux condenser of the fiber extractor for 1 h. The samples were washed 3 times after the reaction with 150 mL of boiling distilled water followed by washing with 20 mL of acetone before oven drying at 103 °C for 24 h. Dried samples were cooled in a desiccator before weighing. The ADF and ADL were determined from the NDF fraction (m_{NDF}). The ADF analysis followed the same procedure as the NDF analysis but using acidic detergents (cetyltrimethylammonium bromide in 1N H_2SO_4) to give ADF fraction (m_{ADF}). The final step involved the hydrolysis of the sample post ADF analysis with 20 mL of 72% H_2SO_4 at 25 °C over a 3 h period with intermittent stirring. The hydrolysate was filtered under vacuum and further washed with distilled water until the filtrate attained pH 7. The ADL fraction (m_{ADL}) was dried at 103 °C overnight in an oven and upon removal placed in a desiccator before weighing. The percentages of hemicellulose, cellulose, and lignin were estimated according to Equations 2-4:

$$Hemicellulose\ (\%) = \frac{m_{NDF} - m_{ADF}}{m_{sample}} \times 100 \quad [2]$$

$$Cellulose\ (\%) = \frac{m_{ADF} - m_{ADL}}{m_{sample}} \times 100 \quad [3]$$

$$Lignin\ (\%) = \frac{m_{ADL} - m_{crucible}}{m_{sample}} \times 100 \quad [4]$$

The water and ethanol extractives were determined by a method (NREL/TP 510/42619) [444] as described in Appendix B1. The percent extractive for each (water and ethanol) was calculated using Equation 5. Total extractives were calculated by summing the ethanol and water extractives.

$$Extractive\ (\%) = \frac{m_2 - m_1}{m_s} \times 100\% \quad [5]$$

Where:

m_1 = Mass of the empty flask,

m_2 = Mass of the flask with extractives

m_s = Initial mass of sample.

Ash content was determined following a method by Sluiter et al. [445]. Approximately 0.5 g of sample was placed in pre-weighed porcelain crucibles, which were incinerated in a muffle furnace at 575 ±25 °C for 8 h. Thereafter, the crucibles were cooled in a desiccator before weighing. Ash content was calculated using Equation 6.

$$Ash\ content\ (\%) = \frac{m_2 - m_1}{m_s} \times 100\% \quad [6]$$

Where:

m_1 = Mass of empty crucible

m_2 = mass of crucible plus ash

m_s = initial mass of sample.

5.5. Hemicellulose extraction

Approximately 10 g milled MSHs samples were placed into 250 mL Scotch bottles to which 100 mL (1–2 M) NaOH solutions containing 20 mM sodium borohydride ($NaBH_4$) were added to prevent peeling reaction [84]. The bottles were heated in a shaking water bath at varying temperatures (40–90 °C) for varying times (2–4 h), conditions that were chosen based on preliminary experiments (Appendix B, Table B1) and literature [83]. The reaction mixtures were centrifuged (Hermie Labortechnik GmbH, Z 366, Germany) at 8000 rpm for 10 min. The supernatant was decanted and neutralized to pH 5.5 with 6 M HCl. The solid residue after centrifugation was washed with distilled water to neutral pH and dried at 40 °C in an oven for 48 h before further analyses. The supernatant was dialyzed with membranes (molecular cut-off of 14000 Da, Sigma-Aldrich, USA) at 25 °C for 72 h followed by precipitation in 95% ethanol (three times the volume of the supernatant) at 4 °C for 24 h. The precipitates were washed with 60% v/v ethanol before oven-drying at 25 °C for 48 h. The dried extracts (MHH) were stored in air-tight plastic bags for further characterization. The hemicellulose yield (%) was calculated according to Equation 7.

$$Hemicellulose\ yield\ (\%) = \frac{W_1}{W_0} \times 100 \quad [7]$$

Where:

W_1 = Dry weight (g) of extracted hemicellulose

W_0 = Initial mass (g) of hemicellulose in the starting material.

5.6. Optimization of extraction conditions

The hemicellulose extraction conditions were optimized in a 3^3 central composite rotatable experimental design (CCD) with six replicate of center points for NaOH

concentration (M), temperature (°C), and time (h), to give a total of 20 runs (Appendix B, Table B1). The dependent variables were yield, XGN/XLN ratio, uronic acids, and lignin contents. Commercial xyloglucan (CXGN) and commercial xylan (CXGN) were used as benchmarks for XGN and XLN, respectively. The effects of the extraction conditions and the optimal conditions were determined from CCD surface plots and desirability analysis in Statistica 13.2 Software. Preferred extraction conditions were set to be those that give maximum yield, minimum XGN/XLN ratio, uronic acid, and lignin contents using the desirability function in Statistica 13.2 as detailed in section 4.4.5. The Zeta (ζ-) potential, molecular weight, and thermal degradation were evaluated as per the details in the subsequent sections.

Non-linear regression analysis of the experimental data was performed to identify significant trends, main effects, and interactions. The adequacy of the regression models was determined based on the regression coefficient (R^2). In addition, analysis of variance (ANOVA) was performed to verify the statistical significance of the effects based on the second-order model Equation (Equation 8) at a 95% confidence level.

$$Y = A_o + \sum A_i X_i + \sum A_{ii} X_{ii}^2 + \sum \sum A_{ij} X_i X_j + \varepsilon \quad [8]$$

Where:

Y = Hemicellulose yield, XGN/XLN ratio, uronic acid, and lignin contents of the hemicellulose extract

A_o = Constant for the model

A_i, A_{ii}, and A_{ij} = Coefficients of the model for linear, quadratic, and interaction, respectively),

ε, = Model error.

5.7. Hemicellulose sugar composition analysis

5.7.1. Determination of neutral sugars

The sugar (cellobiose, xylose, glucose, arabinose) compositions of the hemicellulose extracts were determined based on the method described by Yashoda et al. and Minjares-Fuentes et al. [61], [397] with modifications as presented in Appendix B1. This method allows hydrolysis of non-cellulosic glucose, without the need for a pre-hydrolysis step using 12 M H_2SO_4 for 3 h at room temperature. The sugar determination was done using High-Performance Liquid Chromatography (HPLC) (Thermo Separations Product Spectra System) equipped with a Shodex RI101 detector, UV2000, and a 7.8 × 300 mm Biorad Aminex HPX-87H column. The hydrolysates after cooling to room temperature were vacuum filtered through a por. 3 glass crucible. The insoluble solids remaining in the glass crucible were washed till filtrate attained

pH 6 and dried in the oven at 103 °C overnight, cooled, and weighed. The mobile phase used was 5 mM sulphuric acid and a flow rate of 0.6 mL/min at 65 °C. The acid-insoluble residue was incinerated at 575 ºC to obtain ash. The filtrate obtained was diluted with distilled water and used for the determination of acid-soluble lignin (ASL) at 240 nm using a UV spectrophotometer.

The approximate content of XGN and XLN in the hemicellulose were quantified according to a method described elsewhere [61], [397]. The XGN was calculated as the sum of non-cellulosic glucose obtained after H_2SO_4 hydrolysis (Gl) and the xylose portion of the XGN (Xy) (Equation 9) after using the anhydro correction factor. The xylose portion of the XGN was estimated by subtracting 50% of the value obtained for non-cellulosic glucose (Gl) from the total xylose obtained from HPLC analysis Xy_{total} (Equation 10). XLN was estimated based on the xylose not accounted for as part of XGN (Equation 11).

$$XGN\ (\%) = Gl + Xy \quad [9]$$

$$Xy\ =\ Xy_{total}\ - 0.5Gl \quad [10]$$

$$XLN\ (\%) =\ Xy_{total} - Xy \quad [11]$$

5.7.2. Determination of uronic acids

The uronic acid contents in the untreated biomass and the hemicellulose extracts were measured using the carbazole-sulphuric acid method previously described by other authors [63], [84]. Briefly, 2.4 mL of 98% H_2SO_4 was added to 0.4 mL of the acid hydrolysate (prepared as described previously (section 5.5.1) for sugar analysis) in a glass test tube followed by the addition of 0.1 mL of carbazole solution in ethanol (0.1% w/v). The stoppered test tubes were incubated in a water bath at 100 °C for 20 min. The mixture was cooled to room temperature before reading absorbance at 525 nm on a UV visible spectrophotometer (Varian Cary 50 Bio). A blank sample contained all reagents except the test sample. The uronic acid content was quantified from galacturonic acid standard calibration curves.

5.8. Preparation of biocomposite films

About 0.5 g hemicellulose samples were dissolved in 40 mL deionized water in a 100 mL conical flask with magnetic stirring (400 rpm) at 25 °C (Relative humidity ≈50%) for 12 h. Hemicellulose solutions that contain varied XGN/XLN ratios (0.13, 0.29, and 0.47) representing the lowest to the highest ratios in the hemicellulose extract obtained in the present study were poured into petri dishes (diameters=12.5 cm), which were dried in an oven at 25 °C for 72 h. These ratios (0.13, 0.29, and 0.47) were selected to determine the extent of influence of the XGN content on the film's formation and properties such as thermal stability. For

comparison, films were made from solutions with a mixture of CXGN and CXLN in similar ratios and in a similar way.

5.9. Structural characterization of feedstock, hemicellulose, solid residues, and biocomposite films

The untreated MSHs, alkaline treated residue, extracted hemicellulose, and films made from MHH, CXGN, and CXLN were analyzed by FTIR using Thermo Nicolet NexusTM (470/670/870 FTIR) spectroscopy device fitted with a diffuse reflectance sample holder. A spring-loaded anvil was used to press the sample against a diamond crystal surface and the spectra were obtained in Attenuated Total Reflectance (ATR) mode. A wavelength range of 4000 cm^{-1} to 600 cm^{-1} was used for the experiment with 64 scans per sample at a resolution of 4 cm^{-1}. The data collection and processing were performed using Thermo Scientific OMNIC software.

Nuclear Magnetic Resonance Spectroscopy with cross-polarization and magic-angle spinning, CP/MAS NMR was used to obtain hemicellulose spectra on a solid-state NMR spectrometer (Varian VNMRS 500) operating at a frequency of 125 MHz, with a 6 mm T3 probe at room temperature. Dried hemicellulose samples were placed into zirconium oxide rotors at a rotation speed of 5 kHz, a 1500 µs contact pulse, a 90 ° proton pulse of 5 µs with 5 s repetitions between delays. All chemical shifts were assigned based on literature.

The molecular weights (*Mw*) of the hemicelluloses were determined by size exclusion chromatography (SEC) using HPLC. Hemicelluloses were dissolved in distilled water at 30 °C to give a concentration of 1 gL^{-1}. The solutions were filtered through 0.22 µm nylon syringe filters (Membrane solutions, LLC) before HPLC (Dionex Ultimate 3000 system with ELS detection equipped with a 3 x 300 mm PSS SUPREMA column set) analysis. Ammonium acetate concentration of 0.125 M was used as the eluent at a temperature of 75 °C and a flow rate of 1 mL/min. Pullulan was used as *Mw* standard.

The (ζ-) potential and PDI of the hemicelluloses were obtained on a Zetasizer Nano ZS90 (Malvern Instruments, U.K.). (ζ-) potential was measured by dissolving approximately 2 mg of the hemicelluloses in 1 mL of distilled water at 25 °C. The samples were injected using a syringe, into a folded capillary cell (DTS1060) that was stoppered before inserting it into the Zetasizer. (ζ-) potential was measured at 25 °C at a scattering angle of 90 ° by a Laser Doppler Electrophoresis technique. The PDI was determined by dynamic light scattering based on the in-built cumulant method. Samples were allowed to equilibrate for 120 sec before 100 scans were taken per sample in triplicates. All measurements were taken relative to polystyrene latex.

Thermogravimetric analysis (TGA) of hemicellulose samples and composite films was performed using a TGA 5500 thermogravimetric analyzer unit under nitrogen gas. Briefly, 4–10 mg of hemicellulose was heated in porcelain crucible under nitrogen from 20 °C up to 600 °C using a flow rate of 10 °C/min. The various decomposition patterns (weight loss vs temperature) were obtained from which onset (T_{ons}) and maximum thermal degradation temperatures (T_{max}) were obtained.

The glycosidic linkages of the hemicellulose extract were determined by the method of Ciacanu and Kerek (1984) with modifications. Briefly, 5 mg of hemicellulose extract was dissolved in 0.5 mL dimethyl sulphoxide (DMSO) containing 20 mg of powdered NaOH. The mixture was ultrasonicated (120 W) for 10 min and allowed to stand at room temperature for 60 min before 0.1 mL methyl iodide was added. After 1 h of incubation at room temperature, 1 mL distilled water and 1 mL chloroform were added to extract the methylated polysaccharides. The chloroform layer was removed and washed 3 times with distilled water before drying at low pressures using the rotary evaporator. The methylated polysaccharides were hydrolyzed with 500 µL of 2 M trifluoracetic acid (TFA) at 100 ºC for 3 h. The partially *O*-methylated sugars were reduced using 200 µL of 10 mg/mL sodium borohydride ($NaBH_4$) in 1 M ammonium hydroxide (NH_4OH) solution with subsequent addition of 50 µL of acetic acid after 1 h of incubation at room temperature. This was followed by the addition of 3×200 µL of 1:9 acetic acid/methanol mixture with further evaporation to dryness and then 2×200 µL of methanol. The partially *O*-methylated alditols were *O*-acetylated by the addition of 50 µL of acetic anhydride and 50 µL of pyridine. The mixture was heated at 100 ºC for 3 h, allowed to cool to room temperature before 500 µL of water was added. The acetylated derivatives were extracted with 2 mL of dichloromethane and analyzed by gas chromatography (Agilent, 6890 N, Palo Alto, CA), coupled with an Agilent mass spectrometer detector (Agilent 5975 MS, Palo Alto, CA). The GC-MS system was equipped with a non-polar guardian (30 m; 0.25 mm; 0.25 µm film thickness) ZB 7HG-G027-11 GC capillary column. Helium was used as carrier gas with a flow of 1 mL/min. The injector temperature was maintained at 250 ºC and the oven temperature was as follows: 80 ºC for 1 min; and finally ramped up to 300 ºC at 7 ºC min^{-1} and held for 2 min. The MS was operated in full scan mode and the source and quad were maintained at 240 ºC and 150 ºC, respectively. The scan rate was between 40-600 m/z.

The mechanical properties (tensile strength, elongation at break, and Young's Modulus) of the developed hemicellulose-based films were analyzed using an LRX Instron tensile tester (LLOYD instruments). A gauge length of 27 cm and a crosshead speed of 50 mm/min were set

prior to measurement by the instrument. The films were cut into strips in the shape of a dog bone with a diameter of 1 cm and a length of 6 cm. Furthermore, potential improvements in the mechanical properties of the films were analyzed by the incorporation of different contents of glycerol (10 – 40%).

5.10. Results and discussions

5.10.1. Composition of untreated and alkali-treated mango seed husks

The mango seed husk (MSHs) comprised 50.27% cellulose, 17.98% hemicellulose, 14.77% lignin, and 0.8% ash (Table 5.1). The hemicellulose, lignin, and ash contents were lower than the values reported by Andrade et al. [19] and Henrique et al. [20] who used Ubá mango variety but comparable to the value reported by Elizalde-González et al. [131] except for their lignin content which was <6% for Malina variety. The variations in the MSHs composition from the literature values could be attributed to varietal differences. The presence of high carbohydrates (cellulose and hemicellulose) and low lignin and ash contents in the MSHs (Table 5.1) suggests that it can easily be converted into high-value biopolymers due to reduced recalcitrance compared to other feedstocks [175].

Table 5.1: Composition of untreated and alkaline treated mango seed husk

Component	Untreated mango husks[a] (%)	Alkaline-treated mango husks (%)
Cellulose	50.27 ± 0.35	57.08 ± 0.10
Hemicellulose	17.98 ± 0.42	9.43 ± 0.67
Lignin	14.77 ± 1.20	19.13 ± 1.09
Extractives	12.19 ± 0.61	10.50 ± 0.13
Ash	0.80 ± 0.06	0.27 ± 0.21
Others	3.99 ± 0.02	3.59 ± 0.42

[a] Values are presented in percentages based on a dry weight

The composition of the MSHs was confirmed by FTIR analysis (Figure 5.1a-d), which showed absorption peaks at 1506 and 1595 cm^{-1} wavelengths associated with an aromatic ring in lignin. In addition, an absorption band reflected at 1730 cm^{-1} corresponds to C=O stretching vibration of either aliphatic carboxylic acid groups in *p*-coumaric and ferulic acid, which could be either linked to lignin or are aryl ester and acetyl groups of hemicellulose [20], [446]. Furthermore, the absorption bands at 1422 cm^{-1} and 1369 cm^{-1} in MSHs are attributed to the CH_2 bending in cellulose and xyloglucan residues [447].

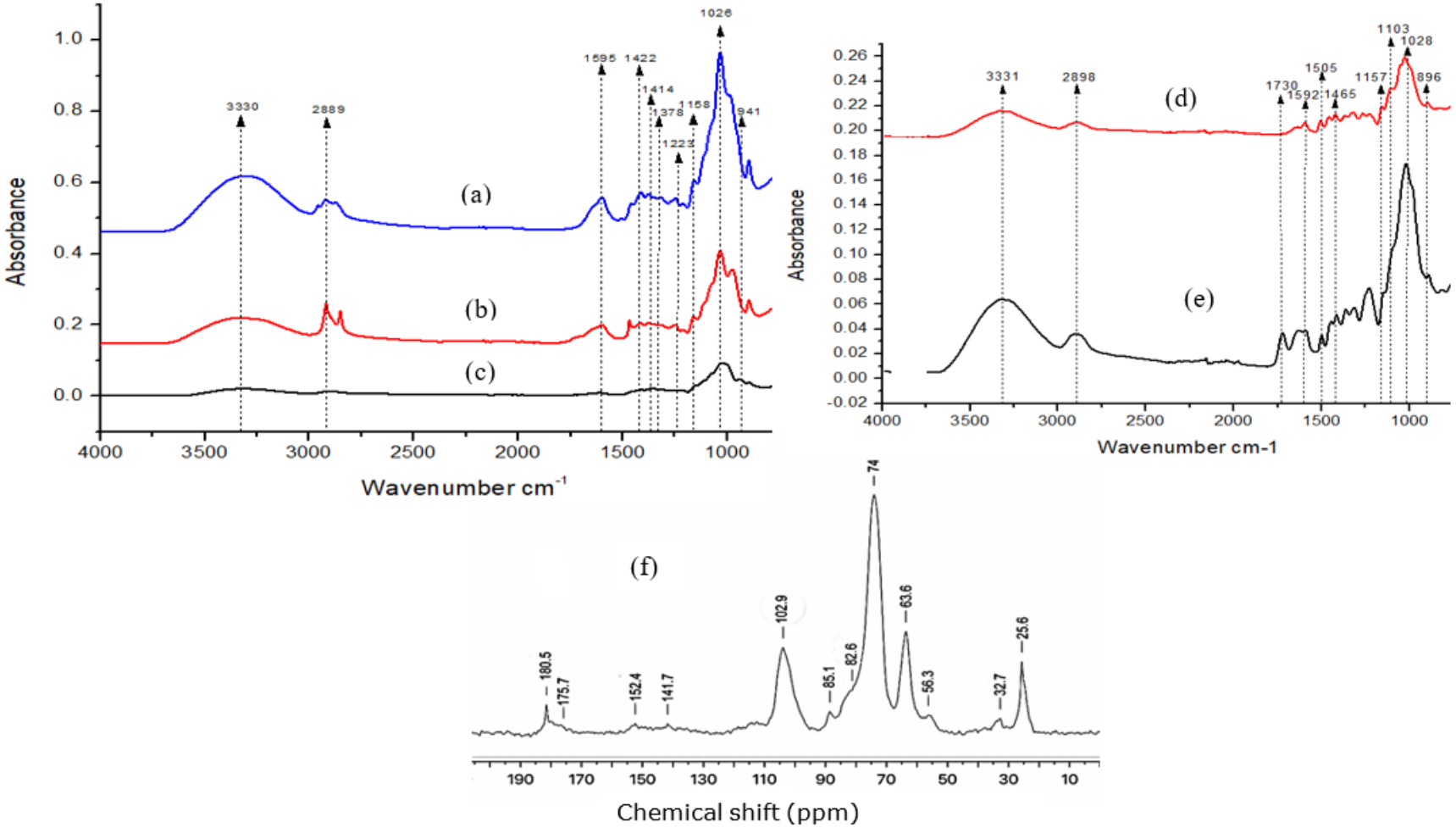

Figure 5.1: Fourier Transform Infra-red spectroscopy (FTIR) spectra showing functional groups in (a) alkaline extracted hemicellulose (b) commercial beechwood xylan (c) commercial tamarind seed xyloglucan (d) alkaline treated mango seed husk and (e) untreated mango seed husk, and (f) CP/MAS solid-state spectra of mango seed husk hemicellulose

5.10.2. Yield and composition of mango seed husk hemicellulose

The hemicelluloses extracted from the MSHs with yields ranging from 16.75 to 48.96% were predominantly a combination of XGN (7.92–16.45%), and XLN (35.64–60.95%) type polysaccharides (Table 5.2). In addition, the extracts (Table 5.2) contained uronic acids (8.43–17.56%) and lignin (17.04–25.97%).

Table 5.2: Yield and composition of hemicellulose extracted from mango seed husk under varying extraction conditions.

NaOH Concentration [M]	Temperature [°C]	Time [h]	Hemicellulose composition					
X1	X2	X3	Yield (%)	XGN (%)	XLN (%)	[a]XGN XLN	Lignin (%)	Uronic acids (%)
1.00	40.00	2.00	21.68	12.58	43.43	0.29	24.22	8.43
1.00	40.00	4.00	23.10	12.46	42.44	0.29	22.05	11.84
1.00	90.00	2.00	23.54	10.11	49.96	0.20	19.98	16.19
1.00	90.00	4.00	23.74	10.51	48.88	0.22	19.36	16.83
2.00	40.00	2.00	27.22	11.53	47.19	0.24	18.60	12.37
2.00	40.00	4.00	25.92	11.28	46.95	0.24	20.85	13.94
2.00	90.00	2.00	48.96	8.46	59.57	0.14	19.38	17.56
2.00	90.00	4.00	48.68	7.92	60.95	0.13	17.04	16.78
0.66	65.00	3.00	16.75	16.45	35.65	0.47	25.97	13.43
2.34	65.00	3.00	44.56	7.56	59.23	0.13	20.95	14.38
1.50	23.00	3.00	18.56	14.68	38.24	0.38	24.35	13.29
1.50	107.00	3.00	33.48	9.49	53.98	0.18	21.42	14.85
1.50	65.00	1.32	30.46	9.73	49.96	0.19	20.22	16.04
1.50	65.00	4.68	31.99	10.28	50.62	0.20	20.52	14.71
1.50	65.00	3.00	33.07	10.55	55.12	0.19	20.63	12.23
1.50	65.00	3.00	34.84	10.45	56.31	0.19	18.73	15.35
1.50	65.00	3.00	34.31	10.36	54.64	0.19	19.21	12.68
1.50	65.00	3.00	37.09	11.60	54.64	0.21	21.09	13.10
1.50	65.00	3.00	33.80	12.46	52.60	0.24	19.89	14.36
1.50	65.00	3.00	34.58	9.78	56.54	0.17	18.01	12.99

[a] Ratio of xyloglucan (XGN) to xylan (XLN) in the hemicellulose extract

The presence of XGN, XLN, lignin, and uronic acids was confirmed by the FTIR spectra (Figures 5.1 a-e). The spectra showed an absorption peak at 896 cm^{-1} attributed to the β- 1,4 glycosidic linkages in hemicellulose units [20]. In addition, the spectra (Figures 5.1 a-b & d-e) showed a peak at 1414 cm^{-1} corresponding to the carboxylic group of uronic acids side chains [282], which suggests the presence of glucuronoxylan that was originally acetylated as per the spectra for the untreated MSHs but was deacetylated during the alkaline extraction. Furthermore, the FTIR spectra (Figure 5.1a) showed peaks at 941 and 1158 cm^{-1}, which are associated with XGN [447] as reflected in the spectra of CXGN (Figure 5.1c), confirming the co-existence of XGN and XLN. Yashoda et al. [397] has also reported the presence of XGN in Alphonso mangoes. The presence of lignin was depicted by peaks at 1265 cm^{-1}, corresponding to the breathing vibration of guaicyl units and a peak at 1223 cm^{-1} (Figures 5.1a & d-e) for syringyl units [448].

The composition of the extracted hemicelluloses, particularly, the co-existence of the XGN and XLN in the extract were further confirmed by CP/MAS solid-state NMR spectroscopy (Figure 5.1f). In the spectra, the peaks at 102.9, 74.1, and 63.6 ppm correspond to C-1, C-3, and C-5 positions of 1,4 β-D-xylopyranosyl unit [176]. The two signals observed at 82.6 and 85.1 ppm show C-4 of glucose residue in xyloglucan [420], [449]. In addition, the presence of the uronic acids is reflected by the signal at 25.6 ppm assigned to the $-CH_3$ and at 180.5 ppm assigned to the carboxylic group in methyl galacturonic acid (MeGlcA) [42]. Furthermore, C-6 and the 4-*O*-methoxyl group of glucuronic acids (Figure 5.1f) are identified by the peaks at 175.7 and 56.3 ppm, respectively [42], [420]. The hemicellulose extract contained both MeGlcA containing XGN and XLN with uronic acid substituents, which confirms the types of hemicelluloses as concluded by the HPLC (Table 5.2) and FTIR (Figure 5.1). Therefore, the properties of the hemicellulose extracted from the mango seed husk can be strategically tuned during extraction to customize composition for applications, which in this case is targeted towards the formulation of biocomposites. However, the FTIR spectra confirmed that the extracted hemicelluloses were contaminated with lignin as depicted by the small peaks at 1265 cm^{-1}, corresponding to the breathing vibration of guaicyl lignin units and a peak at 1223 cm^{-1} (Figure 5.1c) associated with the presence of syringyl lignin units [448]. The presence of the lignin can limit the applications of the extracted hemicellulose, in particular, in food packaging due to the discoloring effect the lignin may have [450], thus, must be minimized during optimization.

Methylation analysis was further used to determine the type of linkages present in the hemicellulose extracts. Table 5.3 shows the mass-to-charge (m/z) ratios of the partially

methylated alditol acetate derivates determined by GC/MS after permethylation. The results showed glucose in the form of 2,6-Me_2 and 2,3,6-Me_3 derivatives, which corresponds to →4,6)-Glc*p*-(1→ and →4)-Glc*p*-(1→ linkage. These fragments suggest the presence of the 1,4-linkage backbone in xyloglucans [397]. Yashoda et al. [397] reported xyloglucan as the major hemicellulose type in mangoes with a 1,4-linked glucan backbone. In addition, some degree of branching was detected on the glucan backbone in this study at the *O*-3 and *O*-6 positions indicated by the presence of 2,6-Me_2 and 2,3-Me_2 glucose derivatives respectively while the presence of 2,3,4,6 Me_4 indicates the non-reducing end of glucose residue [451]. Xylose was found as a substituent at the non-reducing end of glucose due to the presence of a 2,3,4-Me_3-Xylp derivative (Table 5.3). In addition, xylose was also present as 1,4 linked derivatives (presence of 2,3-Me_3 derivative) with multiple branching at *O*-3 and *O*-4 position due to the presence of 2,3-Me_2 derivative (Table 5.3). These linkages confirm the existence of xylan-type hemicellulose in the extract [452], [453].

Table 5.3: *O*-methyl ether derivatives obtained from permethylation of mango seed husk hemicellulose extract

Sugar	Derivative mass-to-charge (m/z) ratio	*O*-methyl ether	Mode of linkage
Glucose	43, 101, 129	2,3,4,6-Me_4	Glc*p*-(1→
	43, 101, 143	2,4,6-Me_3	→3)-Glc*p*-(1→
	43, 173	2,3,6-Me_3	→ 4)-Glc*p*-(1→
	43, 139, 145	2,6-Me_2	→3,4)-Glc*p*-(1→
	43, 129	2,3 Me_2	→4,6)-Glc*p*-(1→
	145,146,217,218,289,290	-	→2,3,4,6)-Glc*p*-(1→
Xylose	43, 129,145	2,3,4-Me_3	Xyl*p*-(1→
	43, 189	2,3-Me_2	→ 4)-Xyl*p*-(1→
	43, 129, 201	2-Me	→3,4)-Xyl*p*-(1→

5.10.3. Effects of extraction conditions on yield and composition of mango seed husk hemicelluloses

The extracted hemicellulose (MHH) varied in XGN, XLN, uronic acid, and lignin contents with values ranging from 7.92–16.45%, 35.65–60.95%, 8.43–17.56%, and 17.04–25.97%, respectively (Table 5.2). The ratio of the XGN/XLN content of the hemicellulose extract ranged from 0.13–0.47 (Table 5.2). The highest MHH yield was obtained with 2 M NaOH, at 90 °C for 2 h giving XGN/XLN ratio, lignin, and uronic acid contents of 0.14, 19.38%, and 17.56% respectively (Table 5.2). The variations in hemicellulose yield and

composition at the different process conditions reflect the differences in reactivity under the extraction conditions, a strategy that is being used in this study to alter or tune the hemicellulose functionality for targeted applications.

The hemicellulose yield increased with an increase in NaOH concentration and temperature but not with time (Figures 5.2a (i-iii)) whereas, the XGN/XLN ratio decreased with an increase in NaOH concentration and temperature but not with time (Figures 5.2b (i-iii)). The increase in yield with NaOH concentration is attributed to the high ion concentration which effectively cleaved ester and ether linkages between hemicellulose and lignin and inter/intramolecular hydrogen bonding between hemicellulose and cellulose thereby releasing hemicellulose in the extraction medium [177]. Likewise, increment in temperature causes the hydrolyzing ions to gain enough energy to effectively diffuse into the cell wall and swell it, leading to weakening and hydrolyses of glycosidic linkages to release the hemicellulose. Similar trends have been reported in the literature [43]. The insignificant effect of time on hemicellulose yield indicates that longer extraction times (<5 h) may not be important for hemicellulose dissolution from mango seed husk [63]. Correlation figures between extraction conditions and the output variables are presented in Appendix B (Figures B2 a-d). Notably, the hemicellulose yield was significantly ($p< 0.05$) affected by the linear, quadratic, and interaction terms of NaOH concentration and temperature (Figure 5.3a). Additionally, both the NaOH concentration and temperature exhibited positive effects towards the hemicellulose yield with the NaOH concentration (linear) having the largest positive effect (Figure 5.3a). The phenomenon is an indication of increased hemicellulose dissolution, effects that have been observed in similar studies [292], [454]. Similar effects were observed with the XGN/XLN ratio except that the interaction (Figure 5.3b) and reaction time were not significant ($p > 0.05$). Thus, controlling either the NaOH concentration or temperature can tune the XGN and XLN composition in the hemicellulose fraction. However, the composition, would be more responsive to the varying of the NaOH concentration than temperature.

The XGN/XLN lowest ratios (0.13-0.14) (Table 4.2) were obtained at various combinations of NaOH (2.0 & 2.32), temperature (65 & 90 ^{o}C) and time (2.0 & 4.0 h) which provide flexible conditions for tuning the hemicellulose composition and functional properties. The higher XLN content in the MHH than XGN can be attributed to the differences in inherent binding mechanism onto cellulose microfibril thus, surface attachment vs crosslinking, respectively, in addition to higher M_w, making XLN more readily cleaved than XGN [438]. Notably, the results suggest that NaOH concentration and temperature are the major influencing parameters in determining the XGN and XLN contents for the tested conditions.

For instance, Minjares-Fuente et al. [61] reported an increase in XGN yield from grape pomace with an increase in KOH concentration in an ultrasonication-assisted extraction. The ultrasonication enhanced swelling and softening of the cell wall [61], but the inherently reduced alkalinity strength of KOH compared to NaOH [455], may explain the differences. These findings are supported by the findings of Kai and Petkowicz [456] and Bashir and co-workers [192] who extracted XGN from *Hymenaea courbaril* and tamarind seeds, respectively, using water and the latter, at room temperature (25 °C). However, the differences in XGN reactivity and dissolution from literature could emanate from the type of feedstock, thus, non-lignocellulosic biomass used in previous studies [195], [439], and lignocellulosic feedstock used in this study. The trend for lignin dissolution in NaOH and response to temperature and extraction time variations is similar to XGN's (Figures 5.2c (i-iii)). The lowest lignin content (17.04%) was at 2 M NaOH, 90 °C and 4 h, which gave hemicellulose yield of 48.68% and XGN/XLN ratio of 0.13 (Table 5.2). Similar yields were obtained at 2 M, 90 °C, and 2 h (48.96%, 18.38%, and 0.14%, respectively). The Pareto chart (Figure 5.3c) shows that negative linear effects of NaOH concentration and temperature, and the quadratic effect of NaOH were significant ($p < 0.05$) for lignin dissolution, a phenomenon that is different from the positive effects displayed for dissolution of lignin from XLN (glucuronoxylans) rich feedstocks such as hardwood [84].

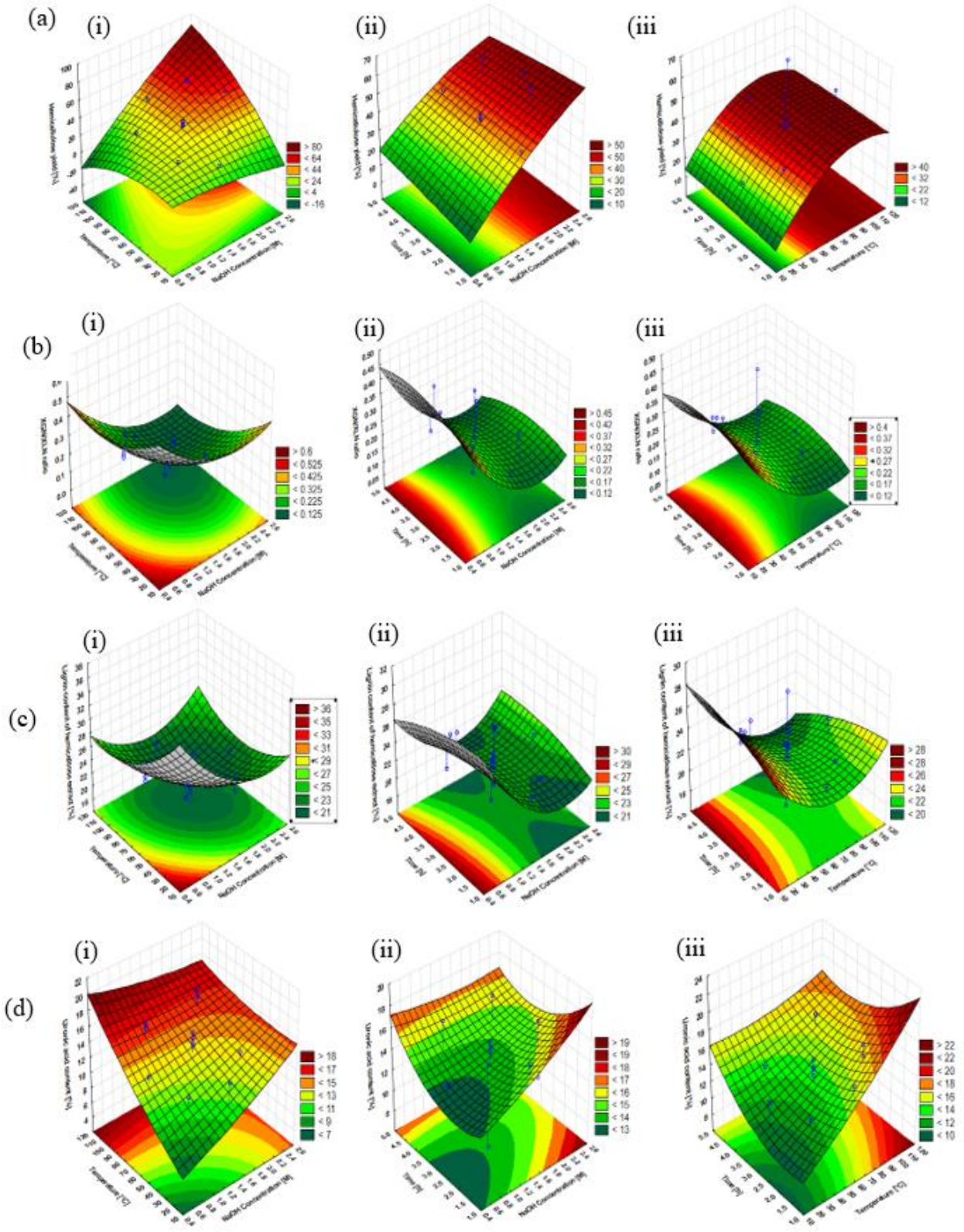

Figure 5.2: Effects of NaOH concentration, temperature, and reaction time on (a) hemicellulose yield, (b) xyloglucan/xylan ratio, (c) lignin, and (d) uronic acid contents of hemicellulose extract with interactions between (i) temperature and NaOH concentration, (ii) extraction time and NaOH concentration and (iii) extraction time and temperature

Notably, the uronic acid content increased with increased NaOH concentration and temperature (Figure 5.2d (i)) but only the temperature effect was significant ($p < 0.05$) (Figure 5.3d). According to Morais De Carvalho et al. [295], uronic acids could act as internal plasticizers during film formation but have a risk of increasing the film's hydrophilicity, thus their content should be minimized during optimization.

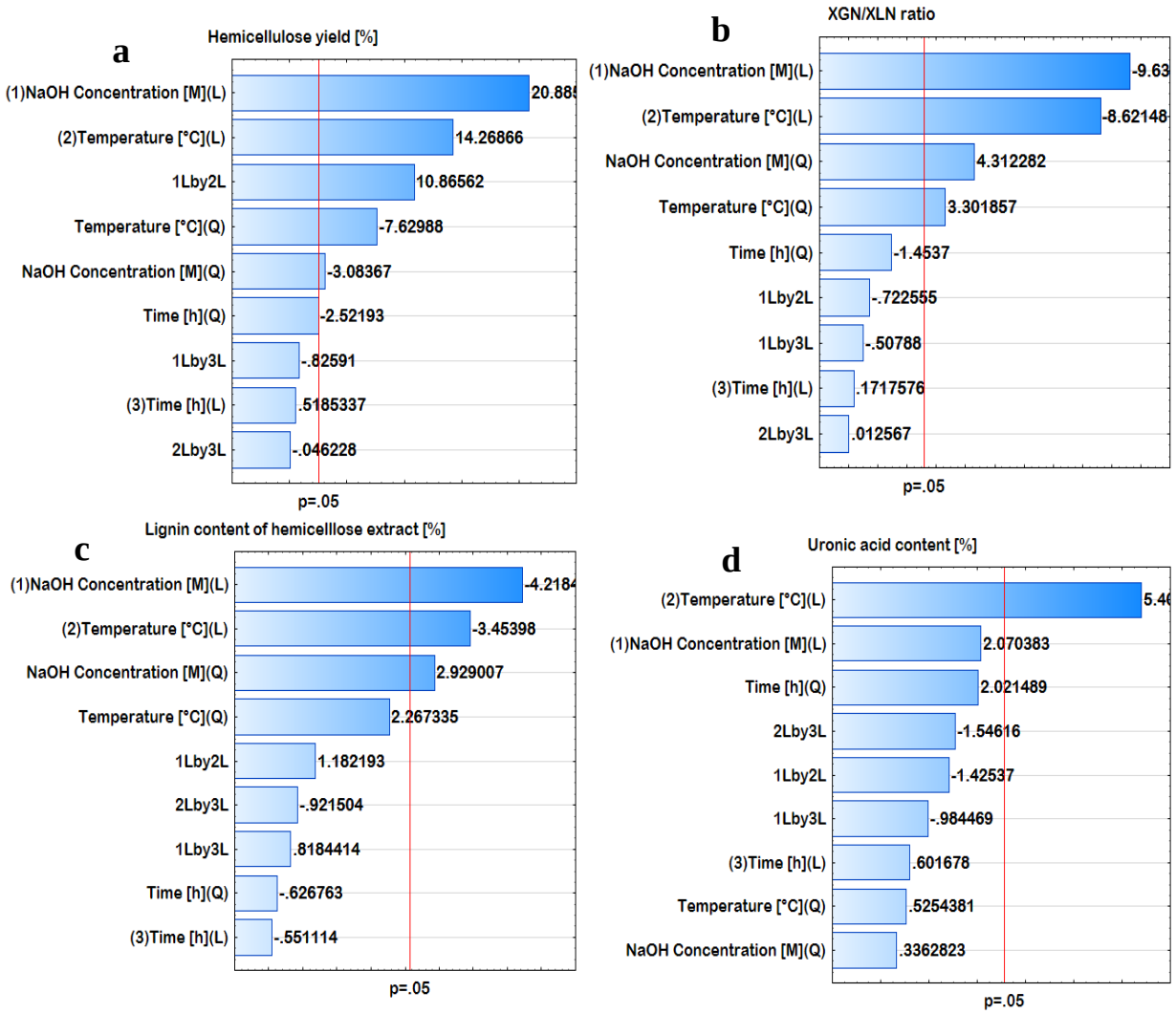

Figure 5.3: Significance and sizes of effects of NaOH concentration, temperature, and reaction time on the (a) yield, (b) xyloglucan/xylan ratio (c) lignin, and (d) uronic acid contents of hemicellulose extract extracted from mango seed husks

5.11. Optimal conditions for extracting hemicellulose suitable for self-forming films from mango seed husks

Optimization of the extraction conditions for high hemicellulose yield, lower XGN/XLN ratio, lower lignin, and uronic acids contents through desirability analysis identified the optimal conditions to be 1.92 M, 86.02 °C, and 3.84 h that gave hemicellulose yield, XGN/XLN ratio, lignin and uronic acids contents of 45.71, 0.13, 18.79 and 15.08%, respectively (Table 5.4). The predicted

values were comparable to observed values except for uronic acid content (12.02%) (Table 5.4). Therefore, the regression equations resulting from the analysis (Appendix B, Equations B1-4) can adequately predict the referred parameters at $R^2 \approx .0.7–0.98$.

Table 5.4: Hemicellulose yield and composition at optimized extraction conditions

Responses	Predicted value %	[a] Observed value %	% Deviation
Yield	45.71	46.24	1.15
Xyloglucan/Xylan	0.125	0.130	3.85
Lignin content	18.79	16.73	10.96
Uronic acid	15.08	12.02	20.29

[a] mean of triplicates determination. Note: Regression equations, Analysis of variance (ANOVA) Tables, and correlation graphs are available in Appendix B1. Optimized extraction conditions were NaOH concentration= 1.92 M Temperature = 86.0 °C and Time = 3.84 h

5.12. Suitability of hemicellulose for self-supporting film formation

Films made using the different hemicelluloses showed varying self-supporting capabilities (Figure 5.4a) and thermal stability, which confirms the complementing properties, thus, thermal stability and flexibility from the XGN and XLN, respectively. Furthermore, the higher MHH M_w (~70189 g/mol) than the CXLN M_w (~27235 g/mol) could be attributed to XGN (M_w ~2372886 g/mol) (Table 5.5). However, high CXGN M_w could be a result of the self-association of the polymers [64], [439]. Generally, molecular weight (M_w), structure, purity, and composition of hemicellulose affect the development of self-supporting films without the application of plasticizers [178], [295]. Higher M_w hemicellulose polymers have resulted in thermally stable self-supporting films without the addition of plasticizers [299], [372]. However, the lower M_w xylan polymers undergo extensive crystallization through inter/intramolecular hydrogen bonding and exhibit high glass transition temperatures which is why plasticizers or higher M_w polymers are added to obtain the desired film property [46], [178]. In addition, various reports highlighted lignin as an additive that contributes to the development of self-supporting xylan films [42], [270], [441]. The presence of the lignin aided in the development of self-supporting films. However, the influence of lignin and its interaction with XGN on the physical attributes of the MHH requires further investigation, which was beyond the scope of this study.

Table 5.5: Molecular weight, polydispersity and zeta potential of mango seed husk and commercial hemicelluloses

Hemicellulose	M_w (g/mol)	M_n (g/mol)	PDI	ζ-potential /mV
Mango husk hemicelluloses	69466 – 70189	42242 – 43756	0.254 ± 0.004	-16.1 ± 1.02
Xyloglucan	2046026 – 2372886	674209 – 707569	1.000 ± 0.000	-5.02 ± 0.34
Xylan	26056 – 27235	9837 – 19201	0.213 ± 0.005	-20.2 ± 2.82
Xyloglucan/Xylan (0.29)	29699 – 3177659	21537 – 1574118	-	-
Xyloglucan/Xylan (0.47)	28519 – 2930472	21756 – 1905882	-	-
Xyloglucan/Xylan (0.13)	28513 – 3479363	21281 – 1627492	-	-

Note: M_w = weighted-average molecular weight, M_n = number-average, mV = milli Volts, 0.29, 0.47 and. 0.13 denote the ratio of xyloglucan to xylan

The MHH had a surface charge, based on (ζ-) potential, of - 16.1 mV > - 5.02 mV of CXGN but < - 20.2 mV of CXLN (Table 5.5). The surface charges associated with the MHH and XLN can be attributed to uronic acid side groups of the xylan moieties in both samples [195]. Additionally, the stability of the hemicellulose in solutions is dependent on (ζ-) potential values with literature suggesting that hemicelluloses with absolute (ζ-) potential values greater than 15 mV become stable in solutions [434]. Therefore, based on the (ζ-) potential, the MHH is likely to form stable solutions, which would favor the formation of smooth biocomposite films. Furthermore, the MHH had a PDI of 0.254, which was between 1 and 0.213 of XGN and XLN, respectively (Table 5.5), further confirming the potential complementary effects between the two hemicelluloses. A (ζ-) potential > 15 mV and PDI < 0.7 may suggest a stable (non-aggregated) [434] and highly monodispersed (ISO 2017) MHH, suitable for the formation of homogenous self-supporting films. The phenomenon is reflected by the morphology of the films presented in Figure 5.4a (i). A PDI value of 0.254 obtained for MHH shows a more monodispersed sample (monodispersed sample ($0 \leq PDI \leq 0.5$)), heterogeneous sample ($PDI \geq 0.5$)). Notably, the MHH film in Figure 5.4a (i) displayed no cracks compared to films formed with a mixture of commercial XGN and XLN in ratios 0.29, 0.47, and 0.13, respectively (Figures 5.4a (ii-iv)) that had no lignin. Thus, the presence of lignin (≈16.0%) in the MHH might be a contributing factor to the film's morphology. Lignin has been reported to act as a plasticizer in biocomposites [295]. All films (Figures 5.4 a (i-iv)) showed similar functional groups

in the FTIR spectra (Figures 5.4b) except for the intense peaks at 1603 cm^{-1} for lignin in MHH film (Figures 5.4a (i)).

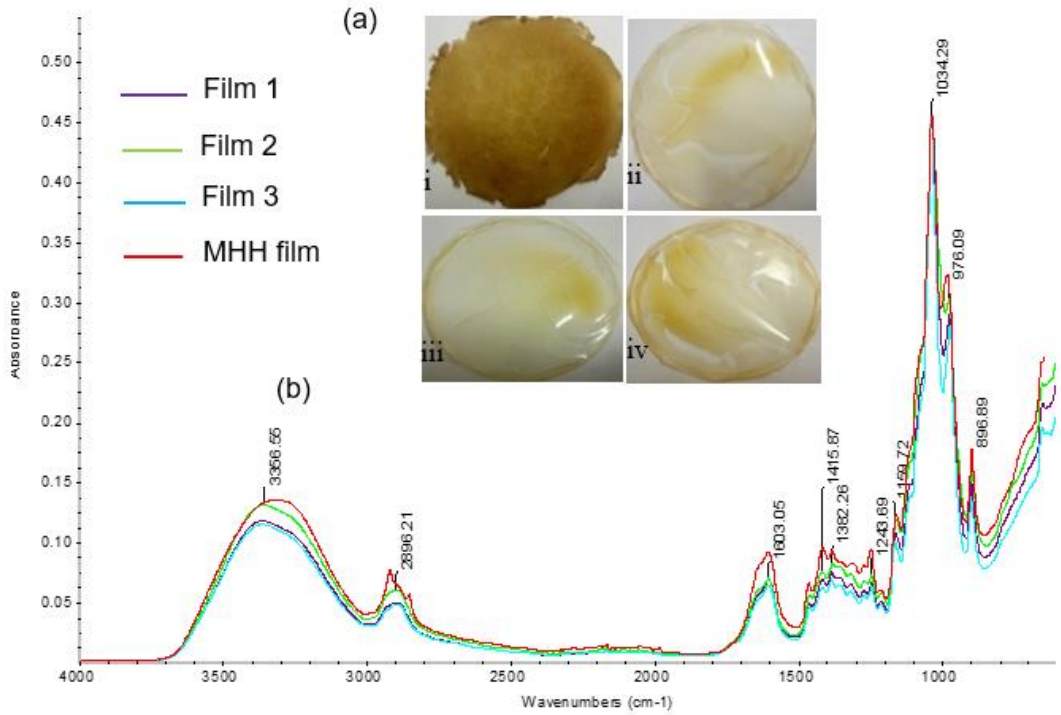

Figure 5.4: Biocomposite films prepared using (a) (i) Mango seed husk hemicellulose (MHH) with xyloglucan (XGN) and xylan (XLN) ratio of 0.13 obtained with mixtures of commercial XGN (CXGN) and XLN (CXLN) and in ratios of 0.29, (iii) 0.47 and (iv) 0.13, (b) Fourier Transform infrared spectra (FTIR) for the films i– iv prepared using CXGN/CXLN ratios of. 0.29, 0.47, 0.13 and MHH with XGN/XLN = 0.13.

An important property of hemicellulose-based films for packaging application in the food industry is thermal stability, particularly if the product may require microwaving [295]. The thermal properties of the MHH, CXGN, and CXLN were evaluated by TGA analysis using a temperature range of 25–600 °C. The total weight loss for the hemicellulose samples in the initial stage (Figure 5.5 and Table 5.6) was less than 10% which was a result of the removal of absorbed water [42], [295]. The XGN in the MHH increased its thermal stability (Figure 5.5a). Thus, a slightly higher initial degradation temperature (T_{onst} = 250 ºC) was observed for MHH (Figure 5.5a) compared to the pure CXLN only (T_{onst} = 230 ºC) (Figure 5.5b) which could be attributed to the presence of CXGN polymers (T_{onst} =380 ºC) (Figure 5.5c). The MHH displayed a maximum thermal degradation temperature (T_{max}) up to 330 °C (Figure 5.5a), which was between that of pure CXLN (290 °C) and CXGN (380 °C).

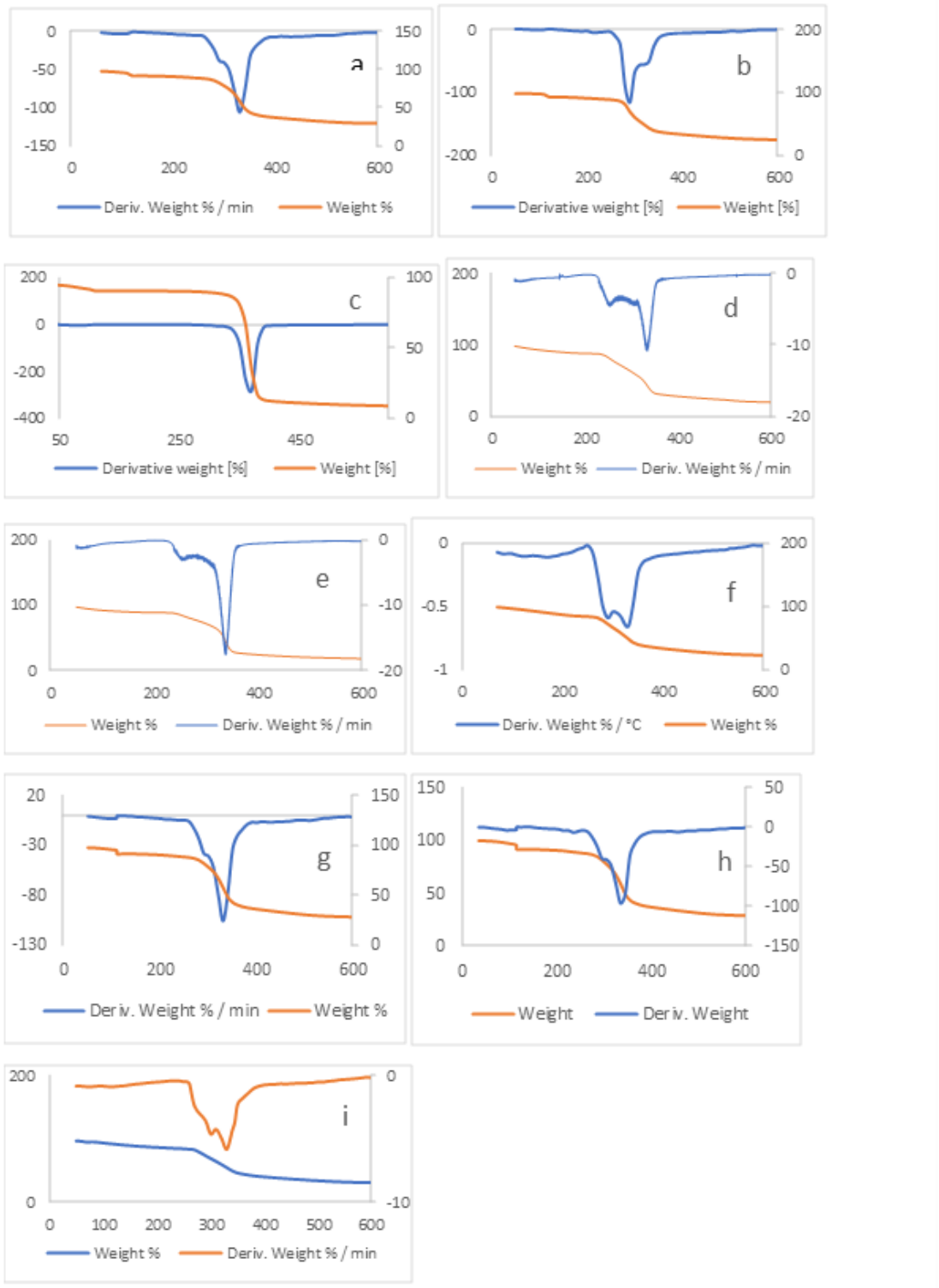

Figure 5.5: Thermal degradation and derivative thermal degradation thermographs of **a**. Mango seed husk hemicelluloses (MHH) at optimum extraction conditions, **b**. Commercial xylan (CXLN), **c**. Commercial xyloglucan (CXGN), **d.** CXGN/CXLN (0.29), **e.** CXGN/CXLN (0.47), **f.** CXGN/CXLN (0.13), **g.** MHH with XGN/XLN (0.29), **f.** MHH XGN/XLN (0.47), and **i.** MHH XGN/XLN (0.13).

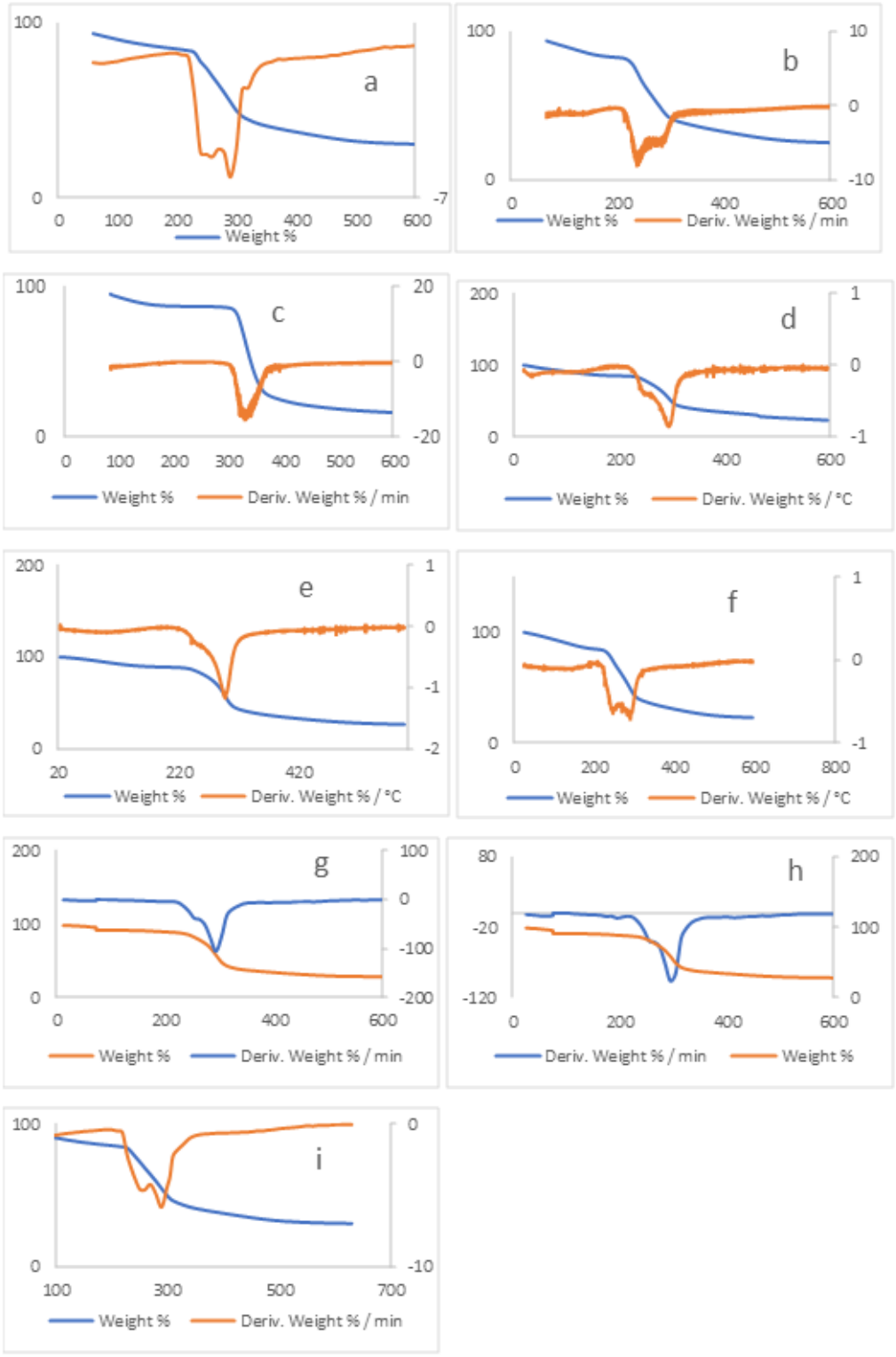

Figure 5.6: Thermal degradation and derivative thermal degradation thermographs of **a**. Mango seed husks hemicellulose (MHH) film at optimum extraction conditions, **b**. Commercial xylan (CXLN) film, **c**. Commercial xyloglucan (CXGN) film, **d.** CXGN/CXLN (0.29) film, **e.** CXGN/CXLN (0.47) film, **f.** CXGN/CXLN (0.13) film, **g.** MHH with XGN/XLN (0.29) film, **f.** MHH XGN/XLN (0.47) film, and **i.** MHH XGN/XLN (0.13) film.

The higher T_{onst} and T_{max} for MHH juxtaposed to CXLN implies the alkaline treatment optimization was effective in liberating the different hemicellulose polysaccharides (xyloglucan and xylan), which further influenced the thermal stabilities. The variation in the thermal stability of MHH due to varying XGN/XLN ratios (0.29, 0.47, and 0.13) as depicted in Figures 5.5 d-i, confirms that thermal properties of the MHH can be influenced by the XGN/XLN ratios (T_{max} (330–338 °C)), which were higher than CXLN T_{max} (290 °C). The influence of XGN was further reflected in T_{onst} and T_{max} of the MHH biocomposite films made with different XGN/XLN ratios (Figure 5.6). For instance, the biocomposite films formulated from the MHH with varying XGN and XLN and from CXGN/CXLN mixtures with varying ratios had T_{onst} and T_{max} ranging 200–296 ºC and 290–298 °C, respectively which were higher than CXLN T_{onst} and T_{max} (194 and 239 °C respectively) (Table 5.6). The addition of XGN in any ratio during the production of xylan composites films can improve the overall thermal stability of the film due to the well-defined structures of the xyloglucan and its stabilized glycosidic linkages. Werner and colleagues [457] reported that xyloglucan was more thermally stable with a T_{max} of about 325 °C compared to xylan whose T_{max} occurred at about 292 °C.

Table 5.6: Maximum degradation temperatures (T_{max}) of MHH, different XGN/XLN ratios, and their corresponding biocomposite films

Hemicelluloses T_{max} [°C]		Corresponding biocomposite films T_{max} [°C]
MHH (optimum point)	330.12	290.03
XLN	290.13	239.93
XGN	380.09	331.97
XGN/XLN (0.29)	335.02	295.17
XGN/XLN (0.47)	338.27	298.09
XGN/XLN (0.13)	332.74	290.01
MHH run 2	332.35	294.16
MHH run 9	335.26	296.23
MHH run 10	331.80	290.43

The mechanical properties (tensile strength, elongation at break, and Young's modulus) of the developed hemicellulose-based films are shown in Figure 5.7. For a film to be used in food packaging, it must be strong but with some level of flexibility [398]. Although the MHH could form

self-supporting films, it was less flexible with a low elongation at break value of 3% vs a reported value of 11% for arabinoxylan films with 40% plasticizer [458]. Thus, varying amounts of plasticizer (glycerol) were incorporated to improve the film's flexibility. The plasticizer had varying effects on the tensile strength, elongation at break, and Young's modulus (Figure 5.7). Relative to the tensile strength value of 11 MPa for the MHH film (Figure 5.7), the film formed from the MHH plus 10% plasticizer had a value of 9 MPa, which reduced with increasing plasticizer contents (< 4 MPa) (Figure 5.7). Similarly, there was a noticeable decrease in Young's modulus from ≈640 MPa to 136 MPa when 10–40% plasticizer was added to the MHH films (Figure 5.7). Similar trends in mechanical properties with respect to plasticizer addition have been reported in the literature [270]. The effect of plasticizer on the elongation at break was the reverse of tensile strength as its value increased from 3% for MHH to 19% for the addition of 10% glycerol (Figure 5.7). Mikkonen et al. [458] reported elongation at break value of 11%, a tensile strength of 4 MPa, and Youngs's modulus of 100 MPa for the film formed from arabinoxylan plus 40% glycerol. Thus, the lower requirement of plasticizer to achieve a high percentage of elongation for the MHH film in the present study (10% glycerol and 19% elongation; Figure 5.7) could save cost in MHH biocomposite film development compared to the requirement of at least 40% plasticizer in xylan-based films. The tensile strength and modulus of the developed hemicellulose-based film compared well with that of commercial low density polyethylene (LDPE) film, however, the elongation at break was low, thus could be improved further using other modification processes for similar applications as the LDPE.

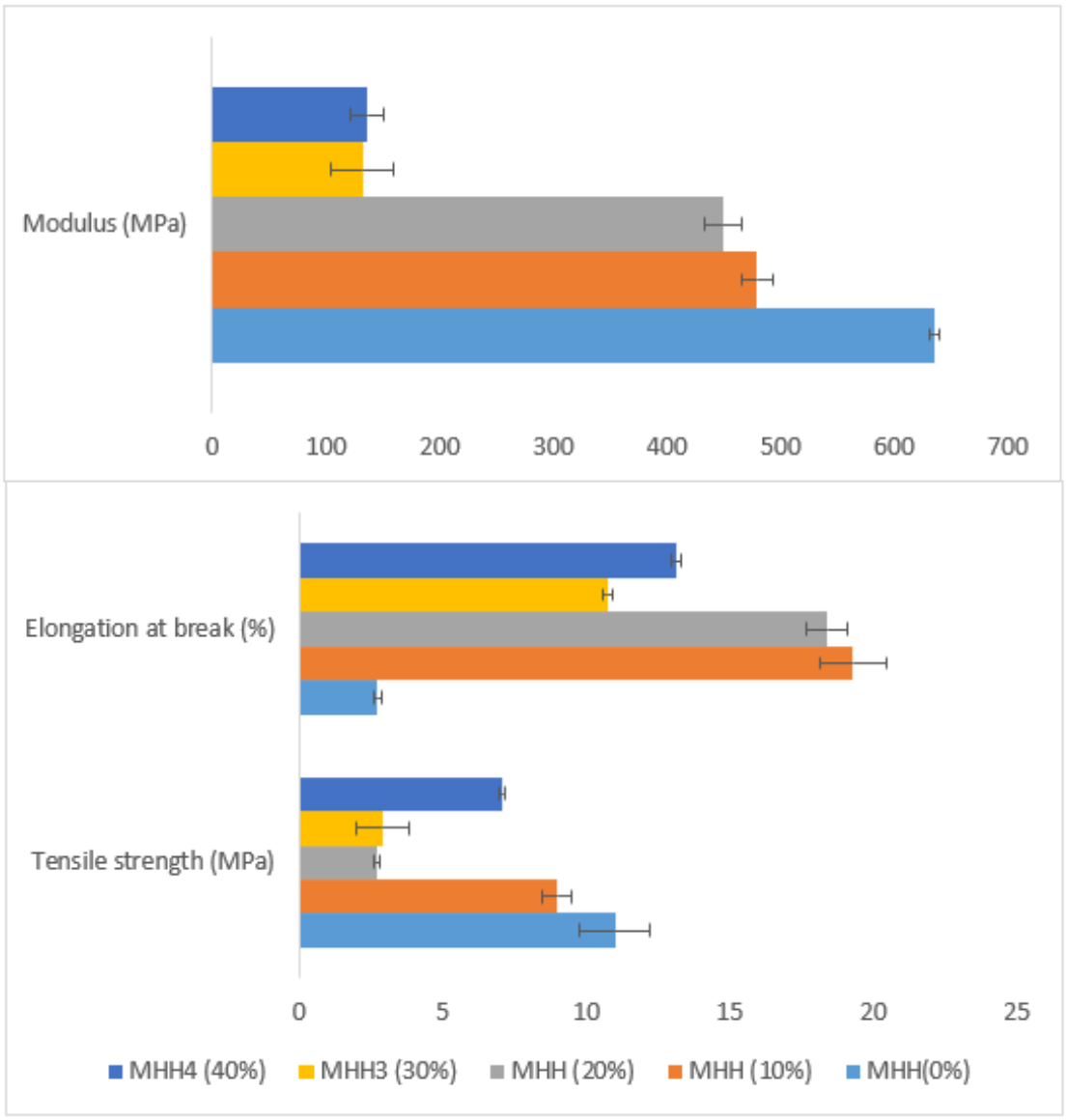

Figure 5.7: Mechanical properties of mango seed husk hemicellulose films with varying percentages (0 – 40%) of plasticizer

5.13. Conclusion

The alkaline-based extraction method was manipulated to produce hemicellulose with varying XGN/XLN ratios while maximizing yield and minimizing the co-extraction of lignin and uronic acids. Permethylation analysis revealed the 1,4 linked glucan backbone in xyloglucan hemicellulose with substituents of xylose at the reducing terminal end. The optimal alkaline extraction conditions for extracting the hemicellulose suitable for thermal stable and self-supporting biocomposite film were 1.92 M, 86.0 °C, and 3.84 h, which gave a yield of 46.24%, XGN/XLN ratio of 0.13, lignin content of 16.73%, and uronic acid content of 12.02%. The customized dissolution of XGN and XLN under varying alkaline extraction conditions is differentiated from the functional properties of the hemicellulose from MSHs in biocomposites. A self-supporting film with a

maximum degradation temperature of 290 °C was obtained from the extracted hemicellulose envisaged for application in food packaging. In addition, biocomposite films produced using MHH with varying XGN and XLN presented higher thermal degradation temperatures than CXLN. Moreover, it was observed that XGN in any ratio during the production of xylan composites films could improve the overall thermal stability of the film. Thus, feedstocks such as MSHs with varying types of hemicelluloses, present ideal feedstocks for obtaining hemicellulose extracts with diversified functionalities. However, the co-existence of different types of hemicelluloses with lignin and cellulose warrants investigation for integration in a biorefinery set-up. Also, the role of residual lignin in biocomposite requires further investigation. Thus, the present study contributes with an innovative optimized process that facilitates the co-extraction of the xylan-xyloglucan complexes (with lignin and uronic acids) from mango seed husks in ratios that show potential one-stop raw material benefits for producing the self-supporting, robust, and thermally stable biocomposite films. In addition, the present study further tests the thermal properties of the xylan-xyloglucan complexes based biocomposite for potential application in thermo-processes or applications requiring microwaving of products. The findings further unlock higher economic potential for mango waste as a suitable raw material for the hemicellulose complex-based biocomposite, which could further enhance economic potential for the mango waste that currently poses environmental cost burdens in the mango processing industry.

5.14. Optimization of lignin extraction from alkaline treated mango seed husk by high shear homogenization-assisted organosolv process using response surface methodology

Published paper: *International Journal of Biological Macromolecules*, 197(2021) 1379-1392

Authors: Fatimatu Bello, Annie Chimphango

5.15. Abstract

Lignin valorization into materials such as resins is essential to increase the value obtained from biomass. However, biomass recalcitrance limits the selective isolation of lignin for economic gains. This study developed a new process for fractionating alkaline treated mango seed husk into high purity lignin and cellulose-rich pulp, using high shear homogenization-organosolv (HSHO) process. The HSHO process conditions (ethanol concentration (50–70%), temperature (130–150 °C), and homogenizing time (10–20 min)) were optimized using response surface methodology to maximize the solubilized lignin with high purity while obtaining a cellulose-rich pulp. Optimum process conditions of 60% ethanol, 148.41 °C, and 15 min homogenization, yielded 70.23% lignin of 96.18% purity, higher than those of the non-assisted process (68.58% and 94.74%, respectively). Nuclear magnetic resonance spectroscopy showed syringyl and guaiacyl lignin units with a molecular weight of 3247 g/mol and thermal degradation temperature of 298 ºC. Sulfur and nitrogen contents in the resulting lignin were lower than 0.15%. Fibrillated cellulose pulp with purity >77% and diameters of <1–10 µm were obtained. This study has established the proficiency of an HSHO process for biomass fractionation and more so, for the extraction of lignin with >90% purity suitable for varied applications.

5.16. Introduction

Most research works were predominantly targeted towards the use of carbohydrates like cellulose and hemicellulose for advanced applications, for example, biocomposite formulation, to substitute the synthetic counterparts [312]. Lignin, on the other hand, received comparatively less attention in this regard due to its complex structural nature arising from the various carbon-carbon, aryl-ether, and alkyl-ether covalent linkages of the monolignols in addition to the ester and ether linkages between lignin and carbohydrates, making it a challenge to selectively isolate it in a less modified form [202], [212]. Therefore, the majority of lignin were recovered and used as a low-purity by-product for heat generation [68]. This current way of disposing of lignin does not account for its full value, thus, the need for novel, and efficient extraction processes for full lignin valorization [459]. Recently, there has been a significant interest in lignin valorization for the generation of valuable materials like phenol-formaldehyde resins, carbon fibers, lignin-based composites among others because of its numerous phenolic compounds [85], [460]. Lignin extraction and valorization in addition to cellulose and hemicellulose will provide the opportunity for recovery of multi-products from a single feedstock through the concept of biorefinery [59], [85]. In biorefinery, biomass is separated into its various components of cellulose, lignin, and hemicellulose and further converted using biochemical and thermochemical processes into fuel, chemicals, and other components [68], [461]. Thus, an important part of the biorefinery is to recover the majority of the lignin as a high-value product rather than using it to generate heat [312]. Despite the many efforts to extract and valorize lignin, there is still the challenge of selectively isolating it in huge volumes with high purity and less modification.

In addition, the application of lignin in resins or carbon fibers depends on the composition and distribution of lignin monolignols, which is not only a function of the biomass source but also the pretreatment techniques employed [239], [461]. Consequently, most recent research works have focused on exploring new lignin feedstock sources and delignification processes [59], [462]. Among the feedstock sources already explored for this purpose are wheat straw, sugarcane bagasse, and oil palm empty fruit bunches [59], [462]. One potential lignin feedstock source is the mango seed husk, which is generated in large quantities after the industrial processing of mango fruits [10]. The husk is composed of 39.4–55.1% cellulose, 15.6–20.6% hemicellulose, and 23.8–26.6% lignin [20], [118]. Most of the research efforts had focused on its usage for activated carbon [463] and nanocellulose production [20]. The lignin content of the husk is comparable to the 17.6% and 18.93% reported for other feedstocks already explored for lignin valorization [59], [228], an indication of the prospect to obtain lignin and other co-products for a sustainable biorefinery. In this respect, appropriate

pretreatment techniques or a combination thereof will be necessary to obtain high purity lignin in addition to value-added co-products of cellulose and hemicellulose.

Conventionally, the established delignification processes: Kraft, lignosulfonate, and alkali result in the extraction of over 70 million tons of lignin annually [85] with the Kraft lignin constituting more than 90% of the total lignin generated [464]. However, Kraft lignin is hydrophobic and less reactive, with significant modification (reduced number of native lignin linkages with the introduction of 1–2% aliphatic thiol groups) due to the application of high temperatures, and strong bases [239]. The alkali and lignosulfonate lignin contain high ash and sulfur contents (10%) respectively, making them less attractive for many applications like in resins, which require less modification and >90% purity [201], [465].

Organosolv is one of the promising pretreatment/fractionation methods that result in the co-production of high purity, less condensed lignin, and cellulose-rich fibers using organic solvents or its aqueous mixtures [59]. Ethanol is used in most organosolv pretreatment processes because of its environmental friendliness, ease of recovery, and its ability to limit the condensation of hydrolyzed lignin [59], [464]. Nonetheless, most ethanol organosolv processes have generally been carried out at relatively severe conditions of temperature (up to 230 ºC), ethanol concentration (up to 80%), and use of acid catalysts (0.5–2 wt% of HCl or H_2SO_4) to achieve high yields and purity of lignin, with highly enzymatically digestible solids [213], [316], [406].

To improve the rate of delignification and limit the use of severe conditions, other mechanical and physicochemical treatments have been combined with organosolv [68], [407]. For example, Matsakas et al. [68] combined steam explosion and organosolv as a hybrid process to achieve high delignification (79.4% w/w) with cellulose-rich solids (72% w/w) from spruce biomass. Sun et al. [466] combined ultrasonication and organosolv to attain up to 78.5% lignin solubilization compared to 61% without ultrasonication. High shear homogenization (HSH) is an economical and efficient mechanical processing method employed purposely for emulsion and dispersion generation of biological tissues [327]. It uses mechanical shear and cavitation to disrupt and fibrillate the cell wall leading to a reduction in crystallinity and particle size with increased porosity [94], [95]. With its open configuration and variable diameters of the probe, the HSH allows repeated circulation of both high and low viscosity samples with minimal issues of clogging [327]. The high shear homogenization has been documented to effectively defibrillate and depolymerize fibers into nanofibrils while consuming low energy when compared to high-pressure homogenization and ultrasonication [467]. This technique, despite its distinctive effectiveness, has been rarely used for pretreatment for lignin extraction or in combination with ethanol organosolv for such purposes. Therefore, combining the HSH and ethanol organosolv in a single process could provide a cost-

effective and industry-applicable method for producing high purity, less condensed lignin, and a cellulose-rich material with separated individual cellulose fibers that can be used for nanocellulose preparation under less severe conditions [20], [98].

As part of a bigger study to develop a process route for producing nanocellulose and high value-added bioproducts from mango seed in a biorefinery concept, the biomass (alkaline treated mango husk) used in this study was obtained after alkaline process conditions were optimized for hemicellulose extraction from dried mango seed husk. This was done to preserve hemicellulose in polymeric form and prevent its exposure to severe delignification conditions [178]. In this study, the alkaline-treated residue was delignified using the high shear homogenization-assisted ethanol organosolv process (HSHO). Firstly, the influence of the HSHO process conditions of ethanol concentration (50–70%), temperature (130–150 ºC), and homogenizing time (10–20 min) on the pretreatment/fractionation of alkaline treated mango seed husk (lignin solubilization and purity, cellulose, and hemicellulose contents of residue) was investigated. The second part involved optimizing the process conditions for maximum solubilization and purity of lignin, and cellulose content of residue, and minimum hemicellulose content. To verify the effect of HSH homogenization on lignin solubilization and purity, cellulose, and hemicellulose contents of residue, a reference non-assisted experiment was performed following the method of Huijgen et al. [59] with modification for comparison. This involved treatment of biomass at 200 ºC, for 90 min using 60% ethanol. The lignin and solid residues were further characterized to determine the effect of the pretreatment on their physicochemical properties.

5.17. Materials and Methods

5.17.1. Materials and sample preparation

All the chemicals used for the experiments are listed in section 5.2.1. The mango seed preparation prior to the experiments is described in section 5.2.2.

5.17.2. Mango seed husk delignification

The set-up for the experiments consisted of homogenization and ethanol organosolv pretreatment. Samples were mixed with ethanol solutions (50–70%) containing 1% NaOH to form a 20% solid loading and left overnight to allow for effective solvent transfer. Thereafter, the samples were placed in an ice bath and homogenized (PRO250, Oxford CT, USA) at a speed of 22000 rpm for varied time intervals based on the experimental design in Appendix B, Table B1. The ice bath was used to avert the heating up of samples during homogenization. Thereafter, homogenized samples were poured into 1 L digester micro bombs and tightly sealed. The bombs were placed in a

15 dm^3 pressurized oscillating (45 °) digestor half-filled with water. A thermocouple and pressure gauge fitted to the digester was used to monitor both temperature and pressure in the digester. The digester was heated to the desired temperatures and maintained at that temperature for 90 min. After the reaction, the pressure build-up in the digester was liberated through a fitted blow valve, and the micro bombs cooled immediately to 40 °C with running water. The suspension was filtered under suction through a membrane filter (1.4 µm) to obtain the black liquor (filtrate). The residue remaining was then washed with 60% ethanol, and then with warm distilled water until the washing solution attained pH 6. The solid residue was dried at 40 °C overnight and kept in sealed plastic bags for further analysis. The obtained filtrate was distilled at low temperatures (40 °C) using a rotary evaporator to recover ethanol and the remaining liquor neutralized to pH 5.5 to 6.0 with acetic acid for lignin precipitation [468], [469]. The precipitated lignin was obtained through filtration by suction using a glass filter with a pore size of 1.4 µm. The lignin recovered was then dried at 40 °C in the oven, cooled, and stored for further characterization. Yields of various fractions were calculated according to Equations 12–14.

$$Total\ solubilised\ lignin\ (\%w/w) = \frac{mass\ of\ lignin\ in\ starting\ material - mass\ of\ lignin\ in\ residue\ (g)}{mass\ of\ lignin\ in\ starting\ material\ (g)} \times 100 \quad [12]$$

$$Recovered\ lignin\ \ (\%w/w) = \frac{mass\ of\ recovered\ lignin\ in\ fraction\ (g)}{lignin\ content\ of\ the\ starting\ material\ (g)} \times 100 \quad [13]$$

$$Solid\ recovery\ (\%) = \frac{mass\ of\ recovered\ solids\ (g)}{mass\ of\ starting\ material\ (g)} \times 100 \quad [14]$$

5.17.3. Experimental design and statistical analysis

The HSH-assisted organosolv pretreatment was carried out in a 3^3 central composite rotatable design (CCD) experiment. The independent variables chosen were ethanol concentration, temperature, and homogenizing time (Appendix B, Table B8). These conditions were chosen based on preliminary experiments (see Appendix B, Figure B3) and from literature studies [215]. A total of 16 runs for the three variables' levels were obtained using Statistica 13.2 software. The dependent variables were solubilized and recovered lignin yields, lignin purity, solid residue, and composition: cellulose, hemicellulose, and lignin.

5.17.4. Regression analysis and optimization

Appropriate models for the responses were developed using regression analysis taking into consideration the parameters of the independent variables and their interactions. Analysis of variance (ANOVA) was used to identify significant factors and coefficients of the second-order model equation (Equation 15).

$$Y = \propto_0 + \propto_1 X_1 + \propto_2 X_2 + \propto_3 X_3 + \propto_{11} X_1^2 + \propto_{22} X_2^2 + \propto_{33} X_3^2 + \propto_{12} X_1 X_2 + \propto_{13} X_1 X_3 + \propto_{23} X_2 X_3 + \varepsilon \quad [15]$$

where Y is the response variable, $\propto_0$, $\propto_1$, $\propto_2$, $\propto_3$, $\propto_{11}$, $\propto_{22}$, $\propto_{33}$, $\propto_{12}$, $\propto_{13}$, and $\propto_{23}$ are the regression coefficients, and X_1, X_2, and X_3 are the independent variables for ethanol concentration, temperature, and homogenizing time respectively and ε is error. A probability value, p<0.05 was used to evaluate the significant relationship of each response variable to the independent variable and optimal extraction conditions were determined using response surface plots (RSM) and desirability analysis (as detailed in section 4.4.5) in Statistica 13.2 software. Further, the regression models' adequacy was determined based on the regression coefficient (R^2).

5.17.5. Characterization of starting material, hydrolysate, recovered lignin, and solid residue

5.17.5.1. Sugars and lignin content determination

The chemical compositions of the starting material and recovered solids were determined based on the method described in section 5.2.2. The sugars and lignin contents of the extracts were determined according to the procedure in section 5.5.1. The structural features of samples were determined based on the method highlighted in section 5.7. The thermal stability of extracts was determined according to the procedure in section 5.7.

5.17.5.2. Elemental analysis

Elemental analysis of lignin samples was performed to determine the relative proportions of hydrogen (H), carbon (C), sulfur, and nitrogen (N) using a Vario EL Cube CHN analyzer (Hanau-Frankfurt, Germany). Acetanilide was used to calibrate the instrument after each analysis. The oxygen percentage was obtained after the sum of the contents of H, C, S, and N were subtracted from 100 percent.

5.17.5.3. Size Exclusion Chromatography (SEC)

SEC was used to determine the molecular weight of extracted lignin. An Agilent 1260 HPLC instrument equipped with a differential refractometer set at 40 °C, a diode array UV detector set at 290 and 320 nm and PSS 10 µm GRAM columns consisting of a guard column and three analytical

columns (2 x 3000 Å and 1 x 100 Å) as the stationary phase, was used for SEC analysis. Dried lignin samples were dissolved in dimethylformamide (DMF) overnight at room temperature before the analysis. The mobile phase was DMF with 0.05 M LiBr at a flow rate of 1.0 mL/min. The injection volume was 100 µL and the sample concentration was 2 mg/mL. The system was calibrated using narrow PMMA calibration standards with a molar mass range of 800 to 2200 000 g/mol.

5.17.5.4. Nuclear magnetic resonance (NMR) spectroscopy

Proton, ^{1}H, and ^{13}C NMR were carried out on the lignin samples for structural characterization using a Varian INOVA 400 MHz spectrometer (USA). Samples were dissolved in Dimethylsulfoxide-*d6* (DMSO-d_6) before the analysis and the instrument was operated in 1D mode at 25 ºC with an acquisition and relaxation times of 2.5 s and 1.0 s respectively. All spectra were noted to the ^{1}H and ^{13}C signals of (DMSO-d_6) at 2.5 ppm.

5.17.5.5. Scanning electron microscopy (SEM)

The morphology and structure of the residue at the optimal high shear homogenization-assisted organosolv process conditions and that of the non-assisted organosolv (control) were analyzed using MERLIN Zeiss scanning electron microscopy (SEM) with an accelerating voltage of 5–20 kV. A layer of gold was coated on the dried samples placed on carbon tapes using an Agar Sputter Coater. A 3-kV electron beam was used for the analysis.

5.18. Results and discussions

5.18.1. Yields and compositions of solubilized lignin and solid residue after homogenization-assisted organosolv pretreatment/fractionation process

Based on the lignin content of the starting material, the total solubilized and recovered lignin yields ranged from 30.32–81.37%, and 20.63–74.79% respectively with purities of 86.55–96.94% (Table 5.7). The solid residues ranged from 66.40–86.64% with cellulose, hemicellulose, and lignin contents of 65.35–78.09%, 9.03–12.25%, and 4.42–16.54% respectively (Table 5.7). The highest solubilization of pure lignin was observed at 156.8 ºC, 60% ethanol, and 15 min homogenization (Table 5.7). In addition, more than 70% solubilized lignin with >90% purity was obtained at different process conditions (Table 5.7).

Table 5.7: Effect of high shear homogenization-organosolv process conditions on lignin yields, purity, solid recovery and composition, sugar, and ash contents of recovered lignin

Ethanol concentration [%]	Temperature [°C)	Homogenizing time [min]	Total solubilized lignin [%w/w]	Total recovered lignin yield [%w/w]	[b]Lignin purity [%w/w]	[a]Sugars in lignin [%w/w]	Ash content of lignin [%]	Solid recovery [%]	Cellulose in residue [%w/w]	Lignin in residue [%w/w]	Hemicellulose in residue [%w/w]
50.00	130.00	10.00	35.37	29.11	88.74	2.60	2.23	80.61	67.77	15.31	10.12
50.00	130.00	20.00	38.15	32.61	90.81	2.01	1.89	80.00	68.06	14.68	10.02
50.00	150.00	10.00	70.21	59.67	94.35	1.51	0.65	70.34	74.36	7.07	11.37
50.00	150.00	20.00	73.33	65.20	96.68	1.15	0.48	69.77	75.03	6.33	11.72
70.00	130.00	10.00	30.32	23.88	94.33	2.02	0.96	80.07	70.97	16.54	10.05
70.00	130.00	20.00	38.90	25.26	93.66	2.18	1.42	78.31	72.41	14.50	10.44
70.00	150.00	10.00	54.82	45.62	96.76	1.22	1.01	71.08	74.90	10.72	11.32
70.00	150.00	20.00	53.26	41.64	90.56	1.68	1.93	70.40	76.20	11.09	11.58
43.18	140.00	15.00	54.03	45.37	86.55	3.39	2.63	77.16	67.03	10.91	10.53
76.82	140.00	15.00	35.09	23.11	91.57	1.48	1.46	76.46	71.52	15.41	10.55
60.00	123.18	15.00	31.57	20.63	89.02	2.56	1.97	86.64	65.35	16.24	9.03
60.00	156.82	15.00	81.37	74.79	96.94	1.03	0.28	66.40	78.09	4.42	12.25
60.00	140.00	6.59	49.71	37.75	93.18	1.72	1.67	78.45	72.90	11.94	10.53
60.00	140.00	23.41	62.81	51.60	96.78	1.12	0.57	75.82	75.20	8.83	10.54
60.00	140.00	15.00	54.93	42.27	96.03	1.74	1.03	77.64	73.07	10.70	10.36
60.00	140.00	15.00	55.50	44.69	95.65	1.96	0.89	78.58	72.50	10.56	10.41

[a]Sugars: total %glucose and %xylose in lignin extract, [b]sum of acid-soluble and acid-insoluble lignin

When compared this study with various organosolv processes in previous studies [85], [470], higher solubilized lignin yields were obtained with the high shear homogenization-assisted organosolv (HSHO) process and at relatively lower temperatures (Table 5.7). The highest solubilized lignin at 156.8 ºC obtained in this study was greater than the reported 66.54% by Nitsos et. al. [85] and 43% by Brahim et al.[470] despite the 182 ºC and 162 ºC employed respectively. The increased solubilization can be attributed to the mechanical shear and cavitation resulting from homogenization that might have led to the peeling of cellulose fibers and the pre-extraction of hemicellulose. Consequently, increasing the surface area and porosity of the biomass [471], for effective penetration of the hydrolyzing ions that depolymerize the lignin. Therefore, the chemical and mechanical pretreatment techniques, when combined, significantly improve the delignification of biomass as demonstrated in this study and other reports [68], [472].

The enhanced solubilization of lignin translated into high lignin purity with low levels of carbohydrates (1.03–3.39%) and ash (0.28–2.63%) (Table 5.7) as impurities that were within the ranges of 0.4–11% and 0.1–2.7%, respectively, reported in other studies [68], [85], [473]. The carbohydrate contaminants could be due to the inability of the process conditions used to hydrolyze all the lignin carbohydrate complexes (LCC) [213]. The ash content may have resulted from the formation of salts during the neutralization for lignin precipitation. In general, purity values achieved are comparable to the 90.5–96.3% reported in the literature [68], [473], [474].

The HSHO process conditions were effective in selectively extracting lignin from the biomass. The yields of the solid residue post-lignin extraction (Table 5.7) fall within the reported range of 14.38–84.4% for ethanol organosolv pretreatment [59], [472]. In addition, the lignin content in the solid residue was reduced (4.42–16.54%), when compared to the 19.13% in the starting material. In contrast, the cellulose and hemicellulose contents of the residue increased (Table 5.7). Although the lignin contents of the solid residues fell within the range of values reported in the literature for organosolv pretreatment, the hemicellulose contents in the residue were higher than the reported values [62], [85]. The hemicellulose content in the residue was higher than reported values due to lignin carbohydrate complexes and the nature of substitution in the hemicellulose type of mango seed husk. The xyloglucans (hemicellulose type in mango) tend to be very stable to hydrolyzing agents such as dilute acids, heat, bases, and shear forces [435] which also explains the lower percentages of sugars in the recovered lignin (Table 5.7).

5.18.2. Optimization of high shear homogenization-assisted organosolv process conditions for isolating pure lignin fraction from alkaline treated mango seed husk

5.18.2.1. Influence of high shear homogenization-assisted organosolv process conditions on lignin solubilization and recovery

Analysis of variance showed that all three process conditions investigated (ethanol concentration, temperature, and homogenizing time) had significant individual influences (p<0.05) on solubilized lignin in addition to the interaction effect of temperature and ethanol concentration (Figure 5.8a). For the recovered lignin, the temperature and ethanol concentration had significant effects (p<0.05), but not the homogenizing time (Figure 5.8b). In addition, the temperature and the homogenizing time had positive effects (Figures 5.8a and c) on both the solubilized and recovered lignin, indicating that higher lignin solubilization and recovery were achieved with an increase in the temperature and homogenization time. This is due to homogenization which increases the accessible cell wall surface area by disrupting the cell wall while temperature provides more heat energy that enhances protonation reactions and induces cleavage of lignin linkages for lignin solubilization and recovery [92], [454]. In contrast, the ethanol concentration showed a negative effect (Figure 5.8a-b) suggesting a decrease in solubilized and recovered lignin with an increase in this variable to an optimum and vice versa.

From Figure 5.8a, the temperature, among the three variables, exhibited the highest effect (p<0.05) on solubilized lignin as confirmed by the largest F-value =16504.83 for the linear term (Appendix B, Table B2). This was followed by the ethanol concentration with F-value =2280.71 and 1117.77 for linear and quadratic terms respectively (Appendix B, Table B2). The interaction effect of temperature and ethanol concentration was moderate (F-value =737.20) but more pronounced than the effect of homogenizing time (F-value =543.81). Similarly, for recovered lignin, temperature exhibited the greatest individual effect with an F-value of 918.92 followed by ethanol concentration (F-value of 190.0) (Appendix B, Table B2).

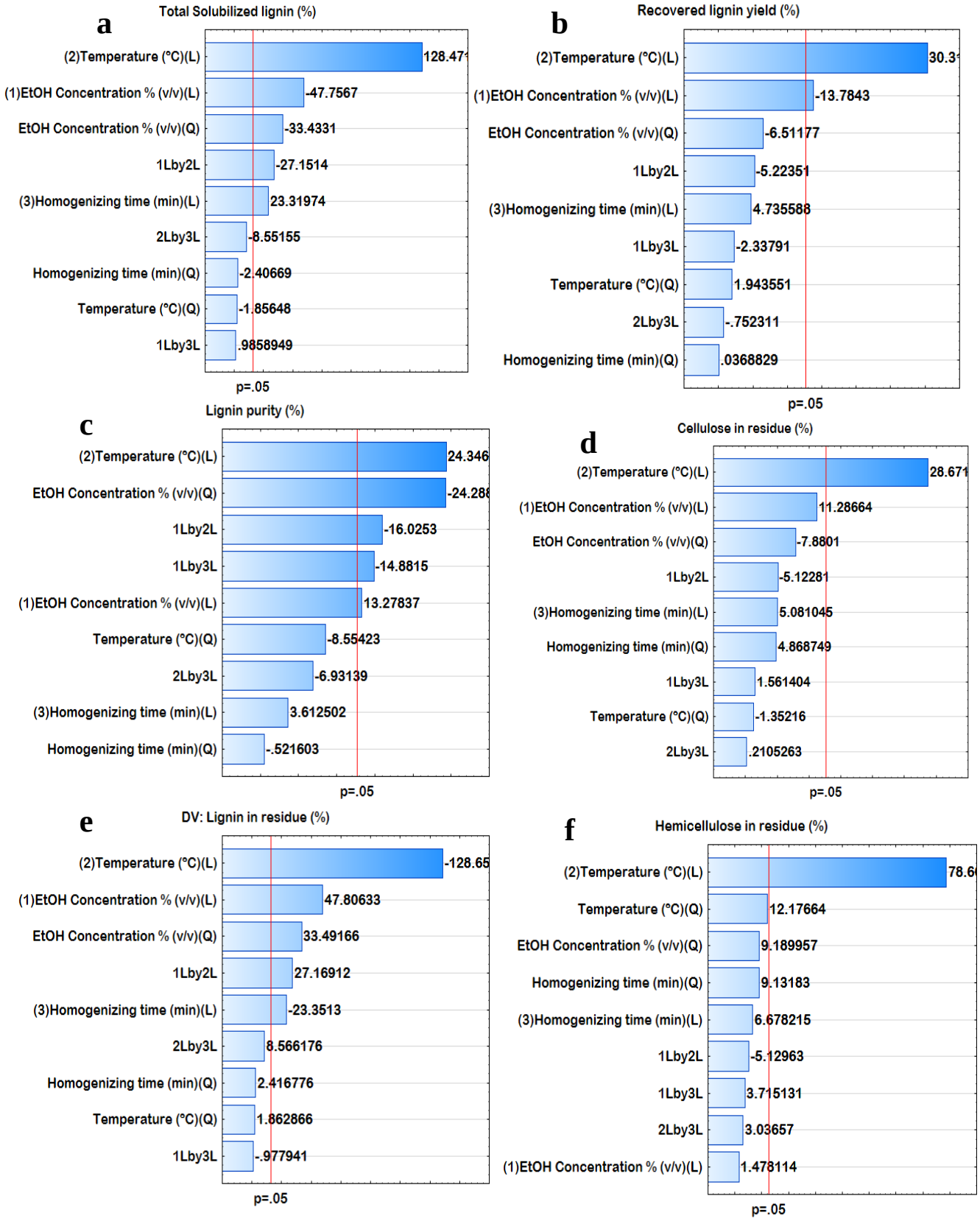

Figure 5.8: Pareto charts showing the significance of the effects of ethanol concentration, temperature, and homogenizing time on (a) solubilized lignin, (b) recovered lignin, and (c) lignin purity, (d) cellulose, (e) lignin, and (f) hemicellulose contents of solid residue.

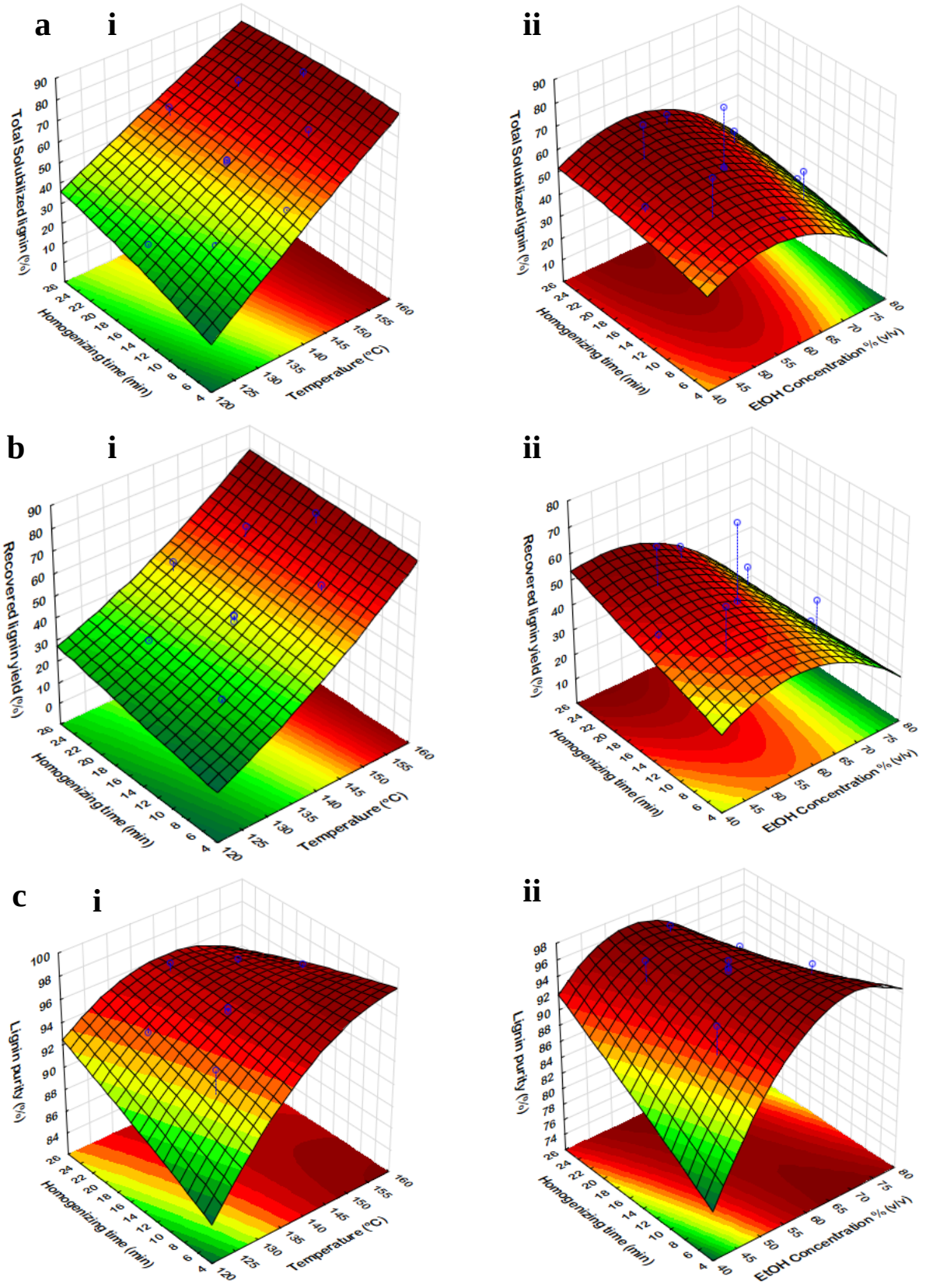

Figure 5.9: Response surface plots showing the effect of ethanol concentration, temperature, and homogenization time on (a) solubilized lignin (b) recovered lignin (c) and lignin purity.

The trends of the effect of the ethanol concentration, temperature, homogenizing time, and their interactions on the total solubilized lignin, recovered lignin and lignin purity are shown on the response surface plots in Figures 5.9a–c. At a constant homogenizing time, an increase in temperature from 123.18 °C to 156.82 ºC increased both solubilized (from 31.57–81.37%) and recovered lignin (20.63–74.79 (Figure 5.9a (i) and Figure 5.9b (i)). The observed trend is due to the progressive hydrolysis of ester bonds between lignin and hemicellulose and lignin ether linkages as the extraction medium becomes more kinetically favored with the application of more heat [59], [419]. In general, at higher temperatures, the ions generated in the reaction medium diffuse rapidly into the cell wall, thus, attacking and cleaving ester and lignin ether linkages, and subsequently resulting in lignin fragmentation and solubilization [215]. This result is in agreement with that reported during organosolv pretreatment of pre-hydrolyzed wheat straw and beech wood [59], [475].

Similar to the temperature, the increase in homogenizing time from 6.59 to 23.41 min at a constant temperature, led to an increment in solubilized lignin (Figure 5.9a (i)) and its recovery (Figure 5.9b (i)). Evidently, an increase in homogenization time directly affected the lignin hydrolysis and consequently solubilization, due to the increased surface area of biomass resulting from mechanical shear and cavitation because of the homogenization. With ethanol concentration, the hydrolyzed lignin was solubilized with a progressive increment until the optimum level was attained at approximately 60% ethanol (Figure 5.9a (ii)). A further increase in ethanol concentration above 60% caused a corresponding reduction in the solubilized (Figure 5.9a (ii)) and recovered lignin (Figure 5.9b (ii)). The trend observed indicates the intricacies involved in lignin extraction from biomass with ethanol organosolv. That is, a reduced proportion of ethanol is required to ensure hydrolytic cleavage of the various ester and ether lignin linkages, whereas, lignin solubilization requires a higher proportion of ethanol since lignin does not dissolve in acid water [472]. Similar scenarios have been reported in the literature for ethanol organosolv pretreatments of wheat straw and Norway spruce [68], [91]. This implies that maximum delignification is a compromise between hydrolysis of linkages and solubility of lignin. It is thus advised that the ethanol content of the solubilizing solvent using the proposed method is limited to a maximum of 60% (v/v) [85]. From Table 5.7, it could be seen that the total solubilized lignin could not be recovered. This is due to the formation of colloidal suspensions whose removal poses various challenges or the presence of very low molecular weight lignin that could pass through the glass filter when vacuum filtration is used. Similar scenarios were reported by Bauer et al. [476] and Nitsos et.al. [85] in their studies.

Therefore, other alternative techniques such as dissolved air floatation are being investigated to improve the recovery of lignin [85].

5.18.2.2. Effect of high shear homogenization-assisted organosolv process conditions on lignin purity

Apart from yield, one other factor that influences lignin utilization in chemical and material production is lignin purity [477]. The sugar content (after sulphuric acid hydrolysis of recovered lignin) and ash content (after incinerating lignin at 575 ºC for 8 h) were considered the main impurities in lignin [478]. As indicated in Figure 5.9c, lignin purity was significantly affected by the individual effects of temperature and ethanol concentration ($p<0.05$) but not homogenizing time ($p>0.05$). Nonetheless, the interaction of ethanol and homogenizing time and that of ethanol and temperature were significant ($p <0.05$) at a 95% confidence level. From Figure 5.9 c, it is evident that the temperature had a positive impact and with the highest F-value of 589.91 (Appendix B, Table B9), therefore promoting an increase in purity when it was raised from a low level (123 ºC) to a high level (156 ºC) at a constant homogenizing time (Figure 5.9 c (i)). This is due to the enhanced cleavage of ester and ether linkages between hemicellulose and lignin and lignin ether linkages resulting from increased heat energy which improves the reactivity of ions to induce catalytic cleavage of bonds [215].

Similarly, the progressive increment of ethanol concentration from ≈43.2% to 60% at a constant homogenizing time slightly improved the purity as the dissolution of lignin in the reaction medium intensified due to enhanced fragmentation (Figure 5.9 a (i)). Nonetheless, a reduction in purity was observed when the ethanol proportion was further increased (Figure 5.9 a (i)). This decrease in purity could have emanated from carbohydrate and ash contamination as discussed in the previous section [59], although the carbohydrate contaminant did not exceed 3.39% and ash, 2.63% (Table 5.7). At the employed conditions, hydrolysis of cellulose is limited and most of the carbohydrates in the lignin could have originated from hemicelluloses. Literature studies have shown that the substitution on xyloglucan (a hemicellulose type in mango seed husk) and its interaction with cellulose microfibrils, allow shielding of the cellulose, protecting it against hydrolyzing agents [179], hence confirming the claim of insignificant degradation of cellulose. Overall, high lignin purities achieved in this study offer the avenue for a wide range of industrial applications compared to Kraft and lignosulphonate lignin [477].

5.18.2.3. Effect of ethanol concentration, temperature, and homogenizing time on the cellulose, hemicellulose, and lignin compositions of the solid residue

The observed trends in solubilized lignin correspond to the data for the composition of cellulose, hemicellulose, and lignin contents of the solid residue (Table 5.7). The cellulose and hemicellulose contents of the solid residue were mainly affected by the reaction temperature (p<0.05) (Figures 5.8 d and f). The effects of ethanol concentration and homogenization time were not statistically significant (p>0.05) towards these responses at a 95% confidence level. In contrast, the individual effect of all three variables investigated: ethanol concentration (linear and quadratic), temperature (linear), and homogenizing time (linear) were significant (p<0.05) towards the lignin content of the solid residue, in addition to the interaction effect of ethanol concentration and temperature (Figure 5.8 e). The response surface plots in Figures 5.10a (i) and 5.10 c (i), depict the cellulose and hemicellulose contents of solid residue as a function of temperature and ethanol concentration when the homogenizing time is fixed at the mid-point level.

In Figures 5.10 a (i) and 5.10 c (i), the reaction temperature showed a positive correlation with cellulose and hemicellulose contents as these responses increased progressively when the temperature was increased. In the case of residual lignin, the opposite was observed as its value decreased with increment in temperature (Figure 5.10b (i)) due to the efficient removal of lignin, which led to the increased cellulose and hemicellulose contents of the solid residue (Table 5.7). This trend complements the lignin solubilization obtained, in that the selective removal of lignin leads to the lowering of the residual lignin content of the solid residue which results in a rise in other cell wall components depending on conditions employed [85]. Similarly, reductions in lignin content of the solid residue occurred with an increase in homogenizing time at constant ethanol concentration (Figure 5.10 c(ii)). For example, a decrease in residual lignin content was observed when the homogenizing time was increased from 6.59 to 23.41 min. The cellulose and hemicellulose contents at these conditions slightly increased (Figures 5.10 a(ii) and 5.10 c (ii)). This is due to the fibrillation of the cellulose microfibrils (shown in SEM images) due to its exposure to mechanical shear and cavitation during homogenization which led to the rapid access of hydrolyzing ions to the cell wall for lignin hydrolysis [92]. The influence of the ethanol concentration on the cellulose, lignin, and hemicellulose contents of solid residue are also depicted in Figures 5.10a-c.

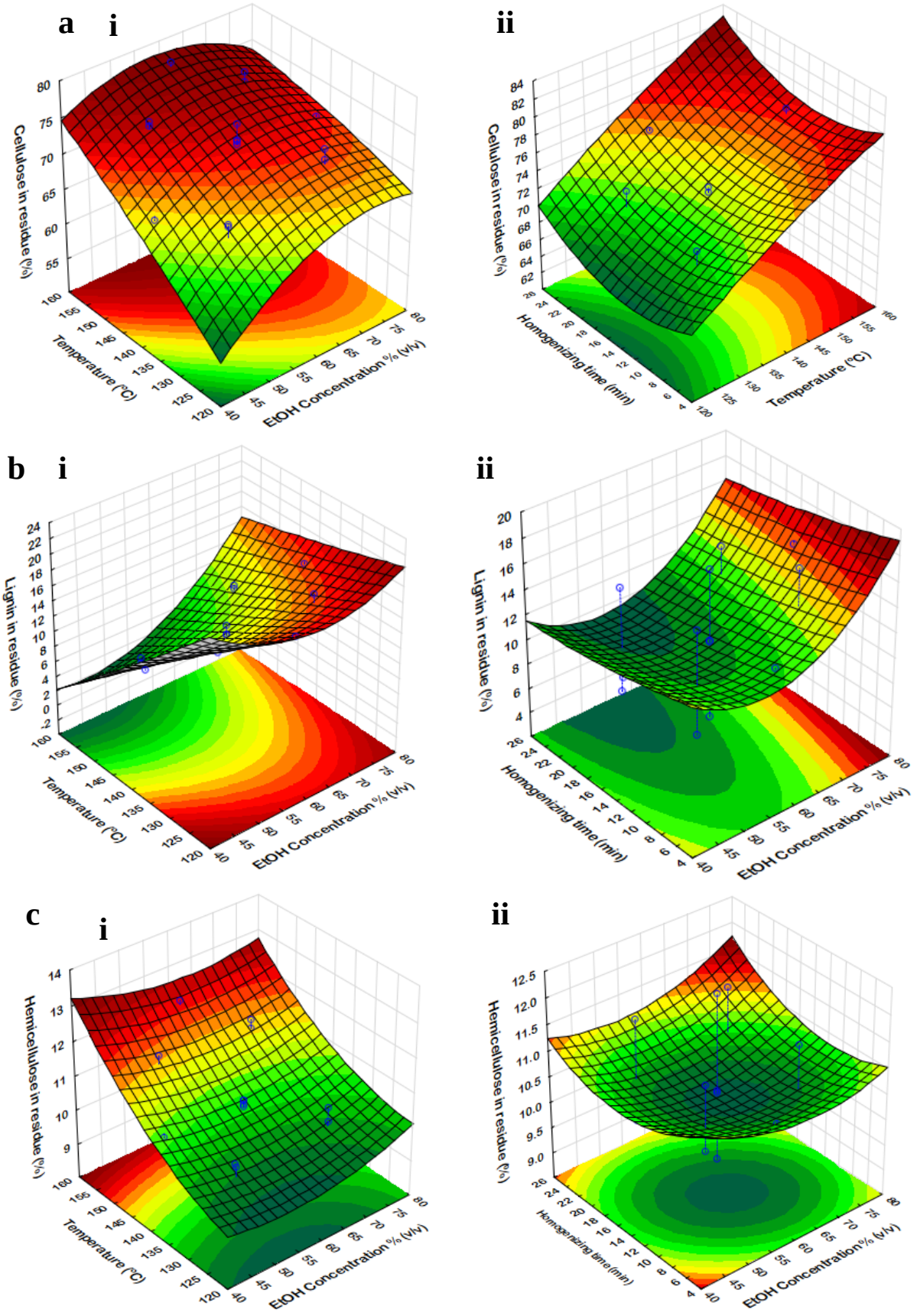

Figure 5.10: Response surface plots showing the effect of ethanol concentration, temperature, and homogenization time on (a) cellulose, (b) lignin, and (c) hemicellulose contents of solid residue.

At a constant temperature (140 ºC), the cellulose content of solids increased, but this time, a slight decrease in hemicellulose content was observed, as the ethanol concentration increased up to 60% (Figures 5.10 a(i) and 5.10 c (i)). This could be due to the favorable conditions of the reaction medium facilitating the hydrolysis of both lignin and hemicellulose. Contrary to the temperature, at the higher ethanol concentration (above 60%), both the residual lignin and hemicellulose contents increased (Figures 5.10 a (i) and 5.10 c (i)) leading to a drop in the cellulose content. This is because of the inadequate water content in the extraction medium to generate enough ions to depolymerize the cell wall linkages for effective lignin extraction. Thus, the lignin content of residue was high for either very low or very high ethanol concentrations.

5.18.3. Optimal conditions for lignin extraction of alkaline treated mango seed husk

The regression models developed for the various response variables are presented in Appendix B Table B9. The coefficient of determination (R^2) for the responses was greater than 0.85, indicating that the experimental data fitted well to the developed models. This was also confirmed by the lack-of-fit *p*-values that were greater than 0.05 (Appendix B Table B9). The results from the desirability profile in Statistica 13.2 software indicated that using 60% ethanol, 148.41 ºC, and 15 min homogenization will achieve maximum solubilized lignin and purity, maximum cellulose content, and minimum hemicellulose contents in solid residue. For confirmation, an experiment was performed using these conditions. A total solubilized lignin of 70.43% and a purity of 96.18% was achieved, similar to the predicted values by the model (Table 5.8). The solubilized lignin and its purity were comparable to that of the non-assisted (reference) process (68.58% and 94.74% respectively) performed at an elevated temperature of 200 ºC. This demonstrates that homogenization enables efficient lignin extraction by the ethanol organosolv at a considerably lower temperature. The solid residue contained cellulose and hemicellulose contents of 77.84% and 10.98% respectively. The optimum temperature and ethanol concentration obtained are lower than the 162 ºC and 65% ethanol reported by Brahim et al. [470] for lignin extraction from rapeseed straw. However, these authors recorded a much lower solubilized lignin (≈43%). The lignin purity obtained is comparable to the 93% recorded by Nitsos *et al.* [85] but higher than the 70.6% reported for oil palm empty fruit lignin [479]. The resultant cellulose content in the solid residue in this study is higher than the 69.07% and 72% reported by Nitsos et al. [85] and Matsakas et al. [68] respectively, despite the higher temperatures (183 ºC and 200 ºC respectively) these authors employed. It can, therefore, be

concluded that the HSHO treatment of alkaline treated mango seed husk resulted in the dissolution of lignin of high purity that can be used in applications like resin and a cellulose-rich pulp that can be valorized further into materials like nanocellulose.

Table 5.8: Predicted and observed values of responses for optimum high shear homogenization-assisted organosolv process conditions

Component	Solubilised lignin [%]	Lignin purity [%]	Cellulose content of solid residue [%]	Hemicellulose content of solid residue [%]
Predicted values	67.18	96.67	75.21	11.13
[a] COL	70.43	96.18	77.84	10.98
% Deviation	4.61	0.51	3.38	1.35
[a] REL	68.58	94.74	76.75	10.16
%Deviation	2.04	1.99	2.00	8.79

[a] mean of triplicates determination. The optimum conditions were Ethanol concentration = 60%, Temperature = 148.41 °C and Homogenizing time = 15 min, COL= Optimum lignin sample, REL= Reference (non-assisted) lignin sample

5.18.4. Structural features of extracted lignin at optimum homogenization-assisted and non-assisted organosolv processes

The structural and functional properties of the lignin samples obtain using the high shear homogenization-assisted organosolv and the non-assisted organosolv process are shown in the FTIR and NMR spectra in Figure 5.11. The homogenization applied during the organosolv (HSHO) process did not change the basic structural features of the lignin under the conditions used. This can be seen in the close resemblance of the FTIR spectra for the HSHO and the non-assisted lignin samples (Figure 5.11 a). The intense and broad peaks shown at 3288 cm^{-1} correspond to the hydroxyl groups of phenolic and aliphatic structures involved in hydrogen bonding [476]. The peaks at 2934 cm^{-1} and 2843 cm^{-1} represent the CH stretching in methyl ($-CH_3$) and methylene ($-CH_2$) groups of side chains [438]. Spectral peaks at 1027 cm^{-1} and 1264 cm^{-1} indicate the presence of guaiacyl lignin monolignol and that at 1329 cm^{-1} is associated with the stretching vibration of the C-O in syringyl lignin units [477], [480]. This implies, both guaiacyl and syringyl lignin monolignols are present in the mango seed husk lignin. A peak at 1365 cm^{-1} is assigned to the phenolic hydroxyl (-OH) groups generated when β-O-4 linkages are cleaved during treatment. This peak was seen to be very weak which

indicates that fewer β-O-4 linkages were cleaved during the HSHO process which was confirmed by the strong peak at 1216 cm^{-1} assigned to ether linkages [481].

The structural features were further confirmed by ^{1}H and ^{13}C-NMR spectroscopy (Figure 5.11 b). In the ^{1}H NMR spectra, the appearance of signals at 2.7–5.18 ppm and 6.5 ppm–6.8 ppm that correspond to protons in guaiacyl and syringyl lignin units respectively were seen [464], [482]. The region between 160 ppm and 103 ppm in ^{13}C-NMR spectra is assigned to the aromatic lignin structural units [483]. Signals at 134.9 ppm and 152.2 ppm corresponds to the C1 of non-etherified and C3/C5 of etherified syringyl lignin units, respectively [480], [482]. The guaiacyl lignin units were confirmed at 147.2 ppm –149.5 ppm for etherified and 145.2 ppm for non-etherified guaiacyl lignin units [203], [481]. In addition, signals at 60.0 ppm, 74.0 ppm, and 86.0 ppm assigned to C-γ, C-α, and C-β in β-O-4 respectively were evident [203], [481]. The lower signals at 86.0 ppm for HSHO than non-assisted lignin samples indicate the cleavage of more β-O-4 linkages in HSHO than in the non-assisted process (Figure 5.11b). The methoxyl groups in both guaiacyl and syringyl lignin are indicted by the strong signal at 55.8 ppm.

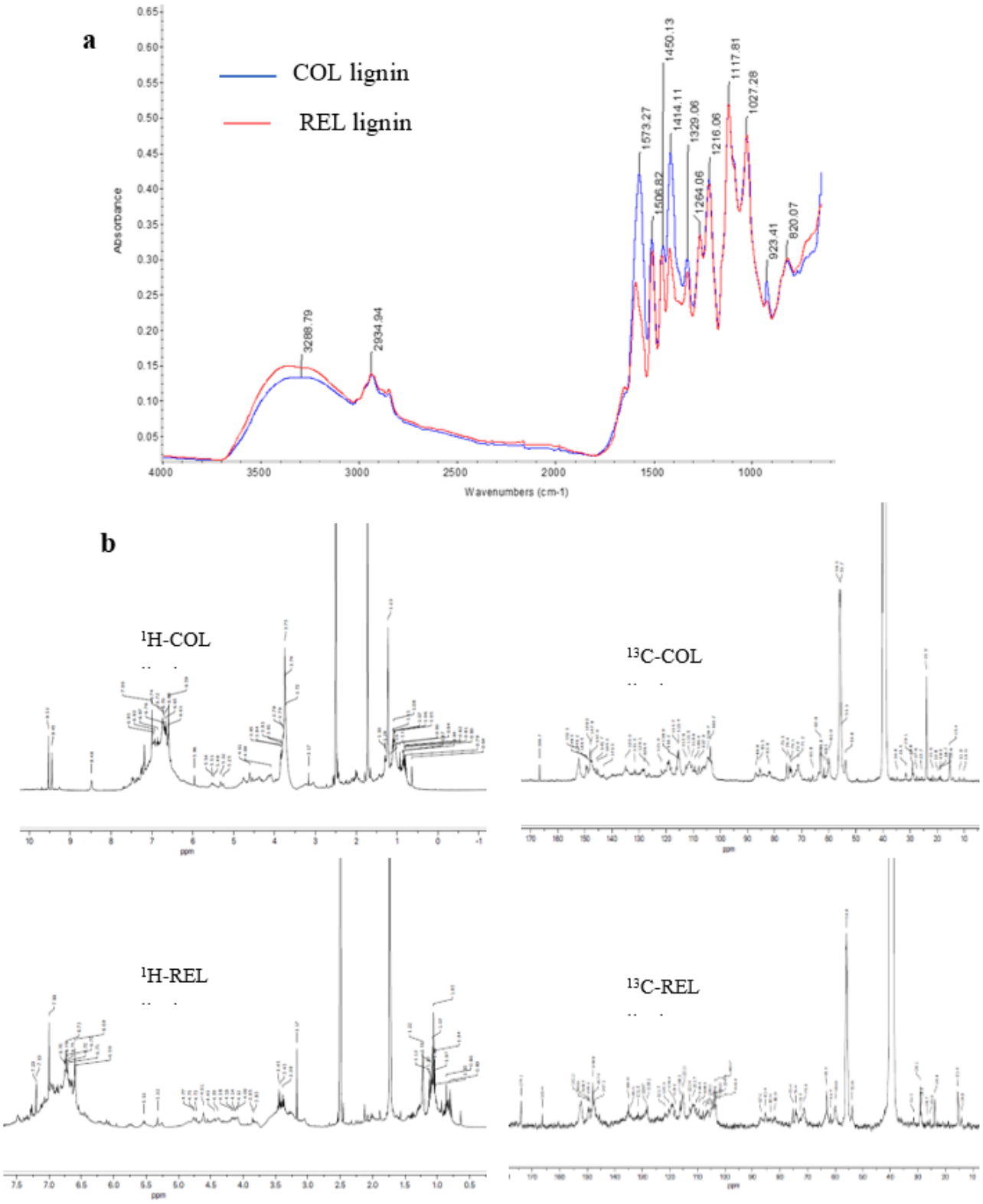

Figure 5.11: Fourier transform infrared and nuclear magnetic resonance spectra of organosolv lignin obtained under optimum high shear homogenization-assisted organosolv process (COL) and non-assisted organosolv process (REL).

Although the lignin samples obtained by the HSHO and non-assisted process showed spectral peaks characteristic of lignin, some of the band intensities differed showing possible differences (Figure 5.11 a). Such observations are evident in the aromatic ring vibration region of the FTIR spectra. The intensities of the bands at 1573 cm^{-1} and 1414 cm^{-1} were stronger for the HSHO lignin (COL) than the intensities of bands at the same absorption band for the non-assisted (REL) lignin while the intensity of bands at 1264 cm^{-1} assigned to C-O stretching of guaiacyl units was similar for both lignin samples (Figure 5.11a). This suggests a higher proportion of syringyl lignin units in the HSHO lignin than in the non-assisted lignin. The higher proportion of syringyl units was also evident in the ^{13}C-NMR spectra for COL lignin (Figure 5.11 b) where the signal at 152.2 ppm associated with syringyl lignin was intense than that of the REL lignin. In addition, the signal at 37.5 ppm associated with methoxyl groups was more intense in the COL lignin than REL lignin (Figure 5.11 b). This could be a result of rapid cleavage of syringyl lignin units (generally regarded to cleave easily due to easier hydrolysis of its β-aryl units) by the action of homogenization [480], [484]. The high lignin purity was also confirmed in the ^{13}C-NMR spectra (Figure 5.11 b), as the intensity of the band associated with neutral sugars was very weak at 103 ppm [466]. Based on the above discussions, it can be concluded that different treatments result in changes in the chemical structure of extracted lignin and consequently their field of application.

5.18.5. Elemental composition of lignin samples

The elemental composition of the two lignin samples obtained at optimal conditions of high-shear homogenization assisted organosolv (COL) and for the non-assisted organosolv (REL) process are shown in Table 5.9. The REL lignin had the highest percentage by weight of carbon and lowest percentage by weight of oxygen while the COL had the lowest percentage by weight carbon and highest percentage by weight oxygen (Table 5.9). From the literature, syringyl lignin is associated with a higher number of methoxyl groups than guaiacyl which translates into a lower percent by weight of carbons [480]. This means the homogenization facilitated the hydrolysis of more syringyl lignin units than guaiacyl units. In addition, the HSHO lignin showed <0.1% sulfur and nitrogen contents (Table 5.9) which are lower than the 0.37%–2.5% sulfur and 0.13%–0.66% nitrogen contents reported for commercial sulfur-free organosolv and Kraft lignin [473], [480]. The presence of nitrogen in the lignin samples could be due to protein or other nitrogenous compounds contamination [480] although, this cannot be confirmed from the present study. Overall, the HSHO lignin has the advantage to be used in a variety of industrial applications including resin production due to its lower sulfur and

nitrogen contents (which reduces the release of toxic gases) and high syringyl lignin content– which limits condensation reactions during depolymerisation processes [202].

Table 5.9: Elemental composition, weighted average, number average and polydispersity of organosolv lignin samples

Lignin sample	C (%)	H (%)	S (%)	N (%)	O (%)	M_w (g/mol)	M_n (g/mol)	*PDI*
COL	56.70	7.15	0.03	0.04	36.08	3247	2349	1.38
REL	58.20	6.21	0.02	0.11	35.46	3325	2424	1.37

COL: optimum high shear homogenization-assisted organosolv lignin, REL: Non assisted organosolv lignin, M_w: weighted average molecular weight, M_n: number average molecular weight, *PDI*: Polydispersity

5.18.6. Molecular weight and molecular weight distributions of lignin samples

Size exclusion chromatography was used to determine the molecular weight (M_w) and diversity of lignin fragments in the solubilized lignin samples [91]. Compared to the average M_w (3325g/mol) of the lignin obtained by the non-assisted process, the HSHO process resulted in a slightly lower average M_w (3247g/mol) (Table 5.9). The lower M_w of HSHO lignin (COL) could be attributed to the cleavage of more ether linkages by the effect of homogenization (opening of the vegetal tissues) and ion catalyzed hydrolysis of lignin by the ethanol organosolv [466]. Furthermore, the stability of C-C covalent bonds existing between guaiacyl lignin units (due to the free C5 position) which is absent in syringyl lignin (C5 substituted with methoxyl group) makes it easier to hydrolyze more syringyl units with the lowest molecular weight [480]. This confirms the lower M_w of the COL lignin (Table 5.9). A similar observation was reported by Sun et al. [466] when they compared M_w of ultrasound-assisted organosolv lignin with a non-assisted product. The polydispersity index (*PDI*) showed similar values for the two lignin samples suggesting less diversity in the lignin fragments. Overall, the HSHO process is effective in obtaining homogeneous lignin fragments of lower molecular weight.

5.18.7. Thermal stabilities of lignin samples

The thermal properties of lignin samples obtained by homogenization assisted organosolv (COL) and non-assisted (REL) process was studied using thermogravimetric analysis (TGA) and thermographs are shown in Figure 5.12. Below 100 ºC, moisture evaporation from both lignin samples occurred resulting in an approximate 5–8% weight loss. At approximately 10% weight loss, the degradation temperature of the COL lignin was at 161.5 ºC and 189 ºC for the REL. The lower initial degradation temperature for COL lignin relates to its slightly reduced weighted-average molecular weight (M_w) as discussed in the previous section (Table 5.8), therefore showing a decrease in thermal stability. The non-

assisted (REL) lignin was the most stable and showed a maximum degradation temperature of 302 ºC with a char content of 42.60% while the homogenization assisted (COL) lignin showed a maximum degradation temperature of 298 ºC and with 41.32% char. This also reflects the effect of the homogenization aiding in effective depolymerization of lignin into lower molecular weight than the non-assisted process. In addition, the existence of highly condensed aromatic structures is associated with the char formation, thereby accounting for the observed 41.32 and 42.60% residual weight at 800 ºC.

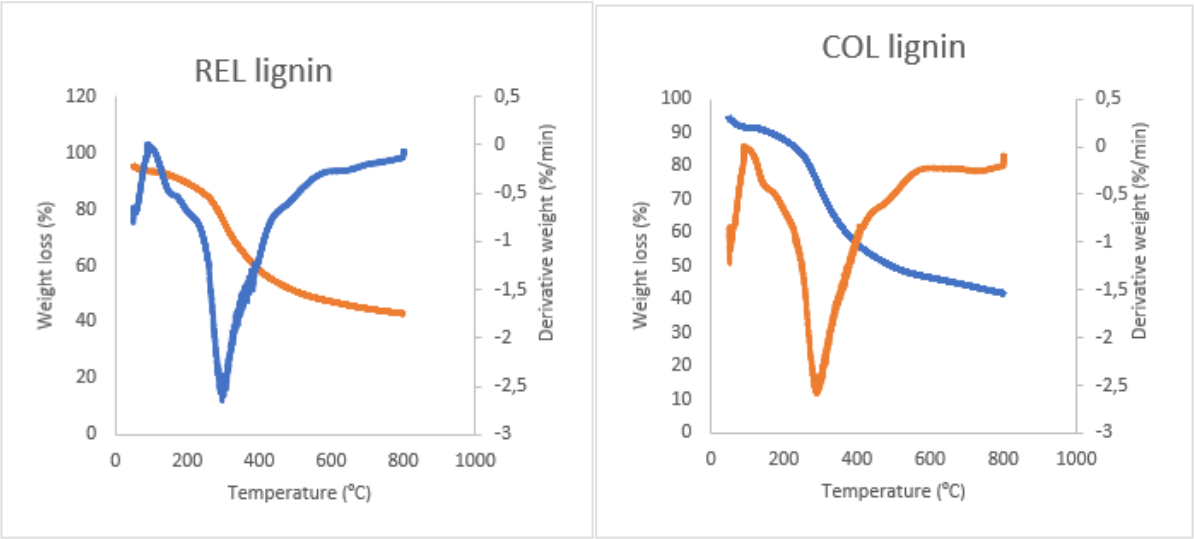

Figure 5.12: Thermogravimetric (TG) and derivative thermogravimetric (DTG) curves of optimum high shear homogenization-assisted organosolv lignin (COL) and non-assisted organosolv lignin (REL).

5.18.8. Scanning electron microscopy analysis for the morphology of solid residue

The structural changes of the residue under the optimal HSHO process conditions were studied by SEM and compared with the non-assisted (Figure 5.13). The surface of the residue for the non-assisted process showed intact fiber bundles with large particle widths (several micrometers) and the appearance of a few separated cellulose microfibrils due to the removal of lignin and some carbohydrates. The surface of the HSHO residue appeared separated and peeled off with the possibility of forming cellulose nanofibers (fiber width ranges from <1-10 µm). The HSHO resulted in disruption of the cellulose fibers, increasing accessibility of ions to the biomass for lignin removal [92] even at a lower temperature (148.4 ºC) when compared to that of the non-assisted process.

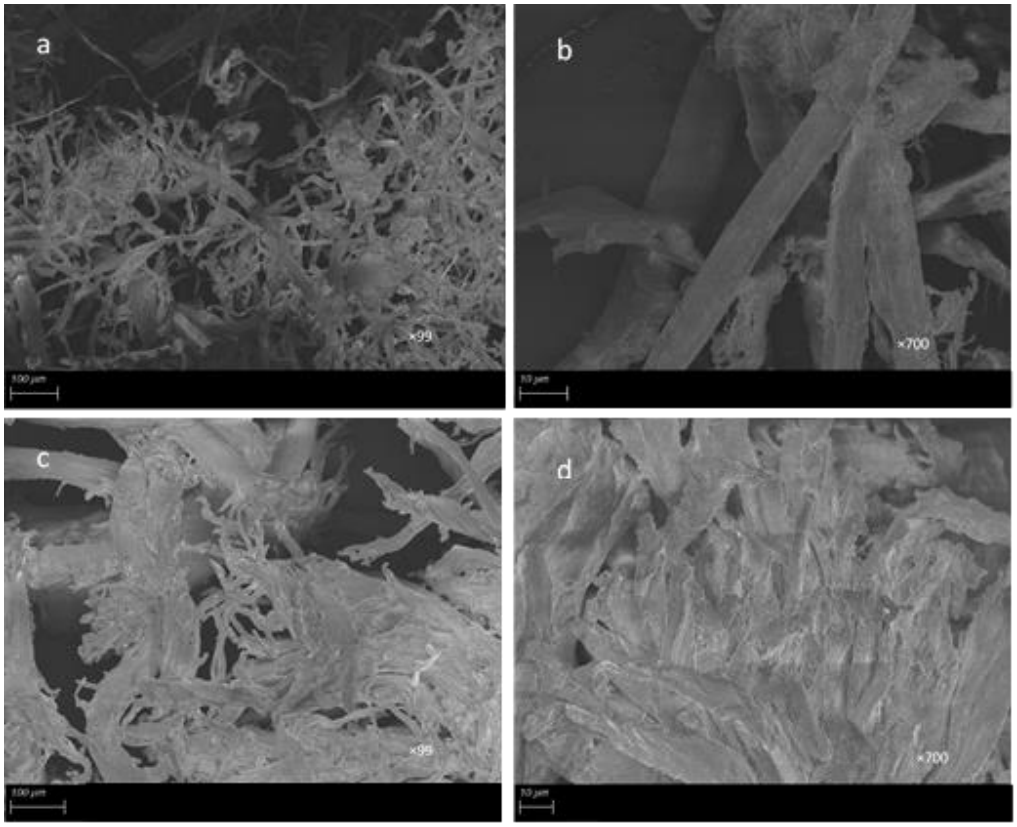

Figure 5.13: Scanning electron microscopy (SEM) images of residues obtained at different magnifications after high-shear homogenization-organosolv process under optimal conditions (a and b) and non-assisted ethanol organosolv (c and d).

5.19. Conclusions

The high shear homogenization assisted-organosolv (HSHO) process developed efficiently pretreat/fractionates alkaline treated mango seed husk into high purity lignin and cellulose-rich fibers in a biorefinery at lower temperatures when compared to the conventional organosolv process. The reaction temperature was the only variable that exhibited a significant effect on all the responses. At the optimal HSHO process conditions, narrow range lignin fragments of purity >90%, with a molecular weight of 3247 g/mol and a maximum degradation temperature of 298 ºC was achieved. The solid pulp showed individual separated fibers with >75% cellulose, <10% residual lignin, and <11% hemicelluloses with a tendency of forming cellulose nanofibers. The high purity and molecular weight with the high thermal stability of the HSHO lignin make it suitable for a wide range of industrial applications including resins and carbon fibers.

6. EFFECT OF THE MULTI-STEP BIOREFINERY PROCESS ON THE YIELD AND PROPERTIES OF CELLULOSE NANOCRYSTALS PRODUCED VIA RECOVERABLE ORGANIC ACID TREATMENTS

Papers contributing to this chapter

1. Optimizing a non-catalyzed formic acid hydrolysis treatment for producing thermally stable cellulose nanocrystals from cellulose-rich pulp obtained via a multi-step biorefinery process
2. Simultaneous preparation and acetylation of cellulose nanocrystals from a cellulose-rich pulp obtained via a multi-step biorefinery route using a non-catalyzed acetic acid-based treatment

Chapter summary

Objective 3, which entails the production of cellulose nanocrystals from the cellulose-rich pulp obtained from a multi-step process that consists of sequential AP and HSHO is highlighted in this chapter (Chapter 6). The main purpose was to investigate the effect of the multi-step biorefinery route on the production and quality of cellulose and its conversion into cellulose nanocrystals using non-catalyzed recoverable organic acids. The effect of each pretreatment step of the multi-step biorefinery process on the quality of cellulose and its suitability to be converted into cellulose nanocrystals through non-catalyzed organic acid-based treatments was investigated. Two organic acids (formic and acetic acids) treatments were tested as alternatives processes to the conventional sulphuric acid-based treatment to produce cellulose nanocrystals. The multi-step biorefinery scheme affected the composition, crystallinity index, and morphology of cellulose in addition to the yield and quality (morphology, crystallinity, thermal stability, hydrophobicity) of the cellulose nanocrystals produced via non-catalyzed organic acid treatments. The first stage of the multi-step process involving alkaline pretreatment improved the cellulose content, crystallinity, and surface area through the removal of hemicellulose. The subsequent stage (homogenization-assisted organosolv process) further removed lignin and improve the cellulose purity, crystallinity, thermal properties, and surface area. The formic acid-based process was performed varying acid-to-pulp ratio and reaction time and the process was optimized for high yield cellulose nanocrystals with high crystallinity and formate content for potential application as fillers in biocomposite. The optimized condition (30: mL/g and 8 h) resulted in 64% nanocellulose yield with, Crl, formate content and average particle of 66.40%, 0.92 mmol/g, and 24.13 nm respectively. For the acetic acid-

based treatment, the effect of acid-to-pulp ratio and reaction on the yield, average particle size, degree of substitution (DS), zeta potential, and polydispersity were investigated. The best condition (1:40 solid-to-acid ratio, and 10 h) resulted in a yield of 17.68% with average particle size, DS, zeta potential, and PDI of 45 nm, 1.833, -19.70 mV, and 0.468 respectively. The yield for the acetic acid-based treatment was lower than both the formic and sulphuric acid-based treatments. Application of homogenization treatment post acetic acid treatment improved CNC yield by >70% but the crystallinity was compromised (61.9 vs 46.7%). The multi-step biorefinery route has proven effective in recovering multiproduct including a cellulose-rich pulp with purity, crystallinity, and morphology suitable to produce cellulose nanocrystals via non-catalyzed recoverable organic acids. Non-catalyzed organic treatment of cellulose-rich pulp from the multi-step process has proven to promote nanocellulose formylation/acetylation and improve thermal stability juxtaposed to the sulphuric acid-based treatment.

Declaration by the candidate:

With regard to Chapter 6, pg. 174–220 the nature and scope of my contribution were as follows:

Nature of contribution	**Extent of contribution**
Planning and execution of experiments, data analysis and interpretation, and writing of the chapter	80

The following co-author (s) have contributed to Chapter 6, pg. 174–220:

Name	**E-mail address**	**Nature of contribution**	**Extent of contribution**
Chimphango, A.	achimpha@sun.ac.za	General discussion and chapter review	15
Görgens J. F.	jgorgens@sun.ac.za	General discussions and chapter review	5

6.1. Optimizing non-catalyzed formic acid hydrolysis of unbleached pretreated mango seed husk pulp to generate cellulose nanoparticles with improved morphology and thermal stability

Manuscript

6.2. Abstract

Biomass pretreatments and nanocellulose treatment process conditions influence the properties of nanocellulose and its field of application. A non-catalyzed formic acid-based treatment (NFAH) with inherent formic acid recycling, was assessed as an alternative to conventional sulphuric acid-based treatment (SA) with a bleaching step, for producing cellulose nanoparticles (CNP) from mango residues. The NFAH of unbleached pretreated mango seed husk pulp (UMP) obtained from a multi-stage biorefinery process consisting of sequential alkaline pretreatment and high shear homogenization-assisted organosolv for hemicellulose and lignin recoveries, was optimized via response surface methodology based on the acid-to-pulp ratio (20:1–40:1 mL/g), and time (6–10 h) variations for maximizing CNP yield, crystallinity (Crl), and CNP formate content while minimizing particle size. The optimum formic acid-to-pulp ratio (30:1 mL/g) and time (8 h) resulted in 64% yield CNP (FCNP) with crystallinity, formate content, particle size, and polydispersity index of 66.40%, 0.92 mmol/g, 24.13 nm, and 0.488, respectively. The FCNP yield was 40% higher and more thermal stable (Tmax=361 ºC vs 309 ºC) than sulphuric acid-based CNP (SCNP). Furthermore, the FCNP were spherical vs. the rod-like SCNP, thus, enabling highly sensitive applications such as in biomedicine. From a technical point of view, the NFAH has shown the potential to be a suitable alternative to SAH for valorizing mango seed husks in a biorefinery. These results showed that the applied pretreatments have a significant influence on CNP formation and properties using organic acids and suggest how biorefining pathways for agro-industrial waste biomass could customize such CNP properties such as morphology and modification. Economic and environmental assessments are required to ascertain its sustainability.

6.3. Introduction

The unique properties of cellulose nanoparticles (CNP) such as high specific surface area, low density (1.57 g/cm^3), and high tensile strength have made it a material of significant interest for advanced and green applications in the fields of nanocomposites, membrane separations, aerogels, drug delivery, and biomedicine [359], [419], [485]. Due to competing uses for wood, the primary cellulose source for CNP production, lignocellulosic residues like wheat straw and mango seed husk have been explored due to their high cellulose and low lignin contents [20], [97]. Conventionally, CNPs production using lignocellulosic biomass involves two major stages: (i) pretreatment/purification stage to remove the cementing components of hemicellulose, lignin, and extractives to obtain a cellulose-rich material, (ii) controlled hydrolysis of the cellulose-rich material using enzymes, acids, among others [144], [145].

The cellulose-rich materials are widely obtained from the pulp and paper industry through combined Kraft pulping and bleaching of the wood [24], [115], [359], [486]. However, the Kraft process, targeted at the removal of mostly the lignin from the feedstock, is expensive and results in considerable degradation of hemicellulose and sometimes the cellulose [177], [208], [237]. The black liquor (i.e. degraded lignin and hemicellulose) is used as boiler fuel due to difficulty in product separation [237]. Given the potential advanced uses for hemicellulose (e.g. biocomposite film, hydrogels, etc.) [42], [487], and its lower heating value (13.6 MJ/kg) vs. lignin (≈27 MJ/kg) [177], boiler fuel is an inefficient use of the hemicellulose [177], [311]. Also, the bleaching agents are costly and environmentally hazardous due to their toxic nature [488]. Similarly, although lignin has valuable industrial uses (e.g. resin, carbon fibers), it is lost through conversion to water-soluble benzoic, oxalic, and vanillic acids during bleaching [489]. Thus, the referred pretreatment processes target a single cellulose product for CNP at the expense of hemicellulose and lignin, impacting sustainable and effective feedstock uses [139], [489].

The environmental concerns and inefficient feedstock usage, therefore, calls for the development of effective processes for obtaining the cellulose for CNP production. In this regard, mild alkaline pretreatment (AP) could be applied to recover the hemicellulose polymers (for composite film development), whereas homogenization-assisted organosolv pretreatment (HSHO) of the alkaline treated solids could result in high purity lignin (for resin/carbon fiber production) and a fibrillated cellulose-rich material (cellulose content= 77%, lignin= <10% and <12% hemicellulose) for the CNP production, thus a multi-step sequential treatment process for potential multi-product recoveries including the cellulose for cellulose nanoparticles. The AP employs reagents such as NaOH to hydrolyze the ester and ether linkages between lignin

and hemicellulose, leaving the glycosidic linkages in hemicellulose polymers unaltered for recovery as shown in previous studies [34]. Subsequent HSHO on the alkaline treated solids can co-produce high purity lignin and cellulose-rich fibers (for CNP production) [14], [59]. Greater economic uses of the feedstock, could, therefore, be anticipated when AP combined with the HSHO is applied in a multi-step biorefinery scheme for multi-products including cellulose for the CNP vs. cellulose for CNP only via the alternate Kraft pulping/bleaching processes.

The next step in the CNP production is controlled treatment of the cellulose-rich pulp using mainly acids (e.g. sulphuric, hydrochloric) [25], [490]. Concentrated sulphuric acid (56–65%) is commonly used due to less severe condition requirements (45 °C for up to 60 min), resultant high crystalline rod-like, whisker-like, and spherical CNPs with sulfate groups which stabilizes the dispersibility of CNPs in aqueous suspension [40], [152], [170]. Spherical CNPs have a large surface area with uniform size mainly desired in applications like biomedicine and drug delivery [151], [174]. The major challenges associated with sulphuric acid include low CNP thermal stability (due to the sulfates groups lowering CNP activation energy) [167], expensive corrosion-resistant equipment, and toxic effluent treatments, which collectively increase the CNP production costs [40], [225], [491]. Concerning the referred setbacks of the inorganic acid-based hydrolysis, techniques involving oxidizing agents [491], enzymatic hydrolysis [163], [170], sonochemical assisted hydrolysis [492], and organic acids [25], [51] are beneficial. Nevertheless, shortcomings of long reaction time (>up to 7 days) and low yields (15%) have been reported for enzymatic and sonochemical hydrolysis [170], [492]. Organic acids such as formic and acetic acids have been used to prepare CNPs with high thermal stability (355–360 ºC). A universal route that produces and functionalizes CNPs through combined formic and hydrochloric acids based hydrolysis has been reported [166]. The CNP had a width of 56 nm with a maximum degradation temperature of 368.9 ºC, which makes it suitable for application as reinforcement agents in thermo-processed nanocomposites. Similarly, Yan et al. [151] reported a one-step process of preparing functionalised CNP from microcrystalline cellulose (MCC) using mixed hydrochloric and formic acids. The CNPs with formate groups were spherical with size distribution ranging 19–29 nm and maximum degradation temperature of 365.4 ºC.

The use of organic acids is preferable to inorganic acids because of their low toxicity, less corrosiveness, and ease of recovery through simple distillation [51], [352], as well as producing CNP with high (355–360 ºC) thermal stabilities [97], [352]. Furthermore, the functional groups on the organic acid can be introduced unto the CNP to make it compatible

with different matrixes, especially for biocomposite formulations. That is, simultaneous formation and functionalization (formylation) of CNPs can be achieved when organic acids such as acetic acid and formic acid are used in CNP production [25], [151]. Nevertheless, the weaker acidity makes organic acids less effective for hydrolyzing the strong hydrogen bonds existing in the high crystalline bleached cellulose-rich fibers [51]. Hence, mineral acids or metal catalysts are incorporated to improve the hydrolytic effect of the organic acids [51], [97], [151]. Conversely, in a multi-product biorefinery scenario focused on hemicellulose, lignin, and CNP production from a single feedstock as aforementioned, the preceding alkaline and HSHO pretreatments (to recover hemicellulose and high purity lignin) yield fibrillated cellulose-rich solids with improved fiber accessibility [205], thus, could be amenable to organic acid (formic acid) hydrolysis to produce the CNP without the need for incorporating the mineral acids/catalysts. However, the feasibility of the postulated multi-step AP and HSHO pretreated solids being suitable for the organic acid treatment without catalysts addition and its effectiveness on CNP properties vs the conventional alkaline/bleaching CNP's need to be investigated.

Therefore, the present study investigates the feasibility of the postulated CNP production using formic acid on the AP plus HSHO treated solids for mango seed husk (MSH). Formic acid (FA) was chosen because of its ease of recoverability and re-usage as a result of its low boiling point (100.8 ºC) [40]. Optimization of the AP and HSHO pretreatment for hemicellulose and lignin recovery from the MSH as valuable co-products have been demonstrated in previous studies [14], [302]. Thus, the present study is focused on the optimization of the FA treatment of the recovered solids (UMP) from the multi-step sequential AP and HSHO pretreatment stages towards obtaining the CNPs. Specifically, the effect of the FA treatment conditions of acid-to-pulp ratio (20–40 mL/g) and reaction time (6–10 h) on the yield, average particle size, ζ-potential, polydispersity, formate content, and crystallinity index of the CNPs were investigated. Reaction conditions were based on literature reports [40], [51], [97], [151], [352] and preliminary studies. In addition, the FA treatment conditions were optimized to maximize the yield and properties of the CNPs. Sulphuric acid CNPs were produced using the conventional approach and compared with the proposed approach. The as-prepared CNPs were characterized by various analytical instruments (section 6.2.4).

6.4. Materials and Methods

6.4.1. Materials

The starting material (UMP) was obtained after dried and alkaline treated (1.92 M NaOH, 86.0 °C and 3.84 h) mango seed husk [302] was subjected to high shear homogenization-assisted organosolv pretreatment (60% ethanol, 15 min homogenization, and 148.41°C) [14]. The UMP was mainly composed of approximately 77% cellulose, 10% hemicellulose, and <10% lignin estimated using the Van Soest method of fiber analysis [493]. Formic acid (88 wt%) and sulphuric acid (64 wt%) were purchased from Sigma Aldrich, South Africa. All chemicals used were of analytical grade.

6.4.2. Preparation of cellulose nanoparticles from unbleached cellulose-rich material from mango seed husk

A modified method of Du et al. [51] was used for cellulose nanocrystal preparation using formic acid treatment. Briefly, a 1 g sample was dispersed in 88 wt% formic acids in a 250 mL three-neck flask connected to a condenser, and the mixture was placed in an oil bath. Following this, the mixture was magnetically stirred at 500 rpm at 95 °C for a period as shown in the experimental design (Appendix C, Table C1). After the reaction was complete, the mixture was immediately cooled to room temperature under running water and centrifuged (Hermie Labortechnik GmbH, Z 366, Germany) at 8000 rpm for 5 min. The formic acid in the supernatant was recovered by distillation. Subsequently, the solids obtained after removal of supernatant were washed several times with distilled water with subsequent centrifugation at 5000 rpm for 5 min until the pH of the suspension reached pH 6. The obtained suspension containing the nanoparticles was dialyzed using a cellulose membrane dialysis tubing with a molecular weight cut-off of 14000 Da (Sigma-Aldrich, USA) for 3 days against distilled water, freeze-dried, and stored in zip lock bags for further analysis.

The sulphuric acid CNPs were produced using the typical alkaline, bleaching, and acid hydrolysis. This involved adding 10 g MSH to 200 mL of 4% w/v NaOH in a 500 mL three-neck flat bottom flask and the mixture heated to 65 ºC. Thereafter, 60 mL of 30% v/v hydrogen peroxide was added and refluxed for 60 min. Extra 60 mL 30% v/v H_2O_2 was added and the reaction was allowed to proceed for a further 90 min. The residue obtained after the reaction was washed until the supernatant reached pH 6 and dried at 40 °C overnight [48]. The composition of the bleached pulp was ≈86% cellulose, ≈2.2% lignin, and ≈10.6% hemicellulose. The bleached pulp was used for CNP preparation using sulphuric acid (64 wt%

for 60 min at 60 °C) at an acid-to-pulp ratio of 30:1. The yields of all CNPs were determined gravimetrically according to Equation 16.

$$Yield\ (\%) = \frac{mass\ of\ freeze-dried\ sample\ (g)}{mass\ of\ starting\ material\ (g)} \times 100\% \quad [16]$$

6.4.3. Experimental design and statistical analysis

The effect of acid-to-pulp ratio (X_1; 20–40 mL/g) and reaction time (X_2; 6–10 h) on the yield, ζ-potential, average particle size, polydispersity (PDI), formate content, and crystallinity of CNPs were investigated in a three-level two factor rotatable central composite design (CCD) experiment. Due to the weaker acidity and lower boiling point of formic acid (100.8 °C), a constant temperature of 95 °C was chosen to allow for efficient preparation of CNPs. A total of 10 runs for the two independent variables, including 4 factorial points, 4 axial points, and 2 center points were obtained. The CCD design in terms of coded variables corresponding to the reaction conditions is shown in Appendix C. The experimental data obtained were analyzed using STATISTICA 13.2 software to develop quadratic regression models. Response surface methodology (RSM) was used to optimize the acid-to-pulp ratio and reaction time that maximize the CNP yield and properties.

6.4.4. Characterization of starting material and cellulose nanocrystals

6.4.4.1. Particle size, ζ-potential, and polydispersity index (PDI)

The particle size, ζ-potential, and polydispersity (PDI) of the cellulose nanoparticles (CNPs) were determined by a Zetasizer Nano S90 instrument (Malvern Instruments Ltd., UK). The sample was prepared in distilled water to obtain a concentration of 0.01%wt and analysis was performed via dynamic light scattering method at 25 °C after an equilibrating time of 120 sec at a 90 ° scattering angle. A cumulant method was used by the instrument to calculate the intensity-weighted mean hydrodynamic diameter of triplicate samples and the particle sizes (length) determined using the intensity peaks that represent most of the particles. ζ-Potential was measured by sucking samples into a syringe and slowly injecting them into a folded capillary cell (DTS1060) with stoppers. The cell was inserted into the Zetasizer, which measured the ζ-potential at 25 °C at a scattering angle of 90° by a Laser Doppler Electrophoresis technique. The PDI was determined by a dynamic light scattering using a cumulant method by the instrument. Samples were equilibrated for 120 seconds before 100 scans were taken per sample for three sample measurements. Samples were prepared to form a

solid concentration of 0.01 wt% with three measurements for each sample. All measurements were taken relative to polystyrene latex.

6.4.4.2. Formate content determination

The formate contents of the FA CNPs were determined by the pH titration through oxime reaction [151]. Briefly, 1 to 10 mL of hydrochloric acid (0.01 M) was added to 25 mL of 0.25 M hydroxylamine hydrochloride solution, and the pH was recorded. A pH vs volume of HCl was then plotted. This was followed by the addition of 0.1 g of freeze-dried CNP to the above-mentioned solutions and stirred using a magnetic stirrer for 24 h at 25 ºC and the pH measured. The volume of HCl was then obtained from the plot of V_{HCl} vs pH without sample. The formate content was then calculated using Equation 17.

$$Formate\ content\ \left[\frac{mmol}{g}\right] = \quad [V_{HCl} \times 0.01]/0.1 \qquad [17]$$

Where V_{HCl} is the volume of HCl added to the sample.

6.4.4.3. Morphological analysis

The structure and morphology of samples were determined by scanning electron microscopy as detailed in section 6.2.5.5. Scanning transmission electron microscopy (STEM) analysis for morphology was performed to obtain images of the UMP, BP, and CNPs in a MERLIN, Zeiss Scanning Electron Microscopy (SEM) equipped with a STEM detector microscope operating at an acceleration voltage of up to 20 kV. CNPs were prepared by dropping 5 µm of 0.01%wt aqueous samples onto a copper grid. After holding for 3 min, excess water was removed, and samples were stained with 10 µL of uranyl acetate (UA-Zero^{TM} EM stain, Agar Scientific) and allowed to dry completely before analysis.

6.4.4.4. Crystallinity index, thermal stability, and structural features determination

The crystallinity index of dried and powdered UMP and cellulose nanoparticles were obtained within a 2θ Bragg angle of 5 to 40° at room temperature using a scan rate of 0.05° per min. A Bruker D2 Phasor diffractometer was used for the analysis, operating at a power of 30 kV with CuKα radiation (1.5406 Å) and 20 mA current. The Crystallinity Index (CrI) was calculated by the Segal method in Equation 18.

$$Cl = \frac{I_{200} - I_{am}}{I_{200}} \times 100\% \qquad [18]$$

Where I_{200} represents the maximum intensity of the crystal plane at 2θ =22.5°; and I_{am} represents 2θ ≈ 18° for the amorphous portion. The thermal stabilities and structural features

of the starting materials and CNPs were determined based on the procedure described in section 5.7.

6.5. Results and Discussions

6.5.1. Preparation and functionalization of cellulose nanoparticles from unbleached organosolv-treated mango seed husk using non-catalyzed formic acid hydrolysis

Table 6.1 shows the non-catalyzed formic acid treatment (NFAH) conditions, yield, and properties of the as-prepared FA cellulose nanoparticles (FCNPs) produced using the previously pretreated (alkaline and HSHO pretreatment) mango seed husk (UMP). The yield (based on the initial mass of dried pulp), average particle size, and ζ-potential ranged from 39.62–65.62%, 22.13–54.78 nm, and -5.70– -19.10 mV respectively.

Table 6.1: Yield and properties of formic acid prepared cellulose nanoparticles from unbleached organosolv-treated mango seed husk

Sample	Acid-to-pulp ratio mL/g	Reaction time [h]	Nanocellulose Yield [%]	Particle size [nm]	ζ-potential [mV]	PDI	CrI [%]	Formate content [mmol/g]
1	20:1	6	59.17	43.09	-5.70	0.887	68.15	0.87
2	20:1	10	51.61	29.05	-9.44	0.538	64.34	0.78
3	40:1	6	65.21	28.07	-11.73	0.519	68.43	0.63
4	40:1	10	39.62	24.78	-13.97	0.451	65.58	0.77
5	15.9:1	8	54.08	54.78	-9.81	0.912	66.74	0.42
6	44.1:1	8	49.96	25.72	-15.18	0.557	67.74	0.69
7	30:1	5.17	60.42	51.80	-9.76	0.905	68.02	0.84
8	30:1	10.83	58.46	22.13	-19.10	0.489	61.74	0.72
9	30:1	8	65.62	24.95	-13.89	0.470	67.86	0.92
10	30:1	8	64.76	25.01	-14.03	0.468	67.59	0.96

PDI= Polydispersity index, Crl= Crystallinity index

The polydispersity index (PDI), formate content and crystallinity (CrI) ranged from 0.451–0.905, 0.42 to 0.96 mmol/g and 61.74–68.43% respectively (Table 6.1). The highest

yield and formate content was achieved at a condition of 30:1 mL/g and 8 h (Table 6.1), while the lowest yield was obtained at 40:1 mL/g and 10 h; however, this condition presented a formate content of 0.77 mmol/g. In addition, the highest Crl (68.43%) was obtained at 40:1 mL/g and 6 h, while the lowest was at 10.83 h and 30:1 mL/g.

The FCNP yields (39.62–65.62%) falls within the reported range for inorganic acid catalysed FA produced CNPs (12.5–70%) [40], [51], [97], but higher than values for sulphuric acid (15–34.5%) [20], [97], [494], hydrochloric acid (18–21%) [355] and enzymes-based (12.3%) [170] produced CNPs using bleached pulp. The relatively high FCNP yields vs the inorganic acids' could be due to the weaker acidity of FA (pKa =3.77 vs pKa =-3.0) to extensively hydrolyze cellulose into simple sugars at the employed reaction conditions [51]. However, the comparable yields of FCNP in this study vs the catalyzed organic acid CNP values could be explained by the physicochemical properties of the starting materials used (bleached pulp vs UMP pulp) due to the different pretreatment approaches employed [14], [115]. The previous pretreatment impact on the starting material, i.e. the combined effect of the high shear homogenization and organosolv pretreatment of the alkaline treated MSH, caused the cellulose fiber bundles to defibrillate and peel off. This increased the accessible surface area of the fibrils to chemicals [471]. Consequently, the hydronium ions (H_3O^+) formed from the dissociation of formic acid (in the presence of water) penetrated effectively into the inner spaces of the fibrillated cellulose, hydrolysed the disordered amorphous portion, and released the CNPs [51].

The hydrolysis of the amorphous cellulose portion resulted in FCNPs with average particle sizes (Table 6.1) that fall within literature reports of length 50–421 nm, but with higher absolute ζ-potential values than reports (-1.7– -14.3 mV) for catalyzed organic acid CNPs [40], [51], [97], [166], [352]. Li et al. [40] obtained particle sizes larger than 2 µm with a corresponding ζ-potential value of -6.7 mV after 6 hr of FA treatment (without a catalyst) of bleached pulp. Du et al. [352] made similar observations when FA was used to prepare CNPs from bleached Kraft pulp whereby the FA alone was insufficient to hydrolyze the cellulose-rich microfibers into nanocellulose at the employed conditions (6 hr of treatment at 95 ºC). CNPs were produced after HCl/$FeCl_3$ catalyst was included in the reaction. Thus, the relatively lower average particle sizes obtained in the present study could be attributed to the easily accessible nature of the starting material used due to the synergist benefits between different pretreatment/fractionation steps, in a multi-step biorefinery process [115].

Degradation of amorphous components exposed more hydroxyl groups on the cellulose nanoparticles and increased the surface charge density, which was measured as the ζ-potential

[495]. At the same time, some of the exposed hydroxyl groups on the FCNP were partially esterified by the carboxyl groups of formic acid (Table 6.1). Generally, FA has been reported to swell cellulose fibers and adsorb unto the surface through hydrogen bonding [352], which complements the observed formate contents in this study (Table 6.1). The two opposing effects, i.e. hydrolysis of glycosidic linkages and esterification of hydroxyl groups, could lead to different formate contents on FCNPs as shown in Table 6.1. The formate contents of the FCNP are however within the reported values in the literature [151], [166]. Thus, the above observations confirm the hypothesis that NFAH could produce the nanocellulose from the UMP. The differences in the properties of the starting raw material, therefore, could account for the contrast findings in the literature [352], that FA must be combined with an inorganic acid/metal catalyst to produce CNPs. However, the properties of the nanocellulose could be impacted by the different pretreatment and nanocellulose treatment approaches. From Table 6.1, different FCNP yields with varied properties were observed for the different reaction conditions, consequently, the treatment conditions have to be optimized to obtain products for diverse applications such as reinforcement agents in nanocomposites.

6.5.2. Optimization of reaction time and acid-to-pulp ratio for cellulose nanocrystal preparation and building of regression models

Optimization of NFAH treatment conditions was performed using response surface methodology (RSM). Multiple regression analysis was applied to the data to reveal the relationships between the independent variables (acid-to-pulp ratio and time) and responses (yield, average particle sizes, ζ-potential, polydispersity index, crystallinity index, and formate content) as indicated by Equations 19 –24.

$$Yield\ [\%] = -83.34 + 5.90x_1 - 0.07x_1^2 + 17.80x_2 - 0.83x_2^2 - 0.23x_1x_2 \quad [19]$$

$$Average\ particle\ size\ [nm] = 227.96 - 5.31x_1 + 0.06x_1^2 - 24.28x_2 + 1.03x_2^2 + 0.13x_1x_2 \quad [20]$$

$$Zeta\ potential\ [mV] = -30.23 + 1.31x_1 - 0.02x_1^2 + 4.07x_2 - 0.144x_2^2 - 0.02x_1x_2 \quad [21]$$

$$PDI = 5.56 - 0.11x_1 + 0.001x_1^2 + 0.59x_2 + 0.02x_2^2 + 0.004x_1x_2 \quad [22]$$

$$CrI = 55.89 - 0.00x_1 - 0.00x_1^2 + 3.79x_2 - 0.32x_2^2 + 0.012x_1x_2 \quad [23]$$

$$Formate\ content = -0.78 + 0.08x_1 - 0.00x_1^2 + 0.13x_2 - 0.00x_2^2 - 0.00x_1x_2 \quad [24]$$

Where x_1 and x_2 are the coded values for acid-to-pulp ratio and reaction time, respectively. Analysis of variance (ANOVA) was carried out to find statistical significance and suitability of the models to predict the responses and determine how important the model variables (x_1

and x_2) and their interaction (x_1x_2) are on the responses. In addition, the coefficient of variation, R^2 values were determined to show how accurate the models could predict the data for the responses. Table 6.2 shows the results of the ANOVA. Concerning the FCNP yield, the quadratic term of acid-to-pulp ratio x_1^2, the linear term of time x_1 and the interaction term x_1x_2 were significant (p<0.05) (Figure 6.1a). The linear term of acid-to-pulp ratio and quadratic term of reaction time were non significant factors (p>0.05) at a 95% confidence level. An optimum acid-to-pulp ratio and reaction time of 30:1 mL/g and 8 h respectively were shown, beyond or below which the yield reduces (Figure 6.1b). With an increase in the contact time and hydrolyzing ions (acid-to-pulp ratio), the diffusion of H_3O^+ ions into the fiber matrix was improved due to a reduction in mass transfer limitations or longer reaction time, which enhanced the hydrolysis of the easily accessible amorphous components from the cellulose-rich fibers [419], [496].

Table 6.2: Analysis of variance for formic acid nanocellulose yield, average particle size, ζ-potential, polydispersity index, crystallinity, and formate content regression models

Response variable	Statistically significant factors	p-value	R^2
Yield (wt%)	x_1^2	0.026	0.80
	x_2	0.030	
	x_1x_2	0.042	
	LOF	0.07	
Average particle size (nm)	x_1	0.001	0.82
	x_1^2	0.002	
	x_2	0.001	
	x_2^2	0.003	
	x_1x_2	0.005	
	LOF	0.004	
Z-potential (mV)	x_1	0.010	0.78
	x_1^2	0.019	
	x_2	0.009	
	LOF	0.023	
Polydispersity index	x_1	0.003	0.91
	x_1^2	0.004	
	x_2	0.003	
	x_2^2	0.005	
	x_1x_2	0.006	
	LOF	0.010	
Crystallinity index (%)	x_2	0.022	0.97
	x_2^2	0.043	
	LOF	0.210	
Formate content (mmol/g)	x_1^2	0.049	0.66
	LOF	0.131	

x_1 =acid-to-pulp ratio, x_2 =reaction time, x_1x_2=interaction of acid-to-pulp ratio and time, LOF=lack of fit

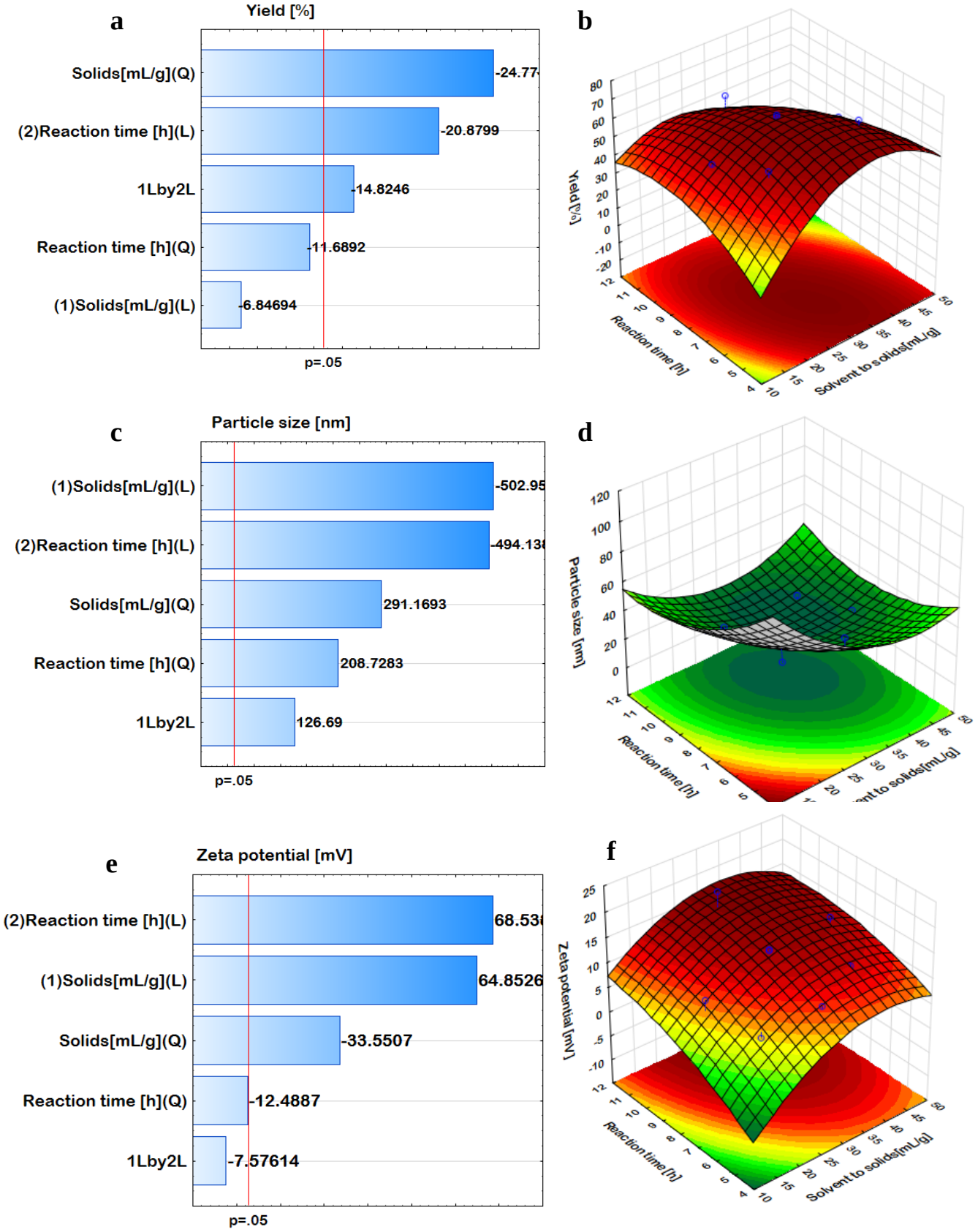

Figure 6.1: Pareto charts and Response surface showing the effect of acid-to-pulp ratio and reaction time on (a, b) cellulose nanoparticle yield, (c, d) average particle size, and (e, f) ζ-potential

Beyond the optimal level, the reduction in yield upon a further increment of acid-to-pulp ratio and reaction time (i.e. high severity conditions) could be attributed to acid hydrolysis of the CNP product into simple sugars [419], which is in agreement with similar findings in related studies [495]. Therefore, the reaction conditions must be restricted to ≤8 h and ≤30:1 mL/g when using the proposed CNP production approach.

For the average particle size of the FCNP, both the acid-to-pulp ratio and reaction time showed negative effects (Figure 6.1c). Therefore, the average particle sizes became smaller and reached an optimum when the acid-to-pulp ratio was increased further (Figure 6.1d) and the average particle size became larger with further increment in the acid-to-pulp ratio (Figure 6.1d). As an example, an increment in acid-pulp ratio from 15.9:1 mL/g to 30:1 mL/g at constant reaction time resulted in average particle size reduction from 54.78 nm to 24.95 nm, which increased to 25.72 nm when the acid-to-pulp ratio was increased to 44.1:1 mL/g. The increased particle size with higher acid-to-pulp ratios could be due to mass transfer limitations as the viscosity of the reaction medium becomes high due to the release of the CNPs into the solvent, thus limiting the effective penetration of ions for further hydrolysis of glycosidic linkages in cellulose fibers. The average particle size decreased progressively when the reaction time was increased from 5.17 h to 10.83 h (Table 6.1), attributable to the improvements in the hydrolysis of the amorphous components of the pulp with reaction time. The elliptical RSM plot (Figure 6.1d) confirms the significance of the interaction between the acid-to-pulp ratio and the reaction time, as well as a reduction in average FCNP particle size with increment in acid-to-pulp ratio or reaction time, which agrees with similar trends from previous reports [419].

The hydrolysis of the glycosidic linkages in cellulose fibers to obtain CNPs exposes more hydroxyl groups which contribute to the ζ-potential, where CNPs with ζ-potential value > 20 mV are considered suitable for forming stable aqueous suspensions [167]. Table 6.1 shows that none of the resultant FCNP met this criterion, and therefore could form aggregates in aqueous suspensions. This could be attributed to the formate groups introduced onto the CNP by FA, which reduced the hydroxyl content and thus the charge density on the CNPs [151]. From the Pareto chart (Figure 6.1e), the linear term of reaction time was the major contributor (p<0.05) to the absolute ζ-potential, followed by the linear and quadratic terms of the acid-to-pulp ratio. The interaction of reaction time and acid-to-pulp ratio and the quadratic term of reaction time was not significant (p>0.05) at a 95% confidence level.

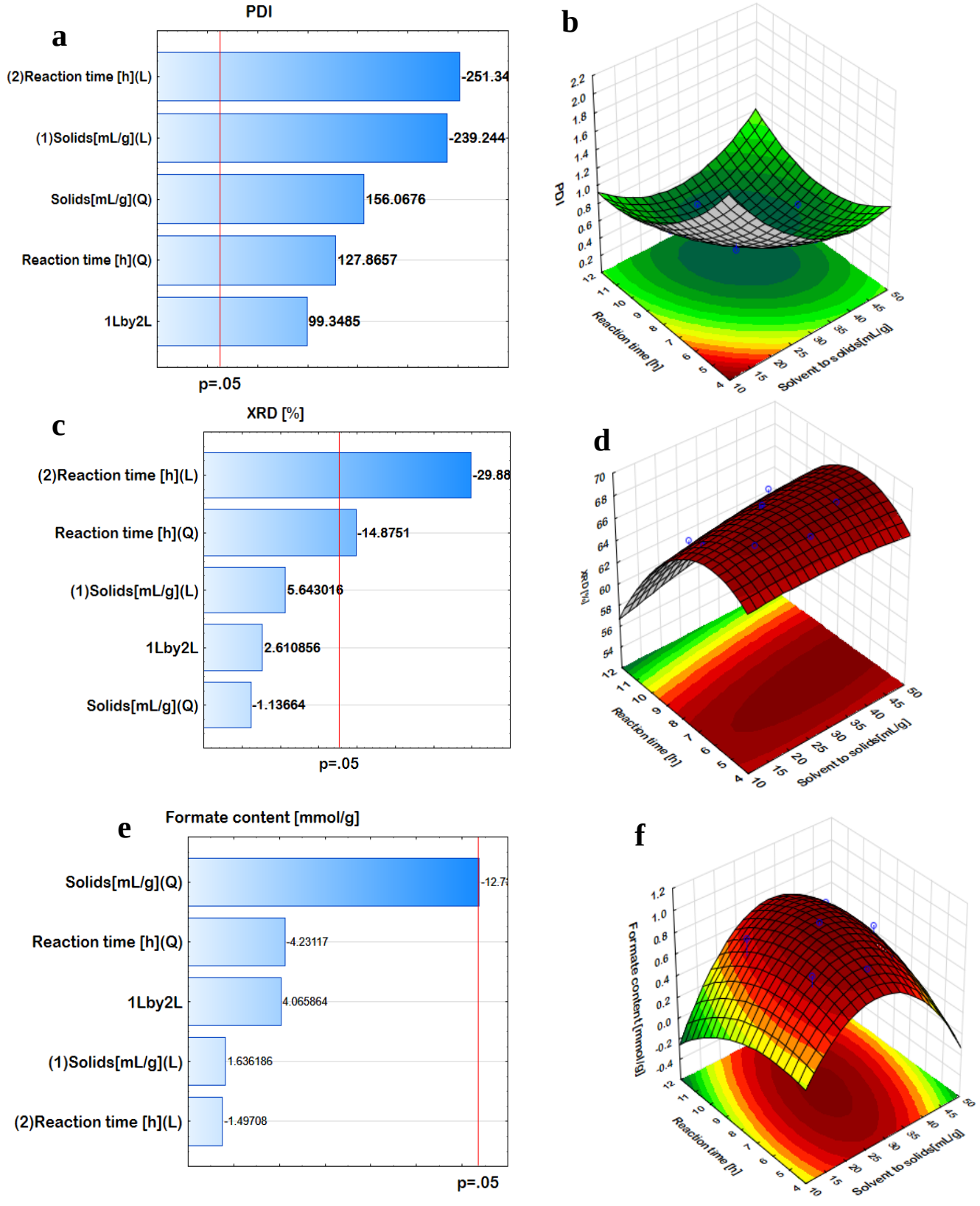

Figure 6.2: Pareto charts and Response surface showing the effect of acid-to-pulp ratio and treatment time on the (a, b) polydispersity index, (c, d) crystallinity, and (e, f) formate content of formic acid nanocellulose

As seen from Figure 6.1f, an increment in reaction time caused an increase in the absolute ζ-potential from approximately 9.7 mV to 19 mV at constant acid-to-pulp ratio due to exposure of hydroxyl groups resulting from hydrolysis of glycosidic linkage in cellulose fibers by the H_3O^+ ions. The absolute ζ-potential also increased when the acid-to-pulp ratio was increased up to 44.1:1 mL/g (Table 6.1). The highest absolute ζ-potential was achieved at 30:1 mL/g and 10.83 h. The effects of reaction time and acid-to-pulp ratio on the FCNP PDI are depicted in Figure 6.2 a–b. The most significant factors (p<0.05) that influenced the PDI of FCNP were the linear term of reaction time (Figure 6.2 a), followed by the linear and quadratic terms of acid-to-pulp ratio, the quadratic term of time, and finally the interaction term of acid-to-pulp ratio and reaction time (Figure 6.2 a). An increase in either acid-to-pulp ratio or reaction time decreased the PDI of the FCNP (Figure 6.2 b). However, an acid-to-pulp ratio of 30:1 mL/g combined with the highest reaction time (10.83h) increased the PDI of the FCNP slightly (Figure 6.2 b).

The crystallinity index (Crl) of nanocellulose is one of the major characteristics that impact mechanical properties and it is dependent on the type of raw material, pretreatment processes, and CNP treatment conditions [419]. In general, from Table 6.1, Crl values of over 60% were achieved for all the FCNPs. These values fall within the reported range of 63.8 to 75% for various inorganic acid/salt-catalyzed FA CNPs [40], [97], [352]. The effect of the acid-to-pulp ratio and reaction time on the Crl is depicted in Figures 6.2 c–d. The reaction time (both linear and quadratic terms) was the only significant factor that influenced the CrI of FCNP (Figure 6.2 c). The acid-to-pulp ratio exhibited a positive influence however its effect was not significant (p>0.05) at a 95% confidence level. From Figure 6.2 d, lower CrI values were achieved at extreme reaction times (>6 h) at a constant acid-to-pulp ratio (30:1 mL/g). Therefore, the part of the crystalline cellulose portion was degraded after the amorphous components were completely hydrolyzed under a long reaction time [166]. For higher Crl of FCNP using the proposed approach, the reaction time should be limited to <8 h. This could save costs and maintain the crystalline nature of cellulose nanoparticles [419].

The effects of acid-to-pulp ratio and reaction time on the formate content of FCNP are shown in Figure 6.2 e–f. Figure 6.2 e demonstrates that the formate contents of FCNP were significantly (p<0.05) affected by only the quadratic effect of the acid-to-pulp ratio. The linear term of acid-to-pulp ratio, linear and quadratic terms of reaction time, and the interaction term of reaction time and acid-to-pulp ratio were not significant at a confidence level of 95% (Figure 6.2 e). From Figure 6.2 f, keeping the acid-to-pulp ratio constant and varying the reaction time from low (5.17 h) to intermediate (8 h) levels increased the formate content. The

formate content, however, decreased at a reaction time of 10.83 h. Similarly, an increment in acid-to-pulp ratio from 15.9:1 to 30:1 mL/g at constant reaction time (8 h) caused an increase in the formate content, nevertheless, a very high acid-to-pulp ratio (44.1:1 mL/g) resulted in lower formate content (Figure 6.2 e). The reduction in formate content at longer contact times and high acid-to-pulp ratios could have resulted from the hydrolysis of the esterified portion of the CNPs since the acid hydrolysis of cellulose to produce CNP occur at the amorphous cellulose region, where the esterification of the hydroxyl groups simultaneously takes place [166]. These two contrasting effects could result in various formate contents of FCNP based on the reaction conditions as indicated earlier [25] with the optimum observed at 8 h in this study (Table 6.1).

The ability of the regression models to accurately predict the responses are determined by the coefficient of determination (R^2 values) that ranges between 0 to 1, where a value close to 1 depicts a good potential for the response prediction. From Table 6.2, the R^2 values for the models for the FCNP's responses of yield, average particle sizes, absolute ζ-potential, PDI, Crl, and formate contents ranged between ≈0.7 and 0.97, suggesting accurate response prediction potential of the respective regression models. Further, lack-of-fit *p*-values > 0.05 indicate that the model is accurate and could predict the response. For the respective regression models for the FCNP's responses of yield, average particle sizes, absolute ζ-potential, PDI, Crl, and formate contents, the lack-of-fit *p*-values of 0.07, 0.004, 0.023, 0.01, 0.21, and 0.13 (Table 6.2) depicts all the models could accurately predict the responses except for the particle size, absolute ζ-potential, and the PDI. Thus, the latter responses were not considered in the further optimization experiment except for the particle size. For the particle size, the lack of fit *p*-value (0.004) was significant ($p<0.05$) at a 95% confidence level, implying the model cannot accurately predict the average particle sizes of the FCNPs. Similar trends have been reported in the literature [497]. Bondeson et al. [497] reported a lack of fit of the developed model to predict the average particle sizes of CNPs prepared from microcrystalline cellulose (MCC) due to wide particle size variations. Similarly, Bester [498] reported a lack of fit *p*-value for the average particle size of CNPs prepared from virgin pulp paper sludge. Thus, variations in particle sizes often account for difficulties in fitting models to such data. Hence, considering the average particle sizes were in the nanometre range (less than 100 nm) with a high R^2 value for the model, it was considered in the further optimization experiments [497].

6.5.3. Verification of optimal formic acid treatment conditions for cellulose nanocrystal preparation

Optimization of the NFAH was carried out to maximize the yield, Crl, and formate content and minimize the average particle sizes of FCNP. The optimum conditions were found to be 30:1 mL/g acid-to-pulp ratio and 8 h. The optimized acid-to-pulp ratio compares favorably with literature values for formic acid treatment [51], [97] whereas the 8 h falls within the 6–12 h reported in the literature for catalyzed formic acid treatment [51], [352]. The predicted values for the responses under these optimum conditions were 65.19%, 25.0 nm, 67.72%, and 0.94 mmol/g for yield, average particle size, CrI, and formate content, respectively (Table 6.3). Experimental validation of the optimal conditions revealed the suitability of the models in predicting the responses as the percentage of deviation between the predicted and observed were 1.84, 3.48, 1.95%, and 2.13% for yield, average particle size, Crl, and formate content respectively.

Table 6.3: Predicted versus observed values of formic acid nanocellulose at optimum conditions and commercial cellulose nanocrystals

Component	Yield [%]	[b]Average particle size [nm]	CrI [%]	Formate content
Predicted	65.19	25.00	67.72	0.94
FCNP	63.99	24.13	66.40	0.92
% Deviation	1.84	3.48	1.95	2.13
SCNP	28.34	175.50	71.02	-

[a]FCNP: Spherical formic acid cellulose nanocrystals, SCNP= sulphuric acid cellulose nanoparticles. [b]Represents particle size (length) obtained from several scanning electron microscopy images using ImageJ software, Crl= crystallinity index

From Table 6.3, more than a 55% increment in yield was achieved for the FCNP when compared to the yield of sulphuric acid CNP (SCNP) (control). The average particle size (length) of the FCNP was more than 80% shorter than the SCNP (Table 6.3), attributable to the preceding multi-step pretreatment/fractionation processes that improved the accessible surface area of the cellulose-rich fibers for effective amorphous cellulose hydrolysis by the FA [20]. The Crl of FCNP was however lower than that of SCNP which could be due to the lower Crl of starting material resulting from the destruction of a portion of the crystalline domain during

the HSHO process, affecting the final Crl of the FCNPs. The optimal FCNP yield is within the range of 41.94% and 79.55% reported in the literature for catalyzed formic acid CNPs [40], [51]. Overall, UMP was easier to hydrolyze using a non-catalyzed FA process to produce functionalized CNPs of high Crl and formate contents with lower average particle sizes compared to the reported values in the literature for catalyzed FA CNPs and sulphuric acid-based CNPs. Thus, FA alone could be used for producing functionalized thermally stable CNPs from a multi-step AP and HSHO treated biomass.

6.5.4. Characterization of pulp and cellulose nanoparticles (at optimum conditions)

6.5.4.1. Morphology and structural changes of unbleached organosolv treated mango seed husk and cellulose nanocrystals

The structural changes and morphologies of the UMP, bleached pulp (BP), FCNP, and SCNP are shown in Figure 6.3. The UMP showed separated and disordered individual cellulose fibers with lengths ranging several microns (Figure 6.3) and diameters ranging ≈1–10 µm due to the removal of non-cellulosic materials particularly hemicellulose and lignin. The organosolv pretreatment, which involved mechanical shear and cavitation (due to high shear homogenization), led to cellulose-rich fibers (Chapter 5, section 5.18.8), thus yielding ruptured fibers that peeled off [92], similar to findings in the literature [94], [491]. Barbash et al. [491] reported a considerable reduction in reed stalks fiber width from ≈100–800 µm to 10–20 µm after two-stage alkaline and organosolv (peracetic acid) pretreatments. The disruption of the cellulose fibers makes it easier for chemicals to access the pulp and hydrolyze the amorphous cellulose to produce CNPs [495]. The morphology changed from microfibrils into nanoparticles with spherical shapes and average particle sizes of approximately 24 nm after the NFAH (Figures 6.3 a and c). This morphology and size differ from previous reports for catalyzed FA CNPs which could be due to the different pretreatment methods used as discussed previously [40], [51].

The HSHO destroys the hydrogen bonding in portions of the crystalline cellulose and converts them into less ordered amorphous fibers [14], [92]. This causes a reduction in the diameter of the crystalline celluloses. Subsequent hydrolysis of the amorphous cellulose with formic acid could result in spherical CNP based on the conditions of operation. On the other hand, the BP exhibited fibrils with diameters in the range of 10–40 µm, which reduced to rod-shaped CNPs of diameter, 175 nm after sulphuric acid treatment (Figures 6.3b and 6.3d). This result confirms the impact of the multi-step pretreatment and hydrolysis route on the properties

of the CNP products [144], [145]. To verify the results of the SEM, a STEM analysis was performed (shown in Figures 6.3e and 6.3f). The STEM image (Figure 6.3e) confirmed the spherical shapes of the FCNP with an average particle size of approximately 25 nm while the SCNP showed rod-like shapes with an average length of approximately 172 nm. It can be concluded that the proposed route in this study could lead to CNPs with spherical morphologies for diverse applications such as in biomedicine, biocomposite, and cosmetics.

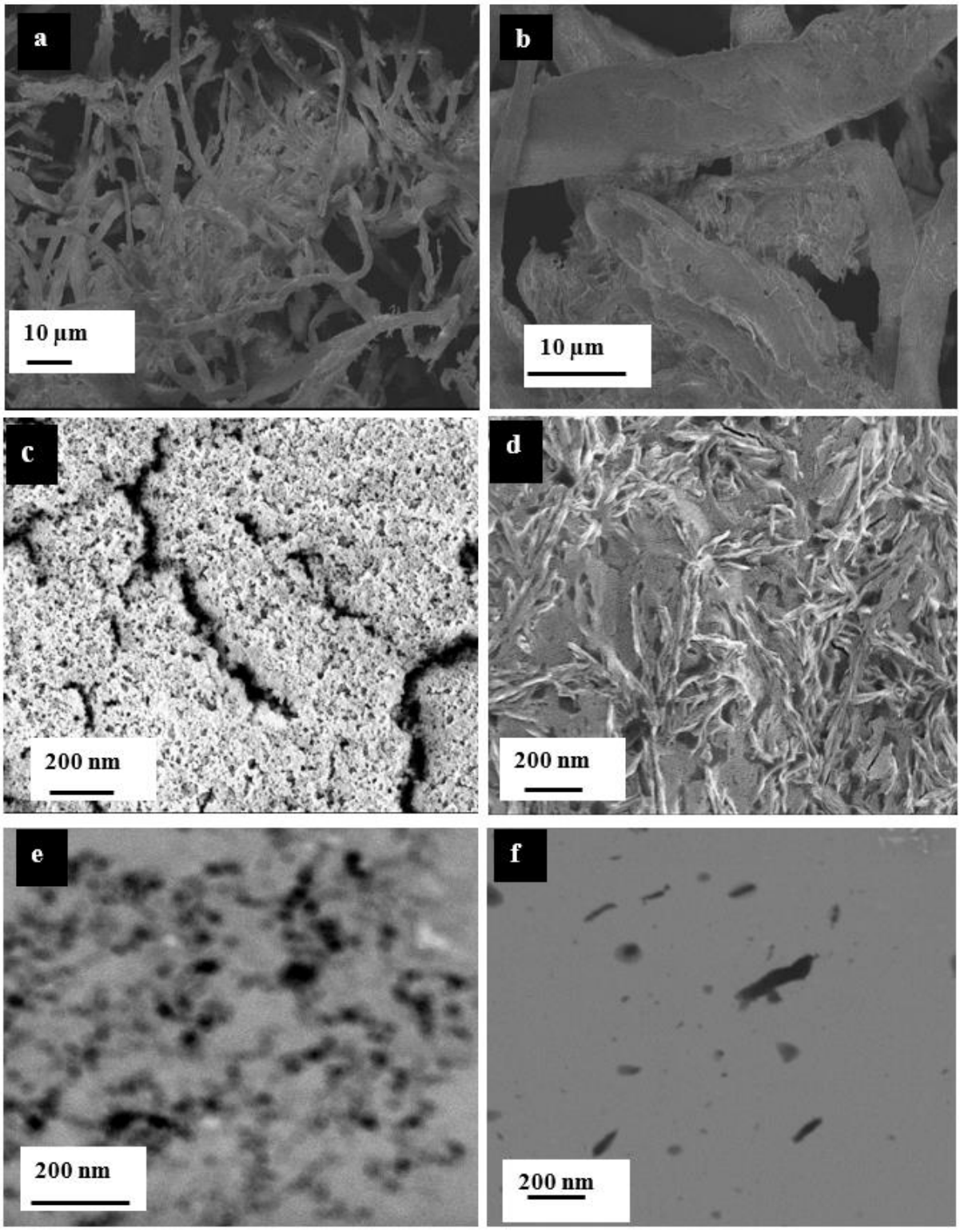

Figure 6.3: Scanning Electron Microscopy images of (a) unbleached organosolv treated pulp (b) bleached pulp (c) formic acid cellulose nanocrystals, (d**)** sulphuric acid cellulose nanocrystals, and Scanning Transmission Electron microscopy of (**e)** formic acid cellulose nanoparticles and (**f)** sulphuric acid cellulose nanocrystals

6.5.4.2. Structural changes and crystallinities of pretreated mango seed husk pulp and cellulose nanocrystals

Figure 6.4 shows the FTIR spectra of UMP, BP, FCNP (obtained at optimum conditions), and SCNP. Apart from the emergence of two new peaks in FCNP and SCNP, most of the bands (897 cm^{-1}, 1028 cm^{-1}, 1104 cm^{-1}, 1426 cm^{-1}, 2902 cm^{-1}, 3330 cm^{-1}) found in the UMP and BP were similar to that of the cellulose nanoparticles. The absorption bands at 3330 cm^{-1} and 2902 cm^{-1} are assigned to the hydrogen-bonded O-H groups of carbohydrates and C-H stretching vibration in methylene groups respectively [352]. The band at 1726 cm-^{1} assigned to the acetyl groups in hemicellulose and that around 1595 cm^{-1} assigned to aromatic ring vibration in lignin were weak in the spectra of UMP and BP. This means the multi-step pretreatments (alkaline/HSHO and alkaline/bleaching) hydrolyzed most of the non-cellulosic components from the biomass as reported in other studies [14], [491].

Compared to the SCNP, the FCNP showed the re-emergence of a strong peak at 1726 cm^{-1} (Figure 6.4a) which is attributed to the C=O stretching of ester fragments formed after partial formylation of cellulose through hydrogen bonding by FA [97]. The re-emergence of the peak at 1726 cm^{-1} confirms the successful modification of the CNP with formate groups and supports the formate contents of the FCNP (Table 6.3). The above observation indicates the successful preparation of CNPs with functionalized surfaces from UMP. Similarly, there is the emergence of two new peaks at 1205 cm^{-1} and 768 cm^{-1} in SCNP that was absent in the UMP and FCNP. These bands are associated with the S=O stretching and C-S vibration of sulfate groups, which also confirms the esterification of hydroxyl groups of cellulose by sulphuric acid [51], [152] which has previously been reported [20]. The band at 1639 cm^{-1} is associated with the bending vibration of hydroxyl groups of absorbed water [169]. Most of the other bands observed in the nanoparticles including 1426 cm^{-1}, 1159 cm^{-1}, 1113 cm^{-1}, 1028 cm^{-1}, and 896 cm^{-1} are typical bands for cellulose Iβ [97], [352]. However, the intensity of the peak at 896 cm^{-1} in the FCNP decreased significantly compared to the UMP, which indicates significant hydrolysis of the β-glycosidic linkages in cellulose microfibers [499]. It can thus be concluded that both pretreatments (alkaline/HSHO) and formic acid treatment did not change the crystalline Iβ characteristic of cellulose which is in accordance with works done by others [51], [97].

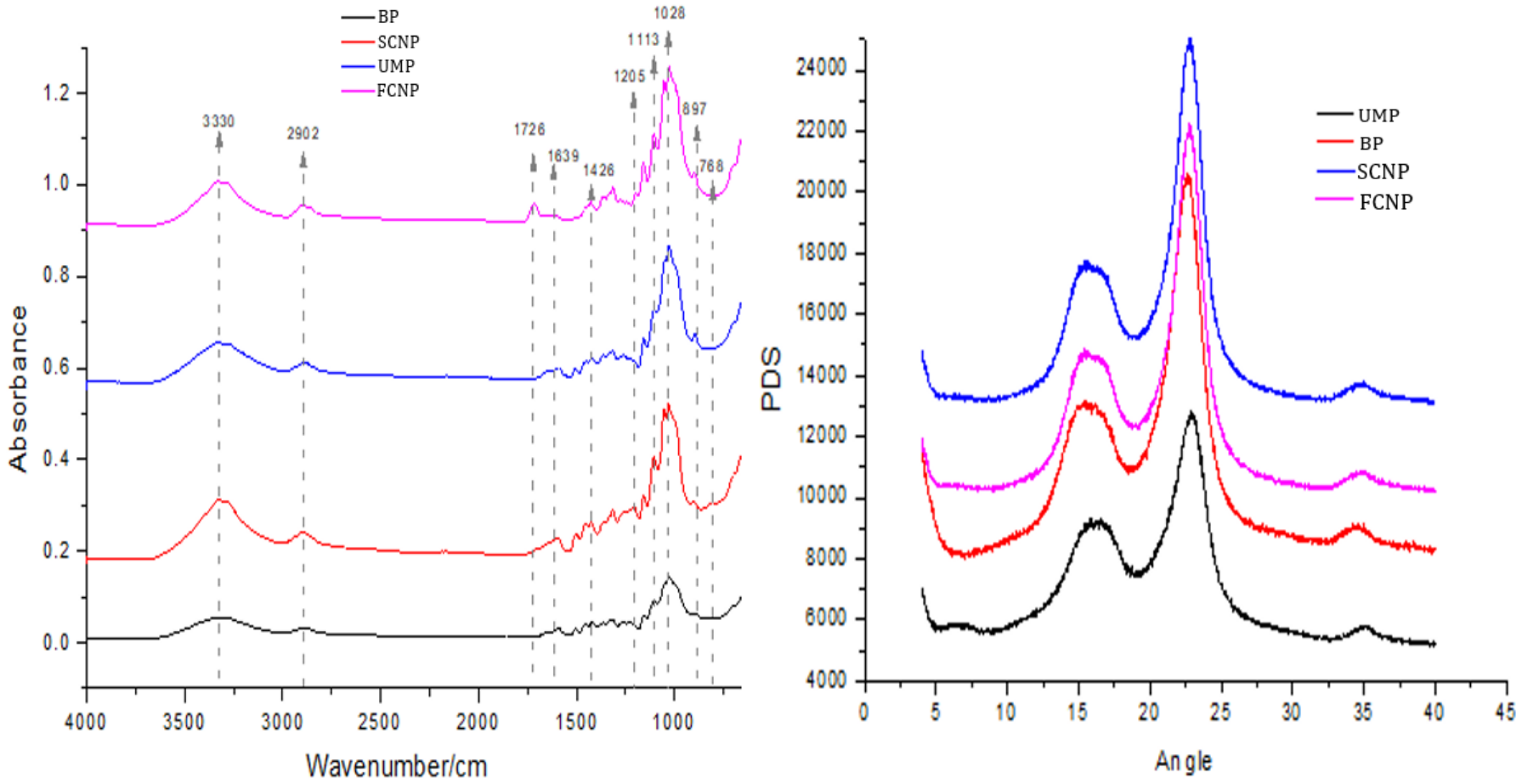

Figure 6.4: (a) Fourier Transform Infrared spectra and (b) x-ray diffractograms of unbleached organosolv treated mango seed husk, bleached pulp, formic acid cellulose nanoparticles, and sulphuric acid cellulose nanoparticles

The X-ray diffractograms showing the crystallinity index (CrI) of pretreated solids and the corresponding cellulose nanoparticles were obtained to provide further details on the structure of cellulose (Figure 6.4b). All the diffractograms showed distinct peaks at a 2θ value of approximately 15 º, 16.5 °, 22.5 °, and 34.5 º which corresponds to (1-10), (110), (200), and (004) crystallographic planes. These peaks are typical characteristics of cellulose Iβ residue– an indication that no significant destruction in the basic structure of cellulose was observed for the developed process [500]. The results are in accordance with the FTIR and other literature reports [40]. The Crl of the FCNP was 66.40%, thus, compared to the Crl of the UMP (55.75%), the FA treatment increased the percentage of the crystalline region by 16% which is ascribed to the removal of amorphous components from the cellulose [500]. The Crl of FCNP compares well with the 63.8% and 66.23% reported by Liu et al. [97] and Du et al. [352] respectively for FA CNPs from the bleached pulp.

The BP showed a Crl value of 66.41% and after H_2SO_4 treatment, the SCNP presented a Crl of 71.02% which agrees with the 72.4% reported by Li et al. [40] for H_2SO_4 CNPs. The referred lower CrI of the FCNPs vs SCNP could be due to the effectiveness of sulphuric acid in hydrolyzing the amorphous cellulose while maintaining the crystalline cellulose. Nevertheless, the FCNP CrI compares well with the 69% reported for sulphuric acid-produced CNP from Kraft loblolly pulp [24]. The lower Crl of Kraft lobloby CNPs and FCNPs could have resulted from the possible adsorption of acid hydrolyzed lignin or hemicelluloses (from the feedstock) unto the CNP which changed the crystallite nature [501]. In addition, hydrolysis of cellulose-rich pulp using strong acids (e.g. sulphuric acid) leads to the removal of amorphous components and leads to higher Crl. However, the strong acidity could also lead to the degradation of crystalline cellulose, consequently lowering the Crl depending on the reaction conditions [97]. Overall, the proposed process route in this study resulted in FCNPs with high Crl comparable to literature values that could have applications as fillers of reinforcement materials in nanocomposites or biomedicine.

6.5.4.3. Thermal stability analysis of pretreated husk and cellulose nanocrystals

Thermogravimetric analysis (TGA) was performed on pretreated pulps, FCNP, and SCNP to assess their thermal stabilities and determine possible fields of application. The TG/DTG curves showed different degradation temperatures for both the SCNP, FCNP, and pretreated pulps (Figure 6.5). An initial weight loss for all samples occurred at ≈100 °C, due to the evaporation of loosely bound water, moisture, and lower molecular weight components [65]. Generally, the degradation of cellulose by heat involves dehydration, depolymerization,

decomposition of glycosidic units, and char formation [166]. Compared to the pretreated pulps, the onset (T_{onst}) and maximum degradation temperatures (T_{max}) for FCNP were observed at higher temperatures (290 °C and 361 °C respectively) indicating improvement in the FCNP thermal stability. This is attributed to the removal of thermally unstable amorphous components by formic acid and reflects the successful introduction of formate groups on the CNP. Formate groups have been reported to improve the thermal stability of CNPs since formylation reduces the less stable hydroxyl groups [151]. The T_{max} for the FCNP agrees with values (355–366 ºC) reported by other authors for FA-produced CNPs [51], [97].

Furthermore, the FCNP was much more stable than SCNP (T_{onst}=233 °C and T_{max}=309 °C respectively) due to the presence of sulfate ester groups which act as dehydrating agents, lowering the activation energy of cellulose chains, and promoting the degradation of CNP [24], [502]. As reported by Roman and Winter, [502], the thermal stability of cellulose crystallites is weakened when sulfate ester groups replace the hydroxyl groups, which favor the dehydration of cellulose and speed up its degradation. This is in agreement with other reports [51], [97]. Thus, even though SCNP exhibited the highest Crl, its thermal stability was lowered by the sulfate groups, which can affect the CNPs application in high-temperature operations [503]. Furthermore, the T_{max} of FCNP is comparable to the reported 355.9 °C to 365.4 °C for mixed formic and hydrochloric acid spherical CNPs [151]. This implies spherical CNPs with better thermal stabilities were prepared from the proposed approach which opens new avenues for application in thermoplastics (as their fabrication requires high temperatures above 200 ºC) and nanocomposites [419].

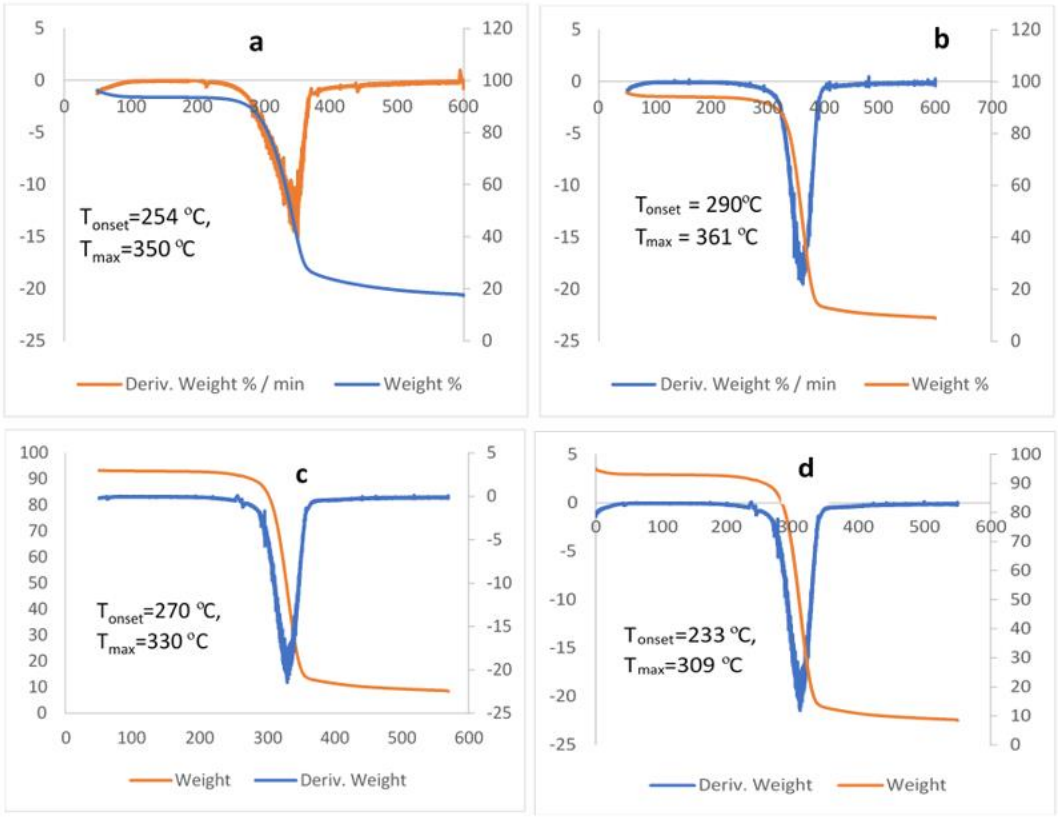

Figure 6.1: Thermograph (TG) and derivative thermogravimetric (DTG) curves for (a) unbleached organosolv treated mango seed husk, (b) formic acid cellulose nanoparticles (at the optimum point) (c) bleached alkaline treated mango seed husk, and (d) sulphuric acid cellulose nanoparticles

6.6. Conclusions

This study reveals the feasibility of using a non-catalyzed formic acid-based treatment on an unbleached mango seed husk obtained by a multi-step biorefinery process that consists of sequential alkaline and HSHO pretreatments to produce spherical cellulose nanoparticles. At the optimum conditions of 30:1 mL/g and 8 h, high yields of crystalline and formylated spherical CNPs were obtained. Compared to the SCNP, the FCNP presented better thermal stability (T_{max}=361 ºC), and hydrophobicity (due to formate groups), making it suitable for varied applications such as in thermo-processed nanocomposites, biomedicine, and cosmetics. Thus, the developed method provides an approach for large-scale production of thermally stable, hydrophobic CNPs compared to the classical sulphuric acid method that has documented environmental and technical problems due to its highly corrosive and toxic nature. Finally, using an unbleached pulp from the two-stage alkaline and HSHO pretreatment instead of alkaline/bleached pulp indicates that the hemicellulose and lignin could be recovered as valuable co-products in the nanocellulose production process instead of being degraded during the conventional bleaching processes.

6.7. Simultaneous preparation and acetylation of cellulose nanocrystals from a cellulose-rich pulp obtained via a multi-step biorefinery route using a non-catalyzed acetic acid-based treatment

Manuscript

Authors: Fatimatu Bello, Annie Chimphango, Ferdinand Görgens

Abstract

In this study, a mild acetic acid-based treatment approach was used to produce acetylated cellulose nanoparticles (ASCN) from an unbleached cellulose-rich pulp obtained from a multi-step sequential alkaline and high shear homogenization-assisted organosolv pretreatment. The influence of pulp-to-acid ratio (1:20–1:40) and reaction time (6–12 h) on the yield, average particle size, and degree of substitution were studied and benchmarked against sulphuric acid produced nanocellulose (SCNP). The nanocelluloses were further characterized by scanning electron microscopy (SEM), Fourier transforms infrared spectroscopy (FTIR), X-ray diffraction (XRD), and thermogravimetric analysis (TGA). Spherical acetylated nanocellulose (ASCN) was obtained by the non-catalyzed acetic acid treatment process. The best result was obtained at a reaction condition of 10 h and 1:40 g/mL solid-to-acid ratio with yield, average particle size, DS, and thermal degradation temperature of 17.68%, 45.0 nm, 1.83, and 352 ºC. Compared to the sulphuric acid nanocellulose (SCNP), the ASCN was thermally stable (T_{max} =352 ºC vs 290 ºC) due to the introduction of acetyl groups. High shear homogenization treatment post acetic acid treatment improved the yield of ASCN by more than 70%, however, there was a reduction in the crystallinity index (61.9% vs 46.7%). Therefore, the non-catalyzed acetic acid-based process has the potential to produce functionalized nanocelluloses that could be applied as fillers of reinforcement agents in hydrophobic nanocomposites due to their acetylation from a cellulose-rich material pretreated using a multi-step biorefinery approach.

6.8. Introduction

Cellulose nanoparticles (CNP) are new bio-based materials with unique chemical and physical properties that have attracted much attention recently for a wide range of industrial applications [166], [495]. CNPs are rod-like, whisker-like, or spherical-shaped cellulose-rich materials with at least one of the dimensions in the nanometre range [24], [409], [419]. The spherical CNPs (SCN) have mostly been applied in food packaging [151], biomedicine and as drug delivery carriers due to their less tendency to injure human cells when compared to the rods and whiskers [170], [171]. Some of the feedstocks that have been used in SCN preparation include waste paper, cotton fabrics, waste cotton, sunflower shells, rice straw, rice husk, coconut coir, jackfruit peel, among others [409], [504], [505]. Mango seed husks as a by-product of the mango processing industry are a potentially suitable feedstock for SCN preparation owing to their high cellulose content of 39.4–55.1% [15], [19].

The characteristics of CNPs such as dimension, morphology, surface charge, thermal stability, and crystallinity, are not only dependent on the cellulose hydrolysis process but also on the pretreatment/purification processes of the starting feedstock [227]. Generally, the conventional practice of obtaining cellulose for CNP production which involves mainly Kraft pulping and bleaching causes severe environmental pollution issues and loss of valuable bioresources such as hemicellulose due to the use of harsh chemicals [24], [359]. Increased environmental safety awareness demands the development of new processes and technologies that produce raw materials for CNP production using recoverable organic solvents [227]. Organosolv is a chemical pretreatment method that employs organic solvents or its aqueous solvents to extract and dissolve lignin from biomass [491]. Organosolv pretreatment effectively breaks the lignin-lignin bonds, especially the β-*O*-4 aryl ether bonds in addition to the ester and ether bonds between lignin and hemicelluloses and releases the lignin into the extraction solvent, leaving a cellulose-rich pulp [228], [314]. Organosolv treated cellulose-rich pulp is a highly digestible and semi-crystalline material used mostly for biofuel production, however, it could be used for CNP production under less severe conditions due to its increased surface area, pore volume, and accessibility [506]. The addition of physicochemical and mechanical pretreatment techniques in ethanol organosolv processes has been reported to improve the accessibility of solvent for lignin hydrolysis and dissolution [62]. Thus, the rupturing of the strong interfibrillar hydrogen bonding via mechanical processes could aid in the usage of less severe hydrolysis conditions such as reduced power or acid concentration on the recovered cellulose-rich solids to produce the CNPs [491].

The production of CNPs from the purified cellulose-rich material has been through sulphuric acid treatment with ultrasonication, mixed acids, and combined enzymatic and mechanical treatments [152], [170]. However, major challenges associated with the use of the referred methods include low thermal stability of SCN, low yields, low crystallinity (Crl), long reaction times, the requirement of corrosive-resistant equipment, and cumbersome downstream processes of toxic effluents, which increases the overall cost of production [145]. For example, Satyamurthy et al. [170] used enzymatic treatment to prepare spherical CNPs (SCNs) from cotton fiber microcrystalline cellulose and reported a yield of 12.3% after 168 h of hydrolysis. The lower yield was attributed to over hydrolysis of glycosidic linkages in cellulose to glucose. In another study, the Crl of SCN produced via NaOH/thiourea/urea was significantly reduced to 48.8% when compared to the starting material (Crl=64.42%) owing to cellulose regeneration [169]. Furthermore, the mixed sulfuric and hydrochloric acids used by Ram and Chauhan [152] presented SCN with reduced thermal stability compared to the thermal stability of the starting material (260.23 ºC vs 284.5 ºC respectively). Therefore, the long treatment period, low yields, Crl, and thermal stability could negatively impact large-scale production in terms of cost and revenue generation.

Although Wang et al. [507] and Chen et al. [508] have optimized the sulphuric acid process conditions to increase the yield of CNP to 70–80% from bleached eucalyptus Kraft pulp, the CNPs exhibited low thermal stability as a result of the surface ester groups [409]. Given these, other methods considered more environmentally friendly have been reported. Such methods include oxidation reactions [157], enzymatic treatment [170], organic acid treatment [25], [40], [51], among others with different levels of efficiency. Of these methods, the organic acid treatment that employs acids such as formic, citric, butyric, oxalic, and maleic has attracted much consideration as a promising alternative to resolve most of the issues associated with the inorganic acids [25], [51], [168]. This is because organic acids are less corrosive, can easily be recovered and reused, and can introduce functional groups onto the CNP [51], [166].

Additionally, organic acid-produced CNPs exhibit high thermal degradation temperatures compared to that of sulphuric acid [51]. For example, Liu et al. [97] compared formic acid treatment (in the presence of hydrochloric acid) with other three different methods to produce CNP from bleached corn cob residue. They reported that both formic and sulphuric acid CNPs had comparable diameters (5.5 nm vs 6.5 nm), but the length of formic acid CNP was much longer (198 nm vs 421 nm). However, the crystallinity and thermal stability of formic acid CNP (63.8% and T_{max}=360 ºC) were higher than sulphuric acid CNP (55.9% and

313 ºC respectively) due to the selective hydrolytic nature of formic acid towards amorphous cellulose and lignin. In addition, Xie et al. [409] produced over 70% yield of thermally stable (T_{max} > 280 ºC) CNPs with diameters in the range of 5–20 nm and lengths of 150–400 nm using mixed sulphuric and oxalic acids treatments on bleached eucalyptus Kraft pulp. The CNPs dispersed well in an aqueous solution due to high ζ-potential values (-30 mV–-42 mV). Acetic acid is the second simplest carboxylic acid after formic acid. Its acidity is almost ten times lesser (pKa=4.75) than formic acid (pKa=3.77) and has been used in various pretreatment/fractionation processes to remove lignin and hemicelluloses [323]. Acetic acid has also been combined with other chemicals including acetic anhydride for modification of CNPs to improve the hydrophobicity [509].

Recently, Wang et al. [25] reported a sulphuric acid intensified acetic acid process to produce CNP from bleached eucalyptus Kraft pulp, in which small doses of sulphuric acid (5–10%) was combined with acetic acid (70–90%). The produced CNPs showed high thermal stability, although the thermal stability was lower than that of the starting material but higher than that of sulphuric acid-based CNPs. Furthermore, the CNPs could disperse well in both organic and aqueous solvents due to the presence of both surface sulfate and acetyl groups. Thus, the CNP was reported to have a bifunctional property with both hydrophilic and hydrophobic groups. Nevertheless, these two different polarities could limit the application of the CNPs in nanocomposites. The sulfate groups on the CNP could also be problematic for application in biocomposite prepared through simple melt blending [408]. Besides, the existence of two different polarities could lead to aggregation and poor dispersion in either a hydrophobic matrix (in which only the hydrophobic portion will interact) or a hydrophilic matrix (in which only the hydrophilic portion will interact) [349], [510]. Therefore, obtaining a more environmentally benign process such as the use of only organic acids without additional mineral acid supplements that produce thermally stable hydrophobic CNPs are relevant for application in nanocomposites.

Due to the semi-crystalline nature, it is anticipated that unbleached AP+HSHO treated mango seed husk (UMP) could be readily hydrolyzed into CNPs with hydrophobic properties using a recoverable acetic acid-based treatment process. In a previous study, we have demonstrated that ethanol organosolv in combination with high shear homogenization treatment (HSHO) is an effective process of obtaining high purity less modified lignin and fibrillated cellulose-rich fibers of reduced particle size and improved surface area from an alkaline treated mango seed husk in a multi-product biorefinery [14]. Alkaline pretreatment

was optimized to recover hemicellulose polymers to prevent their degradation during the CNP production.

Thus, in this study, a simple non-catalyzed acetic acid system was developed to produce acetylated CNPs from unbleached HSHO treated mango seed husk (UMP). Thus, using this approach, the drawbacks of the sulphuric acid-based treatment could be reduced while obtaining an acetylated CNP that may not require further modification for application in fields such as hydrophobic nanocomposites. The dried UMP was subjected to acetic acid treatment [reaction time (8–12 h) and solid-to-acid ratio (20–40 g/mL)]. The yield, average particle size, ζ-potential, polydispersity index, and degree of substitution were investigated. Further, an additional high shear homogenization treatment was included to determine its influence on the yield and properties of the as-prepared SNPs. The morphology, structural features, crystallinity, and thermal stability of CNPs were determined. Sulphuric acid CNP was produced as a benchmark for comparison using the method of Henrique et al. [20] with modifications.

6.9. Experimental

6.9.1. Materials

The starting material was obtained by the procedure described in section 5.2.2. All the chemicals used are highlighted in section 6.2.1.

6.9.2. Acetic acid treatment of unbleached organosolv-treated mango seed husk to produce nanocellulose

The UMP was treated with acetic acid (99.9%) varying the solid-to-acid ratio (20 to 40 g/mL) for a period (6–12 h) in a 250 mL three-neck flask equipped with a condenser. Conditions were chosen from works reported in the literature [40], [51], [97], [151], [352]. The mixture was placed in an oil bath and stirred using a magnetic stirrer (500 rpm) at 110°C. Following this, the mixture was cooled immediately to room temperature under running water, centrifuged for 5 min at 8000 rpm, and the hydrolysate separated. The solids obtained after hydrolysate removal was washed several times with distilled water with subsequent centrifugation at 5000 rpm for 5 min until the pH of the suspension reached pH 6. The obtained suspension was dialyzed using a cellulose membrane dialysis tubing with a molecular cut-off of 14000 Da (Sigma-Aldrich, USA) for 3 days. The dialyzed CNP was freeze-dried and stored in zip lock bags for further analysis. The CNPs produced were annotated as ASCN.

6.9.3. Homogenization of acetic acid produced nanocellulose

The solids obtained after removal of hydrolysate after acetic acid treatment were dialyzed against distilled water for 3 days and homogenized for 15 min with a high shear homogenizer at 22000 rpm using a 2g in 100 mL distilled water. An ice bath was used to maintain the temperature of the samples and prevent heating up during homogenization. Homogenized samples were freeze-dried and stored in zip-lock bags for further analysis. The nanocellulose produced was annotated as HSCN. The yield of cellulose nanoparticles was determined gravimetrically according to Equation 25.

$$Yield\ (\%) = \frac{mass\ of\ freeze\ dried\ sample\ (g)}{mass\ of\ starting\ material\ (g)} \times 100\% \qquad [25]$$

6.9.4. Experimental design and statistical analysis

The effect of reaction time (X_1; 6–12 h) and solid-to-acid ratio (X_2; 1:20–1:40 g/mL) on the yield, average particle size, ζ-potential, polydispersity index, and degree of substitution of cellulose nanoparticles prepared with acetic acid were investigated in a 4×3 factorial design (i.e. reaction time with 4 levels and solid-to-acid ratio with 3 levels). The experiments were randomized to minimize errors. The statistical analysis was conducted with Statistica software (version 13.2) and analysis of variance (ANOVA) was carried out to determine the significance of the solid-to-acid ratio and reaction time on the yield, average particle size, ζ-potential, polydispersity index, and degree of substitution of the cellulose nanoparticles due to changes in process variables.

6.9.5. Characterization of starting material and cellulose nanoparticles

The particle size, ζ-potential, and polydispersity (PDI) of cellulose nanoparticles were determined based on the procedures detailed in section 6.2.4.1, whereas the morphology, thermal stability, crystallinity, and structural features were determined as detailed in section 6.2.4.3 to 6.2.4.4.

6.9.6. Degree of substitution of nanocellulose

The degree of substitution was determined through a saponification reaction of the acetyl groups that replaced the hydroxyl groups in every glucose unit. A mixture containing 0.5 g dry acetylated cellulose in 8 mL of ethanol (75% v/v) was heated at 60 °C for 30 min. Approximately 8 mL of 0.5 N sodium hydroxide (NaOH) solution was added and further heated for 15 min at 60 °C after which the mixture was tightly sealed and stored for 72 h at room temperature. The mixture was then titrated against 0.5 N hydrochloric acid (HCl) using a phenolphthalein indicator. At the titration endpoint, an excess 1 mL of 0.5 N NaOH solution

was added. Blank titration was similarly performed with unmodified CNP, and the data was used as a reference. The acetyl content was calculated with Equation 26:

$$Acetyl\ content(\%) = [(B - A)N_a + (C - D)N_b] \times \left(\frac{4.035}{W}\right) \quad [26]$$

Where A is the volume of acid added to the sample (mL), B is the volume of acid added to the blank (mL), C is the volume of NaOH added to the sample (mL), D is the volume of NaOH added to the blank (mL), W is the weight of the sample (g), and Nc and Nd are the normality of the HCl and NaOH solutions, respectively. The average number of acetyl groups per anhydrous-D-glucose unit of cellulose (DS) could be calculated from Equation 27:

$$DS = \frac{3.86 \times Acetyl\ content(\%)}{102.4 - Acetyl\ content(\%)} \quad [27]$$

6.10. Results and Discussion

6.10.1. Yield and properties of acetic acid produced cellulose nanoparticles from the two-stage alkaline and organosolv treated pulp

In the present study, we try to eliminate the use of inorganic acids and catalysts by employing organic acids (acetic acid, 99 wt%) to treat unbleached cellulose-rich pulp obtained from a multi-step sequential alkaline and homogenization-assisted organosolv treated mango seed husk pulp (UMP) to produce cellulose nanoparticles. Table 6.4 shows the results of the as-prepared CNPs. The results (Table 6.4) showed that indeed cellulose nanoparticles (ASCNs) could be produced from UMP using acetic acid treatment without the addition of inorganic acids contrary to the reported trends in the literature for other organic acid processes [25], [40], [352], [409]. The ASCN yield ranged from 4.21% to 17.68%, accompanied by average particle size, degree of substitution (DS), ζ-potential, and PDI of 28.6–76.2 nm, 0.482–1.833, -16.18–-18.67, and 0.468–0.784, respectively (Table 6.4). The highest ASCN yield was obtained at a solid-to-acid ratio of 1:40 g/mL and reaction time of 10 h which also presented an average particle size and PDI of 45 nm and 0.468 respectively (Table 6.4). Comparatively, the highest yield (17.68%) obtained in this study was higher than yields (5–12.5%) reported in the literature [51], [168] for other organic acid-produced CNPs from Avicel and bleached pulp. This could be due to the different properties of the starting materials used arising from the different pretreatment processes employed.

Table 6.4: Effect of reaction time and solid-to-acid ratio on the properties of acetic acid nanocellulose from organosolv pulp

Run	Reaction time [h]	Solid-to-acid ratio [g/mL]	Yield [%]	[a]Average particle size [nm]	DS	Zeta-potential (mV)	PDI
1	6	1:20	4.21	76.2	0.482	-16.18	0.784
2	8	1:20	5.11	37.9	0.737	-16.90	0.681
3	10	1:20	5.70	37.9	0.930	-18.03	0.607
4	12	1:20	5.99	35.3	1.255	-19.63	0.567
5	6	1:30	8.74	62.3	0.546	-16.77	0.738
6	8	1:30	10.50	43.0	0.909	-17.20	0.594
7	10	1:30	13.31	36.0	1.395	-18.03	0.526
8	12	1:30	15.97	45.7	1.646	-21.53	0.481
9	6	1:40	11.04	61.8	0.712	-16.83	0.758
10	8	1:40	12.95	28.6	1.210	-17.50	0.657
11	10	1:40	17.68	45.0	1.833	-19.70	0.468
12	12	1:40	17.29	51.3	1.801	-18.77	0.535
HSCN	10	1:40	77.70	38.2	1.811	-20.68	0.450
SCNP	1	1:20	28.34	175	-	-34.86	0.215

Where HSCN is the 15 min post-high shear homogenization of nanocellulose obtained using conditions for Run11 and SCNP is the sulfuric acid produced nanocellulose from the bleached pulp.

The application of high-shear homogenization during mango seed husk purification (delignification) increased the surface area and accessibility of the pulp to chemicals [14], [93], and thus, during the acetic acid treatment, hydronium ions could easily penetrate the cell wall and hydrolyze the less ordered amorphous cellulose to obtain CNPs. Other yields that were greater than 15% were observed at 1:30 g/mL and 12 h or 1:40 g/mL and 12 h. The PDI and average particle sizes at these conditions were approximately 0.5 and <51 nm respectively (Table 6.4). On the contrary, the lowest ASCN yield was observed at the least severe conditions of 1:20 g/mL and 6 h, which also presented the largest average particle size and PDI (76.2 nm and 0.784). In addition, the highest DS (1.833) was observed at the same condition for the highest yield (Table 6.4). Therefore, for ASCN yields >15%, with DS >1.8 and with particle sizes ≈50 nm from cellulose-rich pulp obtained from the aforementioned pretreatment process, high reaction severities will be necessary.

6.10.2. Effect of solid-to-acid ratio and reaction time on the yield and properties of acetic acid hydrolyzed nanocellulose

To demonstrate the statistical significance of the solid-to-acid ratio and reaction time and their correlation with the yield and properties of the ASCN, analysis of variance (ANOVA) was performed on the data, and results are shown in Table 6.5. Both the solid-to-acid ratio, reaction time, and their interaction terms were significant ($p<0.05$) towards the ASCN yield. Therefore, an increment in the reaction time and solid-to-acid ratio hydrolyzed the cellulose-rich pulp and increased the formation of CNPs (Table 6.5). This could be explained by the high concentration of H_3O^+ ions in the reaction medium (as the acid content increases) and the longer contact time of pulp with the solvent which allowed efficient diffusion of the acid into the biomass matrix for amorphous component degradation [419]. The ASCN yield increased from 5.99 to 17.68% when the solid-to-acid ratio was increased as expected of an acidic treatment [419]. On the other hand, the yield increased with an increase in reaction time from 6 to 10 h (11.04 to 17.68%) before a slight reduction when the time was prolonged to 12 h.

Table 6.5: Analysis of variance (p-values) for yield, average particle size, degree of substitution, zeta-potential, and polydispersity of acetic acid produced cellulose nanocrystals

	Yield	Average particle size	DS	Zeta-potential	PDI
X_1	0.000	0.000	0.000	0.000	0.000
X_2	0.000	0.745	0.000	0.509	0.002
X_1X_2	0.006	0.000	0.000	0.830	0.703
R^2	96.65%	99.25%	99.34%	59.82%	88.12%

Where X_1, X_2, and X_1X_2 represent reaction time, solid-to-acid ratio, and the interaction of reaction time and solid-to-acid ratio, respectively. R^2 is coefficient of determination. Values were observed at a 95% confidence level.

The reduction in the ASCN yield could be attributed to the extended treatment time resulting in the complete hydrolysis of some of the cellulose which had been broken down into CNPs [511]. Due to the weaker acidity of acetic acid, the optimum yield observed was ≈18%. Literature reports have indicated improved CNP yields with the application of mechanical treatments [168], [492]. Thus, to improve the ASCN yield using the mild acetic acid-based treatment, a separate experiment was performed using the conditions for Run 11 and introducing a high shear homogenization (HSH) and was designated HSCN (Table 6.4). Results showed that 15 min homogenization could improve the ASCN yield by more than 70% (Table 6.4). Hence, an HSH treatment post-acetic acid treatment of UMP presents an effective

method of improving ASCN yield. The average particle size of the ASCN was measured based on dynamic light scattering. From Table 6.5, only the reaction time and its interaction with the solid-to-acid ratio were significant (p<0.05) towards the average particle size. Therefore, when the reaction time was extended from 6 to 10 h, the average particle size reduced significantly from 62.3 nm to 36.0 nm (Table 6.4) due to hydrolysis of amorphous cellulose [51]. At the same time, a reduction in the average particle size occurred with increment in the solid-to-acid ratio up to 1:30 g/mL (at constant time of 10 h), after which the size became bigger with further increase in solid-to-acid ratio (Table 6.4).

Generally, acetic acid partially dissociates to acetate and hydronium ions (H_3O^+) in the presence of water. The H_3O^+ generated assists in the hydrolysis of amorphous cellulose glycosidic bonds to obtain CNPs. At the same time, the acetate groups in the reaction medium react with the exposed cellulose hydroxyl groups, particularly, OH groups in the amorphous cellulose region through Fisher esterification to obtain cellulose acetate [25]. This process known as acetylation has been applied to modify various biopolymers to improve their compatibility with other hydrophobic polymer matrices. The efficiency of this esterification process is measured by the degree of substitution (DS) [166]. In this study, different DS was observed for ASCN due to the varied reaction conditions (Table 6.4). The DS was found to increase with contact time at a constant solid-to-acid ratio. Nevertheless, at the highest solid-to-acid ratio (1:40 g/mL), the DS decreased when contact time was 12 h. As a result, a DS of 1.801 was observed for the severest reaction conditions (12 h and 1:40 g/mL). The reduction in DS is due to hydrolysis of part of the esterified acetyl groups on the CNPs since both hydrolysis of glycosidic linkages and acetylation of OH^- groups occur at the amorphous cellulose region [166]. Similarly, increasing the solid-to-acid ratio from 1:20 to 1:30 g/mL resulted in a corresponding increase in the DS; however, at 1:40 g/mL an inverse effect on the DS was observed. Furthermore, after HSH post acetic acid treatment (HSCN), the DS of HSCN did not change significantly (1.811) indicating that high shear homogenization does not negatively impact the DS of CNPs post acetic acid treatment. The results indicated that, although controlled treatment of cellulose-rich solids from a multi-step process with acetic acid alone results in ASCN with high DS, application of HSH further improves the yield but does not compromise the DS (Table 6.4).

The different reaction conditions hydrolyzed the cellulose to different degrees which resulted in different particle size distributions (PDI) (Table 6.4). From Table 6.5, only the individual effects of reaction time and solid-to-acid ratio were significant (p<0.05) towards the PDI of ASCN with the reaction time exhibiting a stronger effect. The interaction of reaction

time and the temperature was not significant at a 95% confidence level (Table 6.5). As shown in Table 6.5, the PDI reduced when the reaction time was increased (Table 6.4), except for the reaction performed for 12 h using a solid-to-acid ratio of 1:40 g/mL for which the PDI increased to 0.535 from 0.468. This could be due to increased viscosity resulting from the increased density of the reaction medium. On the other hand, the PDI reduced from 0.567 to 0.481 as the solid-to-acid ratio increased from 1:20 to 1:30 g/mL, but the PDI increased (0.535) when the solid-to-acid ratio was 1:40 g/mL. For the HSCN, the PDI decreased from 0.468 to 0.450 showing that although homogenization reduced the average particle size it also caused a slight reduction in the PDI. The results obtained for ASCN PDI conform with the results for the yield and DS which indicates that at the employed condition for Run 11, most of the best responses were received for the produced ASCN.

With the ζ-potential, only the reaction time had a significant (p<0.05) effect at a 95% confidence level (Table 6.5). The solid-to-acid ratio had a positive effect but was not statistically significant. The increment in the reaction time resulted in increased ζ-potential of ASCN at any given solid-to-acid ratio except for 12 h at 1:40 g/mL. The increased ζ-potential with time complements the results of the average particle size as more hydroxyl groups were exposed as the particle size was reduced. This explains that acetic acid treatment for CNPs production can be achieved at the lowest solid-to-acid ratio without a significant reduction in the mean absolute ζ-potential. For the HSCN, the ζ-potential slightly increased (-20.68 mV) with the addition of HSH which was expected with the observed reduction in DS. Overall, the statistical analysis and ANOVA of the results obtained showed that using a reaction time of 10 h and the solid-to-acid ratio of 1:40 g/mL (Run 11) presented the best-combined effect for yield, DS, PDI, and average particle size. In addition, apart from improving the yield and average particle size of the CNPs produced, HSH did not negatively influence the DS. It can therefore be summarised that it is better to include a homogenization treatment after acetic acid treatment to improve the CNP yield rather than using inorganic acids.

6.10.3. Morphology and size distribution analysis

The morphologies of the UMP, BP, and cellulose nanoparticles obtained through acetic acid, sulphuric acid, and acetic-acid/high shear homogenization treatments as observed under SEM are shown in Figure 6.5. The UMP had individual cellulose strands with rough surfaces and diameters in the range of <1 to 10 µm, owing to the removal of amorphous hemicellulose and lignin in addition to the effect of the HSH during organosolv pretreatment (Figure 6.5a). This is in agreement with the work of Wu et al. [512] who asserted that the application of high

shear homogenization leads to hydraulic shear, coalition tearing in the cavity, and centrifugal extrusion that leads to gradual peeling of individual cellulose fibers from the bundle.

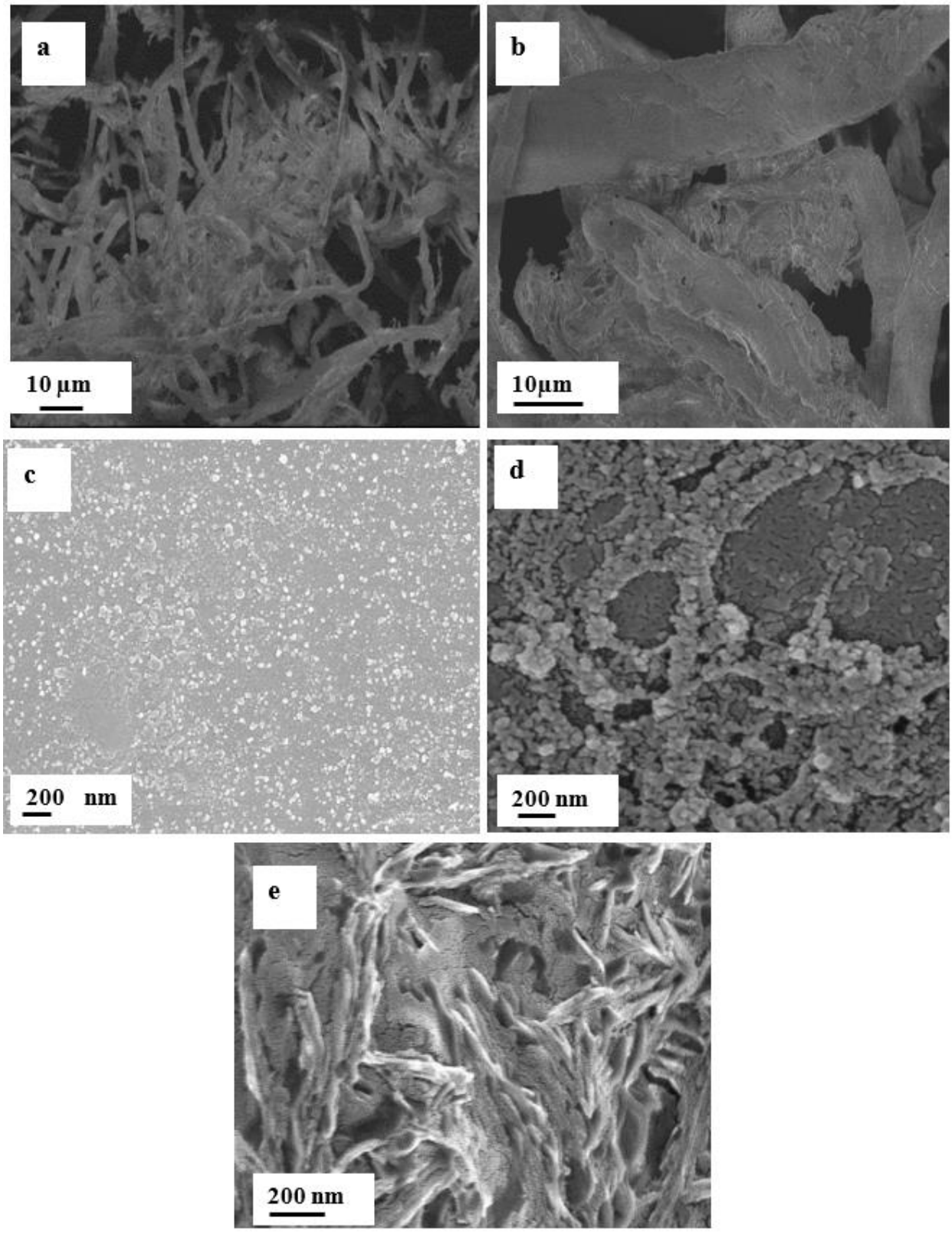

Figure 6.5: Scanning electron microscopy images of (a) unbleached organosolv treated mango seed husk pulp (b) bleached mango seed husk (c) acetic acid cellulose nanocellulose, (d) homogenized acetic acid nanocellulose (e) sulfuric acid cellulose nanocellulose

The rough surface of the fibers of the UMP could favor the production of CNPs due to the cracks and larger surface area and pore volume that will allow easy access of the hydrolyzing ions to the cellulose [419]. After acid treatment of UMP (Figure 6.5b), the rough cellulose fiber dimensions reduced considerably to the nanoscale with irregular spherical shapes. Thus, the micro-sized cellulose fibers were degraded partially with further removal of residual hemicellulose and lignin by the acid [152]. Furthermore, the spherical cellulose nanoparticles produced had particle sizes of 20–80 nm and 10–60 nm respectively for ASCN and HSCN (Figure 6.5b and 6.5c). The effect of the HSH was noticed as the particle size further reduced and narrowed for the HSCN.

In addition, the size distribution graph showed that there was an increase in spherical nanoparticles with a diameter <50 nm (from 70% to 90%) with the introduction of HSH (Figure 6.6b). Nevertheless, there was no statistical difference between the average particle size of ASCN and HSCN (45±14 nm and 38±14 nm, respectively). This was because, although the homogenization treatment reduced and removed the CNPs with particle size >60 nm, most of the particle sizes ended up being between 30–50 nm. Further, the CNPs were spherical with a width of 15–50 nm (Figure 6.5d). Thus, it can be concluded that the use of a non-catalyzed acetic acid-based treatment could produce ASCN from UMP with or without HSH. The spherical-shaped CNPs with modification due to acetylation could be applied in different fields such as green biocomposites [172].

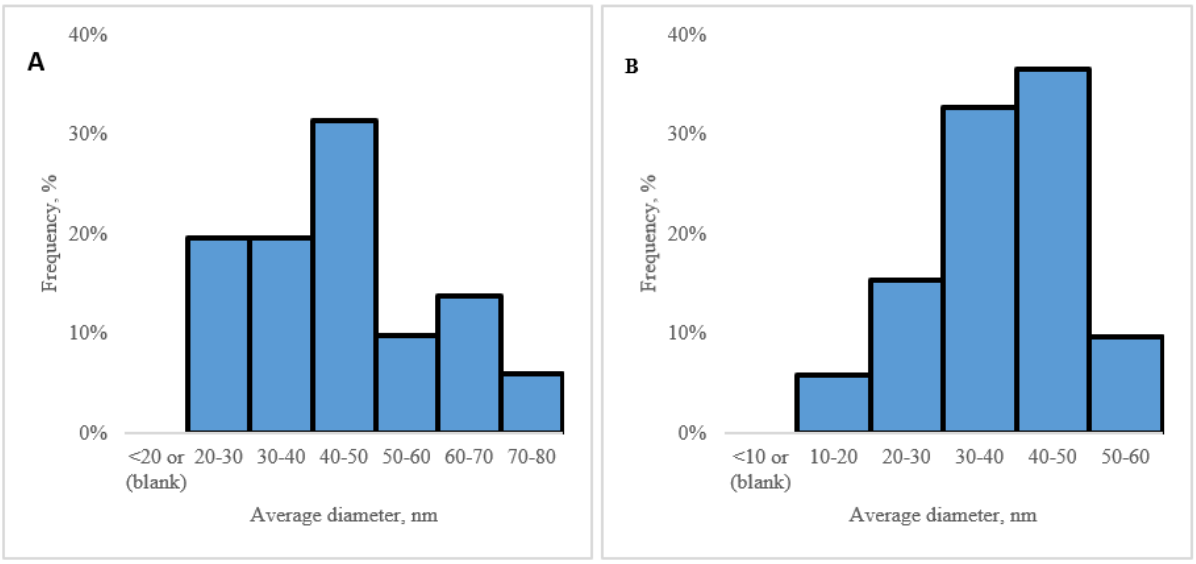

Figure 6.6: Particle distribution analysis of (a) acetic acid cellulose nanoparticles (b) homogenized acetic acid cellulose nanocellulose analyzed using images from scanning electron microscopy

6.10.4. Structural analysis of starting material and cellulose nanoparticles

The FTIR spectra of the UMP, BP, and the produced CNPs showing the changes in surface chemistry are presented in Figure 6.7. The UMP, BP, and CNPs showed broad peaks at 3338–3328 cm^{-1}, 2901–2880 cm^{-1}, and 1160–1155 cm^{-1} assigned to the hydroxyl groups of molecules of cellulose and O– H stretching vibration of intramolecular/intermolecular hydrogen bonding, C–H asymmetric vibration, and C–O–C ring stretching vibration of β-(1,4)-glycosidic linkage in cellulose respectively [166], [419]. Similar findings have been observed in the literature [25], [409]. The 1726 cm^{-1} and 1595 cm^{-1} peaks corresponding to the acetyl groups in hemicellulose and the aromatic ring vibration in lignin respectively were weak in the UMP spectra showing that the sequential AP and HSHO pretreatments hydrolyzed the majority of the non-cellulosic components in the feedstock [14]. Furthermore, the peak at 1595 cm^{-1} was almost invisible in all the CNP spectra after acid treatment, demonstrating that the CNP treatment process removes amorphous hemicellulose and lignin. Meanwhile, all the spectra showed visible peaks at 1640 cm^{-1} assigned to H-O-H bending vibrating of adsorbed water, an indication that even though, the samples were subjected to appropriate drying processes, it is challenging to remove completely moisture because of the strong interaction of bound water with cellulose [419]. Peaks at 1421–1429 cm^{-1}correspond to the asymmetric wagging vibration and bending of $–CH_2$ in cellulose I crystals [419], [513], an indication that the cellulose I crystal structure was maintained even after the pretreatments and acetic acid treatment.

The peak at 894–898 cm^{-1} assigned to the C–H rocking vibrations or the β-glycosidic linkages of the glucose residues in cellulose was more pronounced in the UMP than theCNPs due to removal of amorphous residue [169], [419]. The appearance of a new peak at 1724–1732 cm^{-1} assigned to the alkyl ester of the acetyl group was present in the ASCN and HSCN but not UMP or SCNP indicating that the acetic acid does not only hydrolyzed UMP to CNPs but also introduced its acetyl groups unto the CNPs. This finding agrees with recent studies [25]. The presence of peaks at 1205 cm^{-1} and 768 cm^{-1} in the ASCN is associated with the S=O and C-S stretching vibrations of sulfate groups. This shows that the hydroxyl groups of the CNP were replaced by the sulfate groups during sulphuric acid treatment [152]. In summary, the FTIR spectra showed that the exclusive use of acetic acid maintained the native cellulose structure similar to the sulfuric acid treatment except for the emergence of new peaks at 1726 cm^{-1} due to esterification of hydroxyl groups by the acetyl groups.

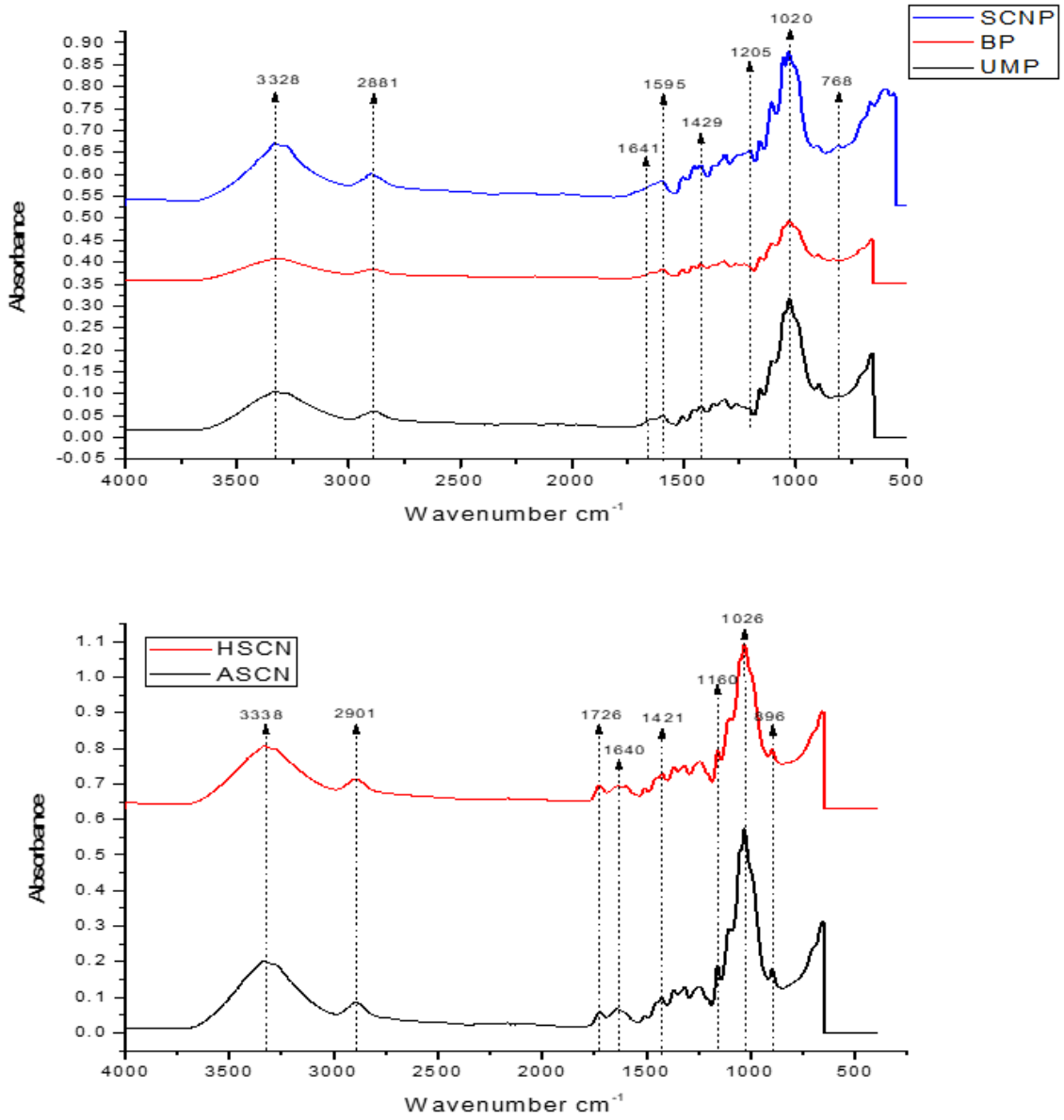

Figure 6.7: FTIR analysis of unbleached pretreated mango seed husk, bleached treated mango seed husk, acetic acid nanocellulose, homogenized acetic acid nanocellulose, and sulfuric acid nanocellulose

6.10.5. Crystallinity analysis of starting material and cellulose nanoparticles using X-ray diffraction

One major factor that determines the mechanical and thermal properties of cellulosic products is the crystallinity index, which is a measure of the relative crystalline portion of the material [349]. X-ray diffraction analysis was used to determine how the crystalline cellulose portion behaved with treatments [169]. The X-ray diffraction pattern for the UMP and CNPs is presented in Figure 6.8. Similar diffractograms for all the samples were observed with each sample displaying a sharp crystalline peak and a broad amorphous bump (Figure 6.8). The diffractogram for UMP showed the typical structure of cellulose I polymorph at miller indices

2θ =14.5 ($1\bar{1}0$), 17.5 (110), 22 (200), and 34.6 (004) [349]. After controlled treatment of UMP, similar crystallinity indexes were observed for both the ASCN and SCNP, however, the addition of homogenization post acetic acid treatment resulted in reduced crystallinity for HSCN (Figure 6.8). This indicates that both acetic and sulfuric acid treatments did not destroy the native cellulose crystalline structure and further improve the crystallinity of UMP through hydrolysis of amorphous components (Figure 6.8). Thus, the effects of the sulfuric acid treatment were similar to that of the acetic acid, making the usage of the acetic acid an adequate substitution for the sulfuric acid for ASCN production from UMP. The initial crystallinity of UMP was 55.75% which increased to 61.9% for acetic CNP. The CrI of the bleached pulp was 66.41% which increased to 71.02% after sulphuric acid treatment due to the successive amorphous components and disordered cellulose removal leading to exposure of highly crystalline CNPs or the resistance of crystalline cellulose to acid degradation [419].

The crystallinity of ASCN is comparable to the reported value (64%) for sulphuric acid CNPs from garlic straw [514]. On the contrary, the inclusion of the high shear homogenization step substantially caused more than a 40% reduction in the crystallinity when compared to ASCN although it improved the yield of CNPs (Table 6.4). Generally, the mechanical properties (flexibility, tensile strength, modulus) of nanocomposites are significantly influenced by the crystallinity of nanocelluloses when added as fillers of reinforcement agents [419], [515]. Therefore, high crystallinity CNPs will be regarded as better strengthening agents in polymer nanocomposites than low crystallinity CNPs. Nevertheless, the low crystallinity CNPs (CNPs with more loose cellulose portions than crystalline) could reduce the stiffness and improve the elasticity of the composite films. In this regard, the mild non-catalyzed acetic acid-based method or in combination with homogenization developed in the present study provides a simple and environmentally benign approach of obtaining CNPs with CrI that could provide the mechanical properties (tensile strength, flexibility, modulus) to nanocomposites without further modifications than the sulphuric acid-based approach. However, the environmental assessment of the proposed process is required.

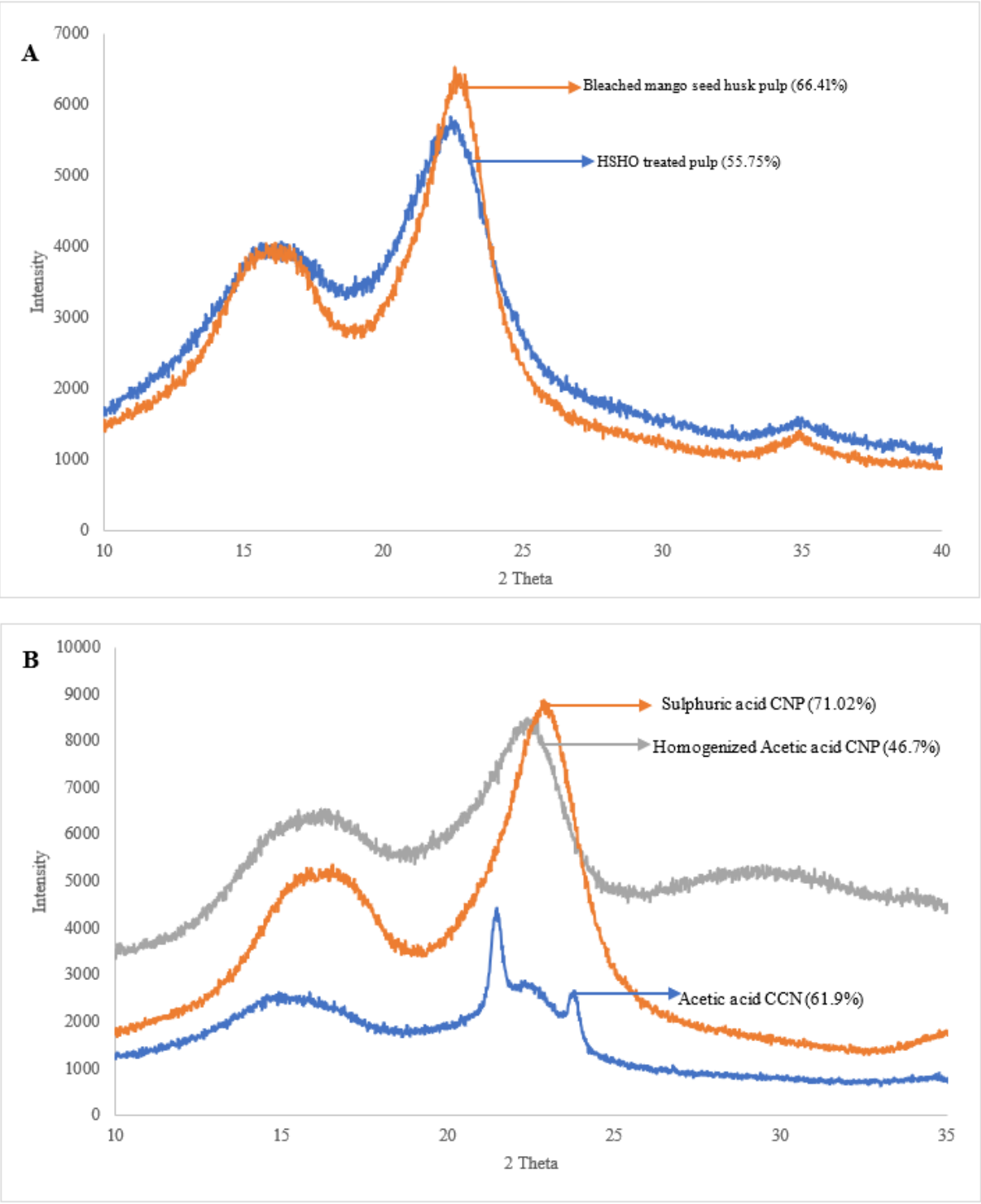

Figure 6.8: X-ray diffractograms of unbleached organosolv-treated mango seed husk, bleached mango seed husk, acetic acid nanocellulose, homogenized acetic acid nanocellulose, and sulfuric acid nanocellulose.

6.10.6. Thermal stability of starting material and cellulose nanocrystals

The thermal stability of CNPs is among the many properties that influence its field of application, especially as reinforcement agents in thermosetting [166]. The thermal stability of the UMP, ASCN, SCNP, and HSCN is illustrated in Figure 6.9. All the samples experienced

about 8% weight loss at 100 ºC due to moisture, and loosely bound water [419]. The onset thermal degradation temperature (T_{onst}) of SCNP and HSCN was lower than that of UMP, which is in agreement with reported literature values [97]. The increased amorphous cellulose region (reduced crystallinity) during homogenization reduced thermal degradation temperature for HSCN while sulfate groups from sulfuric acid esterification promote thermal degradation as observed in most literature [51], [502]. Moreover, the reduction of particle size of CNPs due to hydrolysis of amorphous components could increase the surface area for thermal degradation [25]. The maximum degradation temperature (T_{max}) of the CNPs reduced in the order ASCN > HSCN > SCNP. Of all the CNPs produced, the ASCN exhibited the highest stability with the onset and maximum degradation temperatures of 263 ºC and 352.1 ºC respectively.

The removal of amorphous components of hemicellulose and lignin in addition to disordered cellulose could have caused the better thermal stability of the ASCN. Additionally, the mild acetic acid treatment method used could have caused most of the intermolecular hydrogen bonding to remain intact. Also, the replacement of OH^- groups with bulky acetyl groups contributed to the CNP stability at high temperatures [25]. Chen et al. [419] have reported a similar trend for CNPs from commercial α-cellulose. The higher T_{max} for ASCN is comparable to that (360 ºC and 356 ºC) of other organic acid-produced CNPs reported by Liu et al. [97] and Du et al. [51] for corn cob residue and bleached softwood Kraft pulp respectively. Although the thermal stability of HSCN was lower than UMP and ASCN, its T_{max} (333 ºC) was better than SCNP due to the acetyl groups on the CNP arising from acetylation by acetic acid [499]. Overall, the T_{onst} and T_{max} values indicate that solely producing CNPs with acetic acid results in nanoparticles with the best thermal properties, and the addition of homogenization slightly reduces the thermal stability by ≈5%. The UMP had a char reduction to 18.8%. The acetic acid treatment reduced the char yield to 16.3% whereas there was a slight increase to 18.3% because of homogenization. The lowest char yield (8.5%) observed for the sulfuric acid treatment was expected. The application of CNPs in biocomposite materials or thermoplastics is dependent on thermal stability as the general processing temperature of these polymers is more than 200 ºC [419]. From the results, both ASCN and HSCN presented onset thermal decomposition temperatures above 240 ºC, an indication that they could be appropriate for such applications.

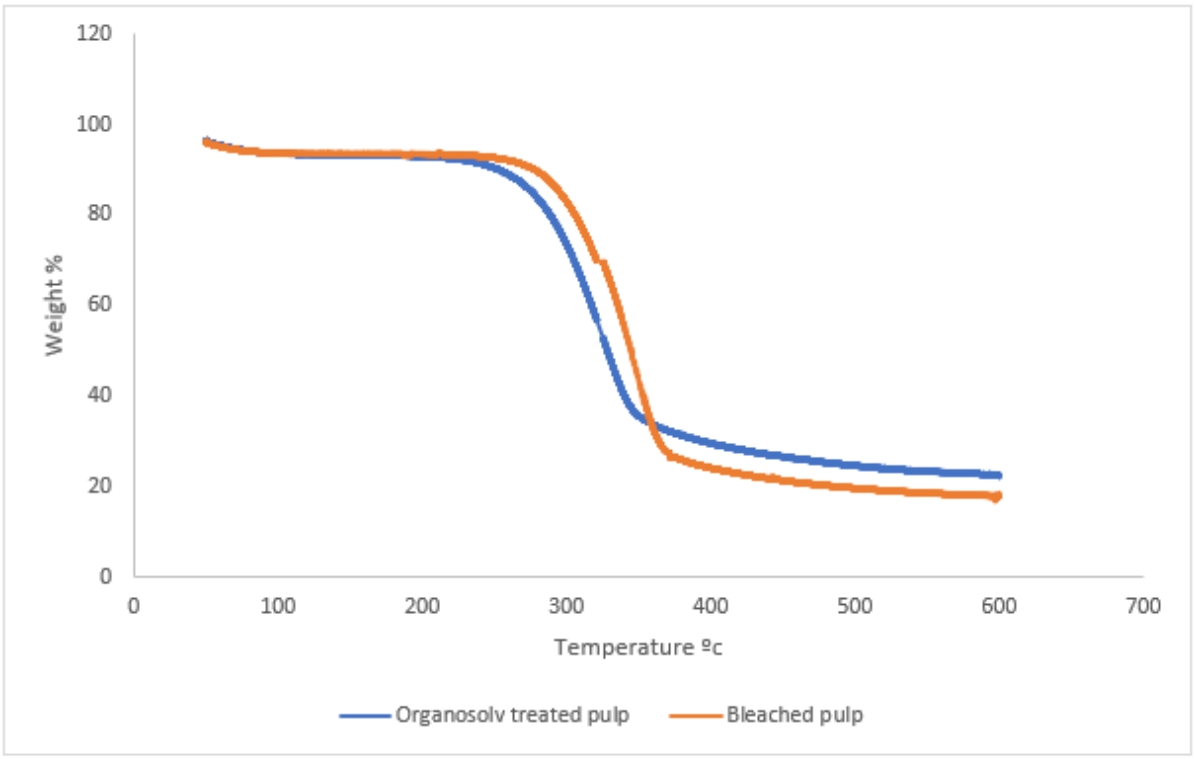

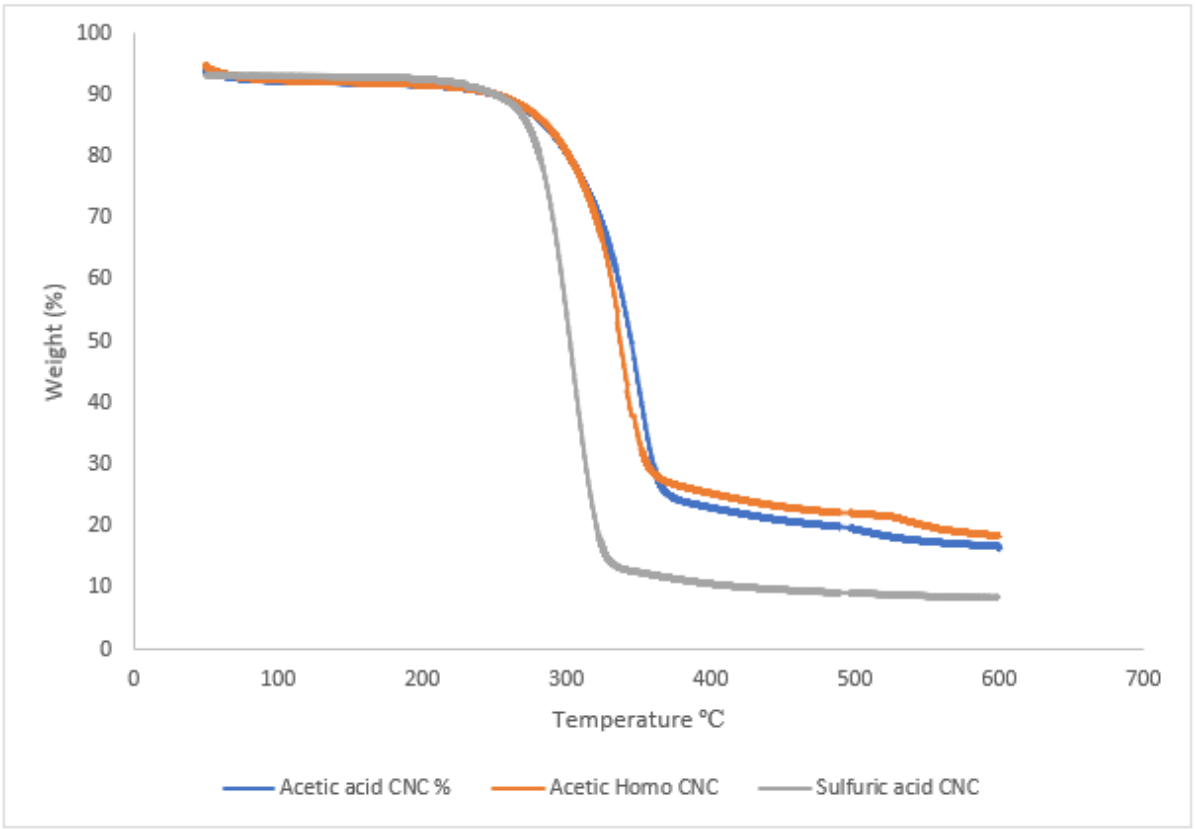

Figure 6.9: Thermogravimetric analysis of organosolv treated mango husk, bleached pulp, acetic acid cellulose nanocellulose, homogenized acetic acid cellulose nanocellulose, and sulfuric acid cellulose nanocellulose.

6.11. Conclusions

The mild acetic acid treatment with (HSCN) and without homogenization (ASCN) successfully produced CNPs from unbleached cellulose-rich pulp obtained from the multi-step sequential AP and HSHO pretreated mango seed husk. At a reaction time of 10 h and a solid-to-acid ratio of 1:40 g/mL, the ASCN produced had a DS of 1.83 and a yield of 17.68%. SEM analysis showed no significant difference in average particle size of the ASCN and HSCN and the morphologies were spherical with only one dimension. Contrarily, the sulphuric acid produced rod-like CNP with a diameter and length of 22.5 and 175.3 nm, respectively. In addition, XRD and FTIR showed that the MSH retained the cellulose I_a crystalline structure with all three CNP samples. The non-catalyzed acetic acid-based process resulted in CNPs with lower crystallinity compared with sulfuric acid-based CNPs due to the relatively low Crl of the starting material (UMP). The homogenization of ASCN resulted in comparable PDI, ζ-potential, DS, and thermal stability, when compared to the non-catalyzed acetic acid CNPs however with lower crystallinity. Conversely, the homogenization of ASCN improved the CNP yield but the Crl was compromised. In summary, this study showed that the solitary use of acetic acid provided a greener method for producing spherical acetylated nanocellulose that may not require further modifications before application in hydrophobic matrix juxtaposed to the sulphuric acid-based treatment process. However, environmental assessment is required.

7. General discussions, conclusions, and recommendations

7.1. Summary of study outcomes and implications

The study findings and general discussions for the MSK and MSH fractionation are detailed in sections 7.2.1 and 7.2.2 respectively. Likewise, the impacts of the pretreatment steps in the subsequent stages of the multi-step biorefinery scheme have been discussed in section 7.3.

7.1.1. Multi-step biorefinery route for mango seed kernel fractionation

Polyphenols, starch, and bioactive hemicellulose were recovered from the MSK based on the composition in Table 7.1 while ensuring minimal cellulose and lignin degradation in the residual solids. The selective extractions of the bioproducts present various challenges due to the differing optimal extraction conditions that could result in low yields, molecular weight, and purity (elaborated in section 4.5). Therefore, a multi-step biorefinery process that consisted of sequential organosolv extraction (OE), enzymatic hydrolysis (EH), and alkaline pretreatment (AP) was developed and optimized to fractionate the MSK into polyphenols, starch, and hemicellulose respectively while minimizing the degradation of cellulose and lignin in the solid residue for potential valorization into other bioproducts (Chapter 4). The effect of each extraction step on the subsequent stage of the multi-step biorefinery process was analyzed.

Table 7.1: Composition of untreated mango seed husk and kernel

Biomass	Cellulose (%)	Hemicellulose (%)	Lignin (%)	Starch (%)	Proteins (%)	Extractives (%)
Mango Husk	50.27	17.98	14.77	-	2.11	12.19
Mango Kernel	3.08	17.28	4.17	33.81	18.01	19.86

Step 1: In the first stage of the multi-step biorefinery scheme, free polyphenols were recovered from the MSK through optimized organosolv extraction (OE) process (ethanol concentration and temperature), aimed at maximizing the total polyphenol content (TPC) and antioxidant activity (AA) of the extract, and the cellulose, lignin, hemicellulose, and starch in the residual solids (Chapter 4, section 4.3.1). The best compromise among the OE conditions that resulted in maximum TPC (TPC= 95.21 mg GAE/g) and AA (AA= 84.69%) of extract and maximum hemicellulose, cellulose, starch, and lignin retention in the solid residue were 64.99% v/v ethanol and 54.18 °C (Chapter 4, section 4.5.2). The TPC of 95.21 mg GAE/g and AA of 84.69 observed in the present study were comparable with values (93.41–101.68 mg GAE and 85.58% respectively) in the literature [135], [235], although the optimal ethanol concentration was slightly higher in the present study (64.99% vs 50%). The higher ethanol concentration could be attributed to the differing present study's additional objective whereby the residual solid substrates (cellulose, lignin, hemicellulose, and starch) retention was taken into consideration for further valorization which was not considered by other authors [135], [235]. The higher ethanol concentration retained the residual solid components because of their low reaction rates at the conditions investigated. The cost implications of the higher ethanol concentrations versus the economic benefits that could be derived from the retained solid components should, however, be investigated to establish the actual economic benefits. The removal of the free polyphenol enriched the composition of the residual solids in terms of cellulose, hemicellulose, lignin, and starch (section 4.3, Table 4.2).

Components such as polyphenols obstruct the accessibility of the pretreatment chemicals and enzymes to the fractionate lignocellulosic biomass [238]. Thus, the OE process for free polyphenols is an important step for reducing the biomass resistance and enriching the biomass components for the subsequent fractionation stages in the multi-step biorefinery process. The percentage cellulose, hemicellulose, lignin, starch, and proteins retained in the solid residue were 98.05%, 93.91%, 97.84%, 92.04%, and 91.17% respectively indicating minimal losses of these components and minimal impact of the treatment process on their degradation (Chapter 4, section 4.5.3). In conclusion, compared to the literature reports of ≥20% losses for the total solid residue's components, the <10% losses obtained for the total MSK solid residue (cellulose, hemicellulose, lignin, and starch) implies the optimized process was effective for achieving part of the study's objective of obtaining an extract with TPC ≥90 mg GAE/g biomass with AA ≥80% whiles retaining ≥80% of the other biomass components in the residue for further fractionation and valorization (Objective 1, section 2.16.2).

Step 2: In the second stage of the multi-step process (i.e., after the OE process above), the recovered OE solids were subjected to an enzymatic treatment to remove >90% starch while retaining ≥ 80 cellulose, ≥80% hemicellulose, and ≥80% lignin in the residual solids for further fractionation (Chapter 4, section 4.4.3). The applied enzymatic hydrolysis (EH) resulted in more than 96% starch removal from the OE solids as simple sugars for potential application in bioethanol production. The 96% starch removal indicates the effectiveness of the EH treatment step in the multi-step biorefinery process. The efficiency of this treatment step compares well with the reported 100% starch removal in the literature [69]. It was further showed that, relative to the initial composition of the starting biomass (i.e., the OE solids), 97.68%, 83.82%, and 99.75% of the cellulose, hemicellulose, and lignin respectively were retained in the solids after the EH (Chapter 4, section 4.5.3) suggesting that these components were minimally disrupted by the treatment process. Enzymes are known to be substrate-specific and thus hydrolyze the starch while causing minimal depolymerization and dissolution of other biomass components [82]. The 83.82% hemicellulose retention was below the reported 98% for destarched wheat bran which could be attributed to hemicellulose dissolution during the starch gelatinization process which required hot water application [69]. Various studies have reported on similar extraction of some hemicellulose polysaccharides such as xyloglucan in water-based extractions [192], [516]. Thus, although EH was targeted towards starch removal, it was not selective enough and resulted in other component removals. The EH could therefore be optimized to ensure favorable conditions for both starch removal and hemicellulose retention in the solid residue. In conclusion, the >96% starch removal in addition to the retention of >80% of the cellulose, hemicellulose, and lignin compositions in the residual solids (Chapter 4, section 4.5.3) suggest that the treatment step was efficient in starch removal with minimal impact on the other components. This implies the referred MSK components could be obtained in good yield and quality (purity, molecular weight, etc.) using appropriate treatment processes in a stepwise manner.

Step 3: Following the sequential OE and EH, the resultant solid residue (destarched MSK solids) was alkaline pretreated (AP) to extract the hemicellulose together with the bound polyphenols which yield a bioactive hemicellulose polymer with antioxidant potential [261]. Literature on the recovery of the free polyphenols from MSK is well established, whereas data on the bound polyphenols is limited [81], [245]. The AP conditions were therefore optimized such that ≥50% yields of the bioactive hemicellulose extract having high bioactivity potential and low lignin contents (i.e., high purity) could be recovered while retaining maximum solid

substrates (≥80% cellulose and ≥80% lignin) composition in the residual solids (Objective 1; Chapter 4, section 4.5.2.1). The optimum AP conditions were found to be 1.07 M NaOH, 44 ºC, and 2.16 h, which resulted in a 55.13% hemicellulose dissolution from the biomass (Table 7.3), with 53.68% recovery attributed to potential losses in the downstream processing such as washing. The bioactive hemicellulose purity was 78.23%, having lignin contents of 6.24%. The 55% hemicellulose dissolution with a purity of 78.23% was higher compared to the 36.98% and 47.6% respectively reported for destarched wheat bran hemicellulose obtained under much higher optimal temperature (68.28 ºC) but with the application of lower (1.27 wt%) NaOH concentration. In addition, the lignin content of hemicellulose extract (6.24%) was far below the 19.5% and 17.5% reported in the literature for destarched wheat bran hemicellulose which could be due to differences such as the starting material composition [69], [238], [517]. The TPC, AA, and *Mw* of the bioactive hemicellulose extract were 34.96 mg GAE/g, 55.05%, and 108163 g/mol respectively (Chapter 4, section 4.5.2). The 55% AA falls within the reported 48–80% for bioactive hemicellulose [282]. From Table 7.3, less than 60% hemicellulose was recovered after the multi-step sequential OE, EH, and AP process, thus, other techniques such as pressure reactors may be explored for higher recoveries of hemicellulose from MSK using the AP process [238], [241]. Relative to the composition of the destarched solids, the cellulose, and lignin retention in the residual solids after AP was 92.20% and 93.37% respectively corresponding to 88.31% and 91.13% of the untreated biomass compositions (Chapter 4, Figure 4.5). Thus, the collective impact of the various pretreatment steps (OE, EH, and AP) in the multi-step biorefinery was minimal on these components' degradation. In conclusion, the developed novel multi-step biorefinery process for MSK could preserve the properties (TPC, AA, and *Mw*) of the free polyphenols and bioactive hemicellulose, remove >95% starch (in the form of simple sugars) and retain >80% lignin and >80% cellulose in the residual solids for valorization into other products. The recovery of multi-products from the MSK feedstock through the sequential optimized OE, EH and AP process revealed potentials for diversified product streams, towards sustainable integrated MSK biorefinery schemes juxtaposed to the single products recoveries reported in the literature with further discard of residual solids, thus, achieving the study's objective 1. FTIR analysis confirmed the effectiveness of the individual treatment steps on the subsequent stages of the process (Chapter 4, section 4.6). There was a slight increment in the intensities of peaks associated with cellulose, hemicellulose and lignin after the OE compared to their almost absence in the untreated MSK, an indication of the removal of polyphenols. Further EH increased the intensities of peaks associated with particularly hemicellulose and lignin. After

the AP, the most prominent peak observed was associated with lignin, showing that the process was less severe to remove the lignin. SEM images (Chapter 4, section 4.6) further confirmed the gradual loosening of the MSK structure after each treatment step, confirming the results of the compositional analysis (Chapter 4, section 4.5.2.2).

7.1.2. Multi-step biorefinery process for fractionating mango seed husk

With respect to the MSH, due to the lower starch and polyphenol contents (not recorded, Table 7.1), they were excluded from the target products, thus, the requisite OE and EH (respectively) were not considered in the MSH multi-step biorefineries. Consequently, a multi-step biorefinery process consisting of a sequential alkaline pretreatment (Chapter 5, section 5.1) and homogenization-assisted organosolv (HSHO) (Chapter 5, section 5.14) pretreatment was developed and optimized to fractionate the MSH into the respective products [hemicellulose (xylan/xyloglucan complexes for potential application in biocomposite films), lignin (for phenol-formaldehyde resin production), and cellulose-rich solids (for nanocellulose production)], while maintaining the properties of the product and retaining ≥80% cellulose, ≥80% hemicellulose and ≥80% lignin in the residual solids after each step of the process. The influence of each extraction step on the properties of products in the subsequent stages of the multi-step biorefinery process was analyzed. Details of the processes are discussed in the following sections.

Step 1: The first stage of the MSH multi-step biorefinery scheme involved an optimized AP to maximize hemicellulose recovery with lower xyloglucan/xylan ratio, lower lignin, and uronic acid contents (enhancing purity), to obtain properties (purity, molecular weight, composition) for potential application in the development of self-supporting thermally stable film for food packaging while retaining ≥80% cellulose and ≥80% lignin in the solid residue for further fractionation and valorization (Chapter 5, section 5.10). The AP process conditions influenced the solubility of the different hemicellulose polysaccharides (xyloglucan and xylan), lignin, and uronic acids due to their structural variations, response to process conditions, and differing optimal extraction conditions, which further influenced the functional property (thermal stability) of the hemicellulose extract (Chapter 5, section 5.8.3). An increment in the AP conditions favored xylan dissolution and vice versa for the xyloglucan (Section 5.8.2, Table 5.2). Previous studies on hemicellulose extraction for biocomposite film development focused mainly on thermally labile xylan based brittle films, where proposed solutions to the inherent limitations of thermally labile brittle film formation included strategies such as the incorporation of plasticizers (e.g., sorbitol, and glycerol) and higher molecular weight polymers

[42], [271], [295]. The strategy in this study involved optimizing the AP process conditions such that the obtained hemicellulose extract (with yields >50%) comprised of lower XGN/XLN ratios, lower lignin, and uronic acid contents (high purity), and higher *Mw*. This strategy is important, particularly when aiming for a hemicellulose extract for the development of thermally stable self-supporting films. It was shown that hemicellulose extract with a XGN/XLN ratio of 0.13, and lignin and uronic acids contents of ≈16 % and 12% respectively could be recovered at the optimal AP conditions (1.92 M, 86 ºC, and 3.84 h), which was able to form thermally stable self-supporting biocomposite film juxtaposed to the brittle and thermally labile xylan-based films [42], [43]. The presence of xyloglucan in any ratio of the extract was found to improve the thermal stability of the films (Chapter 5, section 5.10). The hemicellulose extract with a molecular weight of ≈70189 g/mol had a purity of 79.25% (Table 7.2). The high hemicellulose purity compares well with literature values (≥80% purity), while its *Mw* of 70189 g/mol is greater than 27235 g/mol reported for xylan used in biocomposite film development. The higher *Mw* could be associated with the presence of the xyloglucan moiety in the extract [64], [178], [299], [402].

Table 7.2: Recovered bioproduct yields and properties

Product	Yield [%]	Purity [%]	TPC mg GAE/g	AA [%]	Molecular weight [g/mol]	Crystallinity index [%]	Tmax [ºC]	Surface morphology
MSK								
Free polyphenols	-	-	95.21	84.69	-	-	-	-
Starch	96	-			-	-	-	-
Bioactive hemicellulose	53.13	78.23	34.96	55.05	108163	-	-	-
MSH								
Hemicellulose	46.24	79.25	-	-	70189	-	330	-
Co-lignin	3.26	43.83	-	-		-		-
HSHO lignin	70.23	96.18	-	-	3247	-	298	-
Non-assisted organosolv lignin	68.58	94.74	-	-	-	-	-	-
Cellulose		77.84	-	-	-	-	-	-
FCNP	63.99	-	-	-	-	66.40	361	Spherical
ASCN	17.68	-	-	-	-	61.9	352	Spherical
SCNP	28.34	-	-	-	-	71.02	309	Rod-like
HSCN	77.70	-	-	-	-	46.7	333	Spherical

[a]FCNP: Spherical formic acid nanocellulose, ASCN= Acetic acid nanocellulose, SCNP= sulphuric acid nanocellulose, HSCN= Homogenized acetic acid nanocellulose, Crl= crystallinity index, TPC=Total polyphenol content, AA=Antioxidant activity, Tmax=Maximum degradation temperature

The hemicellulose extract from the MSH demonstrates potential benefits including (i) the elimination of the cost associated with high applications of additives such as plasticizers in the xylan-based composite film development [46], [295], (ii) the reported risk from the potential migration of the unbound lower molecular weight plasticizers (i.e. the additives in the xylan-based films) into packaged food products [295], [299] could be mitigated through the use of the bio-based XGN/XLN packaging films proposed in the present study. Thus, compared to raw materials with no xyloglucan contents such as wheat straw and sugarcane bagasse [69], [83], manipulating the AP process conditions for the hemicellulose extraction from the MSH could yield varying hemicellulose compositions and resultant properties suitable for diverse applications such as thermally stable biocomposite film development. Part of objective 2 was to extract 50% or more of the actual hemicellulose in the raw materials while retaining ≥80% residual cellulose and lignin for subsequent fractionation (Chapter 2, section 2.16). Per the study outcome, at the identified optimized AP extraction conditions, 56.06% of the hemicellulose in the MSH was extracted, while a total recovery of 48.84% (i.e., 46.24% in hemicellulose extract and 2.24% in co-extracted lignin) was achieved (Table 7.2). Approximately 10% hemicellulose was lost due to possible downstream processing of washing, and product transfers.

Although the objective of the AP process was mainly targeted at selective hemicellulose extraction, crude lignin was recovered as a co-product now referred to as co-lignin (Table 7.2) after hemicellulose precipitation, implying the treatment process conditions were not selective enough. Specifically, a co-lignin yield of 3.26% having a purity of 43.83% was recovered (Table 7.2). The co-lignin was mainly contaminated with 36.63% hemicellulose, which accounts for 2.26% of the original hemicellulose in the MSH. The yield of the co-lignin was far lower than the 44.8% reported in the literature [69], although very high hemicellulose impurity (36.63%) was recorded vs the less than 10% reported in the literature [69]. Since lignin contributes to biomass resistance to enzymes and chemicals, the removal of a portion of the lignin during the AP of the MSH implies a reduction of the recalcitrance in the residual solids, leading to potentially less severe condition requirements in the subsequent fractionation stages [336]. At the optimized AP conditions, the cellulose, and lignin compositions in the residual solids improved (50.27% vs. 57.08% cellulose; 14.77% vs 19.13% lignin) when compared to the untreated biomass indicating the success in the removal of hemicellulose (Chapter 5, section 5.10.1). Less than 5% of original cellulose in the MSH was a loss from the biomass, an indication of the retention of more than 95% of original biomass cellulose (Table 7.4). The AP was, therefore, less severe towards cellulose and hardly disrupted it. This

could be attributed to the high selectivity of alkali reagents towards hemicellulose and lignin, and vice versa for cellulose under the considered operation conditions [241]. In conclusion, an optimized condition that favor the recovery of hemicellulose extracts with properties (XGN/XLN ratio, lignin, and uronic acids contents, and *Mw*) that suit thermally stable films formation have been obtained for MSH. Moreover, compared to the ≥20% residual solid substrate losses reported in the literature for the single hemicellulose extraction schemes, the <10% loss indicates that the optimal AP conditions had minimal degradation effect on the solid components (objective 2, section 2.16.2 and Table 7.4).

Step 2: The second step in the MSH multi-step biorefinery scheme involved subjecting the resultant solid residue obtained from the AP process to a novel HSHO treatment to extract lignin and recover cellulose-rich solids (with high cellulose purity and Crl for CNP production). Firstly, the effect of the HSHO process conditions of ethanol concentration (50–70%), temperature (130–150 ºC), and homogenizing time (10–20 min) on the fractionation of AP MSH (lignin solubilization and purity, cellulose, and hemicellulose contents of residue) was investigated followed by optimizing the process conditions for maximum lignin solubilization and purity, and maximum cellulose content (≥70%), and minimum hemicellulose content (≤10%) in the solid residue (i.e., cellulose recovery ≥80%, cellulose content ≥70% and Crl ≥55% for potential application in CNP production). The HSHO process conditions (ethanol concentration, temperature, and high shear homogenization time) showed effectiveness in fragmenting and dissolving lignin while enriching the cellulose content in the residual solids (Chapter 5, section 5.18.2). At the optimized HSHO process conditions (60% ethanol concentration, 15 min homogenization, and 148.41 ºC), >70% lignin dissolution with high purity (≈96%), plus cellulose-rich fibers with a purity of 77%, <10% lignin, and <12% hemicellulose was recovered. The HSHO process presents an advantage as the recovered lignin had a purity >95% with less than 0.15% sulfur and nitrogen contents making it suitable for phenol-formaldehyde resin production contrary to the conventional Kraft/lignosulphonate processes that present over 10% sulfur and ash content and with 1–2% aliphatic thiol groups respectively [201], [239], [465]. The optimized temperature of 148.41 ºC is lower than that of the non-assisted OP process of 200 ºC (Chapter 5, section 5.18.3). Likewise, the optimum ethanol concentration and temperature were below the reported 65% and 165 ºC in the literature for which the authors reported lower lignin solubilization (≈43%). Similarly, the 96% purity compares well with the 93% reported in the literature [85]. In addition, the cellulose content (>77%) in the solid residue is higher than the 69.07% and 72% obtained at much higher

temperatures (183 ºC and 200ºC respectively) in the literature [68], [85]. The lower temperature requirement could be attributed to both the mechanical effect of HSH and the previous AP for hemicellulose extraction (Chapter 5, section 5.11) in the multi-step process which improved the surface area and pore volume and reduced the resistance of the biomass for effective solvent penetration, fragmentation, and dissolution of lignin (Chapter 5, section 5.18.3).

The cellulose content of the recovered solids improved to 77% vs 50.27% and 57.08% for the untreated and AP treated MSH respectively (Chapter 5). This translated into an increase in the crystallinity index from 44% (untreated) to 58.3% (AP treated) and then to ≈58.5% (HSHO), thus Crl increased after each step of the process (Table 7.2). The 58.5% Crl is higher than the minimum value (57%) [37] required to be applied in CNP production (Chapter 2, section 2.4.2). The cellulose content of the MSH, after the multi-step sequential AP and HSHO process, of ≈77% (Table 7.2), falls within the reported range of 60.7–91.8% in the literature for CNP production [40], [98], [157], [226]. Concerning the hemicellulose and lignin content after the multi-step sequential AP and HSHO process, the values of <12 and <10% respectively in the solids fall within the 0.5–26%, and <0.1–16% respectively allowed for CNP production [25], [98], [157]. Furthermore, cellulose-rich pulp with diameters of <1–10 µm (evident in the SEM images, section 5.20) were obtained. Overall, the multi-step biorefinery scheme resulted in the recovery of ≈80% cellulose in MSH, suggesting that ≈20% cellulose was lost in the process (Table 7.4) which is due to solids stuck in the homogenizer and downstream washing and product transfer processes. Although the cellulose loss was significant, the 80% recovery falls within the reports of 70.9–97% for single pretreatment processes [213], [319]. The developed HSHO process, therefore, enhances the beneficial exploitation of the mango seed waste into high-value products. For instance, the derived high-purity lignin from the HSHO process could potentially be applied in higher end-uses such as plasticizers, and phenol formaldehyde resins, while the cellulose-rich pulp could be valorized into high-value bioproducts such as nanocellulose. Thus, the proposed HSHO process in the present study demonstrates potentials for minimizing product losses and enhanced qualities versus the conventional non-assisted process (organosolv only, Kraft, and sulfite pulping), thus may potentially benefit the process economics.

Table 7.3: Mass balance for fractionation of mango seed kernel

Organosolv extraction				
Composition	Untreated MSK	Hydrolysate	OE MSK	% Recovery
Cellulose, g/100g	3.08	n/r	3.02	98.05*
Hemicellulose g/100g	17.58	n/r	16.51	93.91*
Lignin, g/100g	4.17	n/r	4.08	97.84*
Starch, g/100g	33.81	n/r	31.12	92.04*
Protein, g/100g	18.01	n/r	16.42	91.17*
Extractives, g/100g	19.86	n/r	1.33	6.70*
Ash, g/100g	2.29	n/r	0.21	9.17*
Others, g/100g	1.20	n/r	-	-
Total, g/100g	100	-	72.23	72.23
Enzymatic treatment				
	OE MSK	Hydrolysate	Destarched MSK	% Recovery
Cellulose, g/100g	4.16	n/r	4.06	97.60*
Hemicellulose g/100g	22.71	n/r	19.04	83.83*
Lignin, g/100g	5.61	n/r	5.60	99.82*
Starch, g/100g	42.81	41.41	1.39	99.98**
Protein, g/100g	22.59	3.55	18.67	98.36**
Extractives, g/100g	1.83	n/r	0.61	33.61*
Ash, g/100g	0.29	n/r	0.04	13.84*
Others, g/100g	-	-	-	-
Total, g/100g	100	44.96	49.19	94.15
Alkaline pretreatment				
	Destarched MSK	Hydrolysate	AP MSK	% Recovery
Cellulose, g/100g	8.22	n/r	7.58	92.21*
Hemicellulose g/100g	38.55	21.25	17.30	99.89**
Lignin, g/100g	11.34	0.25	10.59	95.59**
Starch, g/100g	2.84	n/r	0.06	2.11*
Protein, g/100g	37.80	12.04	22.48	91.32**
Extractives, g/100g	1.25	n/r	0.10	8.00**
Ash, g/100g	-	-	-	-
Others, g/100g	-	-	-	-
Total, g/100g	100	33.50	58.11	91.61

MSK= mango seed kernel, n/r= no recorded, AP= Alkaline pretreatment, OE= Organosolv extraction, *=based on only solid stream, **=based on solid+liquid streams

Table 7.4: Mass balance for fractionation of mango seed husk

Alkaline pretreatment				
Composition	Untreated MSH	Hydrolysate	AP MSH	% Recovery
Cellulose, g/100g	50.27	-	47.82	95.13*
Hemicellulose g/100g	17.98	8.7	7.90	92.32**
Lignin, g/100g	14.77	2.3	16.03	124.10**
Protein, g/100g	2.11	0.82	0.96	84.36**
Extractives, g/100g	12.19	n/r	10.50	86.14*
Ash, g/100g	0.8	0.11	0.27	47.50**
Others, g/100g	1.88	n/r	0.30	15.95*
Total, g/100g	100	11.23	83.78	95.01
Organosolv pretreatment				
	AP MSH	Hydrolysate	HSHO treated MSK	% Recovery
Cellulose, g/100g	57.08	-	47.59	83.37*
Hemicellulose g/100g	9.43	0.10	7.72	83.01**
Lignin, g/100g	19.13	15.00	4.74	103.19**
Protein, g/100g	1.15	n/r	0.39	33.91*
Extractives, g/100g	10.50	n/r	9.43	89.81*
Ash, g/100g	0.27	0.01	0.24	92.59**
Others, g/100g	2.44	n/r	0.19	7.79*
Total, g/100g	100	15.11	70.30	85.41

MSH= mango seed kernel, n/r= no recorded, AP= Alkaline pretreatment, HSHO= Homogenization assisted organosolv pretreatment, *=based on only solid stream, **=based on solid+liquid streams

7.2. Nanocellulose production

7.2.1. The formic acid-based treatment process for cellulose nanoparticles production

Following the multi-step AP and HSHO pretreatments, the recovered cellulose-rich pulp was used as a starting material to produce nanocellulose using non-catalyzed formic acid-based treatment as an alternative to conventional sulphuric acid-based process. The effect of the FA treatment conditions of acid-to-pulp ratio (20–40 mL/g) and reaction time (6–10 h) on the yield, average particle size, ζ-potential, polydispersity, formate content, and crystallinity index of the CNPs were investigated and the conditions further optimized to maximize the CNP yield and properties. Owing to the weaker acidity of organic acids, challenges of the inability to convert the high crystalline cellulose-rich pulp to the CNPs have been reported in several studies [51], [97], [352]. The addition of inorganic acids (HCl, H_2SO_4) or metal catalysts

($FeCl_3$) has been shown to enhance the CNPs conversions for bleached cellulose pulp [51], [97]. However, due to the synergistic effect of the preceding multi-step pretreatment processes, a cellulose-rich material with Crl ≈55.75% was obtained vs the 66.41% for the bleached cellulose pulp. Lower crystallinity results in increased OH^- content, and cellulose reactivity [169]. Therefore due to the comparatively low crystallinity, plus the individualized cellulose fibers with particle diameters of <1–10 µm, it was hypothesized that the obtained cellulose-rich pulp could be amenable to organic acid treatment for the CNP production without the need for catalysts (Chapter 6, section 6.3). Consequenlty, an experimental work was carried out to establish the feasibility of the hypothesis or otherwise, thus, involved analysis of the effect of the preceding multi-step biorefinery process (that generated the cellulose rich pulp starting material for the CNP production) on the formation of the CNP and its properties using the recoverable organic acids, plus identifying the optimal process conditions (acid-to pulp ratio and reaction time) that favor the desired CNP yields and properties (particle size, crystallinity, formate content, etc.) (Chapter 6, section 6.3.1).

The non-catalyzed FA-based process yielded ≈64% CNPs (Table 7.2) with high thermal stability (361ºC) at optimal conditions of acid-to-pulp ratio of 1:30 g/mL and operation time of 8 h. The referred CNP yield and thermal stability are relatively high versus the reports for the conventional sulphuric acid-based process (i.e., <30% and 290ºC respectively) partly due to the preceding multi-step pretreatment processes (Chapter 6, sections 6.3.3–6.3.4). CNPs produced from highly crystalline bleached cellulose pulp will result in difficult penetration of hydrolyzing ions due to the compact crystalline cellulose structure with fewer hydroxyl ions for reaction. Thus, the multi-step sequential AP and HSHO pretreated cellulose-rich pulp could serve as a good material for CNP production using recoverable and reusable organic acids. The optimal CNP yield is within the range of 41.94% and 79.55% reported in the literature for catalyzed formic acid-based CNPs [40], [51]. In addition, the morphology of the CNP from the proposed FA-based process was spherical vs the whisker shape for the conventional sulphuric acid process (Chapter 6, section 6.3.4), making the former suitable for high temperature and sensitive applications (such as cosmetics, drug delivery, biomedicine, and food packaging) [169], [505]. Therefore, the use of different pretreatment processes could lead to nanocellulose with different properties (particles sizes, morphology, and crystallinity index) [34].

The results further indicate that using the referred multi-step biorefinery process, followed by the organic acid (formic and acetic) treatment could be a more promising and sustainable route for obtaining CNPs with hydrophobic properties (for application in a hydrophobic matrix) as opposed to the post-modification of sulphuric acid-based CNPs for

similar applications. This could save cost and operational time and add more value to the waste. Current studies are focused on developing environmentally sustainable, highly efficient, and low-cost methods for CNP production [25]. The FA could be recovered and reused, therefore contributing to a potential reduction in production costs associated with effluent treatments and related environmental impacts. While the proposed non-catalyzed FA process demonstrate potentials for producing thermally stable CNPs, as well as potentials for economic benefits from the solvent recoverability, the requirement of long reaction times versus the sulphuric acid process (8 h vs 1 h, section 6.3.3 and Table 7.5), due to the weaker acidity of the FA, may impact the economics relative to the production time and inputs (e.g., energy). Implementation considerations of the proposed non-catalyzed FA-based process will, thus, require establishing the true economic benefits. Therefore, selecting appropriate individual pretreatment methods, and the appropriate integration sequence into multi-step biorefinery process and optimizing the process conditions showed potentials for generating multiple bioproducts (i.e., hemicellulose, lignin) and the cellulose-rich pulp having composition and Crl (>55%) favorable for milder organic acid-based (formic and acetic acid) CNP production.

7.2.2. Acetic acid-based treatment for nanocellulose production from cellulose-rich fibers obtained via a multi-step biorefinery process

Formic acid could result in CNPs when applied on the unbleached cellulose-rich pulp obtained via the multi-step sequential AP and HSHO process. However, formic acid is more corrosive and toxic than other acids such as acetic acid [518]. Acetic acid has been reported promising for acetylation effect when applied with acetic anhydride and sulphuric acid [509]. Hence, the potential for the mild acetic acid treatment for producing the CNPs from the referred feedstock was analyzed (Chapter 6, section 6.7). The analysis involved the determination of the influence of acid-to-pulp ratio and reaction time on the CNPs production and the resultant product properties (degree of acetylation, zeta potential, particle size, polydispersity index, etc.). The results showed that the application of a non-catalyzed acetic acid treatment could be promising for the CNPs that have hydrophobic properties (high degree of acetylation; DS= ≈1.8) versus the conventional sulphuric acid-based process (Chapter 6, section 6.11.2) for hydrophilic sulfated CNPs [97]. Moreover, for diverse applications such as hydrophobic biocomposite matrix, the sulphuric acid-based CNPs are hydrophilic and have lower thermal stability (351 ºC vs 290 ºC), thus require further modification to improve both thermal stability and hydrophobicity, often achieved through chemical or enzyme treatments [376], [510]. The simultaneous conversion and acetylation of cellulose into acetylated CNPs in a one-pot non-

catalyzed organic acid-based process has been minimally explored [25], [51]. The feasibility of the non-catalyzed acetic acid-based process to produce the functionalized CNPs was found to be highly dependent on the preceding pretreatment processes (Chapter 6, section 6.11.2). The preceding multi-step pretreatment/fractionation processes of the MSH feedstock (i.e. multi-step sequential AP and HSHO process) increased the surface area and pore volume of the biomass in addition to generating individual cellulose fibers with particle diameter ranging from <1–10 µm for effective solvent penetration [14]. Thus, the preceding pretreatment processes impact the required CNP process conditions and invariably the production cost for both the acetic and formic acid-based treatment processes. Nevertheless, the CNP yields from the acetic acid-based process were relatively low compared to the sulphuric acid or formic acid-based processes (17% vs 28% or 64%, respectively) (Table 7.2). In the literature, various mechanical treatments (such as ultrasonication) have been reported to improve the yield of CNPs [168], [492]. Thus, the potential of high shear homogenization (HSH) treatment for increasing the yield was assessed, which revealed potentials for product yield improvement (77.7% vs 17.68 for HSH assisted vs non-assisted). However, the CNP crystallinity was compromised (46.7% vs 61.9% for HSH vs non-assessed) due to the destruction of portions of the crystalline cellulose.

Table 7.5: Reaction conditions for nanocellulose production

Product	Treatment conditions			
	Temperature [ºC]	Pulp-to-solvent ratio [g/mL]	Time [h]	Homogenization [min]
FCNP	95	1:30	8	-
ASNC	110	1:40	10	-
SCNP	45	1:30	1	-
HSCN	110	1:30	10	15

FCNP=Formic acid nanocellulose, ASCN=Acetic acid-based nanocellulose, SCNP=Sulphuric acid-based nanocellulose, HSCN=Acetic acid +homogenization based nanocellulose

The results indicated that the CNPs from both formic and acetic acid treatments had similar crystallinity, thermal stability, and morphology (Chapter 6), although the formic acid-based treatment performed slightly better in terms of CNP yield, thermal stability, and CrI (Chapter 6, section 6.1 and Table 7.2). However, both treatment processes resulted in improved CNP crystallinity and thermal stability when compared to the starting material (cellulose-rich

fibers). Although the sulphuric acid-based treatment resulted in minimal cellulose deformation (a rod-like shape with high CrI), the CNP thermal stability was lower compared to the alternative treatment processes (acetic and formic acid-based treatment) (Chapter 6) due to the introduced sulfate groups. The formic acid-based treatment, in addition, resulted in a CNP with CrI (66.4%), which was within reports for acetic and sulphuric acid-based processes (61.9 and 71.02%). Consequently, the formic acid-based treatment process can result in higher yields of thermally stable CNPs. Overall, the formic acid-based treatment process performed better in terms of yield and thermal stability than the acetic acid and sulphuric acid-based treatments. The recoverability of the acetic and formic acids serves as added advantage to save cost and time since cumbersome downstream processing of effluents encountered in sulphuric acid-based treatment may not be required. Moreover, the direct application of the CNPs in hydrophobic biocomposite without further modifications could improve the overall economics of the CNP production process and eliminate the cost associated with further modifications for the alternative processes. However, the longer reaction time requirement vs the conventional sulphuric acid (1 h vs 10 h, and 12 h) could imply more process inputs (e.g., energy) that could impact the process economics, which should be assessed to inform implementation decisions.

7.3. Conclusions

Multi-product biorefineries could be considered for integration into the mango fruit processing industries to potentially derive benefits such as reducing the environmental pollution and mitigation costs from the mango waste and increasing the number of products (both food and non-food) that could be recovered from a mango fruit biomass. In the present study, novel multi-step biorefinery schemes have been developed and optimized for the recovery of multi-products from the mango seed waste towards contributing to beneficial mango waste-based multi-products biorefineries. In relation to the MSK, multi-products of polyphenols, starch, bioactive hemicellulose, and solids with >80% cellulose and >80% lignin retentions were recovered via a novel multi-step biorefinery process consisting of sequential organosolv extraction, enzymatic hydrolysis, and alkaline pretreatment without compromising the quality of the bioproducts. The multi-step biorefinery scheme for MSK improved the overall product recoveries from the feedstock contrary to the single extraction processes.

In addition, the developed novel multi-step biorefinery scheme for the MSH valorization, involving sequential alkaline pretreatment (AP) and high shear homogenization assisted organosolv (HSHO) process, resulted in the recovery of hemicellulose, lignin, and cellulose-rich solids (for nanocellulose). Manipulating and optimizing the AP process

conditions facilitated the co-extraction of hemicellulose polysaccharides (xyloglucan and xylan) with lignin and uronic acids from the MSH, which show promises as a raw material for self-supporting hemicellulose-based film development. Additionally, the developed novel HSHO process yielded high purity and less-condensed lignin and highly accessible cellulose-rich fibers (for nanocellulose production) when applied on the AP MSH, compared to the products (lignin and cellulose) obtained from the conventional non-assisted OP process. The integration of high shear homogenization in the OP process led to less heat requirement (148 ºC) to achieve comparable lignin solubilization versus the non-assisted process's temperature (200 ºC). Thus, the developed HSHO process shows potential as an alternative process for the recovery of high purity less modified lignin and cellulose-rich fibers juxtaposed to the conventional non-assisted organosolv and Kraft processes that result in highly modified lignin. The multi-step sequential AP and HSHO process for MSH fractionation therefore is an effective treatment process to produce cellulose-rich pulp with improved cellulose purity (≈77%) and crystallinity index (58%), suitable to produce nanocellulose.

The cellulose-rich solids from the multi-step sequential AP and HSHO process were therefore used to produce nanocellulose via an optimized formic acid-based treatment. The optimized non-catalyzed formic acid-based treatment resulted in higher nanocellulose yields (>60%) with better thermal stability versus the conventional sulphuric acid-based nanocellulose (<30%) produced from the bleached cellulose-rich pulp. The morphology of the nanocellulose from the developed FA-based process was spherical versus rod-like for sulphuric acids CNPs thus, showing potentials for applications in highly sensitive areas such as biomedicine, cosmetics, and food packaging. The previous multi-step AP and HSHO pretreatment processes of the MSH feedstock (for recovery of hemicellulose, lignin, and cellulose-rich solids) highly contribute to the feasibility of the developed non-catalyzed FA-based process for the nanocellulose production. In addition, the thermal properties of the as-prepared FA-based nanocellulose were better than that of the sulphuric acid nanocellulose. Thus, the developed method provides a sustainable approach for large-scale production of thermally stable nanocellulose compared to the conventional sulphuric acid method associated with environmental and technical problems (e.g., highly corrosive, and toxic nature). On the other hand, assessment of potentials for using acetic acid to produce the nanocellulose, which could be more environmentally friendly versus the formic acid, proved technically feasible with similar nanocellulose properties, however, the formic acid-based process performed better in terms of yield (64% vs 17.86%), crystallinity (66.40 vs 61.9%) and thermal stability (361 vs 352 ºC). The integration of high shear homogenization post acetic acid treatment however

improved the nanocellulose yield by more than 70%, although the CNPs crystallinity was compromised. Thus, the findings contribute to strategic mango waste management schemes that could increase revenue and mitigate environmental burdens in the mango processing industry

7.4. Recommendations

Based on the findings, the following recommendations could be considered for implementation considerations.

(a) This study highlighted the potential of mango seed waste as a biorefinery feedstock. The proposed multi-step biorefinery schemes provide a platform for analyzing the holistic environmental impact of the integrated processing routes. It is recommended that the environmental impacts for the development of the multi-step biorefinery bioprocess in this study should be analyzed and compared to the total impact from the individualized conventional approaches for single product recoveries under study. In addition, process pilot and industrial scale-up with further techno-economic and life cycle assessment are required.

(b) The seed waste was separated into the husk and kernel before fractionation due to their structural features and chemical composition. Future studies could focus on combining the waste streams (husk and kernel) in the same biorefinery to determine the feasibility and product ranges and properties that could be obtained.

(c) The solids obtained after the multi-step sequential OE, EH and AP should be fractionated further into lignin and cellulose-rich material for valorization into valuable bioproducts like resin and nanocellulose for industrial application. This will increase the number of products obtained from the MSK and consequently the value of the mango seed waste.

(d) The developed multi-step biorefinery scheme could incorporate an ethanol production process as a side stream product from the glucose obtained after the destarching process prior to AP of MSK, which could improve the overall process economics.

References

[1] L. J. Jönsson and C. Martín, "Pretreatment of lignocellulose: Formation of inhibitory by-products and strategies for minimizing their effects," *Bioresource Technology*, vol. 199. Elsevier Ltd, pp. 103–112, 01-Jan-2016.

[2] D. Wei Kit Chin, S. Lim, Y. L. Pang, and M. K. Lam, "Fundamental review of organosolv pretreatment and its challenges in emerging consolidated bioprocessing," *Biofuels, Bioprod. Biorefining*, vol. 14, no. 4, pp. 808–829, 2020.

[3] G. Taylor, "Biofuels and the biorefinery concept," *Energy Policy*, vol. 36, no. 12, pp. 4406–4409, 2008.

[4] A. García, A. Gandini, J. Labidi, N. Belgacem, and J. Bras, "Industrial and crop wastes: A new source for nanocellulose biorefinery," *Ind. Crops Prod.*, vol. 93, pp. 26–38, 2016.

[5] Z. Zhou, F. Lei, P. Li, and J. Jiang, "Lignocellulosic biomass to biofuels and biochemicals: A comprehensive review with a focus on ethanol organosolv pretreatment technology," *Biotechnol. Bioeng.*, vol. 115, no. 11, pp. 2683–2702, 2018.

[6] S. Farzad, M. A. Mandegari, M. Guo, K. F. Haigh, N. Shah, and J. F. Görgens, "Multi-product biorefineries from lignocelluloses: A pathway to revitalisation of the sugar industry?," *Biotechnol. Biofuels*, vol. 10, no. 1, pp. 1–24, 2017.

[7] V. Galán Saúco, "Trends in world mango production and marketing," *Acta Hortic.*, no. 1183, pp. 351–364, 2017.

[8] C. Torres-León, R. Rojas, J. C. Contreras-Esquivel, L. Serna-Cock, R. E. Belmares-Cerda, and C. N. Aguilar, "Mango seed: Functional and nutritional properties," *Trends in Food Science and Technology*, vol. 55. pp. 109–117, 2016.

[9] J. F. Ekorong Akouan Anta, B. D. Marcelle, B. F. Siewe, and R. K. S. M. S., "Modelling and Optimization of Ultrasound Assisted Extraction of Polyphenols Using Response Surface Methodology," *Eur. J. Eng. Res. Sci.*, vol. 5, no. 9, pp. 1004–1012, 2020.

[10] S. Kittiphoom, "Utilization of mango seed," *Int. Food Res. J.*, vol. 19, no. 4, pp. 1325–1335, 2012.

[11] J. F. E. Akouan Anta, D. M. Biloa, and K. S. M. S. Raghavarao, "Optimization of Extraction Parameters of Polyphenols from Mango Seed Kernel through Response

Surface Methodology," *Eur. J. Eng. Res. Sci.*, vol. 5, no. 8, pp. 877–883, 2020.

[12] J. F. Ekorong Akouan Anta, P. D. Mbougueng, E. Durand, B. Baréa, P. Villeneuve, and R. Ndjouenkeu, "Model Development to Enhance the Solvent Extraction of Polyphenols from Mango Seed Kernel," *J. Biol. Act. Prod. from Nat.*, vol. 8, no. 1, pp. 51–63, 2018.

[13] A. E. Quirós-Sauceda *et al.*, "Dietary fiber and phenolic compounds as functional ingredients: interaction and possible effect after ingestion," *Food Funct.*, vol. 5, no. 6, p. 1063, 2014.

[14] F. Bello and A. Chimphango, "Optimization of lignin extraction from alkaline treated mango seed husk by high shear homogenization-assisted organosolv process using response surface methodology," *Int. J. Biol. Macromol.*, vol. 167, pp. 1379–1392, Jan. 2021.

[15] E. M. S. Cordeiro, Y. L. Nunes, A. L. A. Mattos, M. F. Rosa, M. D. S. M. S. Filho, and E. N. Ito, "Polymer biocomposites and nanobiocomposites obtained from mango seeds," *Macromol. Symp.*, vol. 344, no. 1, pp. 39–54, 2014.

[16] C. Torres-León, R. Rojas, L. Serna-cock, R. Belmares-cerda, and C. Noé, "Extraction of antioxidants from mango seed kernel : Optimization assisted by microwave," *Food Bioprod. Process.*, vol. 105, pp. 188–196, 2017.

[17] C. Hamaio, O. Delgado, and L. F. Fleuri, "Orange and mango by-products : Agro-industrial waste as source of bioactive compounds and botanical versus commercial description — A review," *Food Rev. Int.*, vol. 32, no. 1, pp. 1–14, 2016.

[18] D. S. Sogi, M. Siddiq, I. Greiby, and K. D. Dolan, "Total phenolics, antioxidant activity, and functional properties of 'Tommy Atkins' mango peel and kernel as affected by drying methods," *Food Chem.*, vol. 141, no. 3, pp. 2649–2655, 2013.

[19] L. A. Andrade, M. A. S. Barrozo, and L. G. M. Vieira, "Thermo-chemical behavior and product formation during pyrolysis of mango seed shell," *Ind. Crops Prod.*, vol. 85, pp. 174–180, 2016.

[20] M. A. Henrique, H. A. Silverio, W. P. Flauzino Neto, and D. Pasquini, "Valorization of an agro-industrial waste, mango seed, by the extraction and characterization of its cellulose nanocrystals," *J. Environ. Manage.*, vol. 121, no. march 2013, pp. 202–209, 2013.

[21] A. Dzigbor and A. Chimphango, "Production and optimization of NaCl-activated carbon from mango seed using response surface methodology," *Biomass Convers. Biorefinery*, vol. 9, no. 2, pp. 421–431, 2019.

[22] G. Ganeshan, K. P. Shadangi, and K. Mohanty, "Thermo-chemical conversion of mango seed kernel and shell to value added products," *J. Anal. Appl. Pyrolysis*, vol. 121, pp. 403–408, 2016.

[23] M. FitzPatrick, P. Champagne, M. F. Cunningham, and R. A. Whitney, "A biorefinery processing perspective: Treatment of lignocellulosic materials for the production of value-added products," *Bioresour. Technol.*, vol. 101, no. 23, pp. 8915–8922, 2010.

[24] K. Rajan *et al.*, "Investigating the effects of hemicellulose pre-extraction on the production and characterization of loblolly pine nanocellulose," *Cellulose*, vol. 27, no. 7, pp. 3693–3706, 2020.

[25] H. Wang *et al.*, "Highly Efficient Preparation of Functional and Thermostable Cellulose Nanocrystals via H2SO4 Intensified Acetic Acid Hydrolysis," *Carbohydr. Polym.*, vol. 239, p. 116233, Jul. 2020.

[26] J. O. A. Shatkin, T. H. Wegner, and E. M. T. E. D. Bilek, "Nanocellulose Markets," *Tappi J.*, vol. 13, no. 5, pp. 9–16, 2014.

[27] S. S. Ahankari, A. R. Subhedar, S. S. Bhadauria, and A. Dufresne, "Nanocellulose in food packaging: A review," *Carbohydr. Polym.*, vol. 255, p. 117479, 2021.

[28] Y. Habibi, "Key advances in the chemical modification of nanocelluloses.," *Chem. Soc. Rev.*, vol. 43, no. 5, pp. 1519–42, 2014.

[29] Markets and Markets, "Global Nanocellulose Market (2020 to 2030) - Production and Pricing Report," 2020. [Online]. Available: https://www.marketsandmarkets.com/PressReleases/nanocellulose.asp. [Accessed: 10-Jul-2021].

[30] J. Miller, "Nanocellulose, State of the Industry," in *Nanocellulose state of the industry*, 2015.

[31] A. J. Shatkin, C. John, and W. Theodore, "SWST Conference," *Mark. Proj. nanocellulose-enabled Prod.*, pp. 9–16, 2015.

[32] G. Delepierre, O. M. Vanderfleet, E. Niinivaara, B. Zakani, and E. D. Cranston, "Benchmarking Cellulose Nanocrystals Part II: New Industrially Produced Materials," *Langmuir*, vol. 37, no. 28, pp. 8393–8409, 2021.

[33] M. Rajinipriya, M. Nagalakshmaiah, M. Robert, and S. Elkoun, "Importance of Agricultural and Industrial Waste in the Field of Nanocellulose and Recent Industrial Developments of Wood Based Nanocellulose: A Review," *ACS Sustainable Chemistry and Engineering*, vol. 6, no. 3. pp. 2807–2828, 2018.

[34] A. Garcıa, J. Labidi, M. N. Belgacem, and B. Julien, "The nanocellulose biorefinery : woody versus herbaceous agricultural wastes for NCC production," *Cellulose*, vol. 24, pp. 693–704, 2017.

[35] Z. Anwar, M. Gulfraz, and M. Irshad, "Agro-industrial lignocellulosic biomass a key to unlock the future bio-energy: A brief review," *J. Radiat. Res. Appl. Sci.*, vol. 7, no. 2, pp. 163–173, 2014.

[36] S. B. A. Hamid, S. K. Zain, R. Das, and G. Centi, "Synergic effect of tungstophosphoric acid and sonication for rapid synthesis of crystalline nanocellulose," *Carbohydr. Polym.*, vol. 138, pp. 349–355, Mar. 2016.

[37] A. A. Oun and J. W. Rhim, "Characterization of nanocelluloses isolated from Ushar (Calotropis procera) seed fiber: Effect of isolation method," *Mater. Lett.*, vol. 168, pp. 146–150, 2016.

[38] H. A. Silvério, W. P. Flauzino Neto, N. O. Dantas, and D. Pasquini, "Extraction and characterization of cellulose nanocrystals from corncob for application as reinforcing agent in nanocomposites," *Ind. Crops Prod.*, vol. 44, pp. 427–436, Jan. 2013.

[39] M. Nuruddin *et al.*, "Extraction and Characterization of Cellulose Microfibrils From Agricultural Wastes in an Integrated Biorefinery Initiative," *Cellul. Chem. Technol.*, vol. 45, no. 5–6, pp. 347–354, 2011.

[40] B. Li *et al.*, "Cellulose nanocrystals prepared via formic acid hydrolysis followed by TEMPO-mediated oxidation," *Carbohydr. Polym.*, vol. 133, pp. 605–612, 2015.

[41] P. F. Vena, M. P. García-Aparicio, M. Brienzo, J. F. Görgens, and T. Rypstra, "Effect of alkaline hemicellulose extraction on kraft pulp fibers from eucalyptus grandis," *J. Wood Chem. Technol.*, vol. 33, no. 3, pp. 157–173, 2013.

[42] I. Egüés, A. Eceiza, and J. Labidi, “Effect of different hemicelluloses characteristics on film forming properties,” *Ind. Crop. Prod.*, vol. 47, pp. 331–338, 2013.

[43] A. Svärd, E. Brännvall, and U. Edlund, “Rapeseed straw polymeric hemicelluloses obtained by extraction methods based on severity factor,” *Ind. Crops Prod.*, vol. 95, pp. 305–315, Jan. 2017.

[44] R. N. Tharanathan, H. M. Yashoda, and T. N. Prabha, “Mango (Mangifera indica L.) , ‘The King of Fruits’—An Overview,” *Food Rev. Int.*, vol. 22, no. 2, pp. 95–123, 2006.

[45] F. D. C. Siacor, C. F. Y. Lobarbio, and E. B. Taboada, “Pretreatment of Mango (Mangifera indica L. Anacardiaceae) Seed Husk for Bioethanol Production by Dilute Acid Treatment and Enzymatic Hydrolysis,” *Appl. Biochem. Biotechnol.*, vol. 193, no. 5, pp. 1338–1350, 2021.

[46] C. N. Schnell *et al.*, “Films from xylan/chitosan complexes: preparation and characterization,” *Cellulose*, vol. 24, no. 10, pp. 4393–4403, 2017.

[47] E. Dorta, M. G. Lobo, and M. Gonzalez, “Reutilization of mango byproducts: Study of the effect of extraction solvent and temperature on their antioxidant properties,” *J. Food Sci.*, vol. 77, no. 1, pp. 80–89, 2012.

[48] A. P. M. Silva *et al.*, “Mango kernel starch films as affected by starch nanocrystals and cellulose nanocrystals,” *Carbohydr. Polym.*, vol. 211, pp. 209–216, May 2019.

[49] I. Egüés, A. Eceiza, and J. Labidi, “Effect of different hemicelluloses characteristics on film forming properties,” *Ind. Crops Prod.*, vol. 47, pp. 331–338, 2013.

[50] N. E. El Mansouri and J. Salvadó, “Structural characterization of technical lignins for the production of adhesives: Application to lignosulfonate, kraft, soda-anthraquinone, organosolv and ethanol process lignins,” *Ind. Crops Prod.*, vol. 24, no. 1, pp. 8–16, 2006.

[51] H. Du *et al.*, “Sustainable preparation and characterization of thermally stable and functional cellulose nanocrystals and nanofibrils via formic acid hydrolysis,” *J. Bioresour. Bioprod. bio*, vol. 2, no. 1, pp. 10–15, 2017.

[52] A. K. Bharimalla, S. P. Deshmukh, and P. G. Patil, “Energy Efficient Manufacturing of Nanocellulose by Chemo- and Bio-Mechanical Processes : A Review,” *Would J. Nano Sci. Eng.*, no. December, pp. 204–212, 2015.

[53] K. Saeaurng and D. Kuakpetoon, "A comparative study of mango seed kernel starches and other commercial starches: the contribution of chemical fine structure to granule crystallinity, gelatinization, retrogradation, and pasting properties," *J. Food Meas. Charact.*, vol. 12, no. 4, pp. 2444–2452, 2018.

[54] T. Tesfaye, J. K. Johakimu, R. B. C. Bruce, and D. Ramjugernath, "Valorisation of mango seed via extraction of starch : preliminary techno - economic analysis," *Clean Technol. Environ. Policy*, vol. 20, no. 1, pp. 81–94, 2018.

[55] M. Sonthalia and D. C. Sikdar, "(Mangifera Indica . L) Seed Kernel and Its Characterization," *Int. J. Tech. Res. Appl. e-ISSN*, vol. 3, no. 3, pp. 346–349, 2015.

[56] K. X. Liu, H. Q. Li, J. Zhang, Z. G. Zhang, and J. Xu, "The effect of non-structural components and lignin on hemicellulose extraction," *Bioresour. Technol.*, vol. 214, pp. 755–760, 2016.

[57] J. L. F. Kock, E. G. Groenewald, G. H. J. Krüger, J. N. Eloff, and P. M. Lategan, "Extraction of polyphenols and hydrolysis of birdproof sorghum starch," *J. Sci. Food Agric.*, vol. 36, no. 11, pp. 1140–1144, 1985.

[58] K. H. Daiber, "Enzyme inhibition by polyphenols of sorghum grain and malt," *J. Sci. Food Agric.*, vol. 26, no. 9, pp. 1399–1411, 1975.

[59] W. J. J. Huijgen, A. T. Smit, P. J. de Wild, and H. den Uil, "Fractionation of wheat straw by prehydrolysis, organosolv delignification and enzymatic hydrolysis for production of sugars and lignin," *Bioresour. Technol.*, vol. 114, pp. 389–398, 2012.

[60] Y. N. Guragain, K. P. Bastola, R. L. Madl, and P. V. Vadlani, "Novel Biomass Pretreatment Using Alkaline Organic Solvents: A Green Approach for Biomass Fractionation and 2,3-Butanediol Production," *Bioenergy Res.*, vol. 9, no. 2, pp. 643–655, 2016.

[61] R. Minjares-Fuentes, A. Femenia, M. C. Garau, M. G. Candelas-Cadillo, S. Simal, and C. Rosselló, "Ultrasound-assisted extraction of hemicelluloses from grape pomace using response surface methodology," *Carbohydr. Polym.*, vol. 138, pp. 180–191, 2016.

[62] L. Matsakas *et al.*, "A novel hybrid organosolv : steam explosion method for the efficient fractionation and pretreatment of birch biomass," *Biotechnol. Biofuels*, vol. 11, pp. 1–14, 2018.

[63] M. Brienzo, A. F. Siqueira, and A. M. F. Milagres, "Search for optimum conditions of sugarcane bagasse hemicellulose extraction," *Biochem. Eng. J.*, vol. 46, no. 2, pp. 199–204, 2009.

[64] H. N. Rabetafika, B. Bchir, C. Blecker, M. Paquot, and B. Wathelet, "Comparative study of alkaline extraction process of hemicelluloses from pear pomace," *Biomass and Bioenergy*, vol. 61, no. 0, pp. 254–264, 2014.

[65] B. Deepa *et al.*, "Structure, morphology and thermal characteristics of banana nano fibers obtained by steam explosion," *Bioresour. Technol.*, vol. 102, no. 2, pp. 1988–1997, 2011.

[66] C. G. Yoo, "Pretreatment and fractionation of lignocellulosic biomass for production of biofuel and value-added products," *Iowa State Univ.*, p. 159, 2012.

[67] E. Dorta, M. G. Lobo, and M. González, "Optimization of Factors Affecting Extraction of Antioxidants from Mango Seed," *Food Bioprocess Technol.*, vol. 6, no. 4, pp. 1067–1081, 2013.

[68] L. Matsakas *et al.*, "Lignin-first biomass fractionation using a hybrid organosolv – Steam explosion pretreatment technology improves the saccharification and fermentability of spruce biomass," *Bioresour. Technol.*, vol. 273, pp. 521–528, 2019.

[69] R. Ceaser, "Comparative analysis of methods for producing nanocellulose from wheat straw and bran, with co-extraction of valuable products," Stellenbosch University, 2019.

[70] L. R. Mugwagwa and A. F. A. Chimphango, "Box-Behnken design based multi-objective optimisation of sequential extraction of pectin and anthocyanins from mango peels," *Carbohydr. Polym.*, vol. 219, no. October 2018, pp. 29–38, 2019.

[71] S. Galili and R. Hovav, "Determination of Polyphenols, Flavonoids, and Antioxidant Capacity in Dry Seeds," in *Polyphenols in Plants: Isolation, Purification and Extract Preparation*, Elsevier, 2014, pp. 305–323.

[72] G. A. Akowuah and I. Zhari, "Effect of Extraction Temperature on Stability of Major Polyphenols and Antioxidant Activity of Orthosiphon stamineus Leaf," *J. Herbs. Spices Med. Plants*, vol. 16, pp. 160–166, 2010.

[73] B. Guo, Y. Zhang, G. Yu, W. H. Lee, Y. S. Jin, and E. Morgenroth, "Two-stage acidic-alkaline hydrothermal pretreatment of lignocellulose for the high recovery of cellulose

and hemicellulose sugars," *Appl. Biochem. Biotechnol.*, vol. 169, no. 4, pp. 1069–1087, 2013.

[74] K. Werner, L. Pommer, and M. Broström, "Thermal decomposition of hemicelluloses," *J. Anal. Appl. Pyrolysis*, vol. 110, no. 1, pp. 130–137, 2014.

[75] A. Mehmood, L. Zhao, M. Ishaq, B. Safdar, C. Wang, and M. Nadeem, "Optimization of total phenolic contents, antioxidant, and in-vitro xanthine oxidase inhibitory activity of sunflower head," *CYTA - J. Food*, vol. 16, no. 1, pp. 957–964, 2018.

[76] R. C. de A. Castro, B. G. Fonseca, H. T. L. dos Santos, I. S. Ferreira, S. I. Mussatto, and I. C. Roberto, "Alkaline deacetylation as a strategy to improve sugars recovery and ethanol production from rice straw hemicellulose and cellulose," *Ind. Crops Prod.*, vol. 106, pp. 65–73, Nov. 2017.

[77] P. Correia, L. Cruz-Lopes, and L. Beirão-da-Costa, "Morphology and structure of chestnut starch isolated by alkali and enzymatic methods," *Food Hydrocoll.*, vol. 28, no. 2, pp. 313–319, 2012.

[78] D. Koegelenberg and A. F. A. Chimphango, "Effects of wheat-bran arabinoxylan as partial flour replacer on bread properties," *Food Chem.*, vol. 221, pp. 1606–1613, 2017.

[79] M. Sonthalia and D. C. Sikdar, "Production of starch from mango (Mangifera indica.L) seed kernel and its characterization," *Int. J. Tech. Res. Appl.*, vol. 3, no. 3, pp. 346–349, 2015.

[80] E. M. S. Cordeiro *et al.*, "XRD as an analytical tool for analyses of tommy atkins mango kernel polysacharide," in *International Symposium on Crystallography*, 2014, vol. 3, pp. 18–18.

[81] Y. Zheng *et al.*, "Antioxidant, α-amylase and α-glucosidase inhibitory activities of bound polyphenols extracted from mung bean skin dietary fiber," *Lwt*, vol. 132, no. April, p. 109943, 2020.

[82] M. J. Peña, S. T. Tuomivaara, B. R. Urbanowicz, M. A. O'Neill, and W. S. York, "Methods for structural characterization of the products of cellulose- and xyloglucan-hydrolyzing enzymes," *Methods Enzymol.*, vol. 510, pp. 121–139, 2012.

[83] M. Makhetha, "Fractionation of Lignocellulosic Biomass for Production of Materials and Chemicals," Stellenbosch University, 2016.

[84] A. F. A. Chimphango, W. H. van Zyl, and J. F. Görgens, "Isolation, characterization and enzymatic modification of water soluble xylans from Eucalyptus grandis wood and sugarcane bagasse," *J. Chem. Technol. Biotechnol.*, vol. 87, no. 10, pp. 1419–1429, 2012.

[85] C. Nitsos *et al.*, "Isolation and Characterization of Organosolv and Alkaline Lignins from Hardwood and Softwood Biomass," *ACS Sustain. Chem. Eng.*, vol. 4, no. 10, pp. 5181–5193, 2016.

[86] J. Seok, Y. Y. Lee, and T. Hyun, "Bioresource Technology A review on alkaline pretreatment technology for bioconversion of lignocellulosic biomass," *Bioresour. Technol.*, vol. 199, no. 2016, pp. 42–48, 2016.

[87] X. Zhao, K. Cheng, and D. Liu, "Organosolv pretreatment of lignocellulosic biomass for enzymatic hydrolysis," *Appl. Microbiol. Biotechnol.*, vol. 82, no. 5, pp. 815–827, 2009.

[88] Y. N. Guragain, K. P. Bastola, R. L. Madl, and P. V Vadlani, "Novel Biomass Pretreatment Using Alkaline Organic Solvents : A Green Approach for Biomass Fractionation and 2 , 3-Butanediol Production," pp. 643–655, 2016.

[89] V. B. Agbor, N. Cicek, R. Sparling, A. Berlin, and D. B. Levin, "Biomass pretreatment: Fundamentals toward application," *Biotechnol. Adv.*, vol. 29, no. 6, pp. 675–685, 2011.

[90] M. Norgren and H. Edlund, "Current Opinion in Colloid & Interface Science Lignin : Recent advances and emerging applications," *Curr. Opin. Colloid Interface Sci.*, vol. 19, no. 5, pp. 409–416, 2014.

[91] W. J. J. Huijgen, G. Telysheva, A. Arshanitsa, R. J. A. Gosselink, and P. J. de Wild, "Characteristics of wheat straw lignins from ethanol-based organosolv treatment," *Ind. Crops Prod.*, vol. 59, pp. 85–95, Aug. 2014.

[92] A. Iskalieva, B. M. Yimmou, P. R. Gogate, M. Horvath, P. G. Horvath, and L. Csoka, "Cavitation assisted delignification of wheat straw: A review," *Ultrason. Sonochem.*, vol. 19, no. 5, pp. 984–993, 2012.

[93] R. Terán Hilares, L. Ramos, S. S. da Silva, G. Dragone, S. I. Mussatto, and J. C. dos Santos, "Hydrodynamic cavitation as a strategy to enhance the efficiency of lignocellulosic biomass pretreatment," *Crit. Rev. Biotechnol.*, vol. 38, no. 4, pp. 483–

493, May 2018.

[94] J. Zhao, W. Zhang, X. Zhang, X. Zhang, C. Lu, and Y. Deng, “Extraction of cellulose nanofibrils from dry softwood pulp using high shear homogenization,” *Carbohydr. Polym.*, vol. 97, no. 2, pp. 695–702, 2013.

[95] M. J. Madison, G. Coward-Kelly, C. Liang, M. N. Karim, M. Falls, and M. T. Holtzapple, “Mechanical pretreatment of biomass – Part I: Acoustic and hydrodynamic cavitation,” *Biomass and Bioenergy*, vol. 98, pp. 135–141, 2017.

[96] P. Harmsen, W. Huijgen, L. López, and R. Bakker, “Literature Review of Physical and Chemical Pretreatment Processes for Lignocellulosic Biomass,” *Food Biobased Res.*, no. September, pp. 1–49, 2010.

[97] C. Liu *et al.*, “Properties of nanocellulose isolated from corncob residue using sulfuric acid, formic acid, oxidative and mechanical methods,” *Carbohydr. Polym.*, vol. 151, pp. 716–724, 2016.

[98] E. de Morais Teixeira, A. C. Corrêa, A. Manzoli, F. de Lima Leite, C. de Ribeiro Oliveira, and L. H. C. Mattoso, “Cellulose nanofibers from white and naturally colored cotton fibers,” *Cellulose*, vol. 17, no. 3, pp. 595–606, 2010.

[99] A. K. Kumar and S. Sharma, “Recent updates on different methods of pretreatment of lignocellulosic feedstocks: a review,” *Bioresour. Bioprocess.*, vol. 4, no. 1, p. 7, 2017.

[100] H. Zhang, Y. Xu, and S. Yu, “Co-production of functional xylooligosaccharides and fermentable sugars from corncob with effective acetic acid prehydrolysis,” *Bioresour. Technol.*, vol. 234, pp. 343–349, 2017.

[101] M. G. Papatheofanous, E. Billa, D. P. Koullas, B. Monties, and E. G. Koukios, “Optimizing multisteps mechanical-chemical fractionation of wheat straw components,” in *Industrial Crops and Products*, 1998, vol. 7, no. 2–3, pp. 249–256.

[102] M. Michelin, H. A. Ruiz, M. de L. T. M. Polizeli, and J. A. Teixeira, “Multi-step approach to add value to corncob: Production of biomass-degrading enzymes, lignin and fermentable sugars,” *Bioresour. Technol.*, vol. 247, no. July 2017, pp. 582–590, 2018.

[103] C. M. Ajila, K. A. Naidu, S. G. Bhat, and U. J. S. P. Rao, “Bioactive compounds and antioxidant potential of mango peel extract,” *Food Chem.*, vol. 105, no. 3, pp. 982–988, 2007.

[104] P. W. Mwaurah *et al.*, "Physicochemical characteristics, bioactive compounds and industrial applications of mango kernel and its products: A review," *Compr. Rev. Food Sci. Food Saf.*, vol. 19, no. 5, pp. 2421–2446, 2020.

[105] M. H. A. Jahurul *et al.*, "Mango (Mangifera indica L.) by-products and their valuable components: A review," *Food Chem.*, vol. 183, no. 2015, pp. 173–180, 2015.

[106] C. R. M. Monteiro *et al.*, "Hydrothermal treatment on depolymerization of hemicellulose of mango seed shell for the production of xylooligosaccharides," *Carbohydr. Polym.*, vol. 253, 2021.

[107] C. Torres-León *et al.*, "Food Waste and Byproducts: An Opportunity to Minimize Malnutrition and Hunger in Developing Countries," *Front. Sustain. Food Syst.*, vol. 2, pp. 1–17, 2018.

[108] FAOSTAT, "FAO statistics. Food and Agricultural Oorganization of the United Nations," 2020. [Online]. Available: http://www.fao.org/faostat/en/#data/QC. [Accessed: 17-Mar-2020].

[109] M. H. A. Jahurul *et al.*, "Mango (Mangifera indica L.) by-products and their valuable components: A review," *Food Chemistry*, vol. 183. Elsevier Ltd, pp. 173–180, 2015.

[110] E. A. Evans, F. H. Ballen, and M. Siddiq, "Mango Production, Global Trade, Consumption Trends, and Postharvest Processing and Nutrition," in *Handbook of Mango Fruit: Production, Postharvest Science, Processing Technology and Nutrition*, 2017, pp. 1–16.

[111] P. X. Villanueva, Y. C. Ávila, L. R. Dávila, J. J. Méndez, and W. M. Arango, "Characterization and use of Mangifera indica L. seeds from four varieties," *BioResources*, vol. 15, no. 3, pp. 5264–5280, 2020.

[112] L. Menon, S. Dutta Majumdar, and U. Ravi, "Mango (Mangifera indica L.) kernel flour as a potential ingredient in the development of composite flour bread," *Indian J. Nat. Prod. Resour.*, vol. 5, no. 1, pp. 75–82, 2014.

[113] X. Yang, H. S. Choi, C. Park, and S. W. Kim, "Current states and prospects of organic waste utilization for biorefineries," *Renew. Sustain. Energy Rev.*, vol. 49, pp. 335–349, 2015.

[114] R. S. Orozco *et al.*, "Characterization of lignocellulosic fruit waste as an alternative

feedstock for bioethanol production," *BioResources*, vol. 9, no. 2, pp. 1873–1885, 2014.

[115] A. García, A. Gandini, J. Labidi, N. Belgacem, and J. Bras, "Industrial and crop wastes: A new source for nanocellulose biorefinery," *Ind. Crops Prod.*, vol. 93, pp. 26–38, 2016.

[116] C. Y. Cheok *et al.*, "Current trends of tropical fruit waste utilization," *Crit. Rev. Food Sci. Nutr.*, vol. 58, no. 3, pp. 335–361, 2018.

[117] O. Guzmán, C. Lemus, J. Bugarin, J. Bonilla, and J. Ly, "Composition and chemical characteristics of mangoes (Mangifera indica l .) for animal feeding in Nayarit , Mexico," *Cuba. J. Agric. Sci.*, vol. 47, no. 3, pp. 273–277, 2013.

[118] C. da S. Meireles *et al.*, "Characterization of asymmetric membranes of cellulose acetate from biomass: Newspaper and mango seed," *Carbohydr. Polym.*, vol. 80, no. 3, pp. 954–961, 2010.

[119] J. H. Clark and F. E. I. Deswarte, "The Biorefinery Concept-An Integrated Approach," in *Introduction to Chemicals from Biomass*, 2008, pp. 1–20.

[120] V. G. Zuin and L. Z. Ramin, "Green and Sustainable Separation of Natural Products from Agro - Industrial Waste : Challenges , Potentialities , and Perspectives on Emerging Approaches," *Top. Curr. Chem.*, vol. 376, no. 1, pp. 1–54, 2018.

[121] B. Kamm and M. Kamm, "Principles of biorefineries," *Appl. Microbiol. Biotechnol.*, vol. 64, no. 2, pp. 137–145, 2004.

[122] A. S. Nizami *et al.*, "Waste biorefineries: Enabling circular economies in developing countries," *Bioresource Technology*, vol. 241. Elsevier Ltd, pp. 1101–1117, 2017.

[123] V. Menon and M. Rao, "Trends in bioconversion of lignocellulose: Biofuels, platform chemicals & biorefinery concept," *Progress in Energy and Combustion Science*, vol. 38, no. 4. Elsevier Ltd, pp. 522–550, 2012.

[124] E. De Jong and G. Jungmeier, "Biorefinery Concepts in Comparison to Petrochemical Refineries," in *Industrial Biorefineries and White Biotechnology*, 2015, pp. 3–33.

[125] A. Zabaniotou, P. Kamaterou, A. Pavlou, and C. Panayiotou, "Sustainable bioeconomy transitions: Targeting value capture by integrating pyrolysis in a winery waste biorefinery," *J. Clean. Prod.*, vol. 172, pp. 3387–3397, 2018.

[126] O. Guzmán, C. Lemus, J. Bugarin, J. Bonilla, and J. Ly, "Composition and chemical

characteristics of mangoes (Mangifera indica l .) for animal feeding in Nayarit , Mexico," *Cuba. J. Agric. Sci.*, vol. 47, no. 3, pp. 273–277, 2013.

[127] G. M. Dorta E., Lobo G. M., "Using drying treatments to stabilise mango peel and seed: Effect on antioxidant activity," *LWT - Food Sci. Technol.*, vol. 45, no. 2, pp. 261–268, 2012.

[128] R. C. Rivas-Cantu, K. D. Jones, and P. L. Mills, "A citrus waste-based biorefinery as a source of renewable energy: Technical advances and analysis of engineering challenges," in *Waste Management and Research*, 2013, vol. 31, no. 4, pp. 413–420.

[129] A. E. M. Abdalla, S. M. Darwish, E. H. E. Ayad, and R. M. El-Hamahmy, "Egyptian mango by-product 1. Compositional quality of mango seed kernel," *Food Chem.*, vol. 103, no. 4, pp. 1134–1140, 2007.

[130] J. O. Nwadiogb, A. A. Igwe, N. H. Okoye, and C. C. Chime, "Extraction and characterization of microcrystalline cellulose from mango kernel: A waste management approach," *Der Pharma Chem.*, vol. 7, no. 11, pp. 1–7, 2015.

[131] M. P. Elizalde-González and V. Hernández-Montoya, "Characterization of mango pit as raw material in the preparation of activated carbon for wastewater treatment," *Biochem. Eng. J.*, vol. 36, no. 3, pp. 230–238, 2007.

[132] R. C. Sun, *Cereal Straw as a Resource for Sustainable Biomaterials and Biofuels*, 1st ed. oxford, 2010.

[133] Y. Sun and J. Cheng, "Hydrolysis of lignocellulosic materials for ethanol production : a review q," *Bioresour. Technol.*, vol. 83, no. 1, pp. 1–11, 2002.

[134] M. Kaur, N. Singh, K. S. Sandhu, and H. S. Guraya, "Physicochemical, morphological, thermal and rheological properties of starches separated from kernels of some Indian mango cultivars (Mangifera indica L.)," *Food Chem.*, vol. 85, no. 1, pp. 131–140, 2004.

[135] Y. Y. Soong and P. J. Barlow, "Antioxidant activity and phenolic content of selected fruit seeds," *Food Chem.*, vol. 88, no. 3, pp. 411–417, 2004.

[136] C. Torres-León *et al.*, "Solid-state fermentation with Aspergillus niger to enhance the phenolic contents and antioxidative activity of Mexican mango seed: A promising source of natural antioxidants," *LWT*, vol. 112, p. 108236, Sep. 2019.

[137] N. Yingkamhaeng and P. Sukyai, "The potential of mango peel utilization for cellulose extraction by hydrothermal pretreatment," in *The 26th Annual Meeting of the Thai Society for Biotechnology and International Conference*, 2014, pp. 101–109.

[138] J. Banerjee, R. Vijayaraghavan, A. Arora, D. R. MacFarlane, and A. F. Patti, "Lemon juice based extraction of pectin from mango peels: Waste to wealth by sustainable approaches," *ACS Sustain. Chem. Eng.*, vol. 4, no. 11, pp. 5915–5920, 2016.

[139] H. Nadia, B. Bchir, C. Blecker, M. Paquot, and B. Wathelet, "ScienceDirect Comparative study of alkaline extraction process of hemicelluloses from pear pomace," *Biomass and Bioenergy*, vol. 61, no. 0, pp. 254–264, 2013.

[140] E. de M. Teixeira, A. A. S. Curvelo, A. C. Corrêa, J. M. Marconcini, G. M. Glenn, and L. H. C. Mattoso, "Properties of thermoplastic starch from cassava bagasse and cassava starch and their blends with poly (lactic acid)," *Ind. Crops Prod.*, vol. 37, no. 1, pp. 61–68, 2012.

[141] T. Saleem Khan and U. Mubeen, "Wheat Straw: A Pragmatic Overview," *Curr. Res. J. Biol. Sci.*, vol. 4, no. 6, pp. 673–675, 2012.

[142] H. Chen, "Chemical Composition and Structure of Natural Lignocellulose," in *Biotechnology of Lignocellulose: Theory and Practice*, 2014, pp. 1–511.

[143] J. Xu, E. F. Krietemeyer, V. M. Boddu, S. X. Liu, and W. C. Liu, "Production and characterization of cellulose nanofibril (CNF) from agricultural waste corn stover," *Carbohydr. Polym.*, vol. 192, no. September 2017, pp. 202–207, 2018.

[144] Y. Habibi, "Key advances in the chemical modification of nanocelluloses," *Chem. Soc. Rev.*, vol. 43, no. 5, pp. 1519–1542, 2014.

[145] H. V Lee, S. B. A. Hamid, and S. K. Zain, "Conversion of Lignocellulosic Biomass to Nanocellulose : Structure and Chemical Process," *Sci. World J.*, pp. 1–14, 2014.

[146] T. Stevanovic, "Chemical Composition and Properties of Wood," *Lignocellul. Fibers Wood Handb.*, pp. 49–106, 2016.

[147] H. Krässig *et al.*, "Cellulose," *Ullmann's encyclopedia of industrial chemistry Vol.6*. pp. 565–582, 2012.

[148] Y. C. Ching and T. S. Ng, "Effect of preparation conditions on cellulose from oil palm

empty fruit bunch fiber," *BioResources*, vol. 9, no. 4, pp. 6373–6385, 2014.

[149] H. P. S. Abdul Khalil *et al.*, "Production and modification of nanofibrillated cellulose using various mechanical processes: A review," *Carbohydr. Polym.*, vol. 99, pp. 649–665, 2014.

[150] L. N. Jimenez, C. D. V. Martínez Narváez, and V. Sharma, "Capillary breakup and extensional rheology response of food thickener cellulose gum (NaCMC) in salt-free and excess salt solutions," *Phys. Fluids*, vol. 32, no. 1, p. 12113, 2020.

[151] C. F. Yan, H. Y. Yu, and J. M. Yao, "One-step extraction and functionalization of cellulose nanospheres from lyocell fibers with cellulose II crystal structure," *Cellulose*, vol. 22, no. 6, pp. 3773–3788, 2015.

[152] B. Ram and G. S. Chauhan, "New spherical nanocellulose and thiol-based adsorbent for rapid and selective removal of mercuric ions," *Chem. Eng. J.*, vol. 331, pp. 587–596, 2018.

[153] C. M. Ewulonu, X. Liu, M. Wu, and H. Yong, "Lignin-Containing Cellulose Nanomaterials: A Promising New Nanomaterial for Numerous Applications," *J. Bioresour. Bioprod.*, vol. 4, no. 1, pp. 3–10, 2019.

[154] H. Bian, L. Wei, C. Lin, Q. Ma, H. Dai, and J. Y. Zhu, "Lignin-Containing Cellulose Nanofibril-Reinforced Polyvinyl Alcohol Hydrogels," *ACS Sustain. Chem. Eng.*, vol. 6, no. 4, pp. 4821–4828, 2018.

[155] L. Wei, U. P. Agarwal, L. Matuana, R. C. Sabo, and N. M. Stark, "Performance of high lignin content cellulose nanocrystals in poly(lactic acid)," *Polymer (Guildf).*, vol. 135, pp. 305–313, 2018.

[156] M. Herrera, K. Thitiwutthisakul, X. Yang, P. on Rujitanaroj, R. Rojas, and L. Berglund, "Preparation and evaluation of high-lignin content cellulose nanofibrils from eucalyptus pulp," *Cellulose*, vol. 25, no. 5, pp. 3121–3133, 2018.

[157] R. Sánchez, E. Espinosa, J. Domínguez-Robles, J. M. Loaiza, and A. Rodríguez, "Isolation and characterization of lignocellulose nanofibers from different wheat straw pulps," *Int. J. Biol. Macromol.*, vol. 92, pp. 1025–1033, 2016.

[158] M. Mahardika, H. Abral, A. Kasim, S. Arief, and M. Asrofi, "Production of nanocellulose from pineapple leaf fibers via high-shear homogenization and

ultrasonication," *Fibers*, vol. 6, no. 2, pp. 1–12, 2018.

[159] E. Rojo *et al.*, "Comprehensive elucidation of the effect of residual lignin on the physical, barrier, mechanical and surface properties of nanocellulose films," *Green Chem.*, vol. 17, p. 1853, 2015.

[160] C. Hu, Y. Zhao, K. Li, J. Y. Zhu, and R. Gleisner, "Optimizing cellulose fibrillation for the production of cellulose nanofibrils by a disk grinder," *Holzforschung*, vol. 69, no. 8, pp. 993–1000, 2015.

[161] P. Phanthong, P. Reubroycharoen, X. Hao, and G. Xu, "Nanocellulose : Extraction and application," *Carbon Resour. Convers.*, vol. 1, no. 1, pp. 32–43, 2018.

[162] J. Xu, E. F. Krietemeyer, V. M. Boddu, S. X. Liu, and W. C. Liu, "Production and characterization of cellulose nanofibril (CNF) from agricultural waste corn stover," *Carbohydr. Polym.*, vol. 192, no. March, pp. 202–207, 2018.

[163] L. Brinchi, F. Cotana, E. Fortunati, and J. M. Kenny, "Production of nanocrystalline cellulose from lignocellulosic biomass: Technology and applications," *Carbohydr. Polym.*, vol. 94, no. 1, pp. 154–169, 2013.

[164] M. Yu, R. Yang, L. Huang, X. Cao, F. Yang, and D. Liu, "Preparation and characterization of bamboo nanocrystalline cellulose," *BioResources*, vol. 7, no. 2, pp. 1802–1812, 2012.

[165] H. D. Wang, R. D. Roeder, R. A. Whitney, P. Champagne, and M. F. Cunningham, "Graft modification of crystalline nanocellulose by Cu(0)-mediated SET living radical polymerization," *J. Polym. Sci. Part A Polym. Chem.*, vol. 53, no. 24, pp. 2800–2808, 2015.

[166] G. Y. Chen, H. Y. Yu, C. H. Zhang, Y. Zhou, and J. M. Yao, "A universal route for the simultaneous extraction and functionalization of cellulose nanocrystals from industrial and agricultural celluloses," *J. Nanoparticle Res.*, vol. 18, no. 2, pp. 1–14, 2016.

[167] O. M. Vanderfleet, D. A. Osorio, and E. D. Cranston, "Optimization of cellulose nanocrystal length and surface charge density through phosphoric acid hydrolysis," *Philos. Trans. R. Soc. A Math. Phys. Eng. Sci.*, vol. 376, no. 2112, 2018.

[168] P. B. Filson and B. E. Dawson-Andoh, "Sono-chemical preparation of cellulose nanocrystals from lignocellulose derived materials," *Bioresour. Technol.*, vol. 100, no.

7, pp. 2259–2264, 2009.

[169] S. Zhang *et al.*, "Preparation of spherical nanocellulose from waste paper by aqueous NaOH/thiourea," *Cellulose*, vol. 26, no. 8, pp. 5177–5185, 2019.

[170] P. Satyamurthy and N. Vigneshwaran, "A novel process for synthesis of spherical nanocellulose by controlled hydrolysis of microcrystalline cellulose using anaerobic microbial consortium," *Enzyme Microb. Technol.*, vol. 52, no. 1, pp. 20–25, Jan. 2013.

[171] M. Ioelovich and M. Ioelovich, "Nanoparticles of Amorphous Cellulose and Their Properties The silicates of strong organic bases View project Biofuel View project Nanoparticles of amorphous cellulose and their properties," *Am. J. Nanosci. Nanotechnol.*, vol. 1, no. 1, pp. 41–45, 2013.

[172] D. Zheng, Y. Zhang, Y. Guo, and J. Yue, "Isolation and Characterization of Nanocellulose with a Novel Shape from Walnut (Juglans Regia L.) Shell Agricultural Waste," *Polymers (Basel).*, vol. 11, no. 1130, pp. 1–14, 2019.

[173] S. Ghasemi, R. Behrooz, and I. Ghasemi, "Extraction and characterization of nanocellulose structures from linter dissolving pulp using ultrafine grinder," *J. Nanosci. Nanotechnol.*, vol. 16, no. 6, pp. 5791–5797, 2016.

[174] Y. W. Chen, M. A. Hasanulbasori, P. F. Chiat, and H. V. Lee, "Pyrus pyrifolia fruit peel as sustainable source for spherical and porous network based nanocellulose synthesis via one-pot hydrolysis system," *Int. J. Biol. Macromol.*, vol. 123, pp. 1305–1319, Feb. 2019.

[175] H. Shao, Y. Hu, H. Sun, B. Yang, B. Fan, and H. Zhang, "Response surface optimization of alkali extraction and characterization of poplar hemicellulose," *BioResources*, vol. 14, no. 2, pp. 3844–3859, 2019.

[176] H. Jiang, Q. Chen, J. Ge, and Y. Zhang, "Efficient extraction and characterization of polymeric hemicelluloses from hybrid poplar," *Carbohydr. Polym.*, vol. 101, no. 1, pp. 1005–1012, 2014.

[177] W. Farhat *et al.*, "Hemicellulose extraction and characterization for applications in paper coatings and adhesives," *Ind. Crops Prod.*, vol. 107, no. January, pp. 370–377, 2017.

[178] A. Svärd, E. Brännvall, and U. Edlund, "Rapeseed straw as a renewable source of hemicelluloses: Extraction, characterization and film formation," *Carbohydr. Polym.*,

vol. 133, pp. 179–186, 2015.

[179] R. N. Tharanathan, H. M. Yashoda, and T. N. Prabha, “Mango (Mangifera indica L.), ‘the king of fruits’ - An overview,” *Food Rev. Int.*, vol. 22, no. 2, pp. 95–123, 2006.

[180] R. N. Tharanathan, “Biodegradable films and composite coatings: Past, present and future,” *Trends Food Sci. Technol.*, vol. 14, no. 3, pp. 71–78, 2003.

[181] Z. Jamsazzadeh Kermani *et al.*, “The impact of extraction with a chelating agent under acidic conditions on the cell wall polymers of mango peel,” *Food Chem.*, vol. 161, pp. 199–207, 2014.

[182] V. Menon, M. Rao, and G. Prakash, “Value added products from hemicellulose - Biotechnological perspective,” *Glob. J. Biochem.*, vol. 1, no. 1, pp. 36–67, 2010.

[183] F. B. Sedlmeyer, “Food Hydrocolloids Xylan as by-product of biore fi neries : Characteristics and potential use for food applications,” *Food Hydrocoll.*, vol. 25, no. 8, pp. 1891–1898, 2011.

[184] A. Ebringerová and T. Heinze, “Xylan and xylan derivatives – biopolymers with valuable properties, 1. Naturally occurring xylans structures, isolation procedures and properties,” *Macromol. Rapid Commun.*, vol. 21, no. 9, pp. 542–556, 2000.

[185] C. Laine, “Structures of hemicelluloses and pectins in wood and pulp,” Helsinki University of Technology, 2005.

[186] K. Keegstra, K. W. Talmadge, B. W. D., and P. Albertsheim, “The Structure of Plant Cell Walls,” *Plant Physiol.*, vol. 55, no. 1, pp. 64–68, Jan. 1973.

[187] T. H. M. Vu, H. Pakkanen, and R. Alén, “Delignification of bamboo (Bambusa procera acher) Part 1. Kraft pulping and the subsequent oxygen delignification to pulp with a low kappa number,” *Ind. Crops Prod.*, vol. 19, no. 1, pp. 49–57, 2004.

[188] F. B. Sedlmeyer, “Xylan as by-product of biorefineries: Characteristics and potential use for food applications,” *Food Hydrocoll.*, vol. 25, no. 8, pp. 1891–1898, 2011.

[189] H. V. Scheller and P. Ulvskov, “Hemicelluloses,” *Annu. Rev. Plant Biol.*, vol. 61, pp. 263–289, 2010.

[190] D. U. Lima, W. Loh, and M. S. Buckeridge, “Xyloglucan – cellulose interaction depends on the sidechains and molecular weight of xyloglucan,” *plant physiolgy Biochem.*, vol.

42, pp. 389–394, 2004.

[191] A. P. Busato, C. G. Vargas-Rechia, and F. Reicher, “Xyloglucan from the leaves of Hymenaea courbaril,” *Phytochemistry*, vol. 58, no. 3, pp. 525–531, 2001.

[192] A. Bashir, P. K. Sharma, and M. H. Warsi, “Extraction and Characterization of Tamarind Seed Polysaccharide as a Pharmaceutical Excipient,” *Pharmacogn. J.*, vol. 5, no. 6, pp. 2209–2220, 2016.

[193] Y. B. Park and D. J. Cosgrove, “Xyloglucan and its interactions with other components of the growing cell wall,” *Plant and Cell Physiology*, vol. 56, no. 2. pp. 180–194, 2015.

[194] J. X. Sun, F. C. Mao, X. F. Sun, and R. Sun, “Comparative Study of Hemicelluloses Isolated with Alkaline Peroxide from Lignocellulosic Materials,” *J. Wood Chem. Technol.*, vol. 24, no. 3, pp. 239–262, 2005.

[195] J. Gu and J. M. Catchmark, “The impact of cellulose structure on binding interactions with hemicellulose and pectin,” *Cellulose*, vol. 20, no. 4, pp. 1613–1627, 2013.

[196] R. Sánchez, E. Espinosa, J. Domínguez-Robles, J. M. Loaiza, and A. Rodríguez, “Isolation and characterization of lignocellulose nanofibers from different wheat straw pulps,” *Int. J. Biol. Macromol.*, vol. 92, pp. 1025–1033, 2016.

[197] A. F. A. Chimphango, “Development of enzyme technology for modification of functional properties of xylan biopolymers,” Stellenbosch University, 2010.

[198] T. Egüés, C. Sanchez, and J. Labidi, “Separation and Purification of Hemicellulose by Ultrafiltration,” *Ind. Eng. Chem. Res.*, vol. 51, pp. 523–530, 2012.

[199] W. Stelte, “Steam explosion for biomass pre-treatment,” Gregersensvej, 2013.

[200] A. Kaushik and M. Singh, “Isolation and characterization of cellulose nanofibrils from wheat straw using steam explosion coupled with high shear homogenization,” *Carbohydr. Res.*, vol. 346, no. 1, pp. 76–85, 2011.

[201] Y. H. P. Zhang, “Reviving the carbohydrate economy via multi-product lignocellulose biorefineries,” *Journal of Industrial Microbiology and Biotechnology*, vol. 35, no. 5. pp. 367–375, 2008.

[202] Y. Cao *et al.*, “Advances in lignin valorization towards bio-based chemicals and fuels: Lignin biorefinery,” *Bioresource Technology*, vol. 291. Elsevier Ltd, p. 121878, 01-

Nov-2019.

[203] M. Namane, F. José García-Mateos, B. Sithole, D. Ramjugernath, J. Rodríguez-Mirasol, and T. Cordero, "Characteristics of Lignin Precipitated With Organic Acids As a Source for Valorisation of Carbon Products," *Cellul. Chem. Technol*, vol. 50, pp. 3–4, 2016.

[204] K. Wang, J.-X. Jiang, F. Xu, and R.-C. Sun, "Influence of Steaming Pressure on Steam Explosion Pretreatment of Lespedeza stalks (Lespedeza cyrtobotrya). II. Characteristics of Degraded Lignin," *J. Appl. Polym. Sci.*, vol. 116, no. 5, pp. 2658–2667, 2010.

[205] P. Sannigrahi, S. J. Miller, and A. J. Ragauskas, "Effects of organosolv pretreatment and enzymatic hydrolysis on cellulose structure and crystallinity in Loblolly pine," *Carbohydr. Res.*, vol. 345, no. 7, pp. 965–970, 2010.

[206] M. Yáñez-S *et al.*, "Physicochemical characterization of ethanol organosolv lignin (EOL) from Eucalyptus globulus: Effect of extraction conditions on the molecular structure," *Polym. Degrad. Stab.*, vol. 110, pp. 184–194, 2014.

[207] C. G. Boeriu, D. Bravo, R. J. A. Gosselink, and J. E. G. Van Dam, "Characterisation of structure-dependent functional properties of lignin with infrared spectroscopy," *Ind. Crops Prod.*, vol. 20, no. 2, pp. 205–218, 2004.

[208] R. B. Santos, P. W. Hart, H. Jameel, and H. M. Chang, "Wood based lignin reactions important to the biorefinery and pulp and paper industries," *BioResources*, vol. 8, no. 1, pp. 1456–1477, 2013.

[209] a Cornu, J. M. Besle, P. Mosoni, and E. Grenet, "Lignin-carbohydrate complexes in forages: structure and consequences in the ruminal degradation of cell-wall carbohydrates.," *Reprod. Nutr. Dev.*, vol. 34, no. 5, pp. 385–398, 1994.

[210] C. Campano, R. Miranda, N. Merayo, C. Negro, and A. Blanco, "Direct production of cellulose nanocrystals from old newspapers and recycled newsprint," *Carbohydr. Polym.*, vol. 173, pp. 489–496, 2017.

[211] W. Zhang, Y. Zhang, J. Cao, and W. Jiang, "Improving the performance of edible food packaging films by using nanocellulose as an additive," *International Journal of Biological Macromolecules*, vol. 166. pp. 288–296, 2021.

[212] J. Fernandez-Rodríguez, O. Gordobil, E. Robles, and M. Gonz, "Lignin valorization from side-streams produced during agricultural waste pulping and total chlorine free

bleaching," *J. Clean. Prod.*, vol. 142, pp. 2609–2617, 2017.

[213] J. Wildschut, A. T. Smit, J. H. Reith, and W. J. J. Huijgen, "Ethanol-based organosolv fractionation of wheat straw for the production of lignin and enzymatically digestible cellulose," *Bioresour. Technol.*, vol. 135, pp. 58–66, 2013.

[214] X. Pan, J. F. Kadla, K. Ehara, N. Gilkes, and J. N. Saddler, "Organosolv ethanol lignin from hybrid poplar as a radical scavenger: Relationship between lignin structure, extraction conditions, and antioxidant activity," *J. Agric. Food Chem.*, vol. 54, no. 16, pp. 5806–5813, 2006.

[215] M. N. Borand and F. Karaosmanoğlu, "Effects of organosolv pretreatment conditions for lignocellulosic biomass in biorefinery applications: A review," *J. Renew. Sustain. Energy*, vol. 10, no. 3, 2018.

[216] K. R. Aadil, D. Prajapati, and H. Jha, "Improvement of physcio-chemical and functional properties of alginate film by Acacia lignin," *Food Packag. Shelf Life*, vol. 10, pp. 25–33, 2016.

[217] L. A. Bello-Pérez, A. Aparicio-Saguilán, G. Méndez-Montealvo, J. Solorza-Feria, and E. Flores-Huicochea, "Isolation and partial characterization of mango (Magnifera indica L.) starch: Morphological, physicochemical and functional studies," *Plant Foods Hum. Nutr.*, vol. 60, no. 1, pp. 7–12, 2005.

[218] J. R. Daniel, R. L. Whistler, H. Roper, and B. Elvers, "Starch," *Ullmann's Encycl. Ind. Chem.*, 2007.

[219] A. V. Oliveira, A. P. M. da Silva, M. O. Barros, M. de sá M. Souza Filho, M. F. Rosa, and H. M. C. Azeredo, "Nanocomposite Films from Mango Kernel or Corn Starch with Starch Nanocrystals," *Starch/Staerke*, vol. 70, no. 11–12, 2018.

[220] M. Kaur, N. Singh, K. S. Sandhu, and H. S. Guraya, "Physicochemical, morphological, thermal and rheological properties of starches separated from kernels of some Indian mango cultivars (Mangifera indica L.)," *Food Chem.*, vol. 85, no. 1, pp. 131–140, 2004.

[221] N. Singh, Y. Nakaura, N. Inouchi, and K. Nishinari, "Structure and viscoelastic properties of starches separated from different legumes," *Starch/Staerke*, vol. 60, no. 7, pp. 349–357, 2008.

[222] M. Masibo and Q. He, "Major mango polyphenol and their potential significance to

human health," *Compr. Rev. Food Sci. Food Saf.*, vol. 7, no. 4, pp. 309–19, 2008.

[223] L. Y. Yan, L. T. Teng, and T. J. Jhi, "Antioxidant properties of guava fruit : comparison with some local fruits," *Sunw. Acad. J.*, vol. 3, pp. 9–20, 2006.

[224] C. M. Ajila, S. G. Bhat, and U. J. S. Prasada Rao, "Valuable components of raw and ripe peels from two Indian mango varieties," *Food Chem.*, vol. 102, no. 4, pp. 1006–1011, 2007.

[225] Y. Habibi, L. A. Lucia, and O. J. Rojas, "Cellulose nanocrystals: Chemistry, self-assembly, and applications," *Chem. Rev.*, vol. 110, no. 6, pp. 3479–3500, Jun. 2010.

[226] R. M. dos Santos, W. P. Flauzino Neto, H. A. Silvério, D. F. Martins, N. O. Dantas, and D. Pasquini, "Cellulose nanocrystals from pineapple leaf, a new approach for the reuse of this agro-waste," *Ind. Crops Prod.*, vol. 50, pp. 707–714, Oct. 2013.

[227] V. A. Barbash, O. V Yaschenko, and O. M. Shniruk, "Preparation and Properties of Nanocellulose from Organosolv Straw Pulp," *Nanoscale Res. Lett.*, vol. 12, no. 1, 2017.

[228] L. Mesa, Y. Albernas, M. Morales, G. Corsano, and E. González, "Integration of Organosolv Process for Biomass Pretreatment in a Biorefinery," in *Biomass Fractionation Technologies for a Lignocellulosic Feedstock Based Biorefinery*, 2016, pp. 229–254.

[229] Z. Li *et al.*, "Ethanosolv with NaOH Pretreatment of Moso Bamboo for Efficient Enzymatic Saccharification," *BioResources*, vol. 8, no. 2, pp. 711–4721, Jul. 2013.

[230] P. Dongre, M. Driscoll, T. Amidon, and B. Bujanovic, "Lignin-furfural based adhesives," *Energies*, vol. 8, no. 8, pp. 7897–7914, 2015.

[231] L. R. Mugwagwa, "Fractionation of agro-waste to produce biopolymers and bioactive compounds for active food packaging," Stellenbosch University, 2020.

[232] Y. Chen, H. Luo, A. Gao, and M. Zhu, "Extraction of Polysaccharides from Mango (Mangifera indica Linn.) Seed by Response Surface Methodology and Identification of their Structural Characteristics," *Food Anal. Methods*, vol. 5, no. 4, pp. 800–806, 2012.

[233] H. I. Castro-Vargas, D. B. Vivas, J. O. Barbosa, S. J. M. Medina, F. A. Gutiérrez, and F. Parada-Alfonso, "Bioactive phenolic compounds from the agroindustrial waste of Colombian mango cultivars 'sugar mango' and 'tommy atkins'—An alternative for their

use and valorization," *Antioxidants*, vol. 8, no. 2, 2019.

[234] A. M. Abdel-Aty, W. H. Salama, M. B. Hamed, A. S. Fahmy, and S. A. Mohamed, "Phenolic-antioxidant capacity of mango seed kernels: therapeutic effect against viper venoms," *Rev. Bras. Farmacogn.*, vol. 28, no. 5, pp. 594–601, 2018.

[235] K. J. A. Lim, A. A. Cabajar, C. F. Y. Lobarbio, E. B. Taboada, and D. J. Lacks, "Extraction of bioactive compounds from mango (Mangifera indica L. var. Carabao) seed kernel with ethanol–water binary solvent systems," *J. Food Sci. Technol.*, vol. 56, 2019.

[236] E. Fortunati, F. Luzi, D. Puglia, and L. Torre, "Extraction of Lignocellulosic Materials From Waste Products," in *Multifunctional Polymeric Nanocomposites Based on Cellulosic Reinforcements*, Elsevier Inc., 2016, pp. 1–38.

[237] J. C. Carvajal, Á. Gómez, and C. A. Cardona, "Comparison of lignin extraction processes: Economic and environmental assessment," *Bioresour. Technol.*, vol. 214, pp. 468–476, 2016.

[238] P. F. Vena, "Integration of xylan extraction prior to kraft and sodaAQ pulping from South African grown Eucalyptus grandis, giant bamboo and sugarcane bagasse to produce paper pulps, value added biopolymers and fermentable sugars," Stellenbosch University, 2013.

[239] C. Chio, M. Sain, and W. Qin, "Lignin utilization: A review of lignin depolymerization from various aspects," *Renewable and Sustainable Energy Reviews*, vol. 107. Elsevier Ltd, pp. 232–249, 01-Jun-2019.

[240] E. Abraham *et al.*, "Extraction of nanocellulose fibrils from lignocellulosic fibres: A novel approach," *Carbohydr. Polym.*, vol. 86, no. 4, pp. 1468–1475, 2011.

[241] M. T. Pius, "Alkaline Polyol Fractionation of Sugarcane Bagasse and Eucalyptus Grandis into Feedstock for value added chemicals and materials," Stellenbosch University, 2017.

[242] L. Capolupo and V. Faraco, "Green methods of lignocellulose pretreatment for biorefinery development," *Appl. Microbiol. Biotechnol.*, vol. 100, no. 22, pp. 9451–9467, 2016.

[243] G. Y. S. Mtui, "Recent advances in pretreatment of lignocellulosic wastes and

production of value added products," *African J. Biotechnol. Vol.*, vol. 8, no. 8, pp. 1398–1415, 2009.

[244] N. Mosier *et al.*, "Features of promising technologies for pretreatment of lignocellulosic biomass," *Bioresour. Technol.*, vol. 96, no. 6, pp. 673–686, 2005.

[245] S. Liu *et al.*, "Removal of bound polyphenols and its effect on antioxidant and prebiotics properties of carrot dietary fiber," *Food Hydrocolloids*, vol. 93. pp. 284–292, 2019.

[246] D. S. Sogi, M. Siddiq, I. Greiby, and K. D. Dolan, "Total phenolics, antioxidant activity, and functional properties of 'Tommy Atkins' mango peel and kernel as affected by drying methods," *Food Chem.*, vol. 141, no. 3, pp. 2649–2655, 2013.

[247] S. Tunchaiyaphum, M. N. Eshtiaghi, and N. Yoswathana, "Extraction of Bioactive Compounds from Mango Peels Using Green Technology," *Int. J. Chem. Eng. Appl.*, vol. 4, no. 4, pp. 194–198, 2013.

[248] R. P. F. F. da Silva, T. A. P. Rocha-Santos, and A. C. Duarte, "Supercritical fluid extraction of bioactive compounds," *TrAC - Trends Anal. Chem.*, vol. 76, pp. 40–51, 2016.

[249] K. Kumar, A. N. Yadav, V. Kumar, P. Vyas, and H. S. Dhaliwal, "Food waste: a potential bioresource for extraction of nutraceuticals and bioactive compounds," *Bioresour. Bioprocess.*, vol. 4, no. 1, p. 18, 2017.

[250] R. González-Montelongo, M. Gloria Lobo, and M. González, "Antioxidant activity in banana peel extracts: Testing extraction conditions and related bioactive compounds," *Food Chem.*, vol. 119, no. 3, pp. 1030–1039, 2010.

[251] F. D. C. Siacor, C. F. Y. Lobarbio, and E. B. Taboada, "Optimizing the extraction of phenolic compounds with high antioxidant activity from mango seed kernel wastes using response surface methodology," *Appl. Environ. Res.*, vol. 42, no. 3, pp. 60–76, 2020.

[252] D. Gómez-Maldonado, C. Lobato-Calleros, E. Aguirre-Mandujano, S. G. Leyva-Mir, L. Robles-Yerena, and E. J. Vernon-Carter, "Antifungal activity of mango kernel polyphenols on mango fruit infected by anthracnose," *LWT*, vol. 126, p. 109337, May 2020.

[253] P. Maisuthisakul and M. H. Gordon, "Antioxidant and tyrosinase inhibitory activity of

mango seed kernel by product," *Food Chem.*, vol. 117, no. 2, pp. 332–341, Nov. 2009.

[254] P. Maisuthisakul and M. H. Gordon, "Antioxidant and tyrosinase inhibitory activity of mango seed kernel by product," *Food Chem.*, vol. 117, no. 2, pp. 332–341, 2009.

[255] M. R. Islam, A. R. Haque, M. R. Kabir, M. M. Hasan, K. J. Khushe, and S. M. K. Hasan, "Fruit by-products: the potential natural sources of antioxidants and α-glucosidase inhibitors," *J. Food Sci. Technol.*, vol. 58, no. 5, pp. 1715–1726, 2021.

[256] S. Rawdkuen, S. Sai-Ut, and S. Benjakul, "Optimizing the Tyrosinase Inhibitory and Antioxidant Activity of Mango Seed Kernels with a Response Surface Methodology," *Food Anal. Methods*, vol. 9, no. 11, pp. 3032–3043, 2016.

[257] Y. Y. Soong and P. J. Barlow, "Quantification of gallic acid and ellagic acid from longan (Dimocarpus longan Lour.) seed and mango (Mangifera indica L.) kernel and their effects on antioxidant activity," *Food Chem.*, vol. 97, no. 3, pp. 524–530, Aug. 2006.

[258] R. González-Montelongo, M. G. Lobo, and M. González, "The effect of extraction temperature, time and number of steps on the antioxidant capacity of methanolic banana peel extracts," *Sep. Purif. Technol.*, vol. 71, no. 3, pp. 347–355, 2010.

[259] F. Mas'Ud, M. Mahendradatta, A. Laga, and Z. Zainal, "Optimization of mango seed kernel oil extraction using response surface methodology," *OCL - Oilseeds fats, Crop. Lipids*, vol. 24, no. 5, 2017.

[260] K. Rajbhar, H. Dawda, and U. Mukundan, "Polyphenols: methods of extraction," *Sci. Revs. Chem. Commun*, vol. 5, no. 1, pp. 1–6, 2015.

[261] Z. Kostalova, Z. Hromádková, S. Paulsen Berit, and A. Ebringerová, "Bioactive hemicelluloses alkali-extracted from Fallopia sachalinensis leaves," *Carbohydr. Res.*, vol. 398, pp. 19–24, 2014.

[262] D. Koegelenberg, "Arabinoxylan as partial flour replacer : The effect on bread properties and economics of bread making by," *Food Chem.*, vol. 221, no. March, pp. 427–435, 2016.

[263] T. O. Matavire, "Extraction and Modification of hemicellulose from Wheat bran to produce entrapment materials for the controlled release of chemicals and bioactive substances," Stellenbosch University, 2018.

[264] G. V Chowdary, S. Hari Krishna, and G. Hanumantha Rao, "Optimization of enzymatic hydrolysis of mango kernel starch by response surface methodology," *Bioprocess Eng.*, vol. 23, no. 6, pp. 681–685, 2000.

[265] A. Nawab, F. Alam, and A. Hasnain, "International Journal of Biological Macromolecules Mango kernel starch as a novel edible coating for enhancing shelf- life of tomato (Solanum lycopersicum) fruit," *Int. J. Biol. Macromol.*, vol. 103, pp. 581–586, 2017.

[266] Y. Liu and P. K. W. Ng, "Relationship between bran characteristics and bran starch of selected soft wheats grown in Michigan," *Food Chem.*, vol. 197, pp. 427–435, 2016.

[267] C. Anderson and S. Simsek, "Mechanical profiles and topographical properties of films made from alkaline extracted arabinoxylans from wheat bran, maize bran, or dried distillers grain," *Food Hydrocoll.*, vol. 86, pp. 78–86, 2019.

[268] B. Palmarola-Adrados, P. Chotěborská, M. Galbe, and G. Zacchi, "Ethanol production from non-starch carbohydrates of wheat bran," *Bioresour. Technol.*, vol. 96, no. 7, pp. 843–850, 2005.

[269] E. I. Goksu, M. Karamanlioglu, U. Bakir, L. Yilmaz, and U. Yilmazer, "Production and characterization of films from cotton stalk xylan," *J. Agric. Food Chem.*, vol. 55, no. 26, pp. 10685–10691, 2007.

[270] N. M. L. Hansen, T. O. J. Blomfeldt, M. S. Hedenqvist, and D. V. Plackett, "Properties of plasticized composite films prepared from nanofibrillated cellulose and birch wood xylan," *Cellulose*, vol. 19, no. 6, pp. 2015–2031, 2012.

[271] S. Shankar, J. P. Reddy, and J. Rhim, "Effect of lignin on water vapor barrier , mechanical , and structural properties of agar / lignin composite films," *Int. J. Biol. Macromol.*, vol. 81, pp. 267–273, 2015.

[272] P. F. Vena, M. P. García-Aparicio, M. Brienzo, J. F. Görgens, and T. Rypstra, "Effect of alkaline hemicellulose extraction on kraft pulp fibers from eucalyptus grandis," *J. Wood Chem. Technol.*, vol. 33, no. 3, pp. 157–173, 2013.

[273] F. Hu and A. Ragauskas, "Pretreatment and Lignocellulosic Chemistry," *Bioenergy Res.*, vol. 5, no. 4, pp. 1043–1066, 2012.

[274] A. Verardi, I. De Bari, E. Ricca, and V. Calabrò, "Hydrolysis of Lignocellulosic

Biomass : Current Status of Processes and Technologies and Future Perspectives," *Bioethanol*, p. 290, 2012.

[275] J. Singh, M. Suhag, and A. Dhaka, "Augmented digestion of lignocellulose by steam explosion , acid and alkaline pretreatment methods : A review," *Carbohydr Polym*, vol. 117, pp. 624–631, 2015.

[276] P. Kumar, D. M. Barrett, M. J. Delwiche, and P. Stroeve, "Methods for pretreatment of lignocellulosic biomass for efficient hydrolysis and biofuel production," *Ind. Eng. Chem. Res.*, vol. 48, no. 8, pp. 3713–3729, 2009.

[277] C. E. Wyman, B. E. Dale, R. T. Elander, M. Holtzapple, M. R. Ladisch, and Y. Y. Lee, "Coordinated development of leading biomass pretreatment technologies," *Bioresour. Technol.*, vol. 96, no. 18 SPEC. ISS., pp. 1959–1966, 2005.

[278] L. Capolupo and V. Faraco, "Green methods of lignocellulose pretreatment for biorefinery development," *Appl. Microbiol. Biotechnol.*, vol. 100, no. 22, pp. 9451–9467, 2016.

[279] C. Rezende, M. de Lima, P. Maziero, E. DeAzevedo, W. Garcia, and I. Polikarpov, "Chemical and morphological characterization of sugarcane bagasse submitted to a delignification process for enhanced enzymatic digestibility," *Biotechnol. Biofuels*, vol. 4, no. 1, p. 54, 2011.

[280] R. Gupta and Y. Y. Lee, "Pretreatment of corn stover and hybrid poplar by sodium hydroxide and hydrogen peroxide," *Biotechnol. Prog.*, vol. 26, no. 4, pp. 1180–1186, 2010.

[281] M. Gáspár, G. Kálmán, and K. Réczey, "Corn fiber as a raw material for hemicellulose and ethanol production," *Process Biochem.*, vol. 42, no. 7, pp. 1135–1139, 2007.

[282] A. Ebringerová, Z. Hromádková, Z. Košťálová, and V. Sasinková, "Chemical valorization of agricultural by-products:Isolation and characterization of xylan-based antioxidants from almond shell biomass," *BioResources*, vol. 3, no. 1, pp. 60–70, 2008.

[283] J. Xu, J. J. Cheng, R. R. Sharma-Shivappa, and J. C. Burns, "Sodium hydroxide pretreatment of switchgrass for ethanol production," *Energy and Fuels*, vol. 24, no. 3, pp. 2113–2119, 2010.

[284] W. Geng *et al.*, "The influence of lignin content and structure on hemicellulose alkaline

extraction for non-wood and hardwood lignocellulosic biomass," *Cellulose*, vol. 26, no. 5, pp. 3219–3230, 2019.

[285] W. Geng, R. A. Venditti, J. J. Pawlak, and H. M. Chang, "Effect of delignification on hemicellulose extraction from switchgrass, poplar, and pine and its effect on enzymatic convertibility of Cellulose-rich Residues," *BioResources*, vol. 13, no. 3, pp. 4946–4963, 2018.

[286] P. F. Vena, M. Brienzo, M. D. P. Garc??a-Aparicio, J. F. G??rgens, and T. Rypstra, "Hemicelluloses extraction from giant bamboo (Bambusa balcooa Roxburgh) prior to kraft or soda-AQ pulping and its effect on pulp physical properties," *Holzforschung*, vol. 67, no. 8, pp. 863–870, 2013.

[287] A. J. Joubert, "Integration of Xylan Extraction From E . Grandis , Prior To Pulping , Into Kraft," Stellenbosch University, 2015.

[288] N. Ratanasumarn and P. Chitprasert, "Cosmetic potential of lignin extracts from alkaline-treated sugarcane bagasse: Optimization of extraction conditions using response surface methodology," *Int. J. Biol. Macromol.*, vol. 153, pp. 138–145, 2020.

[289] F. Peng, P. Peng, F. Xu, and R. C. Sun, "Fractional purification and bioconversion of hemicelluloses," *Biotechnol. Adv.*, vol. 30, no. 4, pp. 879–903, 2012.

[290] A. Höije, M. Gröndahl, K. Tømmeraas, and P. Gatenholm, "Isolation and characterization of physicochemical and material properties of arabinoxylans from barley husks," *Carbohydr. Polym.*, vol. 61, no. 3, pp. 266–275, 2005.

[291] Y. Hamzeh, A. Ashori, Z. Khorasani, A. Abdulkhani, and A. Abyaz, "Pre-extraction of hemicelluloses from bagasse fibers: Effects of dry-strength additives on paper properties," *Ind. Crops Prod.*, vol. 43, no. 1, pp. 365–371, 2013.

[292] I. Egüés, C. Sanchez, I. Mondragon, and J. Labidi, "Effect of alkaline and autohydrolysis processes on the purity of obtained hemicelluloses from corn stalks," *Bioresour. Technol.*, vol. 103, pp. 239–248, 2012.

[293] R. Sun, J. M. Lawther, and W. B. Banks, "Fractional and structural characterization of wheat straw hemicelluloses," *Carbohydr. Polym.*, vol. 29, no. 4, pp. 325–331, 1996.

[294] J. C. García, M. J. Díaz, M. T. Garcia, M. J. Feria, D. M. Gómez, and F. López, "Search for optimum conditions of wheat straw hemicelluloses cold alkaline extraction process,"

Biochem. Eng. J., vol. 71, pp. 127–133, 2013.

[295] D. Morais De Carvalho, C. Marchand, J. Berglund, M. E. Lindström, F. Vilaplana, and O. Sevastyanova, "Impact of birch xylan composition and structure on film formation and properties," *Holzforschung*, vol. 74, no. 2, pp. 184–196, 2019.

[296] A. J. Joubert, A. F. A. Chimphango, and J. F. Görgens, "Effect of Integrating Xylan Extraction from E. grandis into the Kraft Pulping Process on Pulp Yield and Chemical Balance," *BioResources*, vol. 11, no. 1, pp. 2417–2437, 2016.

[297] D. L. Júnior, A. Ayoub, R. A. Venditti, H. Jameel, J. L. Colodette, and H. min Chang, "Ethanol precipitation of hetero-polysaccharide material from hardwood by alkaline extraction prior to the kraft cooking process," *BioResources*, vol. 8, no. 4, pp. 5319–5332, 2013.

[298] M. A. Lima *et al.*, "Effects of pretreatment on morphology, chemical composition and enzymatic digestibility of eucalyptus bark: a potentially valuable source of fermentable sugars for biofuel production - part 1.," *Biotechnol. Biofuels*, vol. 6, no. 1, p. 75, 2013.

[299] C. K. Simi and T. E. Abraham, "Biodegradable biocompatible xyloglucan films for various applications," *Colloid Polym. Sci.*, vol. 288, no. 3, pp. 297–306, 2010.

[300] W. B. Wei, L. N. Li, L. Chang, and Z. Wang, "Chemical and structural characterization of alkaline-extractable hemicelluloses from various eucalyptus species," *J. Appl. Polym. Sci.*, vol. 130, no. 4, pp. 2390–2398, 2013.

[301] A. Ayoub, R. A. Venditti, J. J. Pawlak, H. Sadeghifar, and A. Salam, "Development of an acetylation reaction of switchgrass hemicellulose in ionic liquid without catalyst," *Ind. Crops Prod.*, vol. 44, pp. 306–314, 2013.

[302] F. Bello and A. Chimphango, "Tailor-Made Conversion of Mango Seed Husks to Obtain Hemicellulose Suitable for the Production of Thermally Stable Films," *Waste and Biomass Valorization*, vol. 1, p. 3, 2021.

[303] A. Modenbach, "Sodium hydroxide pretreatment of corn stover and subsequent enzymatic hydrolysis: An investigation of yields , kinetic modeling and glucose recovery," University of Kentucky, 2013.

[304] G. Bali, X. Meng, J. I. Deneff, Q. Sun, and A. J. Ragauskas, "The effect of alkaline pretreatment methods on cellulose structure and accessibility," *ChemSusChem*, vol. 8,

no. 2, pp. 275–279, 2015.

[305] Q. Li *et al.*, "Comparison of different alkali-based pretreatments of corn stover for improving enzymatic saccharification," *Bioresour. Technol.*, vol. 125, pp. 193–199, Dec. 2012.

[306] L. D. Khuong, R. Kondo, R. De Leon, T. Kim Anh, K. Shimizu, and I. Kamei, "Bioethanol production from alkaline-pretreated sugarcane bagasse by consolidated bioprocessing using Phlebia sp. MG-60," *Int. Biodeterior. Biodegrad.*, vol. 88, pp. 62–68, Mar. 2014.

[307] M. Kim and D. F. Day, "Composition of sugar cane, energy cane, and sweet sorghum suitable for ethanol production at Louisiana sugar mills," *J. Ind. Microbiol. Biotechnol.*, vol. 38, no. 7, pp. 803–807, 2011.

[308] I. R. S. Arruda *et al.*, "International Journal of Biological Macromolecules Structure and rheological properties of a xyloglucan extracted from Hymenaea courbaril var . courbaril seeds," *Int. J. Biol. Macromol.*, vol. 73, pp. 31–38, 2015.

[309] S. S. Mankar, A. R. Chaudhari, and I. Soni, "Lignin in Phenol-Formaldehyde Adhesives," *Int. J. Knowl. Eng.*, vol. 3, no. 1, pp. 116–118, 2012.

[310] X. Zhao, S. Li, R. Wu, and D. Liu, "Organosolv fractionating pre-treatment of lignocellulosic biomass for effi cient enzymatic saccharifi cation: chemistry, kinetics, and substrate structures," *Biofuels, Bioprod. Biorefining*, vol. 11, no. 2017, pp. 567–590, 2017.

[311] P. Sannigrahi and A. J. Ragauskas, "Fundamentals of Biomass Pretreatment by Fractionation," *Aqueous Pretreat. Plant Biomass Biol. Chem. Convers. to Fuels Chem.*, pp. 201–222, 2013.

[312] K. Zhang, Z. Pei, and D. Wang, "Organic solvent pretreatment of lignocellulosic biomass for biofuels and biochemicals: A review," *Bioresour. Technol.*, vol. 199, pp. 21–33, 2016.

[313] J. Domínguez-Robles, R. Sánchez, P. Díaz-Carrasco, E. Espinosa, M. T. García-Domínguez, and A. Rodríguez, "Isolation and characterization of lignins from wheat straw: Application as binder in lithium batteries," *Int. J. Biol. Macromol.*, vol. 104, pp. 909–918, 2017.

[314] O. Y. Abdelaziz *et al.*, "Biological valorization of low molecular weight lignin," *Biotechnol. Adv.*, vol. 34, no. 8, pp. 1318–1346, 2016.

[315] W. J. J. Huijgen, J. H. Reith, and H. Den Uil, "Pretreatment and fractionation of wheat straw by an acetone-based organosolv process," *Ind. Eng. Chem. Res.*, vol. 49, no. 20, pp. 10132–10140, 2010.

[316] M. Raita, N. Denchokepraguy, V. Champreda, and N. Laosiripojana, "Effects of alkaline catalysts on acetone-based organosolv pretreatment of rice straw," *3 Biotech*, vol. 7, no. 5, pp. 1–10, 2017.

[317] W. J. J. Huijgen, J. H. Reith, and H. Den Uil, "Pretreatment and fractionation of wheat straw by an acetone-based organosolv process," *Ind. Eng. Chem. Res.*, vol. 49, no. 20, pp. 10132–10140, 2010.

[318] A. Romaní, G. Garrote, F. López, and J. C. Parajó, "Eucalyptus globulus wood fractionation by autohydrolysis and organosolv delignification," *Bioresour. Technol.*, vol. 102, no. 10, pp. 5896–5904, 2011.

[319] L. Mesa *et al.*, "Preliminary evaluation of organosolv pre-treatment of sugar cane bagasse for glucose production: Application of 23 experimental design," *Appl. Energy*, vol. 87, no. 1, pp. 109–114, 2010.

[320] H. Amiri, K. Karimi, and H. Zilouei, "Organosolv pretreatment of rice straw for efficient acetone, butanol, and ethanol production," *Bioresour. Technol.*, vol. 152, pp. 450–456, Jan. 2014.

[321] B. B. Hallac, P. Sannigrahi, Y. Pu, M. Ray, R. J. Murphy, and A. J. Ragauskas, "Effect of ethanol organosolv pretreatment on enzymatic hydrolysis of Buddleja davidii stem biomass," *Ind. Eng. Chem. Res.*, vol. 49, no. 4, pp. 1467–1472, 2010.

[322] A. T. W. M. Hendriks and G. Zeeman, "Pretreatments to enhance the digestibility of lignocellulosic biomass," *Bioresour. Technol.*, vol. 100, no. 1, pp. 10–18, 2009.

[323] P. Manara, A. Zabaniotou, C. Vanderghem, and A. Richel, "Lignin extraction from Mediterranean agro-wastes: Impact of pretreatment conditions on lignin chemical structure and thermal degradation behavior," in *Catalysis Today*, 2014, vol. 223, pp. 25–34.

[324] N. Park, H. Y. Kim, B. W. Koo, H. Yeo, and I. G. Choi, "Organosolv pretreatment with

various catalysts for enhancing enzymatic hydrolysis of pitch pine (Pinus rigida)," *Bioresour. Technol.*, vol. 101, no. 18, pp. 7046–7053, 2010.

[325] M. F. Li, S. N. Sun, F. Xu, and R. C. Sun, "Ultrasound-enhanced extraction of lignin from bamboo (Neosinocalamus affinis): Characterization of the ethanol-soluble fractions," *Ultrason. Sonochem.*, vol. 19, no. 2, pp. 243–249, 2012.

[326] F. F. Sun *et al.*, "Biorefining fractionation of the Camellia oleifera Abel. hull into diverse bioproducts with a two-stage organosolv extraction," *Ind. Crops Prod.*, vol. 94, pp. 790–799, Dec. 2016.

[327] P. Dhankhar, "Homogenization Fundamentals," *IOSR J. Eng.*, vol. 04, no. 05, pp. 1–8, 2014.

[328] Y. F. Maa and C. Hsu, "Liquid-liquid emulsification by rotor/stator homogenization," *J. Control. Release*, vol. 38, no. 2–3, pp. 219–228, 1996.

[329] A. O'Driscoll, "The Forces Involved in Homogenization Explained," 2019. [Online]. Available: https://homogenizers.net/blogs/blog/forces-involved-in-homogenization. [Accessed: 16-Aug-2021].

[330] I. Siro´ and D. Plackett, "Microfibrillated cellulose and new nanocomposite materials: A review," *Cellulose*, vol. 17, no. 3, pp. 459–494, 2010.

[331] H. Kargarzadeh, M. Ioelovich, I. Ahmad, S. Thomas, and A. Dufresne, "Methods for Extraction of Nanocellulose from Various Sources," in *Handbook of Nanocellulose and Cellulose Nanocomposites*, 2017, pp. 1–49.

[332] C. G. Vargas-rechia *et al.*, "A profile of the South African table grape market value chain," *Bioresour. Technol.*, vol. 6, no. 1, pp. 1–14, Jan. 2015.

[333] M. López-Rodríguez *et al.*, "Assessment of multi-step processes for an integral use of the biomass of the marine microalga Amphidinium carterae," *Bioresour. Technol.*, vol. 282, no. March, pp. 370–377, 2019.

[334] H. Zhang, Y. Xu, and S. Yu, "Bioresource Technology Co-production of functional xylooligosaccharides and fermentable sugars from corncob with effective acetic acid prehydrolysis," *Bioresour. Technol.*, vol. 234, pp. 343–349, 2017.

[335] A. M. Da Costa Lopes, R. M. G. Lins, R. A. Rebelo, and R. M. Łukasik, "Biorefinery

approach for lignocellulosic biomass valorisation with an acidic ionic liquid," *Green Chem.*, vol. 20, p. 4043, 2018.

[336] J. Varavadekar, P. Konde, S. Adhyapak, S. Gujrathi, A. Pooja, and A. Lali, "A multi step process for fractionation of lignocellulosic biomass," *8th World Congr. Chem. Eng. Inc. 59th Can. Chem. Eng. Conf. 24th Interam. Congr. Chem. Eng.*, no. January, 2009.

[337] T. E. Amidon, B. Bujanovic, S. Liu, and J. R. Howard, "Commercializing biorefinery technology: A case for the multi-product pathway to a viable biorefinery," *Forests*, vol. 2, no. 4, pp. 929–947, 2011.

[338] J. Li *et al.*, "Homogeneous isolation of nanocellulose from sugarcane bagasse by high pressure homogenization," *Carbohydr. Polym.*, vol. 90, no. 4, pp. 1609–1613, 2012.

[339] F. T. Seta *et al.*, "Preparation and characterization of high yield cellulose nanocrystals (CNC) derived from ball mill pretreatment and maleic acid hydrolysis," *Carbohydr. Polym.*, vol. 234, Apr. 2020.

[340] X. Cao, H. Dong, and C. M. Li, "New nanocomposite materials reinforced with cellulose nanocrystals in nitrile rubber," *Biomacromolecules*, vol. 8, no. 3, pp. 899–904, 2007.

[341] P. H. F. Pereira, H. L. Ornaghi Júnior, L. V. Coutinho, B. Duchemin, and M. O. H. Cioffi, "Obtaining cellulose nanocrystals from pineapple crown fibers by free-chlorite hydrolysis with sulfuric acid: physical, chemical and structural characterization," *Cellulose*, vol. 27, no. 10, pp. 5745–5756, 2020.

[342] Y. Liu, H. Wang, G. Yu, Q. Yu, B. Li, and X. Mu, "A novel approach for the preparation of nanocrystalline cellulose by using phosphotungstic acid," *Carbohydr. Polym.*, vol. 110, pp. 415–422, 2014.

[343] P. P. Zhang *et al.*, "Effects of acid treatments on bamboo cellulose nanocrystals," *Asia-Pacific J. Chem. Eng.*, no. 9, pp. 686–695, 2014.

[344] T. M. Koskinen, P. Qvintus, C. Ritschkoff, T. Tammelin, and J. Pere, "Nanocellulose materials - preparation, properties, uses," p. 29, 2013.

[345] M. R. K. Sofla, R. J. Brown, T. Tsuzuki, and T. J. Rainey, "A comparison of cellulose nanocrystals and cellulose nano fi bres extracted from bagasse using acid and ball milling methods," *Adv. Nat. Sci. Nanosci. Nanotechnol.*, vol. 7, 2016.

[346] D. Klemm *et al.*, "Reviews Nanocelluloses : A New Family of Nature-Based Materials Angewandte," *Green Nanomater.*, pp. 5438–5466, 2011.

[347] X. M. Dong, J. F. Revol, and D. G. Gray, "Effect of microcrystallite preparation conditions on the formation of colloid crystals of cellulose," *Cellulose*, vol. 5, no. 1, pp. 19–32, 1998.

[348] S. Bhattacharjee, "DLS and zeta potential - What they are and what they are not?," *J. Control. Release*, vol. 235, pp. 337–351, 2016.

[349] S. Naduparambath, J. T.V., V. Shaniba, S. M.P., A. K. Balan, and E. Purushothaman, "Isolation and characterisation of cellulose nanocrystals from sago seed shells," *Carbohydr. Polym.*, vol. 180, pp. 13–20, Jan. 2018.

[350] T. Lindström, "Current Opinion in Colloid & Interface Science Aspects on nano fi brillated cellulose (NFC) processing , rheology and NFC- fi lm properties," *Curr. Opin. Colloid Interface Sci.*, vol. 29, pp. 68–75, 2017.

[351] A. C. W. Leung *et al.*, "Characteristics and properties of carboxylated cellulose nanocrystals prepared from a novel one-step procedure," *Cellul. Nanoparticles*, vol. 7, no. 3, pp. 302–305, 2011.

[352] H. Du *et al.*, "Preparation and characterization of thermally stable cellulose nanocrystals via a sustainable approach of FeCl3-catalyzed formic acid hydrolysis," *Cellulose*, vol. 23, no. 4, pp. 2389–2407, 2016.

[353] M. A. Torlopov *et al.*, "Cellulose nanocrystals with different length-to-diameter ratios extracted from various plants using novel system acetic acid / phosphotungstic acid / octanol-1," *Cellulose*, vol. 25, no. 2, pp. 1031–1046, 2018.

[354] J. P. Reddy and J. W. Rhim, "Characterization of bionanocomposite films prepared with agar and paper-mulberry pulp nanocellulose," *Carbohydr. Polym.*, vol. 110, pp. 480–488, Sep. 2014.

[355] N. Hastuti, K. Kanomata, and T. Kitaoka, "Hydrochloric Acid Hydrolysis of Pulps from Oil Palm Empty Fruit Bunches to Produce Cellulose Nanocrystals," *J. Polym. Environ.*, vol. 26, no. 9, pp. 3698–3709, 2018.

[356] S. Rebouillat and F. Pla, "State of the Art Manufacturing and Engineering of Nanocellulose: A Review of Available Data and Industrial Applications," *J. Biomater.*

Nanobiotechnol., vol. 04, no. 02, pp. 165–188, 2013.

[357] M. Visanko, "Functionalized nanocelluloses and their use in barrier and membrane thin films," University of Oulo, 2015.

[358] S. Mbakop, L. N. Nthunya, and M. S. Onyango, "Recent advances in the synthesis of nanocellulose functionalized-hybrid membranes and application in water quality improvement," *Processes*, vol. 9, no. 4, 2021.

[359] J. Rojas, M. Bedoya, and Y. Ciro, "Current Trends in the Production of Cellulose Nanoparticles and Nanocomposites for Biomedical Applications," in *Cellulose - Fundamental Aspects and Current Trends*, 2015, pp. 193–228.

[360] I. Siró, D. Plackett, M. Hedenqvist, M. Ankerfors, and T. Lindström, "Highly transparent films from carboxymethylated microfibrillated cellulose: The effect of multiple homogenization steps on key properties," *J. Appl. Polym. Sci.*, vol. 119, no. 5, pp. 2652–2660, 2011.

[361] M. Börjesson and G. Westman, "Crystalline Nanocellulose — Preparation, Modification, and Properties," in *Cellulose - Fundamental Aspects and Current Trends*, 2015.

[362] S. Kamel, "Nanotechnology and its applications in lignocellulosic composites , a mini review," vol. 1, no. 9, pp. 546–575, 2007.

[363] S. Y. Lee, S. J. Chun, I. A. Kang, and J. Y. Park, "Preparation of cellulose nanofibrils by high-pressure homogenizer and cellulose-based composite films," *J. Ind. Eng. Chem.*, vol. 15, no. 1, pp. 50–55, 2009.

[364] E. Dinand, H. Chanzy, and M. R. Vignon, "Suspensions of cellulose microfibrils from sugar beet pulp," vol. 13, pp. 275–283, 1999.

[365] A. Dufresne and M. R. Vignon, "Improvement of Starch Film Performances Using Cellulose Microfibrils," *Macromolecules*, vol. 31, no. 97, pp. 2693–2696, 1998.

[366] M. L. Hassan, A. P. Mathew, E. A. Hassan, N. A. El-Wakil, and K. Oksman, "Nanofibers from bagasse and rice straw: Process optimization and properties," *Wood Sci. Technol.*, vol. 46, no. 1–3, pp. 193–205, 2012.

[367] T. Lindström and M. Henriksson, "Roadmap 2015 to 2025 Materials from

nanocellulose," *Rise*, pp. 1–8, 2015.

[368] R. Ma, A. Pekarovicova, P. D. Fleming, and V. Husovska, "Preparation and characterization of hemicellulose-based printable films," *Cellul. Chem. Technol.*, vol. 51, no. 9–10, pp. 939–948, 2017.

[369] Y. Zhao, H. Sun, B. Yang, and Y. Weng, "Hemicellulose-Based Film: Potential Green Films for Food Packaging," *Polymers (Basel).*, vol. 12, no. 8, p. 1775, Aug. 2020.

[370] S. S. Ahankari, A. R. Subhedar, S. S. Bhadauria, and A. Dufresne, "Nanocellulose in food packaging: A review," *Carbohydr. Polym.*, vol. 255, no. December 2020, p. 117479, 2021.

[371] O. Gordobil, I. Egüés, I. Urruzola, and J. Labidi, "Xylan-cellulose films: Improvement of hydrophobicity, thermal and mechanical properties," *Carbohydr. Polym.*, vol. 112, pp. 56–62, 2014.

[372] Z. Li and X. Pan, "Strategies to modify physicochemical properties of hemicelluloses from biorefinery and paper industry for packaging material," *Reviews in Environmental Science and Biotechnology*, vol. 17, no. 1. pp. 47–69, 2018.

[373] N. M. L. Hansen and D. Plackett, "Sustainable films and coatings from hemicelluloses: A review," *Biomacromolecules*, vol. 9, no. 6, pp. 1493–1505, 2008.

[374] X. Zhang, N. Xiao, M. Chen, Y. Wei, and C. Liu, "Functional packaging films originating from hemicelluloses laurate by direct transesterification in ionic liquid," *Carbohydr. Polym.*, vol. 229, no. June 2019, p. 115336, 2020.

[375] T. Shimokawa, E. Togawa, K. Kakegawa, A. Kato, and N. Hayashi, "Film formation and some structural features of hemicellulose fractions from Pinus densiflora leaves," *J. Wood Sci.*, vol. 61, no. 1, pp. 53–59, 2014.

[376] L. R. Mugwagwa and A. F. A. Chimphango, "Enhancing the functional properties of acetylated hemicellulose films for active food packaging using acetylated nanocellulose reinforcement and polycaprolactone coating," *Food Packag. Shelf Life*, vol. 24, p. 100481, 2020.

[377] K. S. Mikkonen and M. Tenkanen, "Sustainable food-packaging materials based on future biorefinery products: Xylans and mannans," *Trends in Food Science and Technology*. 2012.

[378] J. Manuel Quiroz-Castillo *et al.*, "Preparation and Characterization of Films Extruded of Polyethylene/Chitosan Modified with Poly(lactic acid)," *Materials (Basel).*, vol. 8, pp. 137–148, 2015.

[379] J. M. Quiroz-Castillo *et al.*, "Preparation of extruded polyethylene/chitosan blends compatibilized with polyethylene-graft-maleic anhydride," *Carbohydr. Polym.*, vol. 101, no. 1, pp. 1094–1100, Jan. 2014.

[380] M. Maniruzzaman *et al.*, "A Review of Hot-Melt Extrusion: Process Technology to Pharmaceutical Products," *Int. Sch. Res. Netw. ISRN Pharm.*, vol. 2012, 2012.

[381] J. W. Rhim, A. K. Mohanty, S. P. Singh, and P. K. W. Ng, "Effect of the processing methods on the performance of polylactide films: Thermocompression versus solvent casting," *J. Appl. Polym. Sci.*, vol. 101, no. 6, pp. 3736–3742, Sep. 2006.

[382] L. F. Wang, J. W. Rhim, and S. I. Hong, "Preparation of poly(lactide)/poly(butylene adipate-co-terephthalate) blend films using a solvent casting method and their food packaging application," *LWT - Food Sci. Technol.*, vol. 68, pp. 454–461, 2016.

[383] P. M. Amin, A. B. Gangurde, and P. V Alai, "Oral Film Technology : Challenges and Future Scope for Pharmaceutical Industry," *Int. J. Pharm. Pharm. Res.*, vol. 3, no. 3, pp. 183–203, 2015.

[384] Alibaba, "No." [Online]. Available: https://www.alibaba.com/trade/search?fsb=y&IndexArea=product_en&CatId=&SearchText=hemicellulose&viewtype=&tab=.

[385] F. J. A. A. Ekorong, G. Zomegni, S. C. Z. Desobgo, and R. Ndjouenkeu, "Optimization of drying parameters for mango seed kernels using central composite design," *Bioresour. Bioprocess.*, vol. 2, no. 1, 2015.

[386] F. D. Siacor and E. Taboada, "Integrated processes for the treatment of mango wastes of fruit processing and the preparation of compositions derived thereof," 2013.

[387] B. L. White, L. R. Howard, and R. L. Prior, "Release of Bound Procyanidins from Cranberry Pomace by Alkaline Hydrolysis," *J. Agric. Food Chem*, vol. 58, pp. 7572–7579, 2010.

[388] E. Dorta, M. González, M. G. Lobo, C. Sánchez-Moreno, and B. de Ancos, "Screening of phenolic compounds in by-product extracts from mangoes (Mangifera indica L.) by

HPLC-ESI-QTOF-MS and multivariate analysis for use as a food ingredient," *Food Res. Int.*, vol. 57, pp. 51–60, Jan. 2014.

[389] T. vom Stein, P. M. Grande, H. Kayser, F. Sibilla, W. Leitner, and P. Domínguez de María, "From biomass to feedstock: One-step fractionation of lignocellulose components by the selective organic acid-catalyzed depolymerization of hemicellulose in a biphasic system," *Green Chem.*, vol. 13, no. 7, pp. 1772–1777, 2011.

[390] P. D. Carà *et al.*, "Hemicellulose hydrolysis catalysed by solid acids," *Catal. Sci. Technol.*, vol. 3, no. 8, pp. 2057–2061, 2013.

[391] X. J. Ma *et al.*, "Degradation and dissolution of hemicelluloses during bamboo hydrothermal pretreatment," *Bioresour. Technol.*, vol. 161, pp. 215–220, Jun. 2014.

[392] M. Aguedo, S. Kohnen, N. Rabetafika, S. Vanden, M. Paquot, and C. Blecker, "Composition of by-products from cooked fruit processing and potential use in food products," *J. Food Compos. Anal.*, vol. 27, pp. 61–69, 2012.

[393] B. A. Acosta-estrada, J. A. Gutiérrez-uribe, and S. O. Serna-saldívar, "Bound phenolics in foods , a review," *FOOD Chem.*, vol. 152, pp. 46–55, 2014.

[394] M. Bataillon, P. Mathaly, A. N. Cardinali, and F. Duchiron, "Extraction and purification of arabinoxylan from destarched wheat bran in a pilot scale," *Ind. Crops Prod.*, vol. 8, pp. 37–43, 1998.

[395] K. H. Kim, R. Tsao, R. Yang, and S. W. Cui, "Phenolic acid profiles and antioxidant activities of wheat bran extracts and the effect of hydrolysis conditions," *Food Chem.*, vol. 95, no. 3, pp. 466–473, 2006.

[396] C. M. G. C. Renard, C. Lemeunier, and J. F. Thibault, "Alkaline extraction of xyloglucan from depectinised apple pomace: optimisation and characterisation," *Carbohydr. Polym.*, vol. 28, no. 3, pp. 209–216, 1995.

[397] H. M. Yashoda, T. N. Prabha, and R. N. Tharanathan, "Mango ripening - Chemical and structural characterization of pectic and hemicellulosic polysaccharides," *Carbohydr. Res.*, vol. 340, no. 7, pp. 1335–1342, May 2005.

[398] A. Escalante *et al.*, "Flexible oxygen barrier films from spruce xylan," *Carbohydr. Polym.*, vol. 87, no. 4, pp. 2381–2387, 2012.

[399] J. Kochumalayil, H. Sehaqui, Q. Zhou, and L. A. Berglund, "Tamarind seed xyloglucan - A thermostable high-performance biopolymer from non-food feedstock," *J. Mater. Chem.*, vol. 20, no. 21, pp. 4321–4327, 2010.

[400] K. Liu, H. Li, J. Zhang, Z. Zhang, and J. Xu, "Bioresource Technology The effect of non-structural components and lignin on hemicellulose extraction," *Bioresour. Technol.*, vol. 214, pp. 755–760, 2016.

[401] C. Hutterer, G. Schild, and A. Potthast, "Bioresource Technology A precise study on effects that trigger alkaline hemicellulose extraction efficiency," *Bioresour. Technol.*, vol. 214, pp. 460–467, 2016.

[402] A. Kozioł, J. Cybulska, P. M. Pieczywek, and A. Zdunek, "Evaluation of Structure and Assembly of Xyloglucan from Tamarind Seed (Tamarindus indica L.) with Atomic Force Microscopy," *Food Biophys.*, vol. 10, no. 4, pp. 396–402, 2015.

[403] K. C. Kai and C. L. de O. Petkowicz, "Influence of extraction conditions on properties of seed xyloglucan," *Int. J. Biol. Macromol.*, vol. 46, no. 2, pp. 223–228, 2010.

[404] E. M. Karp *et al.*, "Alkaline pretreatment of corn stover: Bench-scale fractionation and stream characterization," *ACS Sustain. Chem. Eng.*, vol. 2, no. 6, pp. 1481–1491, 2014.

[405] H. Krawczyk, *Separation of Biomass Components by Membrane Filtration Process Development for Hemicellulose Recovery*, no. September. 2013.

[406] T. H. Kim, D. Im, K. K. Oh, and T. H. Kim, "Effects of Organosolv Pretreatment Using Temperature-Controlled Bench-Scale Ball Milling on Enzymatic Saccharification of Miscanthus × giganteus," *Energies*, vol. 11, p. 2657, 2018.

[407] S. Beisl, F. Biermair, A. Friedl, N. Mundigler, and A. Miltner, "Sequential extrusion and organosolv pretreatment for wheat straw valorization," *Chem. Eng. Trans.*, vol. 61, pp. 853–858, 2017.

[408] B. Braun and J. R. Dorgan, "Single-step method for the isolation and surface functionalization of cellulosic nanowhiskers," *Biomacromolecules*, vol. 10, no. 2, pp. 334–341, 2009.

[409] H. Xie *et al.*, "Preparation of thermally stable and surface-functionalized cellulose nanocrystals via mixed H2SO4/Oxalic acid hydrolysis," *Carbohydr. Polym.*, vol. 223, 2019.

[410] S. N. Joglekar, P. D. Pathak, S. A. Mandavgane, and B. D. Kulkarni, “Process of fruit peel waste biorefinery: a case study of citrus waste biorefinery, its environmental impacts and recommendations,” *Environ. Sci. Pollut. Res.*, vol. 26, no. 34, pp. 34713–34722, 2019.

[411] A. Asif *et al.*, “Therapeutic potentials of bioactive compounds from mango fruit wastes,” *Trends Food Sci. Technol.*, vol. 53, pp. 102–112, 2016.

[412] H. N. Rajha, T. Mhanna, S. El Kantar, A. El Khoury, N. Louka, and R. G. Maroun, “Innovative process of polyphenol recovery from pomegranate peels by combining green deep eutectic solvents and a new infrared technology,” *LWT*, vol. 111, pp. 138–146, 2019.

[413] K. Ghafoor, Y. Hee Choi, J. Yeong Jeon, and I. J. Hee, “Optimization of Ultrasound-Assisted Extraction of Phenolic Compounds, Antioxidants, and Anthocyanins from Grape (Vitis vinifera) Seeds,” *J. Agric. Food Chem*, vol. 57, pp. 4988–4994, 2009.

[414] J. E. Cacace and G. Mazza, “Mass transfer process during extraction of phenolic compounds from milled berries,” *J. Food Eng.*, vol. 59, no. 4, pp. 379–389, 2003.

[415] Y. Liu and P. K. W. Ng, “Isolation and characterization of wheat bran starch and endosperm starch of selected soft wheats grown in Michigan and comparison of their physicochemical properties,” *Food Chem.*, vol. 176, pp. 137–144, 2015.

[416] B. Yang, X. Liu, and Y. Gao, “Extraction optimization of bioactive compounds (crocin, geniposide and total phenolic compounds) from Gardenia (Gardenia jasminoides Ellis) fruits with response surface methodology,” *Innov. Food Sci. Emerg. Technol.*, vol. 10, no. 4, pp. 610–615, 2009.

[417] H. Yilmaz Celebioglu, D. Cekmecelioglu, M. Dervisoglu, and T. Kahyaoglu, “Effect of extraction conditions on hemicellulose yields and optimisation for industrial processes,” *Int. J. Food Sci. Technol.*, vol. 47, no. 12, pp. 2597–2605, 2012.

[418] Q. Yuan *et al.*, “Extraction optimization, characterization and antioxidant activity in vitro of polysaccharides from mulberry (Morus alba L.) leaves,” *Carbohydr. Polym.*, vol. 128, pp. 52–62, 2015.

[419] Y. W. Chen, H. V. Lee, S. Bee, and A. Hamid, “Investigation of optimal conditions for production of highly crystalline nanocellulose with increased yield via novel Cr (III) -

catalyzed hydrolysis : Response surface methodology," *Carbohydr. Polym.*, vol. 178, no. April, pp. 57–68, 2017.

[420] J. M. Fang, R. C. Sun, and J. Tomkinson, "Isolation and characterization of hemicelluloses and cellulose from rye straw by alkaline peroxide extraction," *Cellulose*, vol. 7, no. 1, pp. 87–107, 2000.

[421] H. S. Yim, F. Y. Chye, S. M. Koo, P. Matanjun, S. E. How, and C. W. Ho, "Optimization of extraction time and temperature for antioxidant activity of edible wild mushroom, Pleurotus porrigens," *Food Bioprod. Process.*, vol. 90, no. 2, pp. 235–242, 2012.

[422] E. Kiassos, S. Mylonaki, D. P. Makris, and P. Kefalas, "Implementation of response surface methodology to optimise extraction of onion (Allium cepa) solid waste phenolics," *Innov. Food Sci. Emerg. Technol.*, vol. 10, no. 2, pp. 246–252, 2009.

[423] X. F. Sun, Z. Jing, P. Fowler, Y. Wu, and M. Rajaratnam, "Structural characterization and isolation of lignin and hemicelluloses from barley straw," *Ind. Crops Prod.*, vol. 33, no. 3, pp. 588–598, 2011.

[424] H. Peng *et al.*, "Physicochemical characterization of hemicelluloses from bamboo (Phyllostachys pubescens Mazel) stem," *Ind. Crops Prod.*, vol. 37, no. 1, pp. 41–50, 2012.

[425] A. X. Jin *et al.*, "Comparative characterization of degraded and non-degradative hemicelluloses from barley straw and maize stems: Composition, structure, and thermal properties," *Carbohydr. Polym.*, vol. 78, no. 3, pp. 609–619, 2009.

[426] N. Y. Abu-thabit, A. Abu, A. S. Hakeem, A. Ul-hamid, Y. Umar, and A. Ahmad, "Isolation and characterization of microcrystalline cellulose from date seeds (Phoenix dactylifera L .)," *Int. J. Biol. Macromol.*, vol. 155, pp. 730–739, 2020.

[427] M. Morales, K. Zapata, C. A. Sagaste, A. A. Angulo, and B. Rojano, "Optimization of the Ultrasound-Assisted Extraction Expression in Mango Peel (Mangifera Indica) using reponse surface methodology," *Acta Sci. Pol. Technol. Aliment. 19(1)*, vol. 19, no. 1, pp. 5–14, 2020.

[428] R. Ceaser and A. F. A. Chimphango, "Comparative analysis of physical and functional properties of cellulose nanofibers isolated from alkaline pre-treated wheat straw in optimized hydrochloric acid and enzymatic processes," *Int. J. Biol. Macromol.*, vol. 171,

pp. 331–342, 2021.

[429] F. J. Warren, M. J. Gidley, and B. Flanagen, “Infrared spectroscopy as a tool to characterise starch ordered structure- a joint FTIR-ATR, NMR, XRD and DSC study,” *Carbohydr. Polym.*, vol. 15, pp. 1–26, 2015.

[430] H. Wang, Y. Pu, A. Ragauskas, and B. Yang, “From lignin to valuable products – strategies, challenges, and prospects,” *Bioresour. Technol.*, vol. 271, pp. 449–461, 2019.

[431] F. H. Isikgor and C. R. Becer, “Lignocellulosic biomass: a sustainable platform for the production of bio-based chemicals and polymers,” *Polym. Chem.*, vol. 6, no. 25, pp. 4497–4559, 2015.

[432] S. Banerjee, A. F. Patti, V. Ranganathan, and A. Arora, “Hemicellulose based biorefinery from pineapple peel waste: Xylan extraction and its conversion into xylooligosaccharides,” *Food Bioprod. Process.*, vol. 117, pp. 38–50, 2019.

[433] L. S. Monte *et al.*, “Study of time reaction on alkaline pretreatment applied to rice husk on biomass component extraction,” *Biomass Convers. Biorefinery*, vol. 8, no. 1, pp. 189–197, 2018.

[434] I. R. S. Arruda *et al.*, “Structure and rheological properties of a xyloglucan extracted from Hymenaea courbaril var. courbaril seeds,” *Int. J. Biol. Macromol.*, vol. 73, pp. 31–38, 2015.

[435] A. Mishra and A. V. Malhotra, “Tamarind xyloglucan: A polysaccharide with versatile application potential,” *J. Mater. Chem.*, vol. 19, no. 45, pp. 8528–8536, 2009.

[436] T. Hayashi and R. Kaida, “Functions of xyloglucan in plant cells,” *Mol. Plant*, vol. 4, no. 1, pp. 17–24, 2011.

[437] A. Palaniappan, S. S. Yuvaraj, S. Sonaimuthu, and U. Antony, “Characterization of xylan from rice bran and finger millet seed coat for functional food applications,” *J. Cereal Sci.*, vol. 75, pp. 296–305, 2017.

[438] J. Xu, M. Li, and R. Sun, “Successive Fractionations of Hemicelluloses and Lignin from Sorghum Stem by Sodium Hydroxide Aqueous Solutions with Increased Concentrations,” *BioResources*, vol. 13, no. 2, pp. 2356–2373, 2018.

[439] A. Kozioł, J. Cybulska, P. M. Pieczywek, and A. Zdunek, “Evaluation of Structure and

Assembly of Xyloglucan from Tamarind Seed (Tamarindus indica L.) with Atomic Force Microscopy," *Food Biophys.*, vol. 10, no. 4, pp. 396–402, 2015.

[440] A. Ebringerova, "Structural Diversity and Application Potential of Hemicelluloses," *Macromol. Symp.*, no. 333, pp. 1–12, 2006.

[441] G. G. Chen, X. M. Qi, Y. Guan, F. Peng, C. L. Yao, and R. C. Sun, "High Strength Hemicellulose-Based Nanocomposite Film for Food Packaging Applications," *ACS Sustain. Chem. Eng.*, vol. 4, no. 4, pp. 1985–1993, 2016.

[442] N. Verma, V. Kumar, and M. C. Bansal, "Valorization of Waste Biomass in Fermentative Production of Cellulases: A Review," *Waste and Biomass Valorization*, vol. 12, no. 2. Springer Science and Business Media B.V., pp. 613–640, 01-Feb-2021.

[443] Z. Hromádková, J. Hirsch, and A. Ebringerová, "Chemical evaluation of Fallopia species leaves and antioxidant properties of their non-cellulosic polysaccharides," *Chem. Pap.*, vol. 64, no. 5, pp. 663–672, 2010.

[444] A. Sluiter, R. Ruiz, C. Scarlata, J. Sluiter, and D. Templeton, "Determination of Extractives in Biomass: Laboratory Analytical Procedure (LAP); Issue Date 7/17/2005 - 42619.pdf," 2008.

[445] A. Sluiter, B. Hames, R. Ruiz, C. Scarlata, J. Sluiter, and D. Templeton, "Determination of Ash in Biomass:Laboratory Analytical Procedure (LAP) Issue Date: 7/17/2005-42622," 2008.

[446] P. Kampeerapappun, "Extraction and Characterization of Cellulose Nanocrystals Produced by Acid Hydrolysis from Corn Husk," *J. Met. Mater. Miner.*, vol. 25, no. 1, pp. 19–26, 2015.

[447] M. Szymanska-Chargot and A. Zdunek, "Use of FT-IR Spectra and PCA to the Bulk Characterization of Cell Wall Residues of Fruits and Vegetables Along a Fraction Process," *Food Biophys.*, vol. 8, no. 1, pp. 29–42, 2013.

[448] L. Fan, R. Ruan, Y. Liu, Y. Wang, and C. Tu, "Effects of extraction conditions on the characteristics of ethanol organosolv lignin from bamboo (Phyllostachys pubescens mazel)," *BioResources*, vol. 10, no. 4, pp. 7998–8013, 2015.

[449] T. J. Bootten, P. J. Harris, L. D. Melton, and R. H. Newman, "Solid-state 13C-NMR spectroscopy shows that the xyloglucans in the primary cell walls of mung bean (Vigna

radiata L .) occur in differnt domains: a new model for xyloglucan-cellulose interactions in the cell wall," *J. Exp. Bot.*, pp. 1–13, 2004.

[450] S. Shankar, J. P. Reddy, and J. W. Rhim, "Effect of lignin on water vapor barrier, mechanical, and structural properties of agar/lignin composite films," *Int. J. Biol. Macromol.*, vol. 81, pp. 267–273, 2015.

[451] G. Cheng *et al.*, "Modification of hemicellulose polysaccharides during ripening of postharvest banana fruit," *Food Chem.*, vol. 115, no. 1, pp. 43–47, Jul. 2009.

[452] O. Chaikumpollert, P. Methacanon, and K. Suchiva, "Structural elucidation of hemicelluloses from Vetiver grass," *Carbohydr. Polym.*, vol. 57, no. 2, pp. 191–196, 2004.

[453] D. Morais de Carvalho *et al.*, "Isolation and characterization of acetylated glucuronoarabinoxylan from sugarcane bagasse and straw," *Carbohydr. Polym.*, vol. 156, pp. 223–234, Jan. 2017.

[454] X. Zhang, Z. Yuan, T. Wang, Q. Zhang, and L. Ma, "Effect of the temperature on the dissolution of corn straw in ethanol solution," *RSC Adv.*, vol. 6, no. 104, pp. 102306–102314, 2016.

[455] J. Puls, R. Janzon, and B. Saake, "Comparative removal of hemicelluloses from paper pulps using Nitren, cuen, NaOH, and KOH," *Lenzinger Berichte*, vol. 86, pp. 63–70, 2006.

[456] K. C. Kai and C. L. de O. Petkowicz, "Influence of extraction conditions on properties of seed xyloglucan," *Int. J. Biol. Macromol.*, vol. 46, no. 2, pp. 223–228, 2010.

[457] K. Werner, L. Pommer, and M. Broström, "Thermal decomposition of hemicelluloses," *J. Anal. Appl. Pyrolysis*, no. February 2018, pp. 1–8, 2014.

[458] K. S. Mikkonen *et al.*, "Films from oat spelt arabinoxylan plasticized with glycerol and sorbitol," *J. Appl. Polym. Sci.*, vol. 114, no. 1, pp. 457–466, 2009.

[459] C. Huang *et al.*, "A sustainable process for procuring biologically active fractions of high-purity xylooligosaccharides and water-soluble lignin from Moso bamboo prehydrolyzate," *Biotechnol. Biofuels*, vol. 12, no. 1, Jul. 2019.

[460] C. Huang, H. Dong, Z. Zhang, H. Bian, and Q. Yong, "Procuring the nano-scale lignin

in prehydrolyzate as ingredient to prepare cellulose nanofibril composite film with multiple functions," *Cellulose*, 2020.

[461] W. Pei, W. Shang, C. Liang, X. Jiang, C. Huang, and Q. Yong, "Using lignin as the precursor to synthesize Fe3O4@lignin composite for preparing electromagnetic wave absorbing lignin-phenol-formaldehyde adhesive," *Ind. Crops Prod.*, vol. 154, 2020.

[462] L. Mesa, E. González, C. Cara, M. González, E. Castro, and S. I. Mussatto, "The effect of organosolv pretreatment variables on enzymatic hydrolysis of sugarcane bagasse," *Chem. Eng. J.*, vol. 168, no. 3, pp. 1157–1162, 2011.

[463] A. Dzigbor and A. Chimphango, "Evaluating the potential of using ethanol /water mixture as a refrigerant in adsorption cooling system by using activated carbon - sodium chloride composite adsorbent," *Int. J. Refrig.*, 2018.

[464] N. Ramezani and M. Sain, "Thermal and Physiochemical Characterization of Lignin Extracted from Wheat Straw by Organosolv Process," *J. Polym. Environ.*, vol. 26, no. 7, pp. 3109–3116, 2018.

[465] J. L. Espinoza-Acosta, P. I. Torres-Chávez, E. Carvajal-Millán, B. Ramírez-Wong, L. A. Bello-Pérez, and B. Montaño-Leyva, "Ionic liquids and organic solvents for recovering lignin from lignocellulosic biomass," *BioResources*, vol. 9, no. 2, pp. 3660–3687, 2014.

[466] R. Sun, X. F. Sun, and X. P. Xu, "Effect of ultrasound on the physicochemical properties of organosolv lignins from wheat straw," *J. Appl. Polym. Sci.*, vol. 84, no. 13, pp. 2512–2522, 2002.

[467] J. Zhao, W. Zhang, X. Zhang, X. Zhang, C. Lu, and Y. Deng, "Extraction of cellulose nanofibrils from dry softwood pulp using high shear homogenization," *Carbohydr. Polym.*, vol. 97, no. 2, pp. 695–702, 2013.

[468] M. Namane, "Precipitation and Valorisation of lignin obtained from South African Kraft Mill black liqour," University of Cape Town, 2016.

[469] S. H. F. da Silva, O. Gordobil, and J. Labidi, "Organic acids as a greener alternative for the precipitation of hardwood kraft lignins from the industrial black liquor," *Int. J. Biol. Macromol.*, vol. 142, pp. 583–591, Jan. 2020.

[470] M. Brahim, N. Boussetta, N. Grimi, E. Vorobiev, I. Zieger-Devin, and N. Brosse,

"Pretreatment optimization from rapeseed straw and lignin characterization," *Ind. Crops Prod.*, vol. 95, pp. 643–650, 2017.

[471] R. Terán Hilares, J. C. dos Santos, M. A. Ahmed, S. H. Jeon, S. S. da Silva, and J. I. Han, "Hydrodynamic cavitation-assisted alkaline pretreatment as a new approach for sugarcane bagasse biorefineries," *Bioresour. Technol.*, vol. 214, pp. 609–614, 2016.

[472] F. Monteil-Rivera, G. H. Huang, L. Paquet, S. Deschamps, C. Beaulieu, and J. Hawari, "Microwave-assisted extraction of lignin from triticale straw: Optimization and microwave effects," *Bioresour. Technol.*, vol. 104, pp. 775–782, Jan. 2012.

[473] S. Constant *et al.*, "New insights into the structure and composition of technical lignins: A comparative characterisation study," *Green Chem.*, vol. 18, no. 9, pp. 2651–2665, May 2016.

[474] J. J. Bozell, "An evolution from pretreatment to fractionation will enable successful development of the integrated biorefinery," *BioResources*, vol. 5, no. 3, pp. 1326–1327, 2010.

[475] Q. Ibrahim and A. Kruse, "Prehydrolysis and organosolv delignification process for the recovery of hemicellulose and lignin from beech wood," *Bioresour. Technol. Reports*, vol. 11, p. 100506, Sep. 2020.

[476] S. Bauer, H. Sorek, V. D. Mitchell, A. B. Ibáñez, and D. E. Wemmer, "Characterization of Miscanthus giganteus lignin isolated by ethanol organosolv process under reflux condition," *J. Agric. Food Chem.*, vol. 60, no. 33, pp. 8203–8212, 2012.

[477] J. Domínguez-Robles, T. Tamminen, T. Liitiä, M. S. Peresin, A. Rodríguez, and A. S. Jääskeläinen, "Aqueous acetone fractionation of kraft, organosolv and soda lignins," *Int. J. Biol. Macromol.*, vol. 106, pp. 979–987, 2018.

[478] D. R. Naron, F. Collard, L. Tyhoda, and J. F. Görgens, "Characterisation of lignins from different sources by appropriate analytical methods : Introducing thermogravimetric analysis-thermal desorption-gas chromatography – mass spectroscopy," *Ind. Crop. Prod.*, vol. 101, pp. 61–74, 2017.

[479] K. Mondylaksita, J. A. Ferreira, R. Millati, W. Budhijanto, C. Niklasson, and M. J. Taherzadeh, "Recovery of high purity lignin and digestible cellulose from oil palm empty fruit bunch using low acid-catalyzed organosolv pretreatment," *Agronomy*, vol.

10, no. 5, 2020.

[480] J. Sameni, S. Krigstin, and M. Sain, "Characterization of Lignins Isolated from Industrial Residues and their Beneficial Uses," *BioResources*, vol. 11, no. 4, pp. 8435–8456, 2016.

[481] Y. Lu, Y. C. Lu, H. Q. Hu, F. J. Xie, X. Y. Wei, and X. Fan, "Structural characterization of lignin and its degradation products with spectroscopic methods," *Journal of Spectroscopy*. pp. 1–15, 2017.

[482] F. Xu, J. X. Sun, R. Sun, P. Fowler, and M. S. Baird, "Comparative study of organosolv lignins from wheat straw," *Ind. Crops Prod.*, vol. 23, no. 2, pp. 180–193, 2006.

[483] C. Huang, J. He, R. Narron, Y. Wang, and Q. Yong, "Characterization of Kraft Lignin Fractions Obtained by Sequential Ultrafiltration and Their Potential Application as a Biobased Component in Blends with Polyethylene," *ACS Sustain. Chem. Eng.*, vol. 5, no. 12, pp. 11770–11779, 2017.

[484] R. C. Sun and X. F. Sun, "Fractional and structural characterization of hemicelluloses isolated by alkali and alkaline peroxide from barley straw," *Carbohydr. Polym.*, vol. 49, no. 4, pp. 415–423, 2002.

[485] C. H. Kim, H. J. Youn, and H. L. Lee, "Preparation of cross-linked cellulose nanofibril aerogel with water absorbency and shape recovery," *Cellulose*, vol. 22, no. 6, pp. 3715–3724, 2015.

[486] V. A. Barbash, O. V. Yaschenko, and O. M. Shniruk, "Preparation of nanocellulose from organosolv straw pulp," *Nanoscale Res. Lett.*, vol. 195, pp. 497–505, 2017.

[487] F. H. Isikgor and C. Remzi Becer, "Lignocellulosic Biomass: a sustainable platform for production of bio-based chemicals and polymers," *Polym. Chem.*, vol. 6, pp. 4497–4559, 2015.

[488] M. Chen, Q. Ma, J. Y. Zhu, D. Martin Alonso, and T. Runge, "GVL pulping facilitates nanocellulose production from woody biomass," *Green Chem.*, vol. 21, no. 19, pp. 5316–5325, 2019.

[489] G. F. Collings, M. T. Yokoyama, and W. G. Bergen, "Lignin as Determined by Oxidation with Sodium Chlorite and a Comparison with Permanganate Lignin," *J. Dairy Sci.*, vol. 61, no. 8, pp. 1156–1160, 1978.

[490] R. S. A. Ribeiro, B. C. Pohlmann, V. Calado, N. Bojorge, and N. Pereira, "Production of nanocellulose by enzymatic hydrolysis: Trends and challenges," *Eng. Life Sci.*, vol. 19, no. 4, pp. 279–291, 2019.

[491] V. A. Barbash, O. V. Yashchenko, A. S. Gondovska, and I. M. Deykun, "Preparation and characterization of nanocellulose obtained by TEMPO-mediated oxidation of organosolv pulp from reed stalks," *Appl. Nanosci.*, vol. 1, p. 3, 2021.

[492] T. I. Shaheen and H. E. Emam, "Sono-chemical synthesis of cellulose nanocrystals from wood sawdust using Acid hydrolysis," *Int. J. Biol. Macromol.*, vol. 107, pp. 1599–1606, Feb. 2018.

[493] C. Torres-León *et al.*, "Edible films and coatings based on mango (var. Ataulfo) by-products to improve gas transfer rate of peach," *Lwt- Food Sci. Technol.*, vol. 97, no. March, pp. 624–631, 2018.

[494] D. García-García, R. Balart, J. Lopez-Martinez, M. Ek, and R. Moriana, "Optimizing the yield and physico-chemical properties of pine cone cellulose nanocrystals by different hydrolysis time," *Cellulose*, vol. 25, no. 5, pp. 2925–2938, 2018.

[495] Z. Lu, L. Fan, H. Zheng, Q. Lu, Y. Liao, and B. Huang, "Preparation , characterization and optimization of nanocellulose whiskers by simultaneously ultrasonic wave and microwave assisted," *Bioresour. Technol.*, vol. 146, pp. 82–88, 2013.

[496] T. F. Meyabadi and F. Dadashian, "Optimization of enzymatic hydrolysis of wool fibers for nanoparticles production using response surface methodology," *fibers Polym.*, vol. 13, pp. 313–321, 2012.

[497] D. Bondeson, A. Mathew, and K. Oksman, "Optimization of the isolation of nanocrystals from microcrystalline cellulose by acid hydrolysis," *Cellulose*, vol. 13, no. 2, pp. 171–180, 2006.

[498] L. M. Bester, "Development and optimisation of a process for cellulose nanoparticle production from waste paper sludge with enzymatic hydrolysis as an integral part," Stellenbosch University, 2018.

[499] F. Niu *et al.*, "The characteristic and dispersion stability of nanocellulose produced by mixed acid hydrolysis and ultrasonic assistance," *Carbohydr. Polym.*, vol. 165, pp. 197–204, 2017.

[500] C. Jin *et al.*, "Corn stover valorization by one-step formic acid fractionation and formylation for 5-hydroxymethylfurfural and high guaiacyl lignin production," *Bioresour. Technol.*, vol. 299, 2020.

[501] Y. Chen, Q. Wu, B. Huang, M. Huang, and X. Ai, "Isolation and characteristics of cellulose and nanocellulose from lotus leaf stalk agro-wastes," *BioResources*, vol. 10, no. 1, pp. 684–696, 2015.

[502] M. Roman and W. T. Winter, "Effect of sulfate groups from sulfuric acid hydrolysis on the thermal degradation behavior of bacterial cellulose," *Biomacromolecules*, vol. 5, no. 5, pp. 1671–1677, 2004.

[503] M. Cheng, Z. Qin, Y. Chen, S. Hu, Z. Ren, and M. Zhu, "Efficient Extraction of Cellulose Nanocrystals through Hydrochloric Acid Hydrolysis Catalyzed by Inorganic Chlorides under Hydrothermal Conditions," *ACS Sustain. Chem. Eng.*, vol. 5, pp. 4656–4664, 2017.

[504] M. Jonoobi, J. Harun, A. P. Mathew, M. Z. B. Hussein, and K. Oksman, "Preparation of cellulose nanofibers with hydrophobic surface characteristics," *Cellulose*, vol. 17, no. 2, pp. 299–307, 2010.

[505] T. Fattahi Meyabadi, F. Dadashian, G. Mir Mohamad Sadeghi, and H. Ebrahimi Zanjani Asl, "Spherical cellulose nanoparticles preparation from waste cotton using a green method," *Powder Technol.*, vol. 261, pp. 232–240, Jul. 2014.

[506] J. Domínguez-Robles, R. Sánchez, P. Díaz-Carrasco, E. Espinosa, M. T. García-Domínguez, and A. Rodríguez, "Isolation and characterization of lignins from wheat straw: Application as binder in lithium batteries," *Int. J. Biol. Macromol.*, vol. 104, 2017.

[507] Q. Wang, X. Zhao, and J. Y. Zhu, "Kinetics of strong acid hydrolysis of a bleached kraft pulp for producing cellulose nanocrystals (CNCs)," *Ind. Eng. Chem. Res.*, vol. 53, no. 27, pp. 11007–11014, 2014.

[508] L. Chen, Q. Wang, K. Hirth, C. Baez, U. P. Agarwal, and J. Y. Zhu, "Tailoring the yield and characteristics of wood cellulose nanocrystals (CNC) using concentrated acid hydrolysis," *Cellulose*, vol. 22, no. 3, pp. 1753–1762, 2015.

[509] H. P. S. Abdul Khalil *et al.*, "A review on nanocellulosic fibres as new material for sustainable packaging: Process and applications," *Renewable and Sustainable Energy*

Reviews, vol. 64. pp. 823–836, 2016.

[510] R. F. S. Barbosa, A. G. Souza, F. F. Ferreira, and D. S. Rosa, "Isolation and acetylation of cellulose nanostructures with a homogeneous system," *Carbohydr. Polym.*, vol. 218, pp. 208–217, Aug. 2019.

[511] M. Z. Karim, Z. Z. Chowdhury, S. B. A. Hamid, and M. E. Ali, "Statistical optimization for acid hydrolysis of microcrystalline cellulose and its physiochemical characterization by using metal ion catalyst," *Materials (Basel).*, vol. 7, no. 10, pp. 6982–6999, 2014.

[512] Z. Wu *et al.*, "Plant and biomass extraction and valorisation under hydrodynamic cavitation," *Processes*, vol. 7, no. 12, pp. 1–19, 2019.

[513] M. Szymanska-Chargot and A. Zdunek, "Use of FT-IR Spectra and PCA to the Bulk Characterization of Cell Wall Residues of Fruits and Vegetables Along a Fraction Process," *Food Biophys.*, vol. 8, no. 1, pp. 29–42, 2013.

[514] F. Kallel, F. Bettaieb, R. Khiari, A. García, J. Bras, and S. E. Chaabouni, "Isolation and structural characterization of cellulose nanocrystals extracted from garlic straw residues," *Ind. Crops Prod.*, vol. 87, pp. 287–296, 2016.

[515] G. Siqueira, J. Bras, and A. Dufresne, "Cellulosic bionanocomposites: A review of preparation, properties and applications," *Polymers*, vol. 2, no. 4. pp. 728–765, Dec-2010.

[516] R. N. Tharanathan, H. M. Yashoda, and T. N. Prabha, *Mango* (Mangifera indica L.) , *"The King of Fruits"—An Overview*, vol. 22, no. 2. 2006.

[517] D. Koegelenberg, "Arabinoxylan as partial flour replacer : The effect on bread properties and economics of bread making by," 2016.

[518] V. B. Singh and R. N. Singh, "Corrosion and inhibition studies of copper in aqueous solutions of formic acid and acetic acid," *Corros. Sci.*, vol. 37, no. 9, pp. 1399–1410, 1995.

[519] M. A. Mohd Nasir and S. H. Saleh, "Characterization of Hemicelluloses From Oil Palm Empty Fruit Bunches Obtained By Alkaline Extraction and Ethanol Precipitation," *Malysian J. Anal. Sci.*, vol. 20, no. 4, pp. 849–855, 2016.

Appendix

Appendix A

Appendix A1: Compositional analysis of feedstock and solid residue

The organosolv pretreated MSK residue were analysed for Acid detergent fiber (ADF), Neutral detergent fiber (NDF) and acid detergent lignin (ADL) using the Fibertech® system (Velp Scientifica 419278, FIWE, raw fiber extractor) to estimate the cellulose, hemicellulose and lignin contents [136]. Approximately, 1 g of sample was weighed into pre-weighed glass crucibles and placed in a Fibertech® extraction unit. Sodium sulphite (0.5 g) and 100 mL NDF solution were added, and the mixture heated to 100°C. After addition of 0.1 mL heat-stable α-amylase (Sigma #A3306), the temperature was reduced to 50°C and the mixture refluxed for 1 h. Thereafter, samples were washed 3 times with 150 mL boiling distilled water each and then 2 times with 20 mL acetone. The washed samples were oven dried at 103°C for 24 h then stored in a desiccator before weighing to give m_{NDF}. The obtained fraction after NDF analysis was used for ADF analysis following similar procedure but with the use of acid detergents to give m_{ADF}. Finally, the ADF fraction was hydrolysed with 20 mL of 72% H_2SO_4 at 25°C for 3 h with intermittent stirring. The mixture after hydrolysis was vacuum filtered with subsequent distilled water washing till filtrate attained pH 7. The residue left was dried at 103°C overnight, cooled in a desiccator and weighed to give m_{ADL}. The percentages of cellulose, hemicellulose, and lignin were calculated using Equations A1 – 3:

$$Hemicellulose\ (\%) = \frac{m_{NDF} - m_{ADF}}{m_{sample}} \times 100 \quad [A1]$$

$$Cellulose\ (\%) = \frac{m_{ADF} - m_{ADL}}{m_{sample}} \times 100 \quad [A2]$$

$$Lignin\ (\%) = \frac{m_{ADL} - m_{crucible}}{m_{sample}} \times 100 \quad [A3]$$

Appendix A2: Destarching of residual solids from after organosolv polyphenol extraction:

The polyphenol extracted solid residue was first destarched using thermostable α-amylase (Termamyl®SC) and amyloglucosidase (Saczyme®Plus) enzymes (from Novozymes). Briefly, samples were dispersed in deionized water to attain a solid-to-liquid ratio of 1:5. The pH of the mixture was adjusted to 5.5 with HCl before addition of the thermostable α-amylase (300 mL of Termamyl SC per ton starch in MSK), then incubated at 85°C for 2 hours in a water bath. Thereafter, the pH and temperature of the mixture were adjusted to 4.5 and 55°C,

respectively, then amyloglucosidase (800 ml Saczyme Plus/ ton starch in MSK) was added. After 2 hours, the solids were obtained by filtration through a number 5 Munktell filter paper, washed with distilled water, then oven dryed at 25°C for 48 h. Cellulose, hemicellulose, and lignin contents were determined by the Van Soest method of fiber analysis [392].

The starch content was determined using the Megazyme starch assay kit (KSTA 09/14). Briefly a sample or glucose standard of weight approximately 0.1 g was dispersed in 0.2 mL of 80% ethanol in a test tube and vigorously mixed for 1 min. This followed the addition of 3 mL of thermostable α-amylase and the mixture incubated for 6 min at 100 ºC in the water bath. Thereafter, the temperature of the test tube and sample was reduced to 50ºC by placing it in a 50 ºC water bath for 10 min before 0.1 mL amyloglucosidase enzyme was added and the mixture incubated further for 30 min. The content of the test tube after the set time was transferred to a 100 mL volumetric flask and filled to the 100 mL mark using distilled water with intermittent stirring. A 1 mL aliquot of the solution was centrifuged (2000×g) for 10 min and 0.1 mL of the clear portion transferred to a separate glass test tube. GOPOD reagent (3 mL) was added to the test tube with further incubation for 20 min. The absorbance of the glucose standard and the samples were measured against distilled water at 510 nm to calculate for starch content (Megazyme 2016).

Appendix A3: Analysis of total polyphenol content and antioxidant activity of polyphenol extracts [135].

About 10 µL of the organosolv extract was mixed with 1.8 mL of Folin-Ciocalteau reagent (previously diluted with distilled water to obtain a 1:10 solution). The mixture stood for 30 min and the absorbance measured (Varian Cary 50 Bio UV-VIS spectrophotometer) at 765 nm. A blank sample was used as reference and gallic acid of different concentrations (0 – 500 mg/L) used to obtain a standard calibration curve. The TPC was expressed as mg GAE/g extract. For the hemicellulose, 1 gram was homogenized (PRO250, Oxford CT, USA) in 10 mL of ethanol for 15 min and kept at 4 ºC overnight before centrifuging at 10,000 rpm for 15 min (Hermie Labortechnik GmbH, Z 366, Germany) and the supernatant used to determine TPC as described above. The antioxidant activity (AA) of the extracts was estimated by the DPPH method [47]. An aliquot of 200 µl extract was added to 1 ml of 0.1 mM DPPH solution in 80% v/v ethanol, vortex and stood 20 min in the dark. The absorbance was measured at 517 nm against ethanol blanks and control samples using a Varian Cary 50 Bio UV-VIS spectrophotometer. The% DPPH scavenging activity was calculated using Equation A4.

$$Scavenging\ activity, \% = \frac{Abs\ control - Abs\ sample}{Abs\ control} \times 100 \quad [A4]$$

Where $Abs\ control$ is absorbance of DPPH and $Abs\ sample$ is the absorbance of sample-DPPH solution.

Appendix A4: Characterisation of the hemicellulose extracts

The sugar composition of the hemicellulose extracted from the destarched kernel was determined based on a modified method of Yashoda et. al. (2005). Approximately 0.3 g of sample was dispersed in 72% M H_2SO_4 followed by the addition of distilled water to attain a 6% solution. The mixture was autoclaved for 3 h at 121°C and 2 bars. The conditions used allowed the hydrolysis of non-cellulosic glucose. The hydrolysates were filtered through sintered glass filler number 3 under vacuum and the remaining insoluble solids were washed with hot distilled water, dried at 103 ± 2 °C in the oven, cooled in a desiccator, and weighed. The filtrate containing the neutral sugars was neutralized with 7 N KOH to a pH range of 3 – 7, filtered through 2 mL syringe filters into HPLC valves, and analysed by HPLC using Thermo Separations Product Spectra System equipped with UV2000, Shodex RI101 detector, and a Biorad Aminex HPX-51H column (300 × 7.8 mm). Standard solutions of D-glucose, D-xylose, and L-arabinose were used for calibration [83]. All determinations were made in triplicates.

The thermal stabilities of the hemicellulose were determined using Mettler Toledo TGA 5500 thermogravimetric analysers under flowing nitrogen atmosphere (flow rate of 30 mL/min). Samples (5 – 10 mg) were heated in porcelain crucibles to 600°C at a heating rate of 20°C/min.

Molecular weight (Mw) and homogeneity of the extracts were determined by size exclusion chromatography (SEC) using HPLC. The hemicelluloses were dissolved in water at room temperature to obtain a concentration of 1 g/L and filtered through 0.22 µm syringe nylon filters (Membrane solutions, LLC). The HPLC column consisted of Dionex Ultimate 3000 system with ELS detection equipped with PSS SUPREMA column set, 3x300 mm using 0.125 M ammonium acetate as eluent at 75°C and flow rate of 1 mL/min. Pullulan was used as a molecular weight standard. Fourier transform infrared spectroscopy (FTIR) was used to analyse the structural changes in hemicellulose extracts using Thermo Nicolet NexusTM model 470/670/870 spectroscopy device fitted with a diffuse reflectance sample holder. Spectra were recorded in Attenuated Total Reflectance (ATR) mode with 64 scans per sample at a resolution of 8 cm-1 using a wavelength range of 4000 cm-1 to 600 cm^{-1}.

Table A1: Analysis of variance for polyphenol extraction

Response variable	Statistically significant factors	*p*-value	R^2
Total polyphenol content (mg GAE/g)	x_1	0.040	0.88
	x_2^2	0.040	
	Lack of fit	0.124	
Antioxidant activity (%)	x_1	0.019	0.83
	x_2^2	0.048	
	Lack of fit	0.065	
Cellulose content of recovered solids (%)	x_2	0.039	0.96
	LOF	0.325	
Hemicellulose content of recovered solids (%)	x_1	0.010	0.97
	x_1^2	0.014	
	x_2	0.005	
	x_2^2	0.013	
	LOF	0.050	
Lignin content of recovered solids (%)	x_1	0.025	0.99
	x_1^2	0.037	
	x_2	0.015	
	x_2^2	0.035	
	LOF	0.337	
Starch content of recovered solids (%)	LOF	0.584	0.92

x_1 =Temperature, x_2 =Ethanol concentration, x_1x_2=interaction of temperature and ethanol concentration, LOF=lack of fit

Model equations for polyphenol extraction from mango seed kernel

Total polyphenol content =87.6664+14.77772 "Temp [C]" +2.4134 "Temp [C]"*"Temp [C]"– 8.2375 "Conc [M]"- 19.3424 *"Conc [M]"*"Conc [M]"– 11.0085 Conc [M]"*"Temp [C]" [A5]

Antioxidant activity=79.76148+9.75949 "Temp [C]" +3.69227 "Temp [C]"*"Temp [C]"– 3.40742 "Conc [M]"- 5.13560 *"Conc [M]"*"Conc [M]"– 4.09500 Conc [M]"*"Temp [C]" [A6]

Cellulose content of residual solids =4.050150+0.166499 "Temp [C]" -0.134686 "Temp [C]"*"Temp [C]"– 0.324040 "Conc [M]"- 0.1604 *"Conc [M]"*"Conc [M]"– 0.035000 Conc [M]"*"Temp [C]" [A7]

Hemicellulose content of residual solids=22.97577+0.094667 "Temp [C]" -0.88881 "Temp [C]"*"Temp [C]"– 1.83327 "Conc [M]"- 0.97878 *"Conc [M]"*"Conc [M]"+0.23000 Conc [M]"*"Temp [C]" [A8]

Lignin content of residual solids=5.510074+0.253396 "Temp [C]" -0.229149 "Temp [C]"*"Temp [C]"– 0.409615 "Conc [M]"- 0.240549 *"Conc [M]"*"Conc [M]"+0.050000 Conc [M]"*"Temp [C]" [A9]

Starch content of residual solids =40.90185-3.02879 "Temp [C]" +0.71365 "Temp [C]"*"Temp [C]"+2.22947 "Conc [M]"- 0.16504 *"Conc [M]"*"Conc [M]"+1.16500 Conc [M]"*"Temp [C]" [A10]

Table A2: ANOVA for alkaline hemicellulose extraction from destarched mango seed kernel

Response variable	Statistically significant factors	*p*-value	R^2
Hemicellulose yield (%)	x_1^2	0.031	0.80
	x_2	0.021	
	x_2^2	0.010	
	LOF	0.237	
Lignin content of hemicellulose extract (%)	x_2	0.023	0.72
	LOF	0.220	
Total polyphenol content (mg GAE/g)	x_1	0.003	0.87
	x_2^2	0.037	
	LOF	0.252	
Antioxidant activity (%)	x_2	0.030	0.76
	LOF	0.670	
Cellulose content of recovered solids (%)	x_1	0.031	0.81
	x_2	0.016	
	x_2^2	0.007	
	x_1x_3	0.014	
	LOF	0.090	
Hemicellulose content of recovered solids (%)	x_1	0.043	0.79
	x_2	0.002	
	Lack of fit	0.073	
Lignin content of recovered solids (%)	x_1	0.022	0.83
	x_2	0.016	
	LOF	0.308	

x_1 =NaOH concentration, x_2 =Temperature, x_3=reaction time, x_1x_2=interaction of NaOH and temperature, x_1x_3= interaction of NaOH and time, x_2x_3= interaction of temperature and time, LOF=lack of fit

Hemicellulose yield =14.0468+26.968*"Conc [M]"-9.20603*"Conc [M]"*"Conc [M]"+0.619417*"Temp [C]"-0.00556614*"Temp [C]"*"Temp [C]"+4.54273*"Time [h]"-0.781227*"Time [h]"*"Time [h]"-0.009*"Conc [M]"*"Temp [C]"+0.04*"Conc [M]"*"Time [h]"+0.0049*"Temp [C]"*"Time [h]" [A11]

Lignin content of extract=18.4004-6.44129*"Conc [M]"+2.26101*"Conc [M]"*"Conc [M]"-0.124468*"Temp [C]"+0.00157627*"Temp [C]"*"Temp [C]"-5.04795*"Time [h]"+0.793946*"Time [h]"*"Time [h]"-0.00837265*"Conc [M]"*"Temp [C]"+0.694619*"Conc [M]"*"Time [h]"-0.00383649*"Temp [C]"*"Time [h]" [A12]

TPC=15.1271+5.9921*"Conc [M]"+0.866663*"Conc [M]"*"Conc [M]"+0.431456*"Temp [C]"-0.00281552*"Temp [C]"*"Temp [C]"+1.92597*"Time [h]"-0.106836*"Time [h]"*"Time [h]"-0.0019*"Conc [M]"*"Temp [C]"-0.1625*"Conc [M]"*"Time [h]"-0.03385*"Temp [C]"*"Time [h]"[A13]

AA=50.297+9.19965*"Conc [M]"-1.75387*"Conc [M]"*"Conc [M]"+0.174258*"Temp [C]"-0.00310006*"Temp [C]"*"Temp [C]"-1.06689*"Time [h]"-0.307654*"Time [h]"*"Time [h]"-

0.0289*"Conc [M]"*"Temp [C]"-0.4425*"Conc [M]"*"Time [h]"+0.03115*"Temp [C]"*"Time [h]" [A14]

Cellulose content of residue = 17.1017-6.16304*"Conc [M]"+0.548444*"Conc [M]"*"Conc [M]"+0.094379*"Temp [C]"-0.000867651*"Temp [C]"*"Temp [C]"-2.30132*"Time [h]"+0.184761*"Time [h]"*"Time [h]"+0.00956459*"Conc [M]"*"Temp [C]"+1.09341*"Conc [M]"*"Time [h]"-0.00391279*"Temp [C]"*"Time [h]" [A15]

Lignin content of residue =28.0612-12.6853*"Conc [M]"+3.35114*"Conc [M]"*"Conc [M]"-0.139416*"Temp [C]"+0.000462367*"Temp [C]"*"Temp [C]"+3.82244*"Time [h]"-0.463126*"Time [h]"*"Time [h]"+0.0328924*"Conc [M]"*"Temp [C]"-0.700154*"Conc [M]"*"Time [h]"-0.00965319*"Temp [C]"*"Time [h]" [A16]

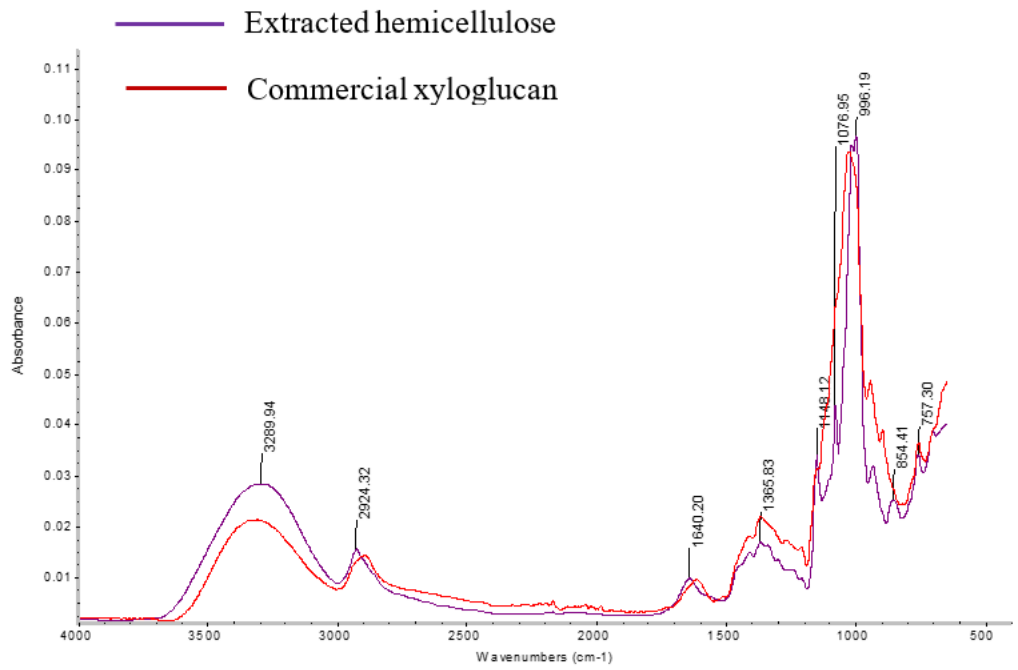

Figure A1: Fourier Transform infrared spectroscopy of bioactive hemicellulose and commercial xyloglucan

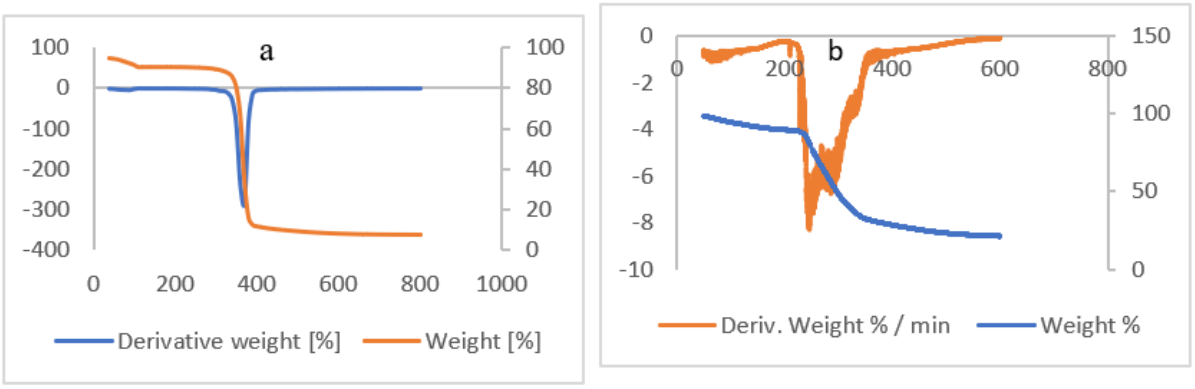

Figure A2: Thermographs and derivative thermographs of (a) commercial tamarind xyloglucan and (b) extracted mango seed kernel hemicellulose.

Table A3: Molecular weight, number average molecular weight and polydispersity of mango seed kernel hemicelluloseand commercial xyloglucan

Sample	MKH	CXGN
M_w (g/mol)	108,163	2372,886
Mn (g/mol)	22,685	707509
PDI	4.77	3.35

Appendix B

Appendix B1: Preliminary experiments for determination of suitable conditions for hemicellulose extraction from mango seed husks

To obtain a range of conditions for optimizing the AP conditions for hemicellulose extraction from mango seed husk, preliminary experiments were performed varying NaOH concentration (0.5, 1, 2, 3 and 4 M), temperature (15, 40, 65, 90 and 115 °C) and time (2, 3, 4, 5 and 6 h). These conditions were chosen from the literature [61], [64], [83]. The response variables were hemicellulose yield and content of monomeric sugars. Hemicellulose yields were based on initial hemicellulose content of the feedstock and the monomeric sugars were determined by HPLC as described in the main text.

Effect of extraction conditions on hemicellulose yield and monomeric sugar content

The increase in NaOH concentration from 0.5 to 4 M increased the yield of hemicelluloses from 10.77% – 54.02% (Figure B1). The hemicellulose yields obtained using 3 and 4 M NaOH concentrations (48.57% and 54.02%, respectively) were not statistically significant (p>0.05), however, both yields were higher than the hemicellulose yields obtained using 2 M, 1 M, and 0.5 M NaOH concentrations. Although higher hemicellulose yields were obtained using 3 and 4 M NaOH, monomeric sugars were observed in these extracts (5.51% and 7.22% monomeric sugars respectively), which is not desirable for the end application of the hemicelluloses as a biomaterial for biocomposites. The degradation of hemicellulose to monomeric sugars at such high alkaline concentrations has been reported in previous studies [519]. Therefore, considering the aim of the study, thus, obtained hemicelluloses in polymeric form, the 2M NaOH concentration was chosen as ideal concentration for further optimisation of the hemicellulose extraction.

To understand the temperature effect on hemicellulose yield, various temperatures (15, 40, 65, 90, and 115 °C) were used at 2 M for 2 h. The yield of hemicellulose increased (Figure B1) as the temperature increased from 15 to 90 °C. This resulted in hemicellulose yields ranging from 9.95% to 48.95%. But when the temperature was increased further to 115 °C, the hemicellulose yield declined to 46.45%. This shows that although higher temperatures are required to help the process in penetrating the cell walls for hemicellulose extraction, extreme temperatures may lead to the co-extraction of other components rather than hemicelluloses [244] resulting in a decrease in the hemicellulose yield.

Further, the effect of time on hemicellulose yield was assessed. Reaction times of 1, 2, 4, and 6 h were evaluated at 2 M and 65 °C, and the results are shown in Figure B1. It was observed that increasing time from 1 – 6 h had a positive influence on the hemicellulose yield, though the yields observed at 4 and 6 h (43.57% and 44.01%) extraction times were not significantly different ($p<0.05$). The insignificant difference between yields obtained at these times may suggest that at longer extraction times, there is the hydrolytic cleavage of bonds in polymers which may lead to structural modification and change in viscosity of reaction medium resulting in a reduction of yield (Mohd Nasir & Saleh, 2016). The hemicellulose yield observed for 1 h extraction time was relatively low (16.35%) compared to the rest of the experimental runs and was therefore excluded in the optimization experiments. Based on these results, a concentration of 1 – 2 M, temperature of 40 – 90 °C and reaction time of 2 – 4 h were chosen for optimization experiments. These selected conditions were within the ranges used for hemicellulose extraction from other agricultural waste residues [61], [64], [83].

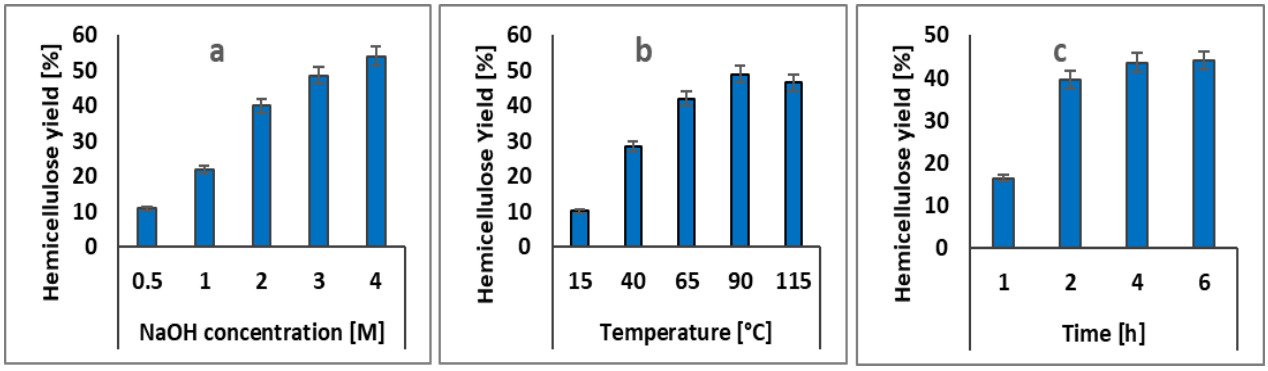

Figure B1: Effect of NaOH concentration (a) temperature (b) and time (c) on the yield and monomeric sugar content of hemicelluloses from mango seed husk.

B2. Mango Seed husks and hemicelluloses characterisation: determination of extractive and sugars

Water extractives were determined from samples weighing 5 g that were placed into extraction thimbles, which were placed in pre-weighed round bottom flasks (500 mL) containing 200 mL of distilled water for refluxing in water for 8 h on a Soxhlet extractor. After extraction, the water was distilled using the Soxhlet extractor until all visible water is gone. The flasks, with the remaining contents, were dried in an oven at 103 °C overnight and weighed after cooled to room temperature. Ethanol extractives were obtained by performing Soxhlet extraction on the residue from the water extraction in the same way as described for the water extractives but in this case, ethanol was used as the extraction solvent.

Sugar composition was determined from approximately 0.3 g of mango seed husks hemicelluloses. The samples in triplicates, were dispersed in 72% H_2SO_4 followed by addition of distilled water to obtain 6% solution and autoclaved at 121 °C for 3 h at a pressure of 2 bar. The hydrolysates were filtered under vacuum through porous sintered glass filter number 3. The filter cakes were washed and subsequently dried at 103 °C in an oven overnight followed by cooling in a desiccator before weighing. The supernatants were neutralized with 7 N KOH to a pH range of pH 3 – pH 7.

Table B1: Central composite experimental design for alkaline extraction of hemicelluloses from mango seed husks

Run	Variable levels		
	NaOH Concentration [M] (X1)	Temperature [°C] (X2)	Time [h] (X3)
1	1.00	40.00	2.00
2	1.00	40.00	4.00
3	1.00	90.00	2.00
4	1.00	90.00	4.00
5	2.00	40.00	2.00
6	2.00	40.00	4.00
7	2.00	90.00	2.00
8	2.00	90.00	4.00
9	0.66	65.00	3.00
10	2.34	65.00	3.00
11	1.50	23.00	3.00
12	1.50	107.00	3.00
13	1.50	65.00	1.32
14	1.50	65.00	4.68
15	1.50	65.00	3.00
16	1.50	65.00	3.00
17	1.50	65.00	3.00
18	1.50	65.00	3.00
19	1.50	65.00	3.00
20	1.50	65.00	3.00

The statistical analysis involved nonlinear regression analysis and Analysis of Variance (ANOVA). The results are presented in Tables A2- A5 for yield, xylan, xyloglucan ratio, uronic acid, and lignin contents

Table B2: Analysis of variance for mango seed husk hemicellulose yield

Source	Sum of squares	Degrees of freedom	Mean square	F-value	*P*-value
X_1	815.08	1	815.08	436.20	0.000
X_1^2	17.77	1	17.77	9.51	0.027
X_2	380.44	1	380.44	203.59	0.000
X_2^2	108.78	1	108.78	58.22	0.000
X_3	0.50	1	0.50	0.27	0.626
X_3^2	11.88	1	11.88	6.36	0.053
$X_1.X_2$	220.61	1	220.61	118.06	0.000
X_1X_3	1.28	1	1.28	0.68	0.446
X_2X_3	0.004	1	0.004	0.002	0.965
Lack of fit	17.09	5	3.42	1.83	0.262
Pure error	9.34	5	1.87		
Total SS	1567.93	19			
R^2	0.98				

X_1, X_2, and X_3 are the coded values for NaOH concentration, temperature, and reaction time respectively.

Table B3: Analysis of variance for Xyloglucan and Xylan ratio

Source	Sum of squares	Degrees of freedom	Mean square	F-value	*P*-value
X_1	0.049	1	0.049	92.91	0.000
X_1^2	0.010	1	0.010	18.60	0.008
X_2	0.039	1	0.039	74.33	0.000
X_2^2	0.006	1	0.006	10.90	0.021
X_3	0.001	1	0.001	0.03	0.870
X_3^2	0.0003	1	0.0003	2.11	0.206
$X_1.X_2$	0.0001	1	0.0001	0.52	0.502
X_1X_3	0.000	1	0.000	0.25	0.633
X_2X_3	0.000	1	0.000	0.00	0.99
Lack of fit	0.023	5	0.005	8.79	0.020
Pure error	0.003	5	0.001		
Total SS	0.129	19			
R^2	0.80				

X_1, X_2, and X_3 are the coded values for NaOH concentration, temperature, and reaction time respectively.

Table B4: Analysis of variance for lignin content of hemicellulose extract

Source	Sum of squares	Degrees of freedom	Mean square	F-value	*P*-value
X_1	24.21	1	24.21	17.795	0.0083
X_1^2	11.67	1	11.67	8.579	0.0326
X_2	16.23	1	16.23	11.930	0.0182
X_2^2	6.99	1	6.99	5.141	0.0727
X_3	0.413	1	0.413	0.304	0.6053
X_3^2	0.534	1	0.534	0.393	0.5583
$X_1.X_2$	1.901	1	1.901	1.398	0.2903
X_1X_3	0.911	1	0.911	0.670	0.4503
X_2X_3	1.155	1	1.155	0.849	0.3991
Lack of fit	21.75	5	4.349	3.197	0.1139
Pure error	6.802	5	1.390		
Total SS	92.10	19			
R^2	0.70				

X_1, X_2, and X_3 are the coded values for NaOH concentration, temperature, and reaction time respectively.

Table B5: Analysis of variance for uronic acid content of hemicellulose extract

Source	Sum of squares	Degrees of freedom	Mean square	F-value	*P*-value
X_1	5.875	1	5.875	4.286	0.093
X_1^2	0.155	1	0.155	0.113	0.750
X_2	40.406	1	40.406	29.26	0.003
X_2^2	0.378	1	0.378	0.276	0.622
X_3	0.496	1	0.496	0.362	0.574
X_3^2	5.601	1	5.601	4.086	0.099
$X_1.X_2$	2.785	1	2.785	2.032	0.213
X_1X_3	1.328	1	1.328	0.969	0.370
X_2X_3	3.277	1	3.277	2.391	0.183
Lack of fit	20.001	5	4.000	2.918	0.132
Pure error	6.853	5	1.371		
Total SS	86.486	19			
R^2	0.70				

X_1, X_2, and X_3 are the coded values for NaOH concentration, temperature, and reaction time respectively.

The output of the analysis of variance (ANOVA) in Tables B2-B5) show that the determination coefficient (R^2) for all the models ranges between 0.7 and 0.99 (Table B2-B5), indicating that 70 to 99% of variations in the response variables are accounted for by the modelled alkaline extraction conditions. Correlation between hemicellulose extraction conditions and responses are shown in Figure B2 a-d. The alkaline extraction conditions had various effects on the different responses. The temperature and NaOH concentration were linearly related to hemicellulose yield. The correlation coefficient (r) for temperature gave 0.49 indicating relatively weak linearity compared to NaOH concentration, r=0.72. The reaction time, on the other hand, exhibited the weakest linear relationship, r=0.02, with yield (Figure B2 a i-iii). Thus, an increase in the extraction conditions especially temperature and NaOH enhanced the dissolution of hemicelluloses. The NaOH concentration and temperature were the major contributors to the hemicellulose dissolution as discussed above. However, among xylan (XLN) and xyloglucan (XGN), xylan was the most favoured during the extraction process, resulting in a lower XGN/XLN ratio in the hemicellulose extracts. The correlation coefficient r= -0.61 (Figure A1b i-iii) indicates a strong inverse correlation between XGN/XLN ratio and NaOH concentration. It follows that approximately 37% of the observed decrease in XGN/XLN ratio was associated with an increase in NaOH concentration. The regression equation (Table B6) shows that for every 1M addition of NaOH, it will result in approximately 0.12 decreases on average in XGN/XLN ratio. A similar trend was observed for XGN/XLN ratio in relation to temperature. Thus, ≈28% on average of the observed decrease in the XGN/XLN ratio is associated with an increase in temperature. The influence of time on the XGN/XLN ratio was negligible with the correlation coefficient, r=0.01, indicating an almost complete absence of correlation. Further, the correlation coefficients, r for NaOH concentration, temperature, and time were -0.53, -0.42, and -0.07 respectively for lignin content of hemicellulose extract (Figure B2 c i-iii).

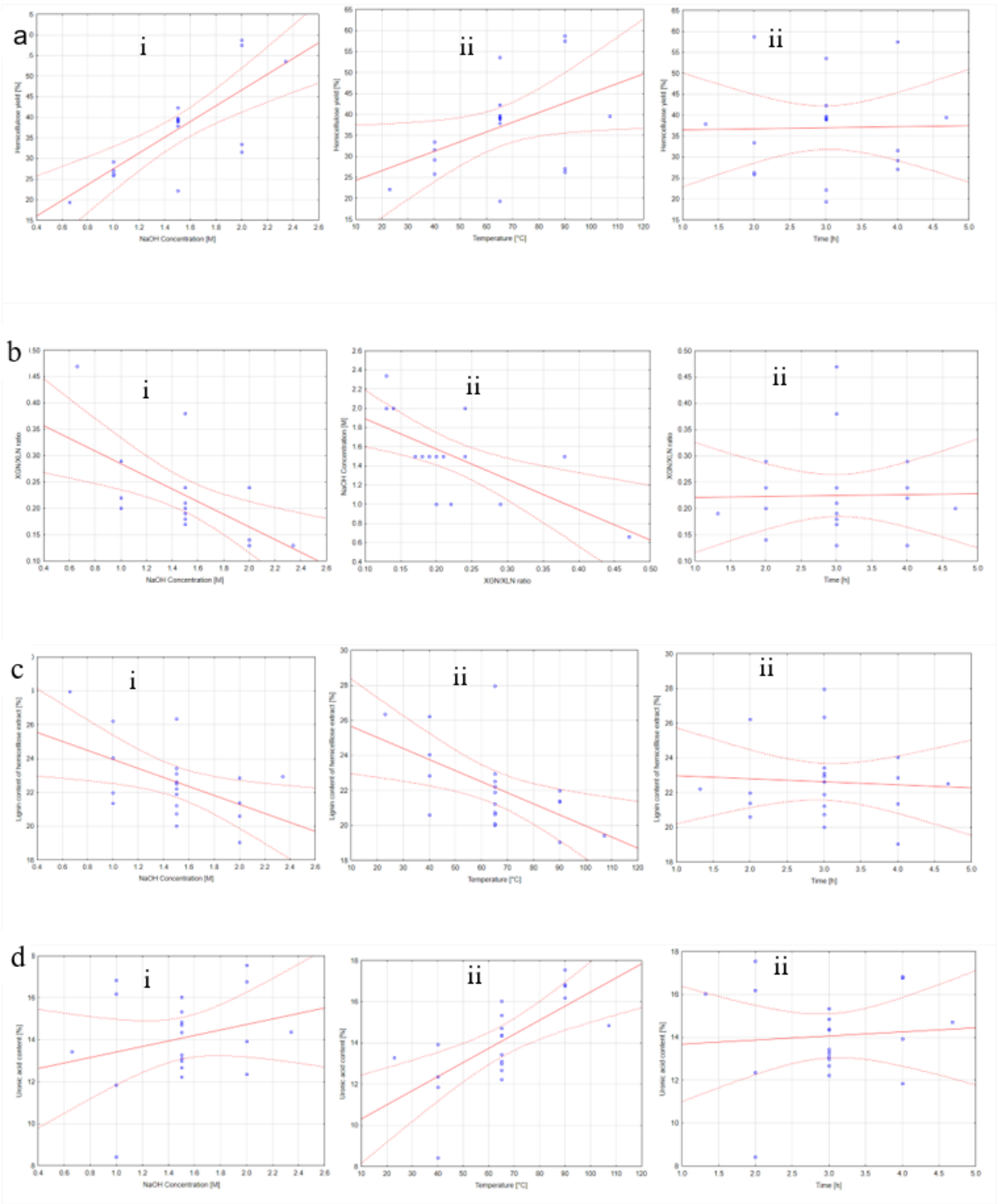

Figure B2: Correlation of hemicellulose extraction conditions and **a**. yield, **b**. XGN/XLN ratio, **c**. the lignin content of hemicellulose extract and **d**. uronic acid content

These indicate inverse correlations with lignin content in the order time < temperature < NaOH concentration. This implies that increases in temperature, NaOH concentration, and time results to decrease in the lignin content. In essence, higher temperatures and NaOH concentrations aided in the breaking of ether, ester, and glycosidic linkages in the cell wall components, resulting in the dissolution of hemicelluloses into the extraction medium [438]. It also follows that the high dissolution of hemicelluloses favoured the extraction of uronic acids (Figure B2d i-iii), although time had the least linear relationship (r=0.08) with uronic acid content in the hemicellulose extract. It could be seen in the figures that the temperature had the strongest linear correlation, r=0.68 while NaOH concentration also had a positive correlation r=0.26 with the uronic acid content.

Table B6: Correlation equations of alkaline treatment conditions with responses

Response (y)	Condition (x)		
	NaOH concentration (M)	Temperature [°C]	Time [h]
Hemicellulose yield [%]	y = 8.348+15.54*x	y = 17.593+0.211*x	y = 30.740+0.1918*x
XGN/XLN ratio	y = 0.405-0.120*x	y = 0.364-0.0024*x	y = 0.2217+0.0011*x
Lignin content of hemicellulose extract [%]	y = 24.618-2.663*x	y = 23.458-0.0436*x	y = 21.145-0.1739*x
Uronic acid content [%]	y = 12.100+1.3118*x	y = 9.612+0.0681*x	y = 13.496-0.1906*x

The regression equations from the optimization of hemicellulose extraction conditions for yield, xyloglucan/xylan ratios, lignin and uronic acid contents are given in Equations B1 to B4, respectively.

Yield= =-2.44989+3.86377*"NaOH Concentration [M]"-4.44153*"NaOH Concentration [M]"*"NaOH Concentration [M]"+0.155105*"Temperature [°C]"-0.00439585*"Temperature [°C]"*"Temperature [°C]"+6.89603*"Time [h]"-0.908111*"Time [h]"*"Time [B1]

XGN/XLN ratio= =0.721466-0.375807*"NaOH Concentration [M]"+0.103854*"NaOH Concentration [M]"*"NaOH Concentration [M]"-0.00557946*"Temperature [°C]"+3.18079e-05*"Temperature [°C]"*"Temperature [°C]"+0.0656257*"Time [h]"-0.00875249*"Time [B2]

Lignin content = =43.9664-18.0217*"NaOH Concentration [M]"+3.59965*"NaOH Concentration [M]"*"NaOH Concentration [M]"-0.201402*"Temperature [°C]"+0.00111459*"Temperature [°C]"*"Temperature [°C]"+0.956966*"Time [h]"-0.192568*"Time [h]"*"Time [B3]

Uronic acid content=0.843385+5.5803*"NaOH Concentration [M]"+0.414842*"NaOH Concentration [M]"*"NaOH Concentration [M]"+0.182442*"Temperature [°C]"+0.000259275*"Temperature [°C]"*"Temperature [°C]"-0.663489*"Time [h]"+0.623434*"Time [h]"*"Time [h]"-0.0472*"NaOH [B4]

Where XGN/XLN is Xyloglucan: Xylan ratio. Coefficients with (-) and (+) signs represent negative and positive correlations as plotted in Figure B2.

Table B7: Neutral sugar composition of extracted hemicellulose from mango seed husk

Total glucose (%)	Total xylose (%)
9.53	54.11
9.44	52.95
7.66	60.60
7.96	59.52
8.73	57.99
8.54	57.62
6.41	70.89
6.00	72.26
12.46	45.74
5.72	70.17
11.12	49.02
7.19	64.94
7.37	60.46
7.79	61.42
8.00	66.63
7.92	67.95
7.85	66.02
8.79	66.49
9.44	64.49
7.41	67.95

Appendix B3: Preliminary experiments for determination of the effect of homogenizing time on lignin dissolution from mango seed husks

To study the effect of high-shear homogenization on lignin dissolution and determine the range of homogenizing time for optimization, preliminary experiments were performed at constant temperature and ethanol concentration (150 °C and 60%v/v ethanol with 0.2% NaOH) after homogenizing the pre-soaked alkaline treated mango seed husk samples at 5, 10, 15, 20, 25 and 30 min. The extraction of the lignin followed the same procedure as in the main text. Lignin solubilisation was calculated as shown in the main text.

Effect of homogenizing time on lignin solubilisation from mango seed husk

Figure B3 depicts the influence of homogenizing time on lignin solubilization. The solubilisation of lignin increased with homogenizing time from 5 min to 15 min and reached its maximum at 20 min. There was significant difference ($p<0.05$) between 5 min and 10 min homogenizing times but no significant difference ($p>0.05$) was observed when the pretreatment was performed at 10 min and 15 min homogenizing times (Figure B3). At 20 min, lignin solubilization reached its maximum and thereafther reduced when homogenizing time was extended to 25 and 30 min, respectively. In addition, the lignin solubilisation obtained at 5 min was relatively lower compared to all other runs and was excluded in the optimization experiment. Though lignin solubilisation at 25- and 30-min homogenizing times were not statistically different from the 20 min, they were considered energy intensive and excluded in the optimization experiment. In all 10 – 20 min was chosen for further optimization experiments.

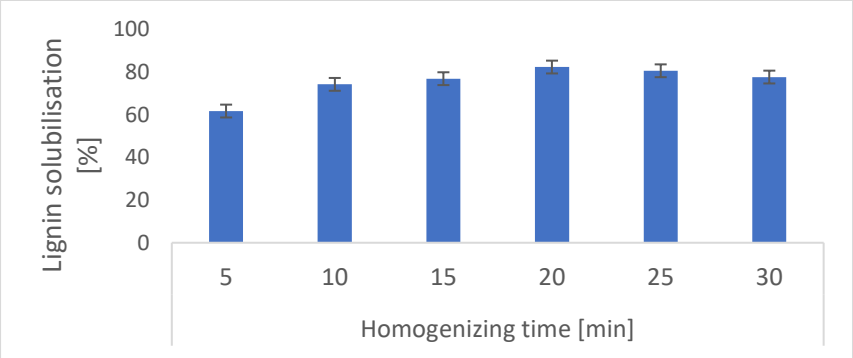

Figure B3: Effect of homogenizing time on lignin solubilisation from mango seed husk

Table B8: Central composite experimental design for alkaline extraction of hemicelluloses from mango seed husks

Run	Variable levels		
	Ethanol concentration [%] (X1)	Temperature [°C] (X2)	Homogenizing time [h] (X3)
1	50.00	130.00	10.00
2	50.00	130.00	20.00
3	50.00	150.00	10.00
4	50.00	150.00	20.00
5	70.00	130.00	10.00
6	70.00	130.00	20.00
7	70.00	150.00	10.00
8	70.00	150.00	20.00
9	43.18	140.00	15.00
10	76.82	140.00	15.00
11	60.00	123.18	15.00
12	60.00	156.82	15.00
13	60.00	140.00	6.59
14	60.00	140.00	23.41
15	60.00	140.00	15.00
16	60.00	140.00	15.00

Table B9: Significant factors obtained from regression analysis and the coefficient of determination

Response variable	Statistically significant factors	F-value	*p*-value	R^2
Lignin solubilisation (wt%)	Ethanol concentration	2280.71	0.013	0.98
	Ethanol concentration × ethanol concentration	1117.77	0.019	
	Temperature	16504.83	0.005	
	Homogenizing time	543.81	0.027	
	Ethanol concentration × homogenizing time	737.20	0.023	
	Lack of fit	79.16	0.085	
Lignin recovery (wt%)	Ethanol concentration	190.01	0.046	0.97
	Temperature	918.92	0.021	
	Lack of fit	6.33	0.291	
Lignin purity (%)	Ethanol concentration	176.32	0.047	0.88
	Ethanol concentration × ethanol concentration	589.91	0.026	
	Temperature	592.73	0.026	
	Ethanol concentration × temperature	256.81	0.039	
	Ethanol concentration × homogenizing time	221.46	0.043	
	Lack of fit	56.86	0.10	
Cellulose content of solids (wt%)	Temperature	822.07	0.022	0.96
	Lack of fit	8.37	0.256	
Residual lignin content (wt%)	Ethanol concentration	2285.45	0.013	0.98
	Ethanol concentration × ethanol concentration	1121.69	0.019	
	Temperature	16551.64	0.005	
	Homogenizing time	545.28	0.027	
	Ethanol concentration × homogenizing time	738.16	0.023	
	Lack of fit	79.20	0.085	
Residual hemicellulose	Temperature	6178.90	0.008	0.94
	Lack of fit	79.62	0.085	

Table B10: Regression models developed for the responses

Lignin solubilisation (%) =-706+10.23 X_1-0.05 X_1^2+4.81 X_2+4.16 X_3-0.04X_1X_2 -0.03X_2X_3
Lignin purity (%) =-341.39+5.22 X_1-0.02 X_1^2+3.39 X_2-0.01 X_2^2 +3.64 X_3-0.02 X_1X_2-0.03 X_1X_3-0.01 X_2X_3
Cellulose content of solids (%) =-103.04+2.33 X_1-0.01 X_1^2+1.24 X_2-1.01 X_3+0.03 X_3^2-0.01 X_1X_2
Residual lignin (%) =191.34-2.43 X_1+0.01 X_2-1.14 X_2-0.99 X_3+0.01 X_1X_2-0.01 X_2X_3
Residual hemicellulose=30.01-0.05 X_1-0.31 X_2-0.29 X_3

Table B11: Carbon chemical shifts (δ, ppm) and assignments of organosolv lignin in ^{13}C NMR spectrum

δ (ppm)	Assignments	δ (ppm)	Assignments
174.4	C-6 in 4-O-MeGluA	115.3	C-3/C-5, p-coumaric acid ester
166.4	C-γ *p*-coumaric acid ester	111.7	C-2, G
152.2	C-3/C-5 in S	103.7	C-2/C-6, S
149.5	C-3, G etherified	74.4	C-3, Xyl internal unit
149.2	C-3, G etherified	72.7	C-α in β-O-4
147.6	C-4, G etherified	63.0	C-γ in β 5
145.2	C-4, G non-etherified	55.8	OCH_3 in S and G units
134.9	C-1, S etherified; C-1 G etherified	33-24	α-, β-Methylene groups
119.2	C-6, G	14.0	γ-Methyl in *n*-propyl side chains

[a] S, syringyl unit; G, guaiacyl unit; H; 4-O-MeGluA, 4-O-methyl glucuronic acid.

Appendix C

Table C1: Central composite experimental design with different combinations of independent variables for formic acid nanocellulose production

Run	Type of point	Coded level	
		X_1	X_2
1	Factorial	-1	-1
2	Factorial	-1	1
3	Factorial	1	-1
4	Factorial	1	1
5	Axial	-α	0
6	Axial	+α	0
7	Axial	0	-α
8	Axial	0	+α
9	Centre	0	0
10	Centre	0	0

X: Coded levels of independent variables